January 19, 1966

MANUFACTURING ENGINEERING LABORATORY

NASA

NASA TMX 57215

ALUMINUM WELD DEVELOPMENT COMPLEX

GEORGE C. MARSHALL SPACE FLIGHT CENTER

HUNTSVILLE, ALABAMA

NATIONAL AERONAUTICS AND SPACE ADMINISTRATION

ALUMINUM WELD DEVELOPMENT
COMPLEX CONFERENCE

BUILDING 4200
January 19, 1966

WELD DEVELOPMENT BRANCH
MANUFACTURING RESEARCH AND TECHNOLOGY DIVISION
GEORGE C. MARSHALL SPACE FLIGHT CENTER
NATIONAL AERONAUTICS AND SPACE ADMINISTRATION
HUNTSVILLE, ALABAMA

ALUMINUM WELD DEVELOPMENT COMPLEX

TABLE OF CONTENTS

SECTION I

REPORT

on

N66 35567

WELDING-BASE METAL INVESTIGATION
Contract NAS8-11445

to

ALUMINUM WELD DEVELOPMENT COMPLEX MEETING

GEORGE C. MARSHALL SPACE FLIGHT CENTER
NATIONAL AERONAUTICS AND SPACE ADMINISTRATION
Huntsville, Alabama

January 19, 1966

by

D. L. Cheever, P. A. Kammer, R. E. Monroe, and D. C. Martin

BATTELLE MEMORIAL INSTITUTE
Columbus Laboratories
505 King Avenue
Columbus, Ohio ·43201

WELDING-BASE METAL INVESTIGATION

by

D. L. Cheever, P. A. Kammer, R. E. Monroe, and D. C. Martin

INTRODUCTION

A program was conducted to investigate the effects of factors associated with aluminum base plate and filler wire on the occurrence of weld defects. The materials studied were experimental alloys of 2219-T87 and 2014-T6 base plate and 2319 and 4043 filler wire. In the program, four factors that determine the weld defect potential of a material were considered: (1) chemical content, (2) internal impurities, (3) hydrogen content, and (4) external impurities.

Chemical content was used to describe all the intentional alloy additions, specified as ranges. Internal impurities were those elements limited by specifications to a maximum level. The hydrogen content was determined by vacuum fusion analysis. External impurities was controlled by moisture additions to the weld shielding gas.

Welds were made with the experimental base plate and filler wire using precisely regulated welding equipment and accurate instrumentation. The welds were then examined by radiographic and sectioning techniques. The occurrence of pores, which were the only weld defects observed, was related to variations of each of the four factors between a high and a low level. Statistical methods were used in this analysis.

The four factors were generally ranked in order of the strength of the relationship between the factor level and the weld porosity level. The external impurities factor was the strongest factor and was followed in strength by the chemical content, internal impurities, and hydrogen content. The hydrogen content

of the experimental base plate was significant only at a level above the hydrogen content of the commercial base plate available and above the majority of the experimental base plate hydrogen contents. The hydrogen content of the filler wire was not significant in the majority of the statistical comparisons studied. An interaction existed between chemical content and internal impurities, which apparently affected the significance of the relationship of each factor to the porosity level. Minimum weld defect potential apparently existed when all four factors were at a low level.

The size and distribution of pores within the welds were related to the composition of the weld metal. Segregation layers were observed in the welds in which pores formed preferentially. The shape of the segregation layer changed for different material compositions.

The hydrogen content of the experimental base plate was low for low chemical content and low internal impurities and was high for high chemical content and high internal impurities. The hydrogen content was independent of the control methods used during casting except for one severe treatment.

The porosity level of the welds increased with increasing hydrogen content of the experimental base plate.

PROGRAM PLAN

In the Saturn rocket program, the weld quality must be kept consistently high. The research described below was initiated and conducted to determine the contribution of four specifically defined factors associated with aluminum welding materials. The factors chosen were suspected to be correlated with the resultant weld quality of gas-tungsten arc (GTA) welds using 2319 filler metal

6

with 2014-T6 base metal and 4043 filler metal with 2219-T6 base metal. The factors chosen were labelled (1) chemical content, (2) internal impurity content, (3) internal hydrogen content, and (4) external impurities. Table 1 shows the specified compositions for the materials studied. The factor of chemical content was defined as the intentionally added metallic alloying elements for which a composition range is specified. The factor of internal impurities was defined as the residual metallic elements present in the weld for which only a maximum composition level is specified. Internal impurities never described non-metallic materials such as dross. The factor of internal hydrogen content was defined as the internal hydrogen content of the welding material prior to welding and as measured by vacuum-fusion analysis. The factor of external impurities was defined as impurities in the welding-arc shielding gas. The impurity addition was made by adding water to the shielding gas to obtain a preset dewpoint. Two levels of each factor were studied in the program. The high level of the chemical content and internal impurities was close to the maximum allowable in Table 1. The low level of these two factors was close to the minimum allowable (chemical content) or was present only in trace amounts (internal impurities).

MATERIALS

The materials used in the program were both experimentally prepared and commercial 1/4- and 3/4-inch-thick 2219-T87 and 2014-T6 base plate. The filler wire, which was used only in the latter half of the program, was experimentally prepared 1/16-inch-diameter X2319 and X4043 filler wire.[*]

----

[*] The prefix "X" will precede alloy numbers for the experimentally prepared materials to distinguish them from the commercial materials used in the program.

TABLE 1. SPECIFIED COMPOSITIONS OF THE ALUMINUM ALLOYS STUDIED[a]

Alloy	Specification Number	Date	Composition, percent by weight										
			Chemical Content					Internal Impurities[b]					
2219	Military Specification MIL-A-8920A (ASG)	5-20-63	Cu 5.8-6.8	Mn 0.20-0.40	Ti 0.02-0.10	V 0.05-0.15	Zr 0.10-0.25	Si 0.20	Fe 0.30	Mg 0.02	Zn 0.10		
2014	Aerospace Material Specification AMS 4014	6-30-64	Cu 3.9-5.0	Mn 0.40-1.2	Si 0.50-1.2	Mg 0.20-0.80		Fe 1.0	Zn 0.25	Ti 0.15	Cr 0.10		
2319	NASA-MSFC Specification M-ME-MPROC-700.1	12-4-62	Cu 5.8-6.8	Mn 0.20-0.40	Ti 0.10-0.20	V 0.05-0.15	Zr 0.10-0.25	Si 0.20	Fe 0.30	Zn 0.10	Mg 0.02	Be 0.0008	
4043	Aerospace Material Specification AMS 4190A	6-15-52	Si 4.5-6.0					Mn 0.05	Cu 0.30	Fe 0.80	Zn 0.10	Mg 0.05	Ti 0.20

(a) Maximum permissible composition of unspecified elements: each 0.05 percent; total 0.15 percent.
(b) Maximum permissible composition.

8

The program studied each of the four factors (chemical content, internal impurity content, internal hydrogen content, and external impurities) at two levels, high and low. Eight of the possible sixteen combinations of the four factors at two levels were selected for study so that statistical analysis of the results could be performed by a one-half fractional factorial analysis. This analysis allows strong conclusions to be quantitatively drawn regarding the effect of the factors on some experimental variable (weld quality in this program). Eight different "types" of each alloy were prepared. Each "type" was cast to produce the desired level for each factor.

MATERIALS PREPARATION

The experimentally prepared materials were melted in a gas-fired furnace. The base-plate ingots and X2319 filler-wire ingots were cast in a massive steel book mold which rotated over a 75 degree arc to minimize turbulence. The X4043 filler-wire ingots were cast in a water-cooled cylindrical mold. All ingots were radiographed to ascertain their soundness. The sound ingots were then topped and surface-milled to remove casting defects. Each ingot was of sufficient size to fabricate all the material needed for a single thickness of a given composition from one ingot.

Base Plate

The base plate was hot-rolled with an average of 12 passes and 4 to 5 reheats. Surface milling at an intermediate stage of rolling removed slight surface cracks. The X2014 base plate was hot-rolled to finished 1/4- and 3/4-inch-thick base plate 36 inches long. The X2219 plate was solution annealed,

water-quenched, and cold-rolled to finished 1/4- and 3/4-inch-thick base plate 36 inches long. The X2219 was heat treated to approximate the T87 temper. The X2014 was heat treated to approximate the T6 temper. All of the fabricated plates were ultrasonically inspected for defects. No defects were found in the X2219 plate; the defects found in the X2014 plate were clearly marked so that weld beads over the defects could be identified.

Filler Wire

The X2319 ingots were cold-rolled to 5/8-inch-diameter rod and then cold swaged to 3/8 inch diameter. The rod was then surface machined to remove any surface defects in the wire. The X4043 ingots were extruded directly from the ingot to 3/8-inch-diameter rod. The rod was drawn to 1/16-inch-diameter filler wire by a commercial welding-wire fabricator using a series of dies and annealing times. Eddy-current techniques were used to inspect the wire prior to level winding on reels. The reels were packed in sealed, evacuated containers and were stored in a low-humidity area until they were opened and immediately used. The wire surface was smooth and was shown in welding tests to have no contamination sufficient to produce observable weld defects.

MATERIALS ANALYSES

The metallic composition of the experimental and commercial welding materials used during the program was determined by spectrographic and wet chemistry methods. Some discrepancy was found between the results reported by two different commercial laboratories even for adjacent specimens from the same material. Since the material composition had only to be at a high or low level,

the discrepancy in analyses did not affect the program results. The experimental materials all had the levels of chemical and internal impurity content specified by the program plan.

Internal Hydrogen Analyses

The internal hydrogen content was determined by vacuum-fusion analysis for a 10-gram base-plate material specimen and a 5-gram sample of filler wire. A standard surface-preparation method was used for each sample so that the analysis could be corrected for the external hydrogen on the sample. This allowed determination of the internal hydrogen content of all but the X2319 and X4043 filler wire. The total hydrogen content only was determined for these alloys. The total hydrogen content was believed to be about 0.5 parts per million (ppm), by weight, higher than the internal hydrogen content. Despite the methods used during casting to control the hydrogen content of the ingot, the resulting internal hydrogen content of the fabricated experimental materials did not correspond to the level specified by the program plan. These results will be discussed later.

WELDING

All of the welding was performed in the horizontal position using the GTA d-c straight-polarity process. The welds were all bead-on-plate both with and without filler-wire addition. The weld bead for each plate was near the center of a plate with a minimum 4-inch width and a standard 36-inch length. The tooling used provided minimum heat sink. The welding was performed in two phases. In Phase I, no filler metal was added to welds on experimental X2219 and X2014 base

plate. In Phase II, experimental X2319 filler wire was added forehand to welds on commercial 2219-T87 base plate. Experimental X4043 filler wire was added to welds on commercial 2014-T6 base plate. Table 2 lists the welding conditions established for each phase. The weld penetration for 1/4-inch plate was nearly complete. Weld penetration on 3/4-inch plate was about 40 percent. Deeper penetration was not possible for the bead-on-plate type welds without encountering severe undercut.

All of the welding parameters were closely regulated and precisely instrumented to eliminate experimental variations due to welding conditions. Although the equipment was capable of completely controlling arc voltage to ± 0.05 volt and arc current to $\pm 0.5\%$ for normal welding conditions, the addition of large amounts of moisture to the shielding gas made the welding arc less stable. In helium with a dewpoint of about 5 F, the arc voltage typically varied ± 0.5 volts and the arc current varied $\pm 2\%$.

The welding was conducted in a controlled-atmosphere chamber which was evacuated to less than 10 microns of mercury pressure and then backfilled with commercial helium gas. The moisture was added to helium to produce a high level of external impurities by evaporating a fixed amount of water in the helium. A dewpoint meter was used to measure the actual moisture in the shielding gas.

All base-plate material was degreased and chemically cleaned in a sodium-hydroxide bath follwed by a nitric-acid bath to remove a dark copper film on the plates. Short, hot water rinses were used. The plates were exposed to air no longer than 1-1/2 hours after cleaning. They were then placed in the chamber and the chamber was evacuated. As many as four identical welds (replications) were made for each of the 8 combinations of factor levels for the four different alloys in two base-plate thicknesses.

12

TABLE 2. WELDING PARAMETERS USED

All welding was d-c straight-polarity,
gas tungsten-arc welding with helium
shielding gas.

Material	Base Plate Thickness, inch	Arc Voltage, volts	Arc Amperage, amperes	Work Travel, inches/minute	Wire Speed, inches/minute
Phase I (No Filler Wire Added)					
X2219-T87	1/4	13.5	140	11.2	--
X2014-T6	1/4	13.5	145	11.2	--
X2219-T87	3/4	13.5	170	11.2	--
X2014-T6	3/4	14.1	220	11.2	--
Phase II (Filler Wire Added)					
2219-T87	1/4	13.5	180	11.2	64
2014-T6	1/4	13.5	180	11.2	64
2219-T87	3/4	13.5	280	11.2	64
2014-T6	3/4	13.5	280	11.2	64

WELD DEFECT ANALYSES

Two methods were used to determine the weld quality. The entire length of all 200 welds made using experimental-welding materials was radiographed. The radiographs all showed the 2T hole in the 2 percent thickness penetrameter at the minimum sensitivity obtained. The radiographic standard used for classifying the radiographs defined five classes for the fine, scattered porosity observed. Because the radiographic method of analysis of weld defects was not sensitive to all of the fine porosity obtained in the program, the results of metallographic analysis were used more during the analysis of the results.

Metallographic Analysis

Over 500 metallographic sections were chosen at random points in each of the 200 welds. Transverse sections of the welds were cut, mounted, polished with a mild oxalic-acid solution in the polishing slurry (etch-polished), and photographed at 20X. Pores were the only weld defects observed in this program. When the negatives were printed, a grid was superimposed across the print. This grid was used for point counting to determine the theoretical volume percent porosity. This was done simply by counting the number of intersections of the grid with pores and then determining the total number of intersections in the weld-fusion zone. The result of dividing the first number by the second and then multiplying the result by 100 yielded the volume percent porosity. Figure 1 illustrates a typical determination of porosity level.
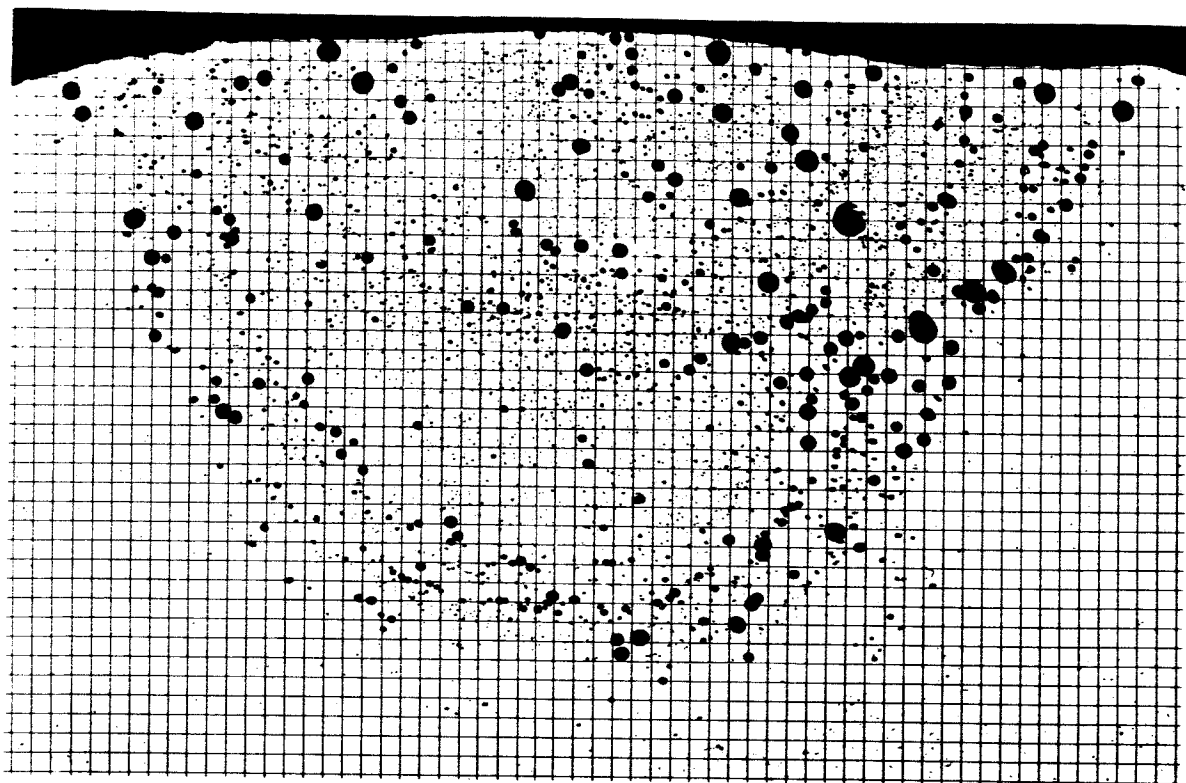
20X   Etch-Polished   RM41742

Area of a fusion zone (measured by polar planimeter) = 13.09 square inches.

Total number of grid intersections in fusion

$$\text{zone} = \frac{100 \text{ grid intersections}}{\text{square inch}} \times 13.09$$

square inches = 1309.

Number of grid intersections coincident with pores in fusion zone (determined by counting) = 288

$$\text{Porosity level} = \frac{\text{coincident intersections}}{\text{total intersections}} \times$$

$$100\% = \frac{288}{1309} \times 100\% = 22.0\%.$$

FIGURE 1. SAMPLE DETERMINATION OF POROSITY LEVEL

PROGRAM RESULTS

A number of interesting observations were made during the program which
are summarized here:

    (1) The dewpoint of the controlled-atmosphere chamber, when backfilled
with uncontaminated helium, was about -60 F. Small, spherical
pores were not observed during welding until the dewpoint was
above -20 F. As the dewpoint increased, the welding arc was less
stable and the weld bead became more rough.

    (2) Regardless of the weld-metal composition, the majority of the welds
made in helium with a -60 F dewpoint (low external impurity level)
contained no porosity. The two exceptions were welds in X2014
base plate. The porosity level for these welds was low and the
results were regarded as anomalous.

    (3) For both the experimental and commercial base plate, pores were
observed to have formed in the base metal beyond the fusion zone
in some of the welds. Figure 2 illustrates that the pores were
formed far beyond the fusion zone and were of a spherical shape.
No satisfactory explanation has been advanced for this phenomenon.

    (4) Welds which were made over plate defects located by ultrasonic
inspection showed no conclusive effect of the defects on the weld
quality or structure.

    (5) Transverse and longitudinal weld sections in both base-plate alloys
revealed macrosegregation in bonds roughly parallel to the fusion
zone boundary. A microhardness traverse revealed a 10 percent
difference in the Knoop Hardness Number for the light and the
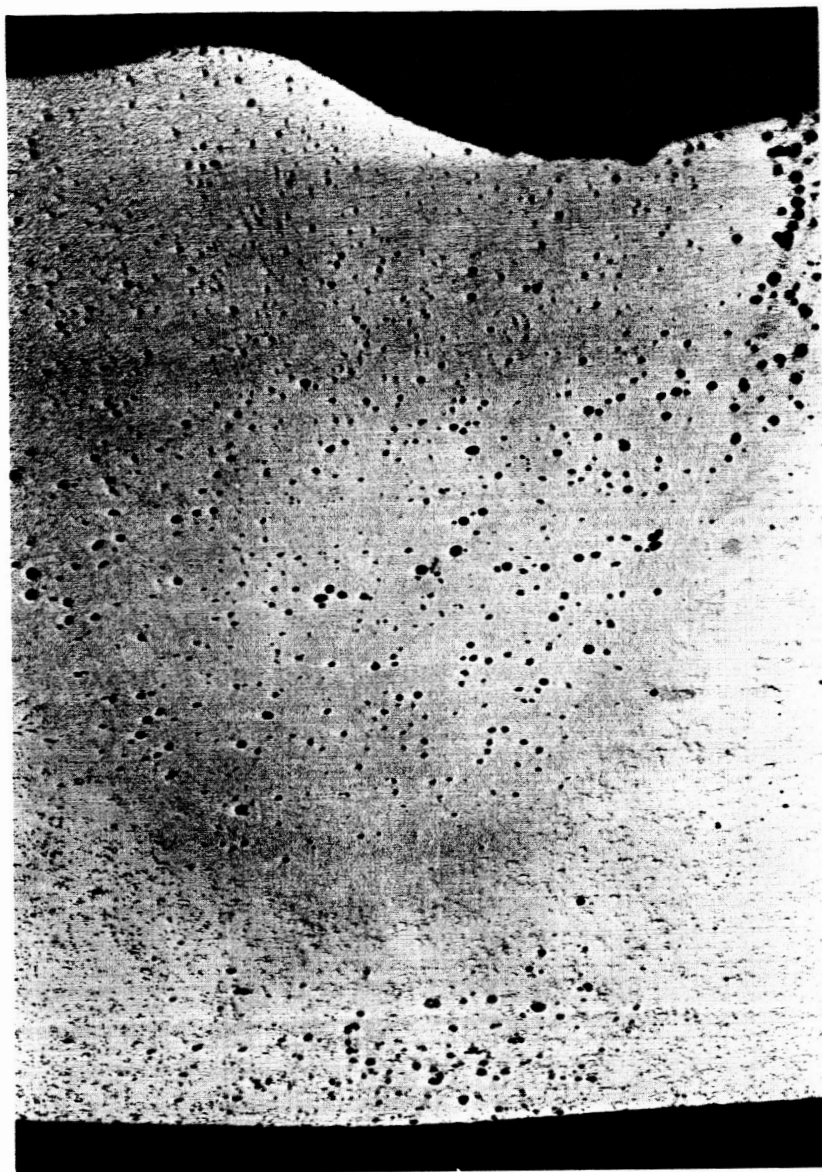
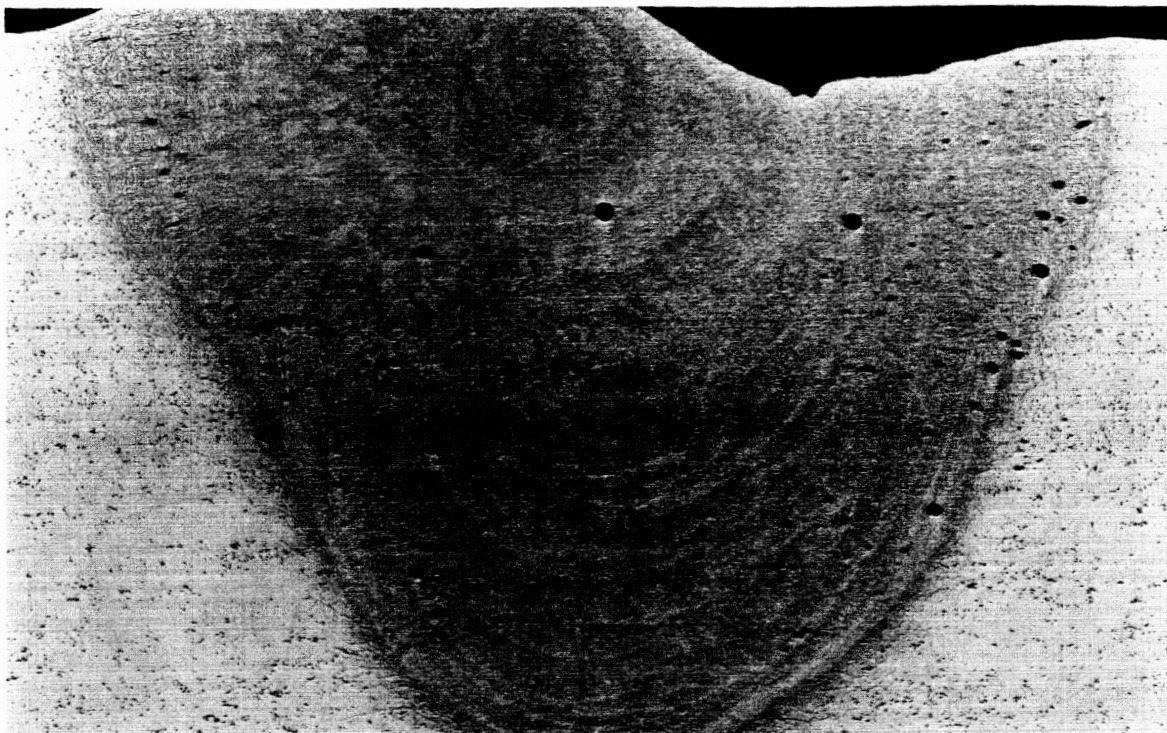20X   Etch Polished   RM40687

FIGURE 2.   PORES OCCURRING OUTSIDE FUSION ZONE IN X2219

High chemical content, low internal impurities,
0.1-ppm hydrogen content.

dark bands. The hardness variation indicated a definite segregation of solute elements in the weld. Figure 3a illustrates this banding in a transverse X2219 weld section. Pores were also found to occur in bands similar to the macrosegregation bands. Figure 3b illustrates pore banding in X2014 alloy similar to solute macrosegregation in X2219 alloy. Figure 4 shows a similar correspondence of pores to the macrosegregation bands found in the longitudinal weld sections. The appearance of the segregation bands in the longitudinal sections was changed by variations of material compositions.

(6) A relationship was observed between the internal hydrogen content of the fabricated X2219 and X2014 base plate. As the chemical content and the internal impurity content increased from the low level to the high level, the internal hydrogen content of the material increased with no dependence on the hydrogen control methods used during casting. Figure 5 illustrates this statistically significant relationship. The single deviation from this relationship was for a composition of 3/4-inch-thick X2014 base plate which had been stirred frequently during melting with a moistened graphite rod to attain a high hydrogen content. Less severe methods were used to control the hydrogen content of the remaining materials. Variations in the chlorination times and the introduction of hydrogen over the surface of the melt were used to control the hydrogen content of the other compositions plotted on Figure 5. Thus, the exception to the relationship observed was an exception to the usual casting technique too.
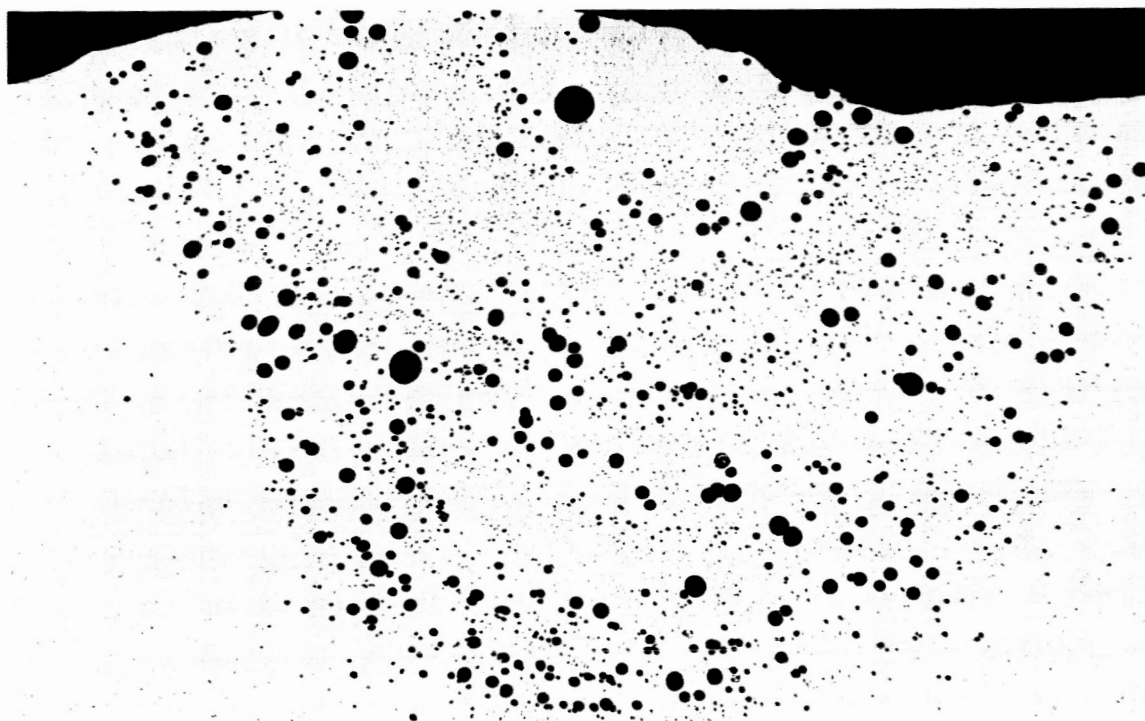
20X Etch-Polished RM40635

a. Segregation and Pores in X2219

20X Etch-Polished RM41743

b. Pores in X2014

FIGURE 3. SIMILARITIES BETWEEN SEGREGATION AND PORE OCCURRENCE IN TRANSVERSE-WELD SECTIONS

Low chemical content and low internal impurity level.
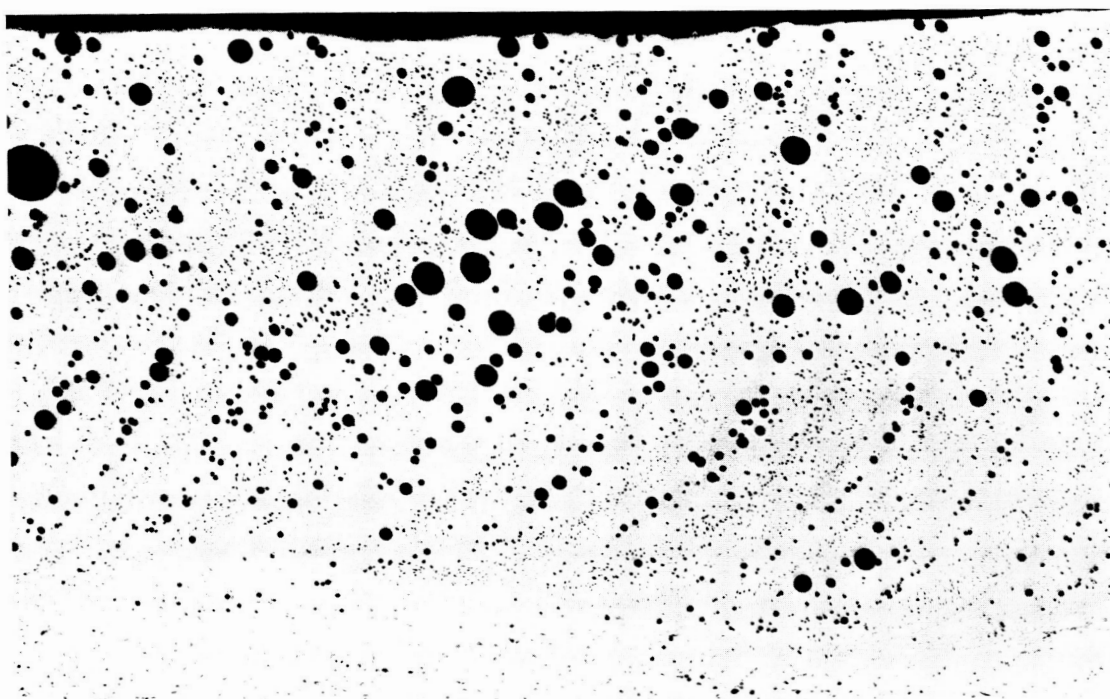
19

20X   5% HF   RM41864

a. Segregation Along High-Chemical-Content and Low-Internal-Impurity Weld

20X   5% HF   RM41860

b. Ordering of Pores Along Low-Chemical-Content and Low-Internal Impurity Weld

FIGURE 4. SIMILARITIES BETWEEN SEGREGATION AND PORE OCCURRENCE IN LONGITUDINAL X2014 WELD SECTIONS

Internal Hydrogen Content, ppm by weight

2.5   2.0   1.5   1.0   0.5   0

Legend:

○ $\frac{1}{4}$-inch-thick X2219
● $\frac{3}{4}$-inch-thick X2219
□ $\frac{1}{4}$-inch-thick X2014
■ $\frac{3}{4}$-inch-thick X2014

Low Chemical Content
Low Internal Impurities
High Chemical Content
Low Internal Impurites

Low Chemical Content
High Internal Impurities
High Chemical Content
High Internal Impurities

26572

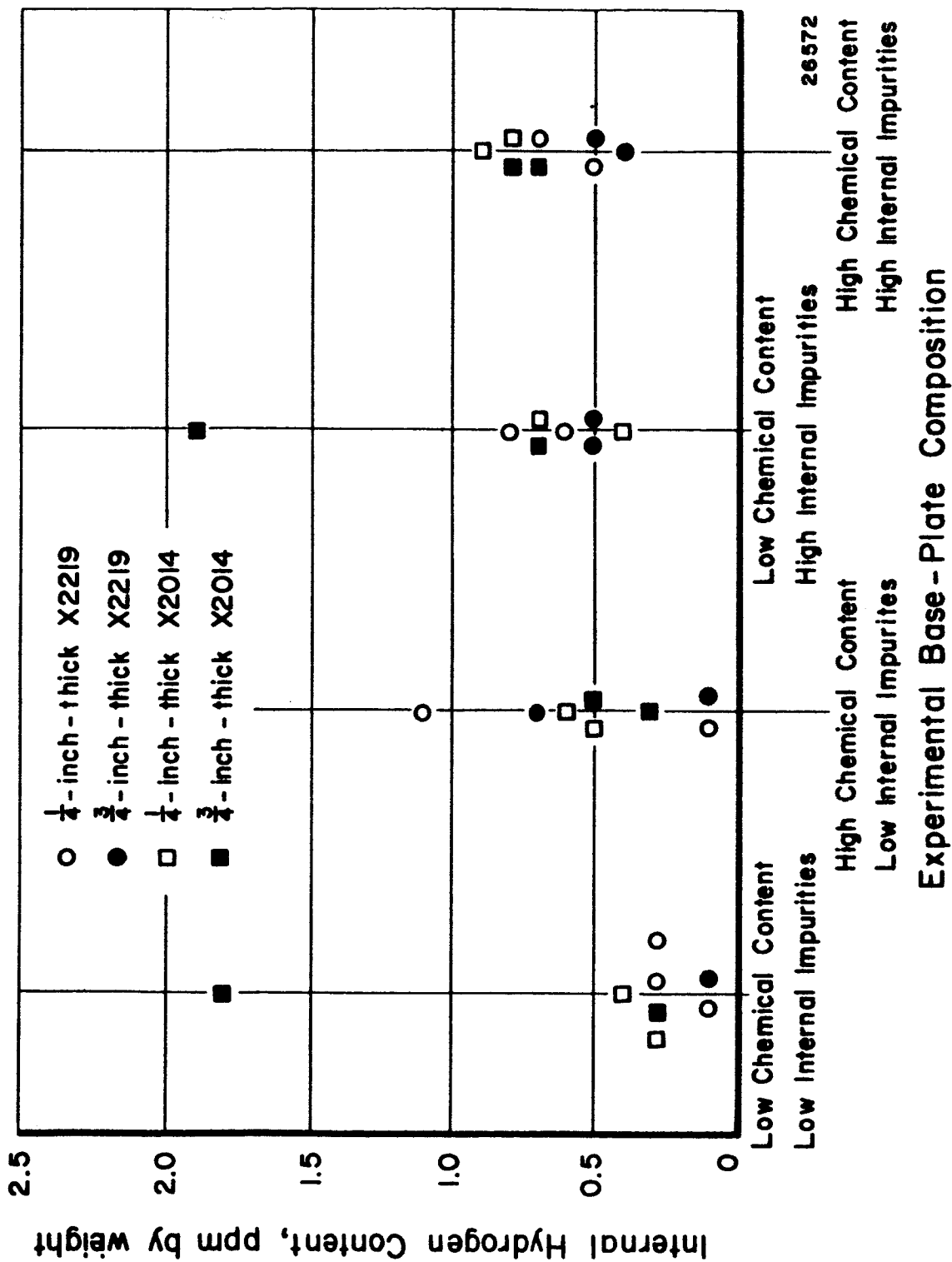Experimental Base-Plate Composition

FIGURE 5. RELATIONSHIP BETWEEN EXPERIMENTAL BASE PLATE
COMPOSITION AND INTERNAL HYDROGEN CONTENT

Hydrogen Content of Base Plate After Fabrication

21

(7) As shown in Figure 6, no relationship existed between filler-wire composition and hydrogen content, such as that observed for the base material. The hydrogen contents for each composition varied about the same median value.

(8) For the welds made with moisture in the arc shielding gas, the porosity level tended to increase as the internal hydrogen content of the experimental base plate increased. Figure 7 shows a typical trend for 1/4-inch-thick X2014. An increase in the internal hydrogen content from 0.4 to 0.8 parts per million (ppm) by weight increased the median porosity level roughly from 5 to 10 percent. There was no relationship between the weld porosity level and the internal hydrogen content of the experimental filler material.

(9) The fact that the factors were not independent of one another (i.e., the relationship of the chemical content and internal impurity content to internal hydrogen content) made the planned fractional factorial analysis impossible. In addition, the fact that almost no defects were observed for low external impurity levels (low moisture content) left less data than might have been obtained for analysis. Accordingly, all welds of experimental filler wire on commercial base plate were made with the external impurity level fixed high so that a base-line porosity level could be introduced. The effect of the other three factors could then be analyzed by the variation of its average porosity level from the base-line level. This procedure supplied a large amount of data for the analysis of the effect of the filler-wire materials.
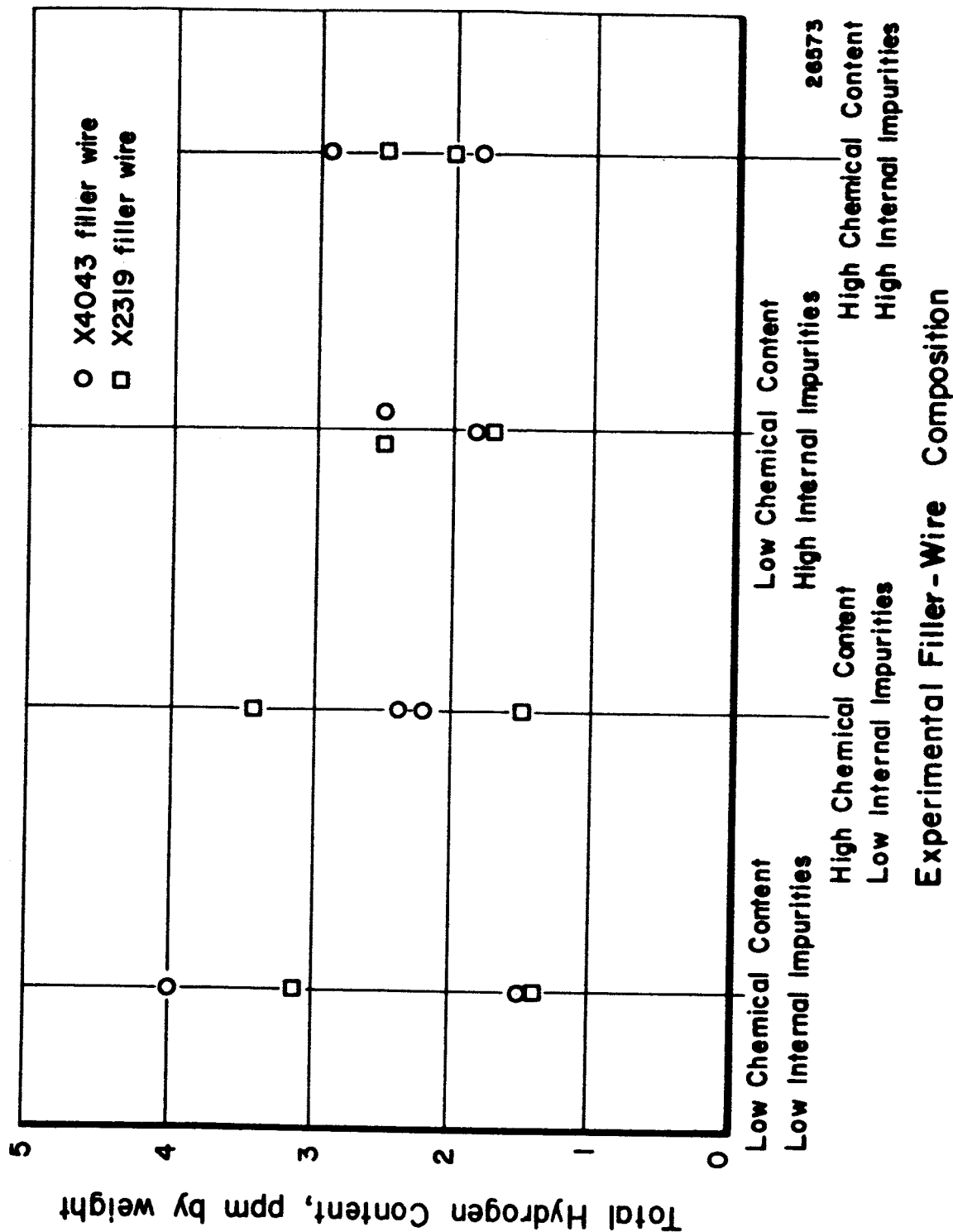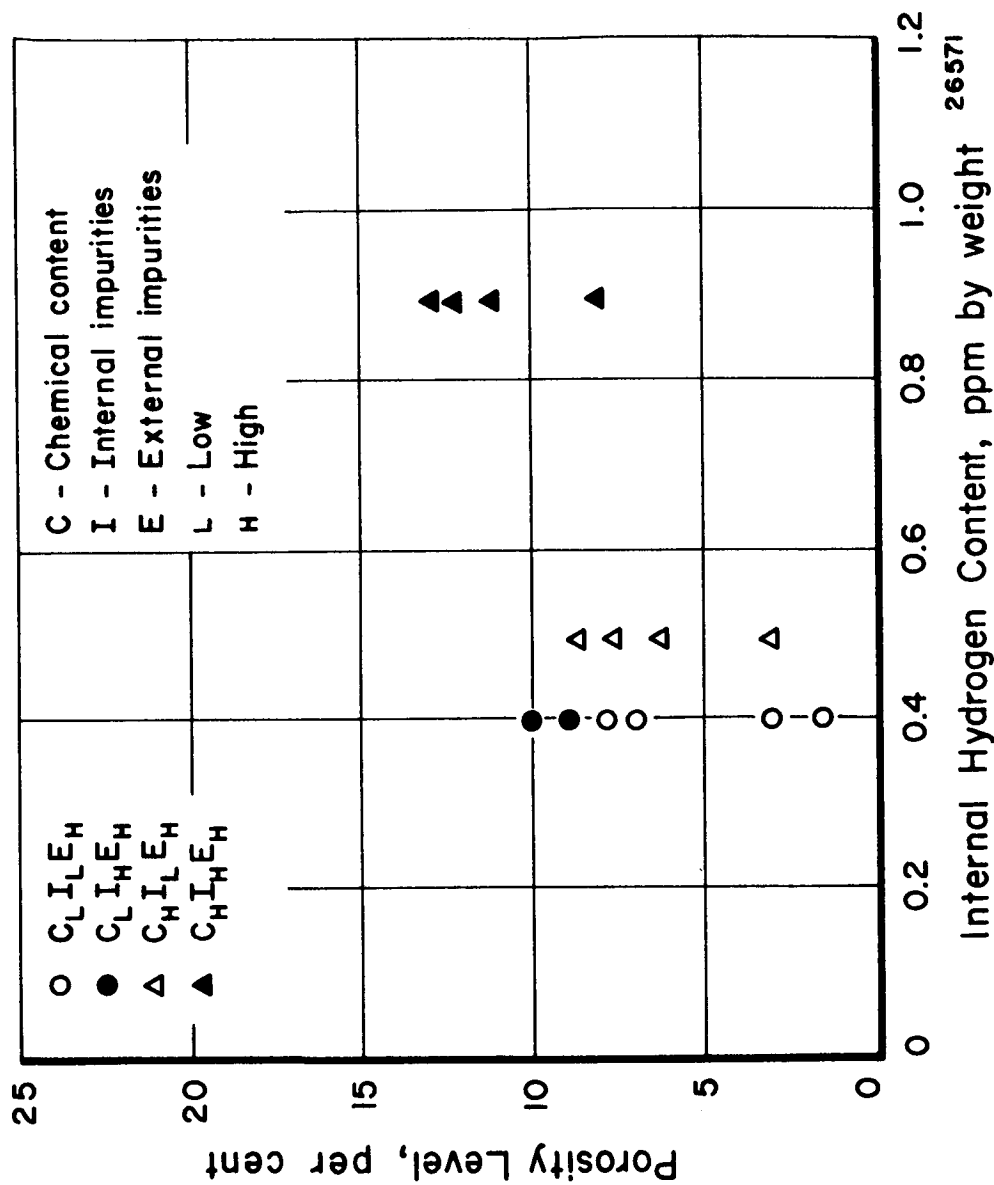
22

FIGURE 6. RELATIONSHIP BETWEEN EXPERIMENTAL FILLER-WIRE COMPOSITION AND TOTAL HYDROGEN CONTENT

Hydrogen Content of 1/16 Inch Diameter Wire after Drawing

FIGURE 7. RELATIONSHIP OF POROSITY LEVEL TO INTERNAL HYDROGEN

For 1/4-inch-thick X2014 Base Plate Welds
Each Plotted Point Denotes the Average Porosity
Level of One Plate.

STATISTICAL ANALYSIS

Because the factors were not independent of one another and the welds made at low external impurities were essentially defect-free, statistical analysis by the planned method was not possible. Sufficient data did exist to permit evaluation of the factors effect on the weld defects (pores). The tests used for the analysis yielded a measure of the significance of the variation of the level of each of the four factors. The degree of certainty for paired comparisons was determined. A degree of certainty under 80 percent is considered not significant. A degree of certainty from 80 to 90 percent is low but should be considered. A degree of certainty from 90 to 95 percent is of interest, but definite conclusions cannot be drawn on the basis of the results. Conclusions based on relationships with a degree of certainty of 95 percent are believed to be sound. Table 3 shows the results of these tests. The material being tested and the thickness of the material or (for experimental filler wire) the base plate it was welded on are listed first. The following column shows the factor(s) for which the significance of a change in level was calculated. The next columns show the levels of the fixed factors and the hydrogen content. The last column shows the degree of certainty. The additional comparisons were made for the filler material when hydrogen content variations of as much as 2.5 ppm, by weight, were not significant in the comparisons made. The additional comparisons therefore assumed that the hydrogen content of two compositions was essentially equal if they varied no more than 0.4 ppm.

TABLE 3. RESULTS OF SIGNIFICANCE TESTS COMPARING COMPOSITIONS

Material	Base Plate Thickness, inch	Factor Tested[a]	Level of Fixed Factors	Hydrogen Content[b], ppm by weight		Statistical Degree of Certainty, percent
				Composition A	Composition B	
X2219	1/4	I and G	C_H	0.1	0.7	98.2
X2219	3/4	C	I_H, E_H, G	0.5	0.5	99.8
X2219	3/4	C	I_L, E_H, G	0.1	0.1	81
X2014	1/4	I	C_L, E_H, G	0.4	0.4	95
X2014	1/4	E	C_H, I_L, G	0.6	0.5	93
X2014	1/4	E	C_H, I_H, G	0.8	0.9	99.9
X2014	3/4	E	C_H, I_H, G	0.7	0.8	>99.9
X2319	1/4	C	I_L, E_H, G	1.4	1.5	Not significant
X2319	1/4	C	I_H, E_H, G	2.5	2.5	83
X2319	1/4	C and I	E_H, G	1.5	1.7	93.5
X2319	1/4	G	C_L, I_L, E_H	1.4	3.1	Not significant
X2319	1/4	G	C_L, I_H, E_H	1.7	2.5	84
X2319	1/4	G	C_H, I_L, E_H	3.4	1.5	85
X2319	1/4	G	C_H, I_H, E_H	2.5	2.0	Not significant
X2319	3/4	C	I_L, E_H, G	1.4	1.5	Not significant
X2319	3/4	C	I_H, E_H, G	2.5	2.5	Not significant
X2319	3/4	C and I	E_H, G	1.5	1.7	90.5
X2319	3/4	G	C_L, I_L, E_H	1.4	3.1	Not significant
X2319	3/4	G	C_L, I_H, E_H	1.7	2.5	81
X2319	3/4	G	C_H, I_L, E_H	3.4	1.5	Not significant
X2319	3/4	G	C_H, I_H, E_H	2.5	2.0	Not significant
X4043	1/4	C	I_H, E_H, G	1.8	1.8	Not significant
X4043	1/4	C and I	E_H, G	2.5	2.4	Not significant
X4043	1/4	G	C_L, I_L, E_H	1.5	4.0	Not significant
X4043	1/4	G	C_L, I_H, E_H	1.8	2.5	89
X4043	1/4	Error	C_H, I_L, E_H, G	2.4	2.2	Not significant
X4043	1/4	G	C_H, I_H, E_H	1.8	2.9	97.1
X4043	3/4	C	I_H, E_H, G	1.8	1.8	91
X4043	3/4	C and I	E_H, G	2.5	2.4	Not significant
X4043	3/4	G	C_L, I_L, E_H	1.5	4.0	Not significant
X4043	3/4	G	C_L, I_L, E_H	1.8	2.5	Not significant
X4043	3/4	Error	C_H, I_L, E_H, G	2.4	2.2	Not significant
X4043	3/4	G	C_H, I_H, E_H	1.8	2.9	Not significant

Additional Comparisons[c]

Material	Base Plate Thickness, inch	Factor Tested[a]	Level of Fixed Factors	Composition A	Composition B	Statistical Degree of Certainty, percent
X2319	1/4	I	C_L, E_H, G	1.4	1.7	77
X2319	1/4	C	I_H, E_H, G	3.1	3.4	97.8
X2319	1/4	C	I_H, E_H, G	1.7	2.0	93.5
X2319	3/4	I	C_L, E_H, G	1.4	1.7	85
X2319	3/4	C	I_H, E_H, G	3.1	3.4	98.7
X2319	3/4	C	I_H, E_H, G	1.7	2.0	Not significant
X4043	1/4	I	C_L, E_H, G	1.5	1.8	87.5
X4043	1/4	C and I	E_H, G	1.5	1.8	91
X4043	1/4	I	C_H, E_H, G	1.8	2.2	91
X4043	3/4	I	C_L, E_H, G	1.5	1.8	Not significant
X4043	3/4	C and I	E_H, G	1.5	1.8	93
X4043	3/4	I	C_H, E_H, G	1.8	2.2	Not significant

(a) C – chemical content, I – internal impurities, G – hydrogen content, E – external impurities, L – low, H – high.
(b) G assumed to be constant if the hydrogen content difference was 0.1 ppm unless noted.
(c) Based on the previous comparisons, G was assumed to be constant for the additional comparisons if the hydrogen content difference was 0.4 ppm.

DISCUSSION OF RESULTS

Tables 4 and 5 list the compositions for each alloy and base-plate thickness studied in the program which resulted in the highest or the lowest weld porosity level for a high level of external impurities (shielding gas dewpoint). Table 4 shows that all of the experimental base-plate and filler-metal compositions associated with the highest weld porosity level had a high chemical content level with one exception. The exception was the 3/4-inch-thick X2014 composition which had been stirred with a moist graphite rod during the melting prior to casting. This was also the highest hydrogen content X2014 composition welded at a high level of external impurities. The base plate associated with high porosity levels also had a high level of internal impurities with an exception again in the case of 3/4-inch-thick X2014 base plate. The levels of the hydrogen content of the base-plate compositions in Table 4 were all high, but this could be expected from the observed relationship of high chemical content and high internal impurities to a high hydrogen content. The X2014 and the X2219 could be expected to have somewhat the same relationship between composition and weld porosity level since both were essentially copper-aluminum alloys. However, the filler metals were two different aluminum alloys and would be expected to show dissimilar behavior. The X4043 filler wire was essentially an aluminum-silicon alloy while X2319 filler wire was an aluminum-copper alloy. Table 4 also showed that X2319 filler wire with low internal impurities was associated with the highest weld porosity level. The X4043 filler wire showed no such definite relationship. Both filler-wire alloys listed in Table 4 showed no correlation between their hydrogen content and the resultant porosity level.

Table 5 shows the experimental-material composition for each alloy and base-plate thickness studied that was associated with the lowest weld porosity level at a high level of external impurities.

TABLE 4. COMPOSITIONS WITH HIGHEST CONSISTENT POROSITY LEVELS

| Material | Base Plate Thickness, inch | Composition | | Hydrogen Content, ppm |
		Chemical Content	Internal Impurities	
X2219	1/4	High	High	0.7
X2219	3/4	High	High	0.5
X2014	1/4	High	High	0.9
X2014	3/4	Low	Low	1.8
X2319	1/4	High	Low	3.4
X2319	3/4	High	Low	1.5
X4043	1/4	High	High	1.8
X4043	3/4	High	Low	2.4

TABLE 5. COMPOSITIONS WITH LOWEST CONSISTENT POROSITY LEVELS

| Material | Base Plate Thickness, inch | Composition | | Hydrogen Content, ppm |
		Chemical Content	Internal Impurities	
X2219	1/4	High	Low	0.1
X2219	3/4	High	Low	0.1
X2014	1/4	Low	Low	0.4
X2014	3/4	High	Low	0.3
X2319	1/4	Low	High	1.7
X2319	3/4	Low	High	1.7
X4043	1/4	High	High	2.9
X4043	3/4	Low	Low	1.5

Of the base-plate materials associated with low porosity levels, the majority had a high chemical content and all had a low level of internal impurities. The hydrogen content of these base-metal compositions was low despite the influence of the composition on hydrogen content. The X2319 filler wire associated with low porosity levels had a low chemical content and high internal impurity content, exactly the opposite of the compositions of X2319 wire in Table 4. The hydrogen content values were not significantly low or high. No general trends could be determined between the X4043 filler-wire composition and the resultant porosity level.

External Impurities

As shown in Table 3, the level of the external impurities was more significantly related to weld porosity than any of the three remaining factors. When the external impurity level was low, all but a few anomalous welds showed no porosity at 20X enlargement. Moisture can readily be introduced into the arc in amounts sufficient to cause porosity either by incomplete shielding, contamination of the shielding gas flow, or by contamination of the welding materials. This program has reaffirmed the necessity of preventing moisture in the welding arc when high-quality welds are desired.

Chemical Content

The level of the chemical content of the experimental materials was, in general, the second most significant factor related to weld porosity. For X2319 filler wire, a change from high chemical content to low decreased the weld porosity level quite demonstrably. For the X2219 and X2014 base plate and the X2319 filler wire, an interaction appeared to occur between the level of chemical

content and internal impurities. For the X2219 base plate a change in the chemical content level was not significant when the internal impurity level was low and the hydrogen content was 0.1 ppm. When the internal impurity level was high and the hydrogen content was 0.5 ppm, an increase in the chemical content level very significantly increased the porosity level of the weld. The effect of the hydrogen content upon these observations was complicated by the observed relationship between chemical content, internal impurities, and hydrogen content.

Internal Impurities

In general, a change in the internal impurities from low to high was associated with increasing porosity levels. However, the significance of the internal impurity level seemed somewhat less than that of the chemical content level. The results for X2319 filler metal, however, indicated that a high level of internal impurities was associated with a low weld porosity level. As noted above, internal impurities were thought to interact with the chemical content level. In many cases, it was felt that the level of the chemical content determined the significance of the internal impurity level.

Hydrogen Content

For the ranges of hydrogen content studied, the level of the hydrogen content had significance in only one situation. This was the 3/4-inch-thick X2014 base-plate composition which had been stirred with a moistened graphite rod during melting prior to casting. The resultant high hydrogen content of 1.9 ppm (more than 2 times the highest hydrogen content found for commercial 2014 used in the program) resulted in a low chemical content, low internal impurity composition becoming the composition with the highest weld porosity

level. The other base-plate compositions with the highest porosity all had high levels of chemical content and internal impurities. However, changes in the internal hydrogen content of the filler wire of as much as 2.5 ppm had little or no significant effect on weld porosity. For 1/2 inch X4043, a decrease in hydrogen content increased the porosity level with a 97.1 percent degree of certainty to produce an anomalous result. All other tests of the hydrogen content levels showed no significance to changes in the levels.

Implications

The results of this program show that, for the experimental materials studied, the composition can change the severity of weld porosity. However, factors external to the welding materials such as surface contamination and shielding gas contamination are more important because they produce porosity more readily. In general, it would appear that weld quality would be increased somewhat if welding materials contained low levels of each composition factor. Welds made with materials with low levels of chemical content, internal impurities, and internal hydrogen content would be less sensitive to arc and welding-material composition variations. These less sensitive materials would develop less volume percent porosity than other welding-material compositions if occasionally exposed to poor shielding conditions.

Macrosegregation

The macrosegregation observed in these aluminum alloys has been reported previously by Gurev and Stout[1] and by Makara and Rossoshinskii[2] for steel. The latter, in reviewing Russian literature regarding this macrosegregation, related the bands to the ripple marks found on the surface of welds. He suggested

31

that these were formed by the periodic growth of solid metal in welding. This periodicity is thought to be due to the latent heat of fusion of the solidifying metal building up to a point where growth of the solid actually stops or is reversed, melting some of the solidified metal. The periodicity presumably allows diffusion of active elements out of the solid nearest the solid-liquid interface to the liquid.

CONCLUSIONS

The following conclusions were drawn from this work:

(1) Generally, for the four factors studied, changes in the level of the external impurities (shielding gas dewpoint) were most significantly related to the resultant weld porosity. The chemical content level was much less significant than the external impurity level, but it still was more significant than the remaining two factors. An interaction between the chemical content and internal impurity level caused the significance of the relation between the level of internal impurities and the resultant porosity to be dependent upon the level of the chemical content. For the ranges studied, the relation of hydrogen content level of the filler wire to weld porosity was the least significant relationship. In one case for the experimental base plate, the hydrogen content was a more significant factor than chemical content or internal impurities. In general, increasing porosity occurred as each factor level was changed from low to high.

(2) For the experimental base plate, the porosity of the bead-on-plate welds with no filler wire addition increased as the hydrogen content of the base plate increased. For the experimental filler wire, increasing hydrogen content of the filler wire was not related to increased weld porosity levels.

(3) A relationship was found to exist between the composition of the fabricated experimental base plate and the internal hydrogen content. Despite the use of methods during melting and casting to achieve two levels of hydrogen content for each composition, the hydrogen content significantly increased as the base-plate composition was changed from a low level of chemical content and a low level of internal impurities to a high level of these two factors.

(4) Macrosegregation bands were observed in aluminum welds which were created during the weld solidification. Porosity occurrence in welds was related to the bands of segregation. The shape of the bands was dependent on the weld-metal composition.

ACKNOWLEDGEMENTS

FUTURE RESEARCH

Additional research is being planned to test the conclusions for the experimental materials with the results for the welding of commercial materials. A large number of commercial-material compositions will be located, welded, and analyzed with the methods reported here. In addition, an evaluation of the use of a radioactive hydrogen isotope, tritium, will be made. The studies will attempt to use this tracer to locate preferential occurrence of hydrogen in welded materials. The results of this additional work will test the applicability of the program conclusions to the welding of commercial alloys and will result in a further understanding of the problems encountered in welding of the alloys studied.

REFERENCES

1. Gurev, H. S., and Stout, R. D., "Solidification Phenomena in Inert Gas Metal-Arc Welds", Welding Journal Research Supplement, Vol. 42, No. 7, pp 298-s to 310-s (July, 1963).

2. Makara, A. M. and Rossoshinskii, A. A., "Segregation in Fusion Zone and in Solidification Layers as Related to the Diffusion Between Solid and Liquid Phases in the Freezing of Welds", Automatic Welding, Vol. 9, No. 6, pp 65-76 (1956) (Henry Brutcher Translation No. 3991).

SECTION II

PROGRESS REPORT

ON

STUDY OF THE MECHANISM OF POROSITY FORMATION IN WELDS

CONTRACT NAS 8-11332

PRESENTED TO

ALUMINUM WELD DEVELOPMENT COMPLEX CONFERENCE

MARSHALL SPACE FLIGHT CENTER

January 19, 1966

BY

D. D. POLLOCK
AND
W. V. MIXON

DOUGLAS AIRCRAFT CO., INC.
SANTA MONICA, CALIFORNIA

INTRODUCTION

This work represents an attempt to explain the mechanisms responsible for porosity in aluminum welds in terms of metallurgical phenomena as well as welding parameters. Hydrogen is considered to be largely responsible for this problem.[1] The kinetics of this behavior are not well known. Thus, the major emphasis is being directed toward an attempt to determine the way in which porosity forms and grows.

The program is divided into two phases. The first phase considers porosity effects in static fusion welds; the second phase considers the same variables in bead-on-plate welds. Both phases employ 2219-T87 and 2014-T6 materials.

THEORETICAL BACKGROUND

Consider a molten metal, or alloy, of a given initial composition which is exposed to a gas under equilibrium conditions. This assumes that the temperature of the liquid-gas system and the composition and pressure of the gas will remain constant. The composition of the gas is considered to be constant because the vapor pressure of most liquid metals is small near the melting point. Under these conditions, some of the gas will be absorbed by the liquid metal. The amount of such absorption is a function of the partial pressure of the gas. Another way of expressing this is: the amount of gas absorbed by the liquid metal will depend upon the quantity of that gas in contact with the liquid metal. This will be a constant for any given set of "equilibrium" conditions.

If the equilibrium conditions change, the amount of gas dissolved by the liquid will change. If the composition and pressure of the gas are held constant and the temperature is increased, the amount of dissolved gas will usually increase. If the temperature is decreased, the quantity of

PRECEDING PAGE BLANK NOT FILMED.

dissolved gas will also decrease. Thus, for most liquid metals, as the temperature of the melt decreases, the amount of gas which the liquid can contain in solution decreases sharply. That portion of the gas which the liquid metal cannot retain is rejected from the melt as the familiar porosity seen in castings and welds.

The question is how does such rejection of gas from the melt occur? The most convenient way of understanding this behavior is based upon thermodynamics and provides a probability of whether or not the reaction will occur. The thermodynamic measure of this behavior is called the change in free energy of the system (ΔF). It, however, does not provide information as to the rate of the reaction.

Under the equilibrium conditions previously noted, the quantity of gas in solution in the liquid metal was constant; in this case $\Delta F = 0$ and no change will occur. When the temperature of the melt is decreased, ΔF will be negative and a decrease in the solubility of the gas is expected. Conversely, when the melt temperature is raised, no gas rejection will occur; actually, more gas will be dissolved. Under these conditions, ΔF will be positive. Thus, the sign of ΔF indicates whether a reaction will or will not occur.

In order to employ this concept for evaluating porosity formation something must be known about the behavior of a molten liquid which contains gas atoms in solution. A convenient picture of this consists of an assembly of metal atoms and some gas atoms which are in rapid, random motion. In this state several gas atoms will occasionally encounter each other. They may remain together, or they may separate. If the conditions are proper, they remain together and little clusters of gas atoms will persist and

42

grow in the melt. These are known as gas nuclei and are assumed to be tiny spheres. Changes in the pressure and composition of the gas and the temperature of the melt can cause these nuclei to grow or to disperse.

For a given set of conditions the formation or dissolution of nuclei can be predicted by the sign of ΔF. The temperature, pressure and composition of the gas over the melt and an approximation of the smallest size of a stable nucleus must be considered for this prediction. When the other variables are maintained at a constant level, the size of the smallest stable nuclei can be used to predict the sign of ΔF.

This approach readily provides an approximation for ΔF; ΔF is found to vary inversely as the square of the radius of the nucleus. This information permits an approximation of the nucleation rate. This is also found to vary inversely as the square of the radius of the nucleating particle. Unfortunately, the radius of the nucleus cannot be measured directly during the welding cycle.

One way of circumventing this problem is to utilize the time-temperature cycle that the weld undergoes during solidification. This will provide a measure of nucleus size.

Since the aluminum alloys under consideration here are representative of eutectic systems (which show a pronounced thermal arrest upon solidification), their thermal arrests may be used as an "anchor point" upon which to base the subsequent calculations. For a given heat input per unit volume of metal and relatively constant cooling conditions, the temperature of this thermal arrest will occur at a nearly constant temperature. This fact is useful in simplifying the expressions for approximating

43

the rate at which these nuclei form. It is also important to note that most of the porosity formation will have been completed by the time that this temperature is reached. Thus, this temperature marks the lower limit of pore formation.

Since heating and cooling rates are very fast and temperatures are difficult to measure, the time to reach the eutectic or "anchor" temperature is used to measure the time available for pore formation. This also gives a readily measurable but indirect approximation of the temperatures and cooling rates that are of interest in welding.

Now, knowing the time for a weld to reach the eutectic temperature and the relationship previously obtained for the nucleation rate, the nucleation rate is found to be approximately inversely proportional to the square of the time required to cool the weldmetal to the eutectic temperature - a more readily useable relationship than one based upon exact temperatures or nuclei sizes.

In a similar way the growth rate of the nuclei can be shown to be approximately directly proportional to the square of the time required for the weld to cool to the eutectic temperature. Other quantities such as the area fraction occupied by pores and the average pore size can also be approximated in this way. The derivations of these relationships are given in the appendix.

In order to make practical use of these relationships the way in which they were derived must be kept in mind. The precise mechanism of nuclei formation is not known on an atomic scale and is considered to be based upon the laws of probability. Further, the theoretical relationships

used in the present work are approximations. The experimental methods used for pore detection and measurement provide average values of those pores which are visible; many pores, particularly those formed just before solidification is completed, are sub-microscopic in size and cannot be included in this analysis because of the practical difficulties of counting and measuring them. In addition, the welds which are being studied here are not true welds in the sense that two pieces of metal are being joined. When these factors are considered in the light of practical applications to real welds, where many additional variables are operative, then it becomes apparent that it is imperative that the general understandings of the formation and growth of porosity be obtained. (The acquisition of extremely detailed relationships would be very difficult to apply to real situations.) Thus, the primary objective of this work is to establish broad relationships regarding the factors affecting the formation of porosity which can be used to understand and minimize this problem in a practical way.

In order to establish these relationships, the variables have been selected so that they include situations encountered in welding practice. The variables being investigated are: the contamination level of the atmosphere, the arc current and voltage, the arc time and the material thickness. Combinations of these five factors are being tested according to a statistical plan given in Table I. This plan will permit the determination of the individual effects of the variables and will also help to indicate if any two-way interactions exist between the variables.

EXPERIMENTAL TECHNIQUES

A schematic diagram of the test apparatus for the static welds is given

45

TABLE 1

PHASE 1 AND 2 BASIC DESIGN
(ALL MATERIAL IS 2219-T87)

Experi- ment No.	Block No.	Arc Atmosphere Contami- nent Level	Arc Cur- rent Level	Arc Volt- age Level	Arc Time or Travel Speed	Material Thick- ness	
1	1	M	M	M	M	L	Center
2		L	L	L	L	L	
3		H	H	H	H	L	
4	2	H	H	H	L	H	
5		L	L	L	H	H	
6		H	H	L	H	H	
7		L	L	H	L	H	
8	3	L	L	H	H	L	
9		H	H	L	L	L	
10	4	M	M	M	M	L	Center
11		H	L	H	H	H	
12	5	L	H	L	L	H	
13		L	H	L	H	L	
14		H	L	H	L	L	
15		L	H	H	L	L	
16	6	H	L	L	H	L	
17		H	L	L	L	H	
18		L	H	H	H	H	
19	7	M	M	M	M	L	Center
20		H	M	M	M	L	
21		L	M	M	M	L	
22		M	H	M	M	L	
23	8	M	L	M	M	L	
24		M	M	H	M	L	
25		M	M	L	M	L	
26		M	M	M	H	L	
27		M	M	M	L	L	

L = Low, M = Medium, H = High

In Figure 1. Two-inch discs are being used for Phase I of the program. The specimens are cleaned with a mixture of nitric and hydrofluoric acid, rinsed in water and dried. They are then cleaned in Freon T-F vapor. The specimens are then stored in the Eringard welding box, Figure 2, where they are kept in either an atmosphere of dry helium or in a vacuum.

Prior to welding, the specimens are briefly removed from the chamber and are drilled to receive the thermocouple wires. They are again degreased in Freon T-F vapor and returned to the chamber. The specimens are kept in the chamber overnight under a vacuum before testing. This procedure is used to minimize surface contamination, particularly moisture, which might influence the experimental results.

The specimen is placed upon the fixture, Figure 3, and the assembly is inserted into the test chamber within the Eringard welding box. A shim, Figure 4, is used to ensure that the desired distance between the top of the specimen and the electrode will be within 0.005 in. The test chamber is sealed and the controlled atmosphere is introduced into it and monitored, Figure 5, until the outlet sampling indicates that the desired atmosphere moisture content has been established. The devices which are used to measure and record welding variables are shown in Figure 6. The prescribed welding cycle is then applied to the specimen. Upon completion of this cycle the atmosphere is again analyzed. At this point, pure dry helium is used to purge the test chamber. This is done to prevent contamination of interior of the Eringard welding box. When the purge is completed, the welded sample is removed for examination. Figure 7 shows a radiograph of a typical specimen.

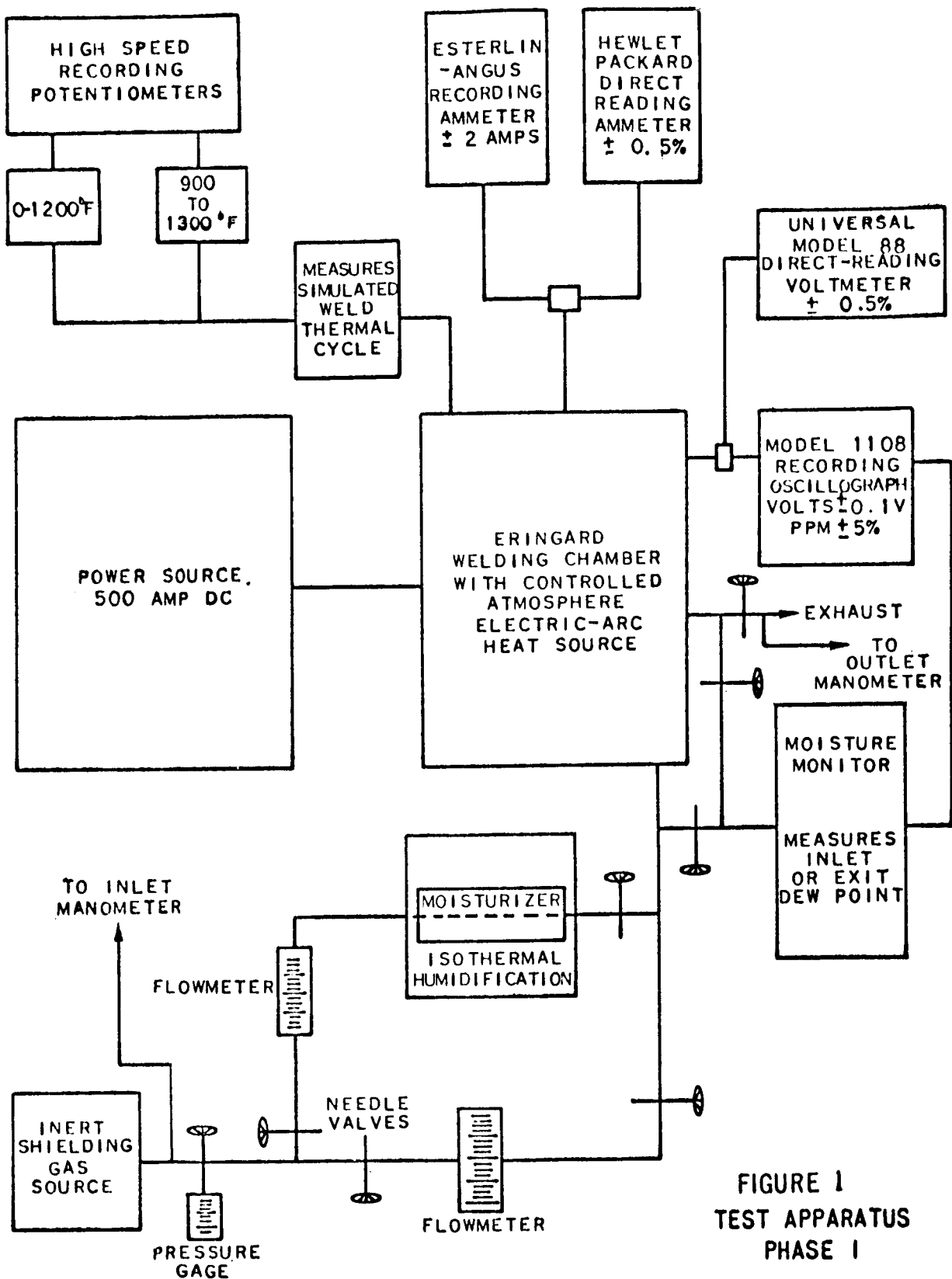After the radiograph is made, a macrophotograph of the top surface is made.
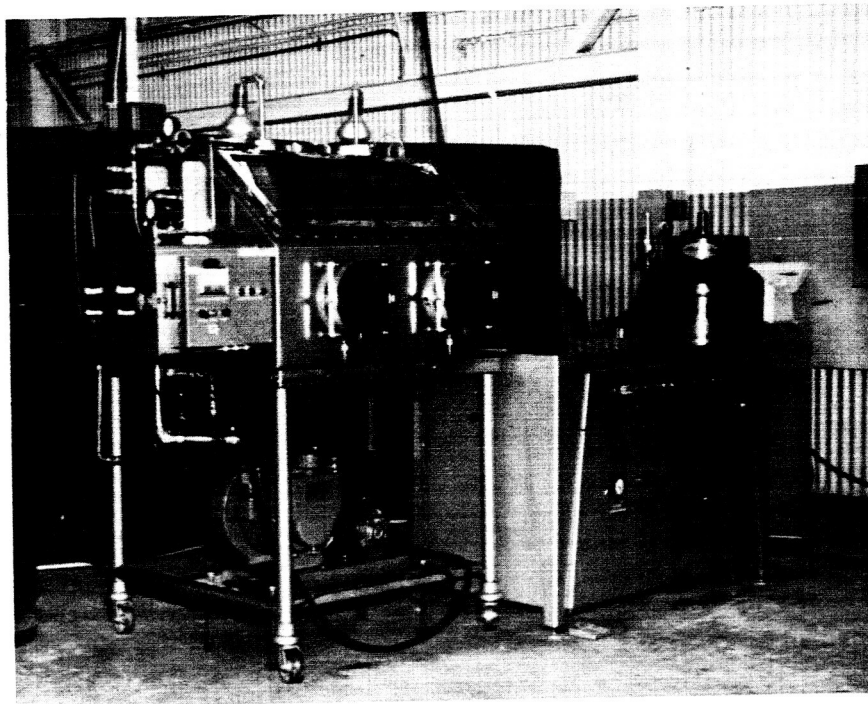
FIGURE 1
TEST APPARATUS
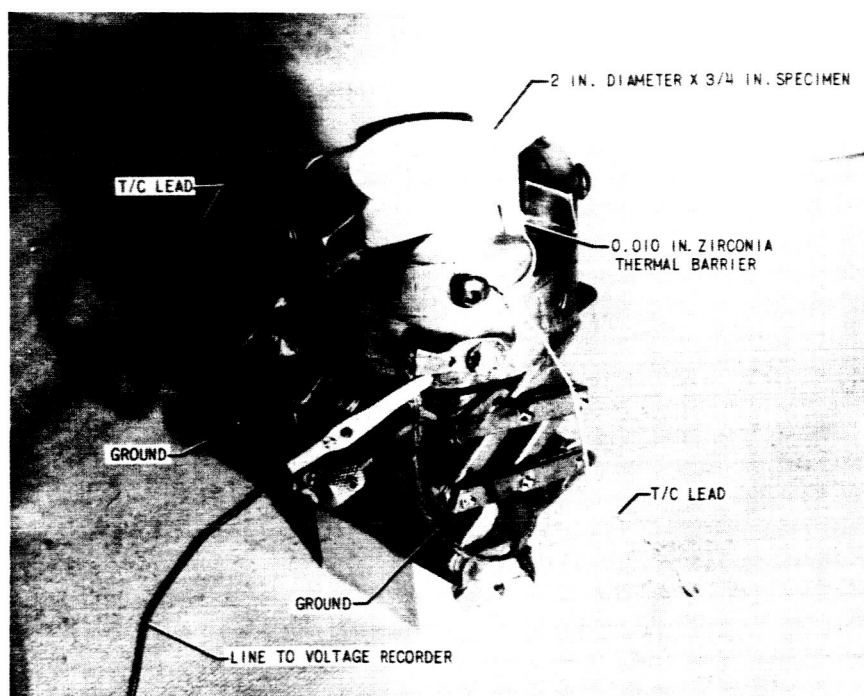PHASE I

FIGURE 2

ERINGARD CHAMBER

2 IN. DIAMETER X 3/4 IN. SPECIMEN

T/C LEAD

0.010 IN. ZIRCONIA
THERMAL BARRIER

GROUND

T/C LEAD

GROUND

LINE TO VOLTAGE RECORDER

FIGURE 3

WELDING FIXTURE WITH SPECIMEN IN PLACE

49

WATER JACKET

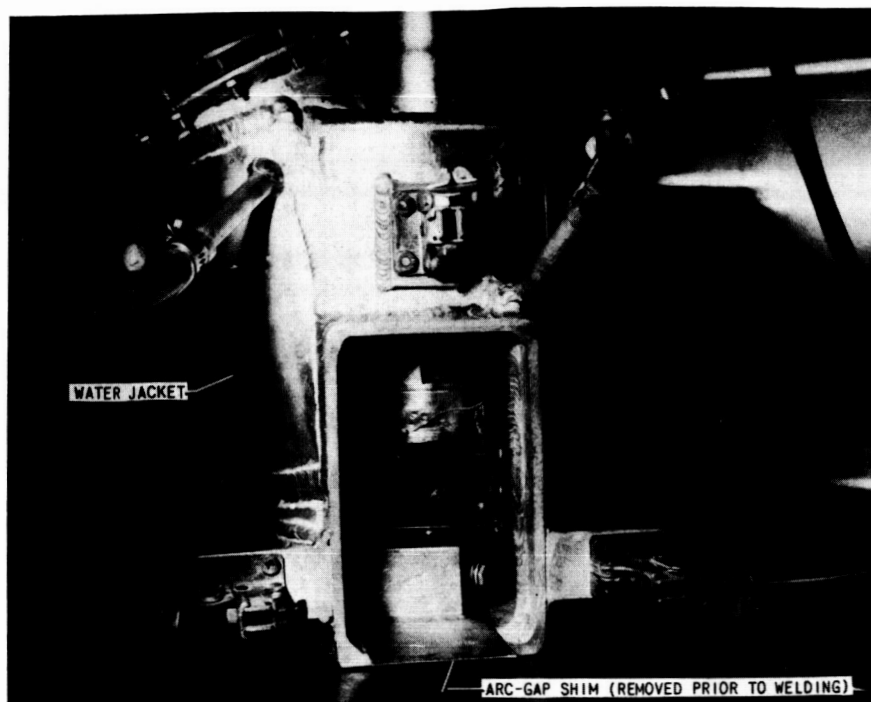ARC-GAP SHIM (REMOVED PRIOR TO WELDING)

FIGURE 4

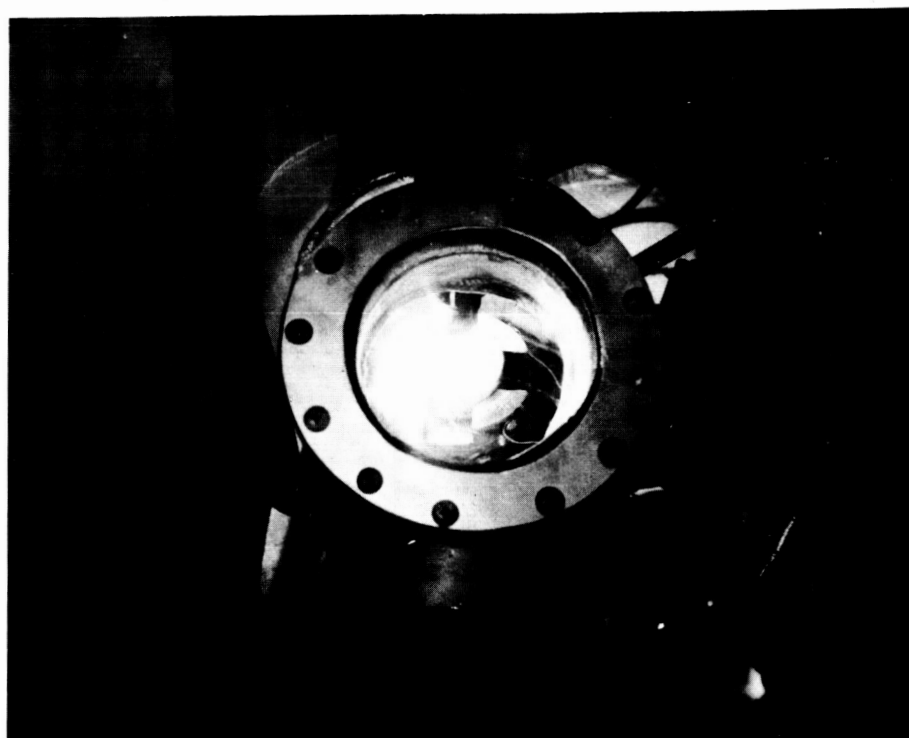FIXTURE IN WELDING CHAMBER WITH SHIM IN PLACE

FIGURE 5

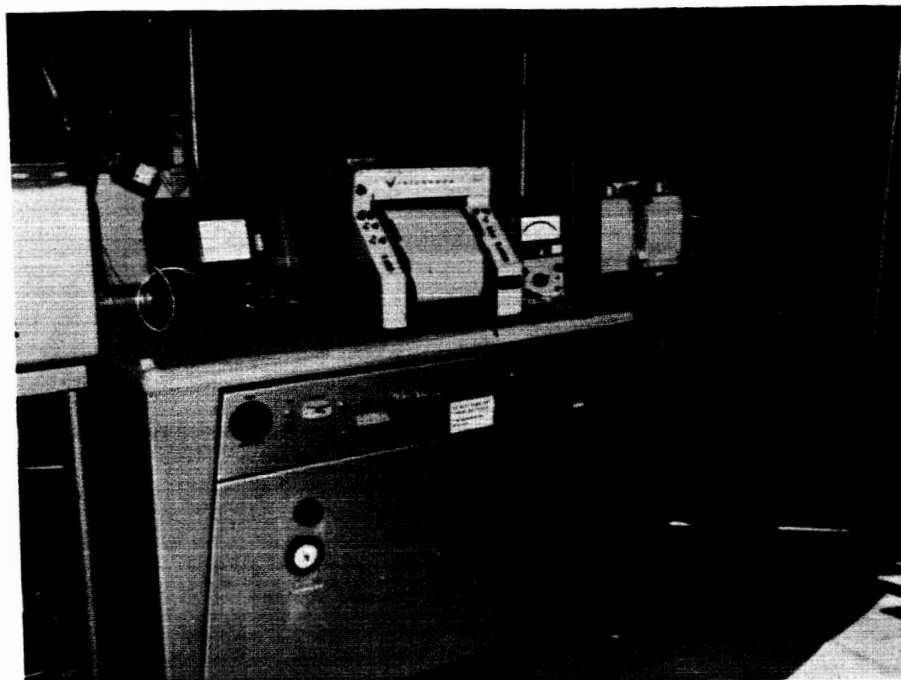FIXTURE INSIDE CHAMBER PRIOR TO WELDING

50

FIGURE 6

DEVICES TO MEASURE AND RECORD WELDING VARIABLES
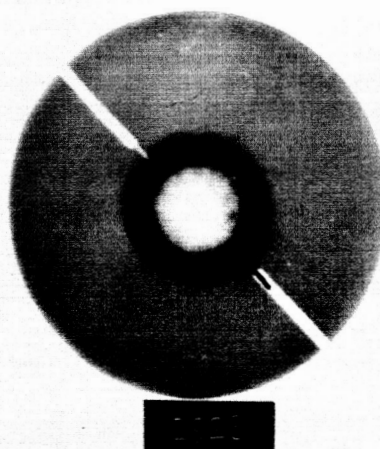

FIGURE 7

RADIOGRAPH OF TYPICAL 1/4-INCH SPECIMEN
SHOWING POROSITY AND LOCATION OF THERMOCOUPLE WIRES

(POSITIVE REPRODUCTION)

51

The specimen is then sectioned to provide a portion of the weld which contains the center and is about 1/8-in. thick. This specimen is polished with 600 grit Al_2O_3, etched with Flick's reagent and repolished with the Al_2O_3 followed by MgO. The polished specimens are used to determine the average pore volume fraction and the average pore diameter.

Sections of a given weld nugget are examined under 20X magnification using a grid area which is about 0.04 x 0.04 inches and contains 144 squares. The number of pores in each grid are counted and the total length of the grid segments which traverse the pores is measured. The total length of the grid lines in each small grid area is also determined. This process is continued until the entire section has been explored, Figure 8. The sums of all the grid segments and grid lines are then determined. These data permit the calculation of the pore volume fraction and the average pore diameter by the method of Guttman and Smith (2). The equations for these calculations are:

$$\text{Pore Volume Fraction} = \frac{La}{L} \qquad (1)$$

$$\text{Average Pore Diameter} = \frac{Lad}{M} \qquad (2)$$

where La is the sum of the grid segments which traverse pores, L is the total length of all of the grid lines, d is the spacing of the grid lines and M is the number of pores.

The pore volume fraction determined in this way was compared to percent porosity as determined by specific gravity measurements. The porosity values based upon equation (1) were approximately 30% higher than those from the gravimetric measurements.
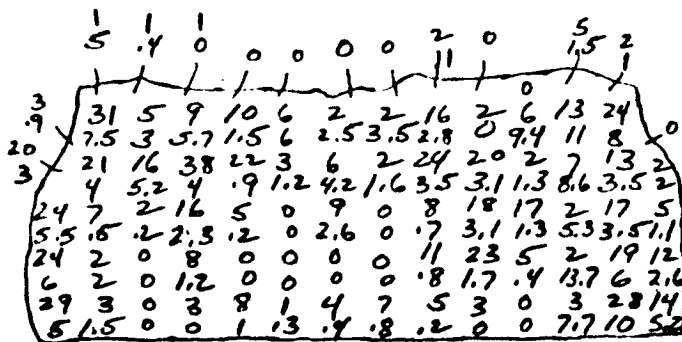
#2973   10-22-65

#8 GRAIN SIZE EYEPIECE, 2.5/0.08 OBJECTIVE
(SILVER)

DIMENSIONS OF 1 MAJOR GRID = $0.0478'' \times 0.0478'' = 22.8 \times 10^{-4} in^2$.

AREA BY OVERLAY:

$$3.00$$
$$.18$$
$$.76$$
$$.20$$
$$\overline{4.34} \; sq.\,in.$$


```
 1  1  1              2   0    5 2
 5 .4  0  0  0  0  0  1 1   1.5 1
3
.9  |31  5  9 10  6  2  2 16  2  6 13 24\
20 |7.5 3 3.7 1.5 6 2.5 3.5 2.8  0 9.4 11  8 | 0
3  |21 16 38 22  3  6  2 24 20  2  7 13 2
   | 4 5.2 4 .9 1.2 4.2 1.6 3.5 3.1 1.3 8.6 3.5 2
24 | 7  2 16  5  0  9  0  8 18 17  2 17 5
5.5 |.5 .2 2.3 .2  0 2.6  0 .7 3.1 1.3 5.3 3.5 1.1
24 | 2  0  8  0  0  0  0 11 23  5  2 19 12
6  | 2  0 1.2  0  0  0  0 .8 1.7 .4 13.7 6 2.6
29 | 3  0  3  8  1  4  7  5  3  0  3 23 14
5 |1.5 0  0  1 .3 .4 .8 .2  0  0 7.7 10 5.2
```

100 65 24 75 45 10 21 11 66 66 30 32 103 33 = 681 = TOTAL NO. OF PORES
20.4 20.5 9.8 13.2 3.6 7.5 9.7 6.9 9 7.9 12.4 47.8 32 10.9 = 209.6 = LINE INTERCEPT

%Porosity by specific gravity = 2.82%

actual area of nugget = $(4.34)\left(\frac{0.0478}{0.250}\right)^2 = (4.34)(0.0365) = .158 \; sq.\,in.$

L, TOTAL LINE LENGTH = $\frac{0.158}{22.8 \times 10^{-4}}$ = 69.5 GRID UNITS

La, TOTAL LINE INTERCEPTED = $(0.0282)(69.5 \; GRID \; UNITS)$
= 1.96 GRID UNITS

$\bar{A} = \pi \bar{r}^2 = \frac{(La)(0.0478)^2}{n} = \frac{(1.96)(0.0478)^2}{681} = 6.56 \times 10^{-6} in^2$

$\bar{r} = 1.446 \times 10^{-3} in. = 0.00145 \; in.$

FIGURE 8

RECORD OF PORE COUNTING AND LINE INTERCEPT COMPUTATION

The planar technique given above is only as good as the degree to which a random plane is representative of the porosity of the sample. The gravimetric method provides a reliable measure of the amount of porosity in the sample but does not give information regarding its size and distribution. A combination of these two methods was used to obtain a more reliable measure of the average pore size. The gravimetrically-determined specific gravity was used in equation (1) to determine the quantity La. This factor was inserted into equation (2) to calculate the average pore diameter. The two largest sources of error in the Guttman and Smith approach are the factors La and M. The use of the gravimetric specific gravity in these calculations minimizes the error in La. The error in the calculations for the average pore diameter is very small and is principally due to that in the determination of the value of M. The factor M is the easiest to determine; its error is smaller than those of the other factors but it still is not representative of all of the sample.

A method for the determination of M which is more representative of the entire sample is now being used. This technique employs the difference in the density between wrought material and a given weld. This permits the calculation of the total volume of porosity in a volume equivalent of one gram of weld metal. The average pore volume, as determined from the combined planar-gravimetric method, is divided into the total pore volume and gives the average number of pores in the volume equivalent of one gram of weldmetal.

The sectioned specimen is radiographed for X-ray density measurements, Figure 9. Such measurements have not been helpful because of the very large amount of very fine porosity. These pores are too fine to permit estimates of pore fraction by X-ray techniques. After this, micrographs are made for the determination of dendrite-cell size (Figure 10).

FIGURE 9

TRANSVERSE RADIOGRAPH OF TYPICAL 1/4-INCH THICK SPECIMEN
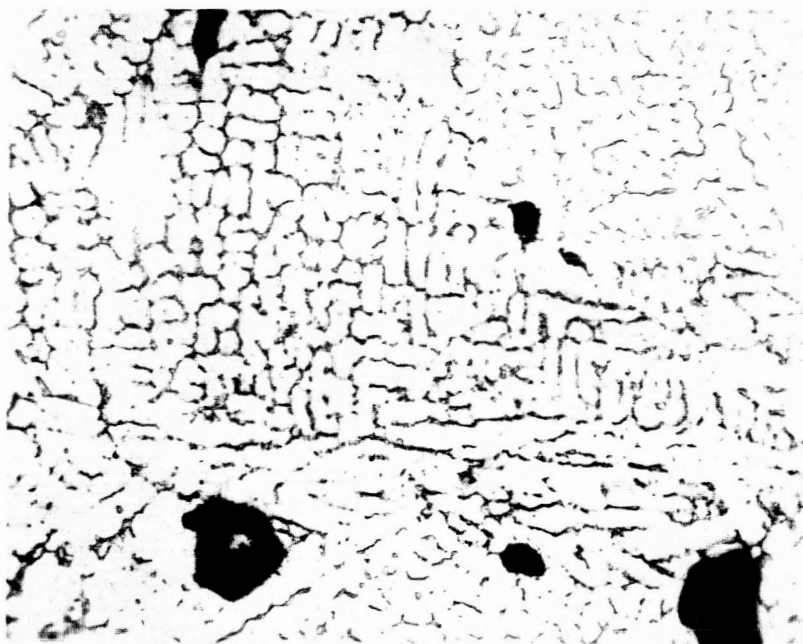
(POSITIVE REPRODUCTION)

FIGURE 10

MICROGRAPH OF TYPICAL DENDRITE CELL STRUCTURE

The nugget is then carefully excised with a jewellers saw and its specific gravity is measured. Following this, the nugget is chemically analyzed for hydrogen content. Selected nuggets are also given complete chemical analyses. Measurements of surface ripples have not been possible to make because these do not appear on the surface of the specimens. These will be measured on the bead-on-plate specimens.

The bead-on-plate specimens, Figure II, are prepared and tested in as nearly the same way as the static fusion weld specimens as is possible. These specimens permit the use of two thermocouples instead of one. They also require a larger test chamber, Figure 12. The only other change is that travel speed is used instead of arc exposure time. The porosity measurements are made on a 1/8-in. section excised one inch away from the thermocouple which showed the clearest thermal arrest.

Present Status of Program

Phase 1

The testing conditions and results of the static fusion welds made on 2219-T87 with moisture contamination are given in Tables 2 and 3. These data were statistically analyzed by means of a Bi-Med 34 routine on the Douglas 7094 computer. Response surfaces were determined for each of the five dependent variables with respect to the five independent variables. The independent variables are: X_1, water vapor present in the shielding gas; X_2, amperage; X_3, voltage as a function of arc-gap; X_4, arc-exposure time; and X_5, thickness of the material. The dependent variables are: Y_1, percent porosity; Y_2, solidification time; Y_3, the hydrogen content of a weld nugget; Y_4, dendrite spacings and Y_5, the number of pores in a volume equivalent of one gram cube of weldmetal. The following equations have been found at the 95% confidence level:
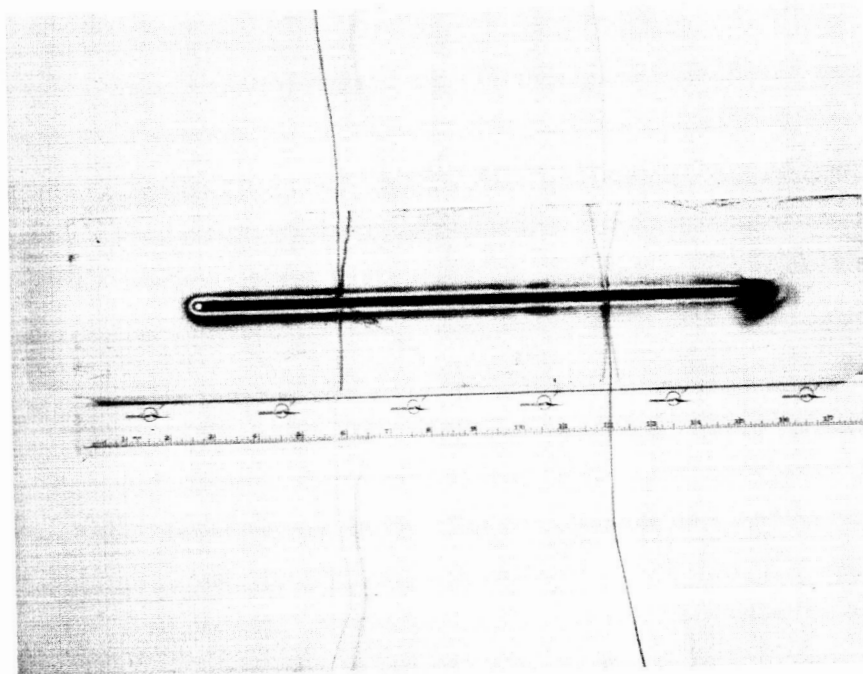
56

FIGURE 11

APPEARANCE OF TYPICAL BEAD-ON-PLATE WELD SPECIMEN. 2219-T87
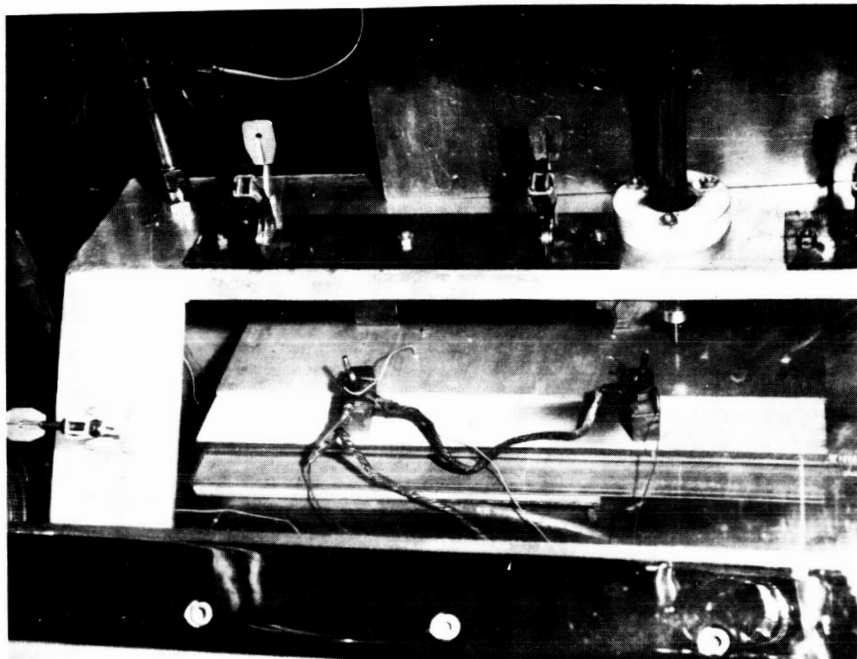MATERIAL PHASE 2 PART A.

FIGURE 12

VIEW OF BEAD-ON-PLATE SPECIMEN IN PLACE READY FOR
CLOSURE OF CHAMBER

TABLE 2

ACTUAL TESTING CONDITIONS FOR PHASE I, PART A
(2219-T87 MATERIAL)

EXPERIMENT AND SPECIMEN NUMBER *	ATMOSPHERE (WATER VAPOR CONTENT PPM ± 5%)	AMPERAGE (AMPS ± 1 AMPS)	VOLTAGE (VOLTS ± 0.1 VOLTS)	ARC EXPOSURE TIME (SEC ± 0.5 SEC.)
1				
1951	250	119.0	15.0	60
19103	250	119.5	15.0	60
1912	250	119.5	14.0	60
2				
191	<15	98.0	13.9	40
19125	<15	88.0	13.8	40
19111	<15	89.0	13.8	40
3				
1962	500	144.0	14.9	80
193	500	146.0	19.0	80
1924	500	150.0	15.2	80
4				
A198	500	154.0	14.5	40
A1926	500	148.0	14.8	40
A1937	500	148.0	12.0	40
5				
A1922	<15	91.0	14.5	80
A193	<15	90.0	15.5	80
A1925	<15	90.0	15.5	80
6				
A195	500	151.0	13.2	80
A1910	500	150.0	13.7	80
A1923	500	154.0	12.8	80
7				
A1935	<15	89.0	17.6	40
A1932	<15	91.0	17.7	40
A1915	<15	89.0	17.5	40
8				
19128	<15	90.0	17.3	80
19102	<15	88.0	19.0	80
1983	<15	88.0	16.5	80
9				
198	500	153.0	14.8	40
1981	500	148.0	15.0	40
19112	500	148.0	15.0	40

* Prefix "A" indicates 3/4-in. material; all others 1/4-in.

TABLE 2 (CONT'D)

ACTUAL TESTING CONDITIONS FOR PHASE I, PART A
(2219-T87 MATERIAL)

EXPERIMENT AND SPECIMEN NUMBER*	ATMOSPHERE (WATER VAPOR CONTENT PPM ± 5%)	AMPERAGE (AMPS ± 1 AMPS)	VOLTAGE (VOLTS ± 0.1 VOLTS)	ARC EXPOSURE TIME (SEC ± 0.5 SEC.)
10				
19121	250	117.0	15.0	60
1936	250	124.0	14.3	60
1953	250	116.0	16.0	60
11				
A1919	500	89.0	15.1	80
A1921	500	91.0	15.9	80
A192	500	91.0	17.0	80
12				
A1938	<15	143.0	12.3	40
A1941	<15	149.0	13.8	40
A194	<15	147.0	12.8	40
13				
19113	<15	147.0	14.8	80
19119	<15	148.0	15.0	80
19127	<15	148.0	13.4	80
14				
1980	500	89.6	17.2	40
1958	500	89.0	16.8	40
19114	500	88.0	16.5	40
15				
19107	<15	154.0	17.0	40
1994	<15	149.0	16.2	40
1915	<15	151.0	16.3	40
16				
1973	500	88.0	13.0	80
1954	500	90.0	13.8	80
19176	500	92.0	13.0	80
17				
A1936	500	85.0	12.5	40
A1933	500	88.0	13.0	40
18				
A1927	<15	144.0	15.0	80
A191	<15	143.6	15.5	80
A197	<15	148.0	15.0	80

* Prefix "A" indicates 3/4-in. material; all others 1/4-in.

TABLE 2 (CONT'D)

ACTUAL TESTING CONDITIONS FOR PHASE I, PART A
(2219-T87 MATERIAL)

EXPERIMENT AND SPECIMEN NUMBER*	ATMOSPHERE (WATER VAPOR CONTENT PPM ± 5%)	AMPERAGE (AMPS ± 1 AMPS)	VOLTAGE (VOLTS ± 0.1 VOLTS)	ARC EXPOSURE TIME (SEC ± 0.5 SEC.)
19				
1992	250	128.0	15.0	60
1996	250	113.6	14.9	60
1931	250	116.0	14.3	60
20				
1969	500	119.4	15.8	60
19104	500	119.0	15.1	60
19123	500	117.0	14.6	60
21				
1929	<15	124.0	16.4	60
1933	<15	117.4	14.1	60
1995	<15	120.0	15.0	60
22				
1934	250	148.0	13.5	60
1916	250	156.0	14.8	60
1971	250	147.5	14.9	60
23				
1987	250	91.6	15.5	60
1945	250	89.6	16.0	60
19179	250	89.0	16.0	60
24				
1997	250	117.0	16.3	60
1928	250	117.4	16.5	60
19108	250	119.0	16.5	60
25				
19130	250	120.0	12.0	60
19120	250	123.0	12.8	60
19-X	250	120.0	14.0	60
26				
1985	250	117.0	15.8	80
1957	250	120.0	14.6	80
1925	250	115.0	15.5	80
27				
19101	250	120.0	14.7	40
1919	250	120.0	14.7	40
19147	250	118.0	18.4	40

* Prefix "A" indicates 3/4-in. material; all others 1/4-in.

TABLE 3

RESULTS FROM PHASE I, PART A
(2219-T87 MATERIAL)

EXPERIMENT AND SPECIMEN NUMBER*	PERCENT POROSITY (GRAVI-METRIC)	Δt (±0.25 SEC)	N AVERAGE (PORES/Δt BY VOLUME)	AVERAGE PORE RADIUS (INCHES X10^{-4})	G AVERAGE (IN^3/SEC X 10^{-9})	DENDRITE SPACINGS (INCHES X10^{-4})	HYDROGEN (PPM, 0.01 ± 0.5%)
1							
1951	ND	2.75	NA	NA	NA	6.67	24.7
19103	7.14	2.75	68,024	12.7	3.11	11.20	ND
1912	4.93	2.25	140,509	9.3	1.49	5.02	ND
2							
191	0	NA	---	---	---	6.80	ND
19125	0	NA	---	---	---	3.36	29.0
19111	0	NA	---	---	---	3.97	ND
3							
1962	6.70	11.0	3,121	22.1	4.09	11.90	33.6
193	6.99	12.5	7,996	15.7	1.29	ND	ND
1924	5.40	11.5	9,168	14.0	1.01	9.61	27.8
4							
A198	4.92	NA	---	---	---	8.20	ND
A1926	ND	NA	---	---	---	4.27	ND
A1937	ND	NA	---	---	---	3.25	45.0
5							
A1922	0	NA	---	---	---	2.69	ND
A193	0	NA	---	---	---	ND	ND
A1925	0	NA	---	---	---	ND	ND
6							
A195	3.64	5.50	14,435	38.8	1.86	7.46	ND
A1910	3.69	9.25	880	28.3	10.20	9.09	5.5
A1923	ND	11.25	NA	NA	NA	12.50	ND
7							
A1935	0	NA	---	---	---	2.32	21.5
A1932	0	NA	---	---	---	3.09	ND
A1915	0	NA	---	---	---	2.89	ND
8							
19128	0	NA	---	---	---	5.81	ND
19102	0	NA	---	---	---	ND	ND
1983	0	NA	---	---	---	5.05	53.0
9							
198	7.74	5.0	17,169	16.8	3.93	8.62	ND
1981	5.34	NA	---	ND	---	11.36	ND
19112	4.72	3.25	17,546	16.5	5.76	7.81	44.0

* Prefix "A" indicates 3/4-in. material; all others 1/4-in.
ND = Not determined; NA = Not available.

TABLE 3 (CONT'D)

RESULTS FROM PHASE I, PART A
(2219-T87 MATERIAL)

EXPERIMENT AND SPECIMEN NUMBER	PERCENT POROSITY (GRAVI-METRIC)	Δt (±0.25 SEC)	N AVERAGE (PORES/Δt BY VOLUME)	AVERAGE PORE RADIUS (INCHES $\times 10^{-4}$)	G AVERAGE (IN^3/SEC $\times 10^{-9}$)	DENDRITE SPACINGS (INCHES $\times 10^{-4}$)	HYDROGEN (PPM, 0.01 ± 0.5%)
10							
19121	3.88	2.75	110,429	8.8	1.04	5.43	57
1936	2.90	3.00	16,403	14.6	4.34	5.21	ND
1953	3.11	2.75	120,433	7.9	0.757	5.38	ND
11							
A1919	5.72	1.75	348,915	8.0	1.22	2.99	88
A1921	S	1.50	---	ND	--	5.56	ND
A192	3.56	1.25	114,175	11.0	4.46	4.17	ND
12							
A1938	0	NA	--	---	--	2.98	ND
A1941	0	5.25	--	---	--	3.11	56
A194	0	5.75	--	---	--	3.21	ND
13							
19113	0	10.0	--	---	--	7.25	ND
19119	0	9.50	--	---	--	8.33	170
19127	0	9.25	--	---	--	7.46	ND
14							
1980	6.75	4.25	1278	40.9	67.3	3.82	118
1958	9.04	5.25	240,470	7.4	0.32	4.00	ND
19114	7.52	4.50	6142	23.8	14.1	2.84	ND
15							
19107	0	9.0	--	---	--	7.58	ND
1994	0	9.0	--	---	--	6.76	68
1915	0	3.75	--	---	--	7.69	ND
16							
1973	4.10	3.00	70,259	10.2	1.45	3.65	ND
1954	8.26	3.75	20,752	18.1	6.64		121
19176	6.88	NA	---	21.8	--	--	ND
17							
A1936	S	NA	---	---	--	1.81	ND
A1933	2.01	2.25	19.203	13.5	4.54	2.40	ND
18							
A1927	0	NA	---	---	--	10.20	ND
A191	0	6.75	---	---	--	10.00	49
A197	0	7.00	---	---	--	7.04	ND

S Indicates specimen too small for removal.

TABLE 3 (CONT'D)

RESULTS FROM PHASE I, PART A
(2219-T87 MATERIAL)

EXPERIMENT AND SPECIMEN NUMBER	PERCENT POROSITY (GRAVI-METRIC)	Δt (±0.25 SEC)	N AVERAGE (PORES/Δt BY VOLUME)	AVERAGE PORE RADIUS (INCHES $\times 10^{-4}$)	G AVERAGE (IN^3/SEC $\times 10^{-9}$)	DENDRITE SPECIMENS (INCHES $\times 10^{-4}$)	HYDROGEN (PPM 0.01 ±0.5%)
19							
1992	3.50	3.0	59,023	10.2	1.47	4.90	43
1996	6.70	2.75	93,858	11.3	2.18	6.94	ND
1931	3.56	2.75	16,632	16.1	6.32	5.38	ND
20							
1969	5.80	7.00	13,825	14.8	1.95	6.10	ND
19104	3.71	8.50	10,763	12.9	1.06	4.42	ND
19123	5.47	3.00	34,380	14.4	4.13	ND	86
21							
1929	0	4.50	---	--	--	5.56	ND
1933	0	4.25	---	--	--	5.10	ND
22							
1934	3.11	4.50	33,003	10.5	1.06	6.49	ND
1916	2.58	3.25	4775	20.6	11.28	5.26	ND
1971	4.41	3.00	44,374	12.6	2.78	6.94	60
23							
1987	1.84	4.75	68,576	8.4	0.494	5.95	36
1945	4.98	2.50	63,650	11.9	2.83	3.97	ND
19179	6.32	3.50		13.8			
24							
1997	5.01	2.75	18,766	17.4	8.00	4.59	ND
1928	5.96	3.50	439,375	6.8	0.377	ND	79
19108	4.06	3.0	52,473	11.1	1.93	4.63	ND
25							
19130	1.69	4.0	107.920	4.63	0.215	4.63	ND
19120	3.56	NA	---	4.06	---	4.06	ND
19-X	3.64	3.50	102,686	5.15	0.645	5.75	118
26							
1985	3.78	4.0	14,192	24.2	14.87	5.38	42
1957	3.99	3.25	296,258	9.0	0.928	6.49	ND
1925	3.99	4.50	7,458	30.6	26.63	7.14	ND
27							
19101	2.48	3.25	261,799	5.4	0.205	5.38	ND
1919	2.93	2.25	76,527	9.7	1.68	4.42	72
19147	9.24	2.0		46.1			ND

$$Y_1 = 0.4 + 0.0124 \, X_1 \tag{3}$$

where

Y_1 = percent porosity determined gravimetrically

X_1 = water vapor present in the shielding gas in PPM

$$Y_2 = 6.2 - 0.024 \, X_1 + 0.000048 \, X_1^2 \tag{4}$$

where

Y_2 = Thermal arrest in seconds

X_1 = Water vapor present in the shielding gas in PPM

$$Y_3 = -161.8 + 1.590 X_1 - 0.415 X_2 + 22.05 X_3 - 0.735 X_4 - 355.8 X_5 - 0.00282 X_1 X_2$$
$$- 0.0882 X_1 X_3 + 2.23 X_2 X_5 + 1.47 X_4 X_5 \tag{5}$$

where

Y_3 = Hydrogen content in PPM

X_1 = Water vapor present in the shielding gas in PPM

X_2 = Measured amperage

X_3 = Measured voltage

X_4 = Arc-exposure time

X_5 = Thickness of parent plate

Y_4 = Dendrite spacings

Analysis of the data showed that the dendrite spacings were not a function of any of the independent variables.

$$Y_5 = 64,420 + 1200 X - 2.40 X^2 \tag{6}$$

where

Y_5 = Number of pores in a volume equivalent of one gram of weldmetal

X_1 = Water vapor present in the shielding gas in PPM

Equation (3), for the gravimetrically determined percent porosity, is only a function of the water vapor in the shielding gas. None of the other independent variables influenced this behavior. In other words, within

the 95% confidence limits, the degree of dryness of the shielding gas determines the extent to which porosity will occur.

The time for the weld metal to reach the eutectic temperature, equation (4), is also only affected by the moisture in the arc atmosphere. This, however, is a more complex relationship than that of equation (2). The time required for the molten metal to reach the eutectic temperature decreases with increasing water vapor until a minimum is reached at 250 PPM. The solidification time then increases with increasing moisture content in the arc atmosphere. This is thought to be a result of two simultaneous, competing processes. One of these is a cooling process; the other is a heating process. The cooling process probably results from the removal of heat from the melt by the hydrogen bubbles as they leave the melt. The heating process is caused by the liberation of the latent heat of solution by the hydrogen as it precipitates from the melt. Small quantities of hydrogen, precipitating from the liquid, give up a smaller amount of latent heat than they remove by absorption when they pass through and leave the melt.

Larger quantities of hydrogen probably liberate more heat of solution than they remove from the melt. In the system under study, the heat removed and that liberated by the hydrogen are most closely matched when the atmosphere above the melt contains 250 PPM of water vapor.

Equation (5), for the quantity of hydrogen in the weld nugget, is the most complex of all of the equations. It is a function of all of the independent variables. Again, water vapor, in the arc atmosphere plays an important role even though its coefficient is relatively small. This results from the fact that the water vapor is in hundreds of PPM; this gives a large

66

contribution to the equation. By the same token the effects of thickness are considerably smaller than they appear to be, because 1/4 and 3/4-in. specimens were used. This was the only case where any of the variables, other than the composition of the arc atmosphere, had significance at the 95% confidence level. A more complete explanation of this complex behavior is beyond the scope of the present investigation.

Repeated analyses of the data for dendrite spacings, Y_4, showed that it was not a function of any of the independent variables. Plots of this quantity versus the other dependent variables provided no significant relationships.

Equation (6), as for equations (3) and (4), is only a function of the amount of water vapor in the arc atmosphere. In a manner analogous to equation (4), equation (6) shows that a maximum number of pores occurs at 250 PPM of water vapor in the arc atmosphere. This behavior is in agreement with equation (4). Where long solidification times are predicted by equation (4), correspondingly low porosities are given by equation (6); the reverse of this is also true. This behavior may be explained by the mechanism that long solidification times permit a high degree of escape of the hydrogen from the melt; shorter solidification times result in a greater degree of entrapment of the hydrogen bubbles.

The volumetric nucleation rate has been defined as the number of pores formed in a given welding situation divided by the time that the weldment took to cool to the eutectic temperature. Equations (4) and (6) were used to calculate the nucleation rates for the solidification times representative of the majority of the data in Table 3. Both of these equations are dependent only upon the amount of water vapor in the arc atmosphere.

Water vapor contents ranging from 250 to 500 ppm were employed for these calculations. Smaller quantities of moisture were not considered since the low value used in this work, < 15 ppm, is uncertain. The volumetric nucleation rate as a function of the inverse square of solidification time is shown In Figure 13. Short solidification times of about three seconds showed high nucleation rates; long solidification times of about six seconds showed low nucleation rates. This indicates that the weldments whould took longest to solidify provided the most time for the entrapped gas to agglomerate and/or escape; those with the shortest solidification times entrapped the greatest number of pores. However, as will be shown later, the growth rate of pores formed during long solidification times was much greater than that of pores formed during short solidification times.

Equations (3),(4) and(6) along with the known density of the parent plate were used to calculate the average growth rate of the pores. As in the previous calculations, these equations are functions only of the amount of water vapor in the arc atmosphere. Equation (3) provided the gravimetrically-determined porosity for a given level of water contamination. This information along with the known density of the parent plates permitted the calculation of the total volume occupied by the pores. These data divided by corresponding data from equation (6), for the number of pores, provided the average pore volumes for given contamination levels. The average pore volumes thus obtained were then divided by their corresponding solidification times calculated by means of equation (4) to provide the average growth rates. These are shown in Figure 14 as functions of the square of the solidification time. The data for contamination levels lower than 250 ppm of moisture are considered to be interpolations because of the previously-noted uncertainty in the low hydrogen levels used in this work.
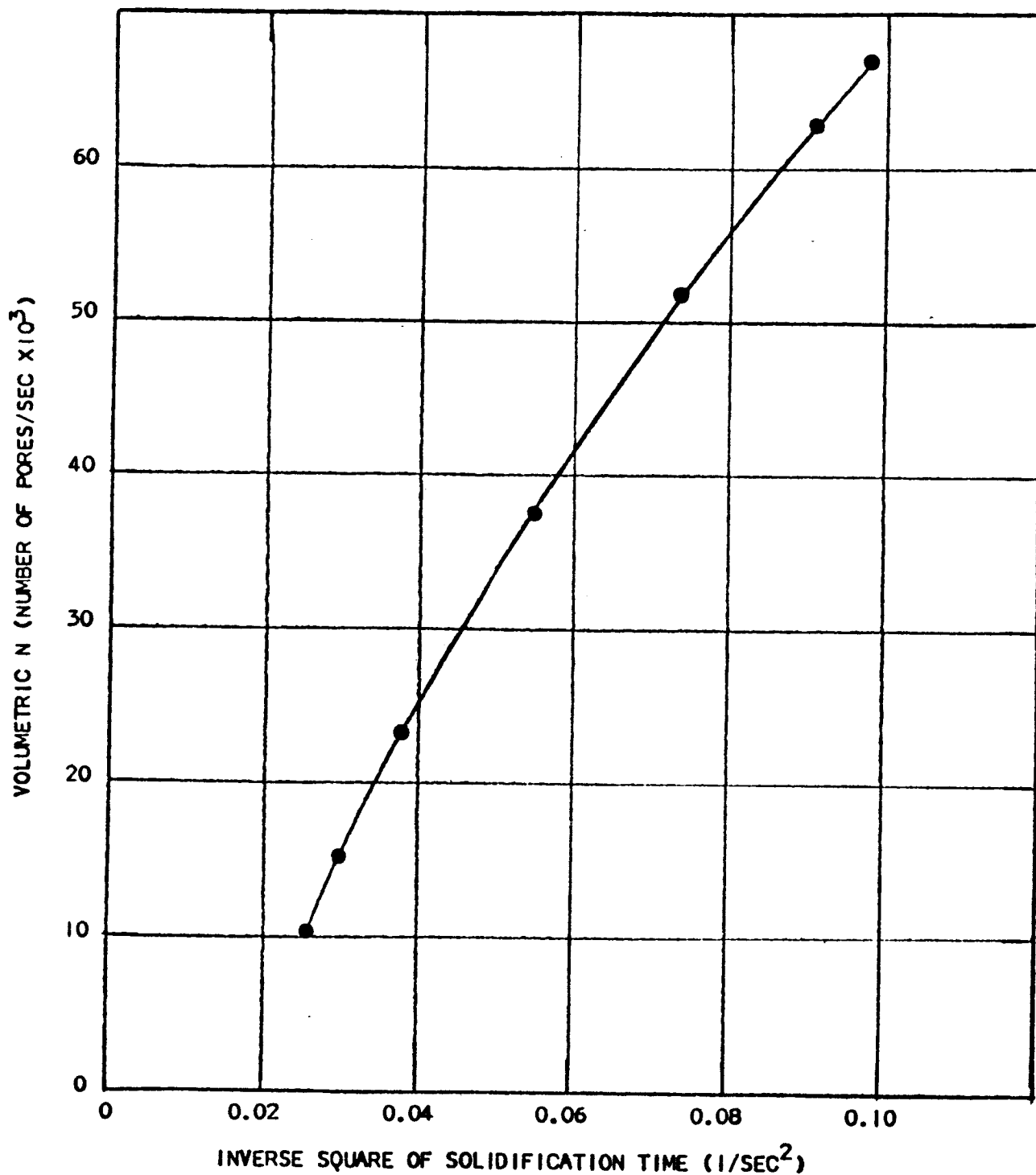
FIGURE 13
VOLUMETRIC NUCLEATION RATE AS A FUNCTION OF THE INVERSE SQUARE OF
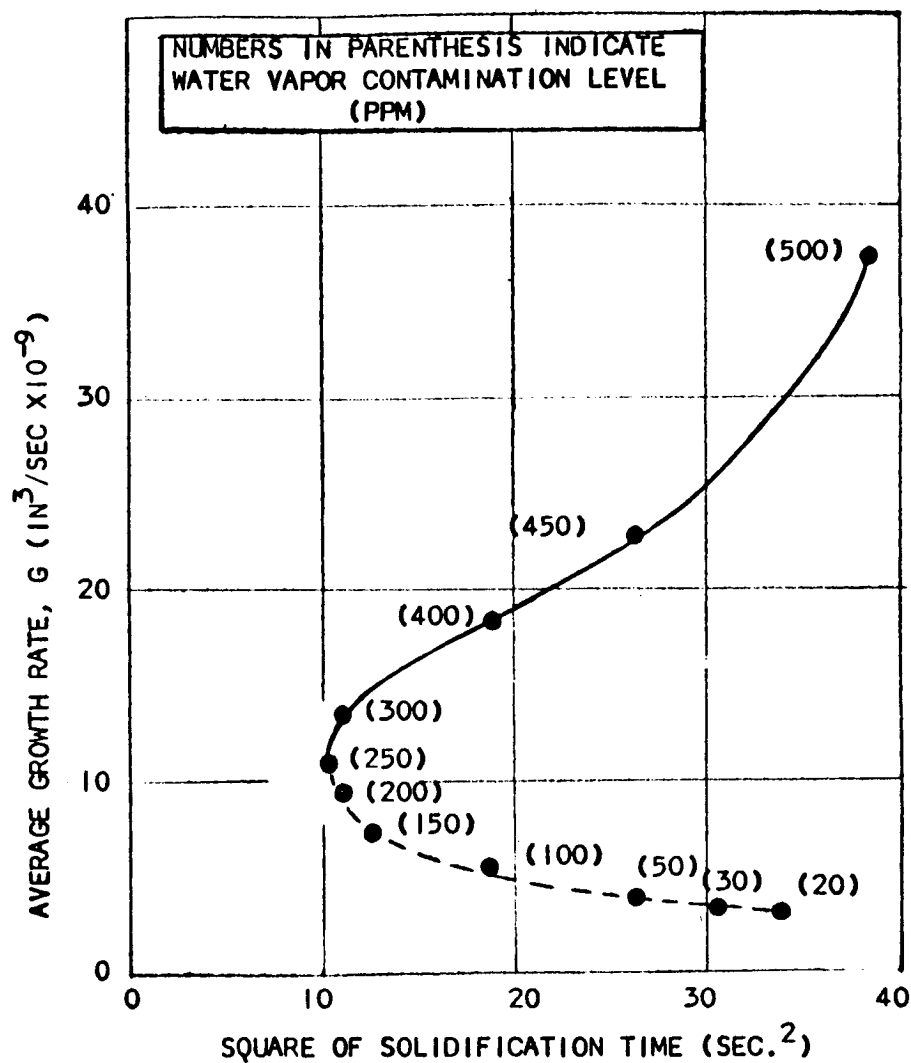SOLIDIFICATION TIME.   PHASE I, PART A 2219-T87 MATERIAL.

NUMBERS IN PARENTHESIS INDICATE
WATER VAPOR CONTAMINATION LEVEL
(PPM)

FIGURE 14
APPARENT GROWTH RATE AS A FUNCTION OF SOLIDIFICA-
TION TIME FOR VARIOUS WATER VAPOR CONTAMINATION
LEVELS. PHASEI, PART A, 2219-T87 MATERIAL.

70

The data plotted in Figure 14 show a "C" type relationship. Samples demonstrating long solidification times coupled with high contamination levels showed more rapid porosity growth rates than those which showed shorter solidification times and lower contamination levels. This effect is probably a result of agglomeration, since the number of pores, Figure 13, is small for these conditions. A "knee" appears in the curve at a solidification time of about three seconds and a contamination level of 250 ppm. If the trend indicated for the interpolated portion of the curve is correct, then the longer solidification times at decreasing contamination levels indicate a decrease in the average pore growth rate.

The curve shape indicated in Figure 14 appears to be reasonable because lower contamination levels (less than 250 ppm) would be expected to induce less porosity than higher amounts of water vapor. In addition, longer solidification times would provide a better opportunity for the escape of such low levels of porosity. Thus, the water vapor level in the arc atmosphere should be kept as low as possible and solidification times should be at least three seconds in order to keep the porosity growth rate as small as possible.

The pore volume fraction as a function of the Johnson-Mehl parameter, NG^3T^4, was calculated from the data previously obtained for N,G and T as noted above. The results are given in Figure 15. Again, the data for contamination levels less than 250 ppm are considered to be interpolations. A sharp discontinuity appears in this curve. Two mechanisms appear to be operative. For the low levels of contamination and their correspondingly short solidification times the controlling factor is probably that of. entrapment. However, at contamination levels of 250 ppm and greater the mechanism appears to be that of the escape of porosity as well as entrapment. This is in agreement with
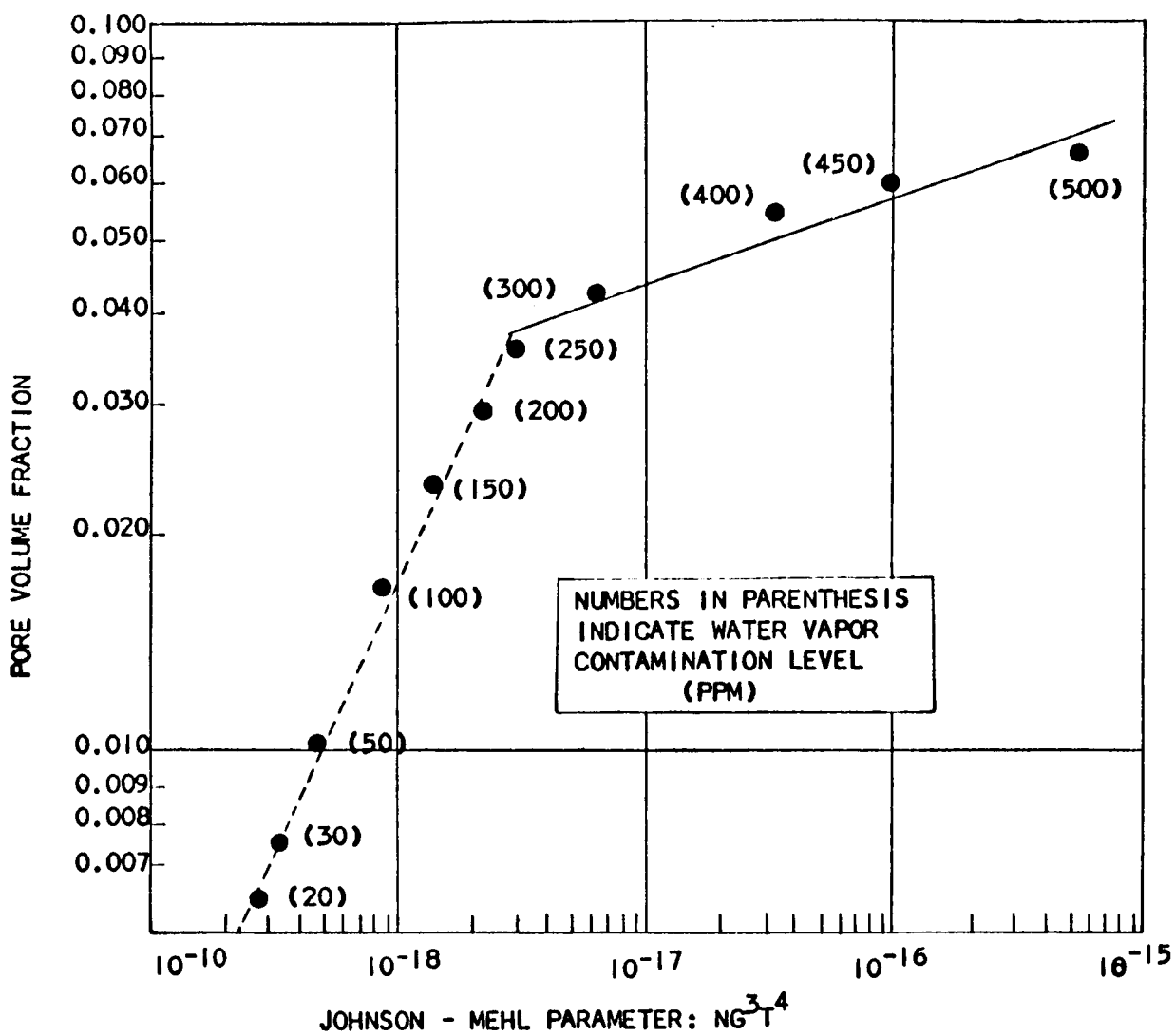
71

FIGURE 15

PORE VOLUME FRACTION AS A FUNCTION OF THE JOHNSON-MEHL PARAMETER FOR VARIOUS CONTAMINATION LEVELS.   PHASE I, PART A, 2219-T87 MATERIAL.

the behaviors previously noted for both the nucleation and growth rates.

The second part of Phase I has two purposes. The first of these is to correlate the behavior of 2014-T6 with that of 2219-T87 in water-contaminated arc atmospheres. The second purpose is to describe the reactions of both alloys when pure hydrogen, in amounts equivalent to those employed in the water-vapor studies, is used in the arc atmosphere. The test conditions and results are given in Tables 4 and 5.

Preliminary statistical analyses show that more samples are needed before any correlation can be made between the behaviors of 2014-T6 and 2219-T87 in water-contaminated arc atmospheres. This work has been scheduled.

The results of the influence of free hydrogen in the arc atmosphere are very interesting. The data, Table 5, show that free hydrogen, in the amount equivalent to more than 500 ppm of water vapor, caused no observable porosity. This is true for both 2219 and 2214 aluminum alloys. This is considered to be conclusive evidence for the statement that hydrogen must enter the weld pool after dissociation from water vapor. It is also indicated that the free hydrogen is much more difficult to ionize than is water vapor. This may provide an explanation for the observed differences in the porosities of welds made under nearly identical welding conditions except for the fact that they had been welded during different days. Differences in the humidities of the two days could account for the porosity differences.

Since weld porosity appears to result from a source of readily-ionizable hydrogen, other sources could be the presence of organic materials in or near the joint preparation. It is considered that the behavior of such compounds would behave in a way similar to that of water vapor.

TABLE 4

ACTUAL TESTING CONDITIONS FOR PHASE I, PART ∟
(2219-T87 AND 2014-T6 MATERIAL)

EXPERIMENT AND SPECIMEN NO. *	AVAILABLE FREE HYDROGEN (PPM)	AMPERAGE (AMPS ± I AMP)	VOLTAGE (VOLTS ± 0.I VOLTS)	ARC EXPOSURE TIME (SEC ± 0.5 SEC)
II				
A19100	71	92.4	18.0	80
A19102	71	87.8	18.1	80
A19104	71	88.2	17.5	80
A14105	71	88.4	16.5	80
A14106	71	88.4	16.55	80
A14107	71	88.0	17.0	80
A14108	71	88.4	16.5	80
13				
1429	<15	148.0	NA	80
1473	<15	149.4	15.0	80
1458	<15	149.0	14.1	80
14				
19144	71	97.6	16.6	40
19169	71	88.0	16.7	40
19143	71	87.8	17.9	40
1420	71	90.0	16.6	40
142	71	88.2	16.5	40
1412	71	88.4	16.8	40
	WATER VAPOR CONTENT (PPM ± 5%)			
II				
A1415	500	88.0	14.0	80
A1417	500	88.6	14.5	80
A1420	500	88.2	14.8	80
14				
1435	500	92.0	5.5	40
1427	500	92.0	15.0	40
1451	500	92.0	14.0	40

* Prefix "A" indicates 3/4-inch material; the others are 1/4-inch.
  The first digit indicates Phase I.
  The second digit indicates type of material
      9 Indicates 2219-T87
      4 Indicates 2014-T6

TABLE 5

RESULTS FROM PHASE I, PART B; BLOCK 5
(2219-T87 AND 2014-T6 MATERIAL)

FREE HYDROGEN AVAILABLE = 71 PPM

EXP & SPECIMEN NO.*	PERCENT POROSITY (AT 27X MAGN.)	Δt (±0.25SEC)	N AVERAGE (PORES/Δt BY VOLUME)	AVERAGE PORE RADIUS (INCHES X 10-4)	G AVERAGE (IN.3/SEC. X 10^{-9})	DENDRITE SPACINGS (INCHES X 10^{-4})	HYDROGEN (PPM 0.01 ± 0.5%)
11							
A19100	0	NA	0	0	0	4.6	
A19102	0	7.7	0	0	0	3.9	
A19104	0	3.4	0	0	0	8.3	
A14105	0	NA	0	0	0	2.9	
A14106	0	3.1	0	0	0	5.0	
A14107	0	3.8	0	0	0	7.0	
A14108	0	NA	0	0	0	2.7	
13							
1429	0	NA	0	0	0	7.5	
1473	0	2.5	0	0	0	7.2	
1458	0	NA	0	0	0	6.6	
14							
19144	0	1.1	0	0	0	5.9	
19169	0	1.75	0	0	0	2.9	
19143	0	NA	0	0	0	8.1	
1420	0	2.4	0	0	0	3.5	
142	0	2.0	0	0	0	3.4	
1412	0	1.2	0	0	0	3.8	
WATER VAPOR = 500 PPM							
11							
A1415	4.68**	2.8	648	73	591	4.7	
A1417	4.83**	2.6	47,897	18	8.89	5.7	
A1420	5.22**	2.4	2,499	49	200	---	
14							
1435	3.96**	2.1	13,965	25	30.6	3.1	
1427	11.42**	2.8	8,448	43	118.6	2.6	
1451	22.59**	2.3	11.118	51	249	1.9	

* Prefix "A" indicates 3/4-in material; the others are 1/4-in.
** Gravimetric Determinations.

Phase 2

The first portion of Phase 2 employs bead-on-plate welds on 2219-T87 and parallels the work described in Phase I for the static fusion welds. The welding parameters are the same as those given in Table I.

The actual test conditions and the available results are given in Tables 6 and 7. The preliminary statistical analyses will be made when the hydrogen contents of the specimens become available. These have been delayed because of a mechanical failure of the gas analyzer.

One preliminary observation may be made. The porosity of the bead-on-plate welds is considerably larger than that of the static welds. This has permitted better X-ray observation of the presence of porosity. A comparison of the percent porosity as determined by X-ray and by gravimetric means is given in Figure 16. It appears that a fair agreement exists between these two methods up to about 20% porosity.

References

1. Saperstein, Z.P. and D. D. Pollock, "Porosity and Solidification in Aluminum Welds" Douglas Aircraft Co., Engineering Paper 3046, Presented to MSFC Aluminum Welding Symposium, Huntsville, Ala., July 1964. (This paper contains a comprehensive list of references on the effects of hydrogen in aluminum welds.)

2. Smith, C. and Guttman, L., Trans. AIME, Jan. 1953, p. 81.

3. Cottrell, A. H., "Theoretical Structural Metallurgy", Edward Arnold, London, p 241, 1951.

TABLE 6

ACTUAL TESTING CONDITIONS FOR PHASE II, PART A
(2219-T87 MATERIAL)

EXPERIMENT AND SPECIMEN NUMBER*	ATMOSPHERE (WATER VAPOR CONTENT PPM, ± 5%)	AMPERAGE (AMPS ± 1 AMPS)	VOLTAGE (VOLTS ± 0.1 VOLTS)	WELDING TRAVEL SPEED (IN/MIN ± 0.10 IN)
1				
2927	250	120.0	15.7	1.5
294-C	250	121.0	17.0	1.5
2942	250	122.0	16.5	1.5
2				
2921	<15	91.6	15.8	1.0
2946	<15	90.0	15.5	1.0
2972	<15	91.0	16.5	1.0
3				
2923	500	149.0	18.5	2.0
2970	500	151.2	21.5	2.0
2971	500	150.0	20.7	2.0
4				
A2915	500			1.0
A2923	500			1.0
A2958	500	160.0	19.0	1.0
5				
A295	<15	90.0	13.5	2.0
A2936	<15	88.0	13.0	2.0
A2961	<15	94.0	16.0	2.0
6				
A2922	500	150.0	14.0	2.0
A2930	500	150.0	14.0	2.0
A2931	500	153.0	13.0	2.0
7				
A2927	<15	90.0	18.0	1.0
A2955	<15	91.0	20.0	1.0
A2963	<15	91.0	19.0	1.0
8				
294-B	<15	90.0	21.5	2.0
2953	<15	89.0	19.5	2.0
2959	<15	88.0	20.0	2.0
9				
2950	500	150.0	17.0	1.0
2957	500	150.0	17.5	1.0
2984	500	148.0	18.0	1.0

* The prefix "A" indicates 3/4-in. material; the others are 1/4-in.

TABLE 6 (CONT'D)

ACTUAL TESTING CONDITIONS FOR PHASE II, PART A
(2219-T87 MATERIAL)

EXPERIMENT AND SPECIMEN NUMBER*	ATMOSPHERE (WATER VAPOR CONTENT PPM, ± 5%)	AMPERAGE (AMPS ± 1 AMPS)	VOLTAGE (VOLTS ± 0.1 VOLTS)	WELDING TRAVEL SPEED (IN/MIN ± 0.10 IN)
10				
2920	250	120.0	16.0	1.5
2979	250	120.0	20.1	1.5
11				
A2913	500	90.0	18.0	2.0
A2952	500			2.0
A2966	500	91.0	18.0	2.0
12				
A292	<15	149.0	15.2	1.0
A2950	<15	150.0	15.0	1.0
13				
2914	<15	149.0	15.0	2.0
2975	<15	150.0	15.0	2.0
14				
291	500	89.0	22.5	1.0
2974	500	90.0	18.5	1.0
15				
2955	<15	149.0	19.0	1.0
2983	<15	149.0	19.0	1.0
16				
2954	500	90.0	14.0	2.0
2976	500	90.4	18.0	2.0
17				
A2919	500	89.5	14.0	1.0
A2926	500	90.0	15.0	1.0
A2941	500	90.6	15.0	1.0
18				
A2934	<15	149.0	18.5	1.0
A2937	<15			1.0
19				
2928	250	121.0	17.0	1.5
2973	250	120.0	19.5	1.5
2977	250	120.0	19.8	1.5

* The prefix "A" indicates 3/4-in. material; the others are 1/4-in.

TABLE 7

RESULTS FROM PHASE II, PART A
(2219-T87 MATERIAL)

EXPERIMENT AND SPECIMEN NUMBER *	PERCENT POROSITY (GRAVI-METRIC)	Δt (±0.25 SEC)	N AVERAGE (PORES/Δt BY VOLUME)	AVERAGE PORE RADIUS (INCHES X 10⁻⁴)	G AVERAGE (IN³/SEC X 10⁻⁹)	DENDRITE SPACINGS (IN X10⁻⁴)	HYDROGEN (PPM, 0.01 ±0.5%)
1							
2927	2.64	7.5	13.031	11	0.80	9.6	
294-C	2.08	5.5	8324	13	1.81	9.3	
2942	5.58	4.75	7828	20	7.18	9.4	
2							
2921	0	6.25	--	--	--	9.8	
2946	0	6.5	--	--	---	9.8	
2972	0	6.0	--	--	---	11.1	
3							
2923	4.05	13.0	6944	13	0.77	10.0	
2970	5.00	13.5	976	27	6.37	5.9	
2971	2.75	12.75	5878	12	0.64	3.8	
4							
A2915	4.90	--	--	23		11.6	
A2923	3.56			19		11.4	
A2958	4.27			16		11.4	
5							
A295	0	0.8	--	--	--		
A2936	0	0.6	--	--	--	3.2	
A2961	0	0.5	--	--	--	5.6	
6							
A2922	6.3	3.5	47,003	13	2.51	4.0	
A2930	10.3	3.0	112,485	12	2.44	5.2	
A2931	16.5	2.7	64,552	17	7.79	5.3	
7							
A2927	0	4.0	--	--	--	7.7	
A2955	0	4.3	--	--	--	5.1	
A2963	0	4.3	--	--	--	6.6	
8							
294-B	0	6.2	--	--	--	9.1	
2953	0	6.1	--	--	--	5.6	
2959	0	6.9	--	--	--	7.9	
9							
2950		24.5					
2957	4.65	25.6	4872	13	0.33	8.9	
2984	4.86	29.5	702	23	1.80	10.6	

* The prefix "A" indicates 3/4-in. material; the others are 1/4-in.

TABLE 7 (CONT'D)

RESULTS FROM PHASE II, PART A
(2219-T87 MATERIAL)

EXPERIMENT AND SPECIMEN NUMBER	PERCENT POROSITY (GRAVI-METRIC)	Δt (± 0.25 SEC)	N AVERAGE (PORES/Δt BY VOLUME)	AVERAGE PORE RADIUS (INCHES X 10^{-4})	G AVERAGE (IN^3/SEC X 10^{-9})	DENDRITE SPACINGS (IN X 10^{-4})	HYDROGEN (PPM, 0.01 $\pm 0.5\%$)
10							
2920	5.67	3.7	17,994	17	5.25		
2979	3.49	4.9	3934	16	3.67	11.1	
11							
A2943	21.8	3.3	10,730	34	51.03	3.2	
A2952	16.3	3.5	165,970	11	1.53	4.1	
A2966	16.58	3.5	24,748	23	14.09	4.1	
12							
A292	0	5.3	---	--	---		
A2950	0	6.0	---	--	---	6.1	
13							
2914	0	4.7	---	--	---	4.8	
2975	0	4.7	---	--	---	7.6	
14							
291	4.52	5.8	79.491	8.1	0.38	9.6	
2974	6.50	3.3	3533	31	38.75		
15							
2955	0.32	20.2	10,521	5.4	0.032	10.9	
2983	0	20.1	--	--	--	8.8	
16							
2954	9.88	5.3	5064	28	16.55		
2976	15.88	5.4	2153	44	64.54	3.5	
17							
A2919		6.1				3.4	
A2926	15.63	5.3	8341	28	17.02	3.6	
A2941	4.10	5.7	933	35	30.24	5.6	
18							
A2934	0	3.0	---	--	---	6.6	
A2937	0	5.0	---	--	---	5.8	
19							
2928	5.32	5.5	14,803	15	2.70	10.9	
2973	2.82	5.25	9368	14	2.42	10.6	
2977	3.70	7.6	77.594	6.9	0.18	6.2	

PERCENT POROSITY (X-RAY)

FIGURE 16
COMPARISON OF PERCENT POROSITY DETERMINED BY X-RAY AND
GRAVIMETRIC METHODS. PHASE 2 PART A, 2219-T87 MATERIAL

APPENDIX

POROSITY FORMATION AS A NUCLEATION AND GROWTH PROCESS

The evolution of gas from a melt is a process which is dependent upon two major mechanisms: the nucleation of stable agglomerations of gas molecules and the growth of such nuclei into bubbles, which appear as voids or porosity in the solidified matrix. Classical thermodynamics (Reference 3) may be used to demonstrate the factors affecting the two major parameters and to show how these may be used to explain observed, experimental behavior.

Nucleation

A stable nucleus of formerly dissolved gas will form when the Gibbs free energy (ΔF) becomes negative. This quantity may be expressed as the sum of component free-energies:

$$\Delta F = -\Delta F_m + \Delta F_s + \Delta F_c , \qquad (1)$$

Where ΔF_m is the chemical free energy of the nucleating gas, ΔF_s is its surface free energy and ΔF_c is its strain energy. Since this work is primarily concerned with gas evolution in the liquid state, ΔF_c will be negligible. Under these conditions, ΔF_s set the lower limit on the size of the stable nucleus. If ΔF_s is too large (molecular agglomeration too small), the nucleus will redissolve. If ΔF_s is small (molecular agglomeration large), the nucleus will grow.

Equation (1) may be rewritten as

$$\Delta F = -k_1 a^3 + k_2 a^2 , \qquad (2)$$

where k_1 is the chemical energy per unit volume and k_2 is the surface energy per unit area and a is the radius of the nucleating particle. The equilibrium nucleus size derived from equation (2) is found to be

$$a_0 = \frac{2}{3}\frac{k_2}{k_1} \qquad (3)$$

and the change in free energy thus becomes

$$\Delta F = \frac{4}{27}\frac{k_2{}^3}{k_1{}^2}$$

The smallest stable nucleus that will form an observable void in a eutectic system, such as under consideration in this work, is that which forms at the eutectic temperature and has sufficient time to grow. Under these conditions, the equilibrium nucleus size, a_0 of equation (3), will be a constant, and equation (3) may be employed to reexpress equation (4) as

$$\Delta F = \text{Const. } k_2 \qquad (5)$$

Thus, the change in free energy will be an inverse function of the radius (r) of the particle as given by

$$\Delta F = \text{Const. } \frac{1}{r^2} \qquad (6)$$

since the surface energy varies inversely as the area of the gas nucleus.

In the liquid state considered here, the diffusion of the gas atoms through the liquid to the growing nuclei will be relatively unimpeded (Reference 13). The nucleation rate, N, may be approximated by

$$N = \text{Const. } \exp.^{-\Delta F/RT} \qquad (7)$$

However, the temperature at the eutectic is constant until solidification is completed, so that equation (7) may be rewritten (using equation (6) and a series approximation for e^x) as

$$N = \frac{Const.}{r^2}$$

Pore Growth

Equation (8) provides an approximation of the rate of nucleation of the smallest observable gas bubbles which grow at the eutectic temperature. The rate of growth, G, of these bubbles must now be described. The growth rate of a sphere is given by (Reference 14)

$$G = \frac{dV}{dt} = 4\pi r^2 \frac{dr}{dt} \quad , \tag{9}$$

where V is the volume of the growing bubble and t is the time. At a given temperature, the eutectic temperature, the bubbles may be assumed to grow at an essentially constant rate. Expressed mathematically,

$$dr = Const. \, dt. \tag{10}$$

Integration of this equation gives

$$r = Const. \, (t - t_E) \tag{11}$$

where t_E is the time of growth at the eutectic temperature. For a given aluminum alloy composition subjected to a given amount of superheating, t_E will be very nearly a constant value. Thus, all bubbles which grow larger than what was previously defined as the smallest observable bubble will have radii that are a direct function of the time that the molten material was allowed to grow at temperatures above the eutectic.

Equation (11) may also be employed to provide further insight into the nucleation rate as given by equation (8); this becomes

$$N = \frac{Const.}{(t - t_E)^2} \tag{12}$$

Thus, the nucleation rate is shown to be inversely proportional to the time

that the melt is kept above the eutectic temperature - in agreement with ob-
served behavior.

In applying equation (11) to equation (9), the growth rate may be rewritten as

$$G = \text{Const.} \ (t - t_E)^2 \tag{13}$$

Integration of both sides of this equation with respect to time, between the
limits of t_E and t, gives

$$\int_{t_E}^{t} G dt = \text{Const.} \ (t - t_E)3 \tag{14}$$

This is an expression for the total volume of all bubbles at an initial time,
t. The total volume of voids grown after that is

$$df = \left[\int_{t_E}^{t} G dt \right] \ N \ (1 - f) \ dt \ , \tag{15}$$

where f is the fraction of the gas that is contained in the bubbles. When
equation (15) is integrated and equation (12) is substituted for N,

$$f = \frac{\text{Const.} \ t^4}{(t - t_E)^2} \tag{16}$$

Thus, the fraction of the gas that has precipitated from the melt and coalesced
to form bubbles is primarily a function of the time that the melt spent above
the eutectic temperature. To a first approximation, equation (16) may be shown
schematically as in Figure IA, where most of the bubble formation occurs
before t_E. The volumetric fraction of porosity is also expressed by equation
(16), except that the proportionality constant is different.

FRACTION OF VOLUME OF AVAILABLE GAS IN BUBBLES
(THE FRACTION OF VOID FORMATION AFTER t_E IS LARGELY UNOBSERVABLE).
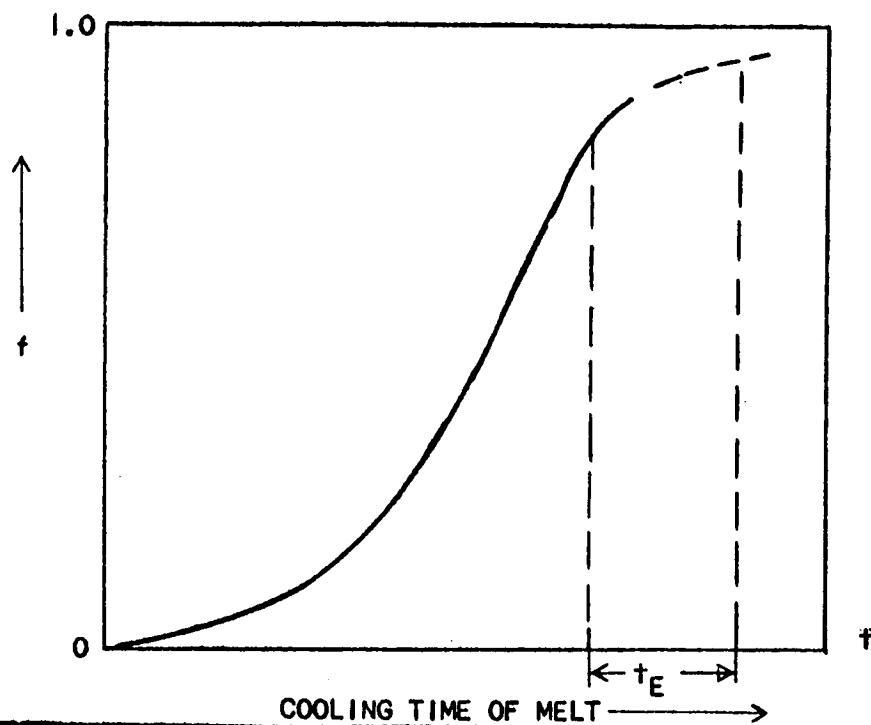
FIGURE IA

A QUANTITATIVE STUDY OF THE ROLE OF GAS

CONTAMINANTS AS A SOURCE OF DEFECTS IN WELDS

PRESENTED AT THE

ALUMINUM WELD DEVELOPMENT COMPLEX CONFERENCE
MARSHALL SPACE FLIGHT CENTER
HUNTSVILLE, ALABAMA

19 January 1966

Prepared and Presented by

W. Evan Strobelt

QUALITY CONTROL RESEARCH
THE BOEING COMPANY
SEATTLE, WASHINGTON

INTRODUCTION

The effects of contamination influx into the inert helium shielding envelope during production welding of 2219-T87 aluminum has been a controversial problem for a number of years. The continued increase in requirements toward ultra high reliability in aluminum weldments has emphasized the need to quantitatively define the effect of this uncontrolled variable on weldment quality.

To evaluate various gas contamination effects on 2219-T87 aluminum a study program was initiated for the NASA/MSFC Welding Development Laboratory by The Boeing Quality Control Research Section. The four gases - hydrogen, oxygen, nitrogen and water vapor - were the major variables, maintaining other parameters such as voltage, amperage, joint preparation and cleaning procedures constant.

Since porosity is recognized as one of the major problems in aluminum weldments, the program was designed primarily to determine the magnitude, frequency and level of porosity that would result from the specific gas contaminants when introduced into the arc zone. However, the physical properties (bend ductility, fatigue life, and tensile strength) are yet to be evaluated with only bend ductility being studied in the initial phase of work.

The experimental approach was based on a gas sampling concept developed at Boeing, where it was established that gases extracted near the weld arc and analyzed could be related to weldment quality.

The initial phase of the Effects Study program has been completed. The initial study included (1) the determination of the relationship of the contaminants to weld characteristics, (2) the establishment of general concentration range of the contaminants requiring quantitative definition and (3) the design of a quantitative study.

PROGRAM DESIGN

A statistical program was designed as a guide to experimental weldment preparation and evaluations. The objectives of the design were to determine:

1. The variability between panels welded under similar conditions (used to test for significance of the variables);

2. Whether variability between welded panels made under similar conditions is the same with or without the presences of contaminants;

3. Whether contaminants have a significant effect on weldment quality; and

4. Whether there are any significant interactions among contaminants.

The design included a total of 39 treatments (experimental runs) which were broken down into the following parts.

1. A complete 2^4 factorial requiring 16 panels;

2. A high level of each contaminant with other at their lowest measurable level, seven panels;

3. Repeated runs at the center of the factorial to determine variability with contaminants present, four panels;

4. Repeated runs with the lowest measurable levels of contaminants to determine variability under similar conditions, 12 panels.

A 30 inch test weldment was prepared and evaluated for each of the required test runs.

EXPERIMENTAL PROCEDURES

Step One

The chemically cleaned panel was removed from the plastic wrapping and placed on the workbench as shown. A triangular file, ground smooth on the flat surfaces to produce a knife edge, was used to scrape the surface adjacent to the joint. Particular care was taken to scrape the panel from the freshly cleaned area toward the oxide-coated surface. In this manner the scraper cuts beneath the oxide surface reducing the possibility of imbedding contamination into the base metal. The scraping process was carried out on both sides of the panel until the surface oxide was removed 3/4-inch back from the panel edge.

Step Two

The weldment panel was placed in a vise and the butt joint filed in the same manner as the sides, filing from freshly exposed metal toward the oxide-coated surface. In this case the file proved to be more effective for cleaning the butt joint than the triangular scraper because it was easier to keep the tool flat on the joint when removing the oxide layer.

Step Three

The top panel was placed in the weldment fixture and aligned by placing two alignment arms on the jig table. A metal finger projected from each of the arms at a height equivalent to the centerline of the backup bar. The top panel was positioned to rest on the alignment arm fingers and securely clamped in place using a torque wrench on the finger bolts.

Step Four

The bottom panel was inserted, pressed tightly against the top panel butt edge, and clamped with torqued finger pressure.

Step Five

The matched pair of panels mounted in the fixture was loaded into the chamber. The chamber was evacuated to a pressure ranging from 3×10^{-5} to 6×10^{-6} mm Hg, pumps valved off, and backfilled with helium in approximately 30 seconds.

Step Six

After backfill of the chamber, the mass spectrometer was calibrated to check for sensitivity. The gas flows in the backup bar and weld cup were then adjusted to the predetermined setting of 15 cu ft/hr in the torch cup and 1/4 cu ft/hr in the backup groove.

Introduction of the N_2, H_2, O_2, and H_2O gas components into the shielding gas was made quite simple by using the measurement instrumentation. The highest contaminant to be added was admitted to the helium stream until the required concentration was reached. The next highest concentration of gas was then added, and so on until all contaminants required were flowing into the shielding gas. The concentrations were then rechecked and re-adjusted, since change in the gas flows as a result of the additions had caused variations in the initial concentration setting. The process of making a flow change to effect the desired mass spectrometer reading for each gas was repeated several times; with each adjustment, the required mixture was more closely approximated. This process was carried out in a relatively few minutes since the response time of the instrument to changes in concentration is less than 30 seconds. Gas flows through the torch and backup were established and controlled with calibrated flowmeters located in the exhaust tube of the atmosphere control chamber.

Calibration was performed before and after welding to establish sensitivity variance of the mass spectrometer. Calibration was established by:

1. Running pure helium through the torch to establish background levels;

2. The sensitivity for each gas was found by flowing gas mixtures (analyzed independently with a gas chromatograph and by the manufacturer) past the inlet port.

Step Seven

In the welding operation, three people were required to produce a test weldment. The gas analysis specialist monitored gas concentration during the operation. The welder observed the weld as it was formed and corrected any mechanical deviation in arc length, wire feed, and fluctuation in arc characteristics. The technical weld specialist monitored voltage and amperage settings and made minor changes as required.

As would be expected when fusion-welding aluminum in the horizontal position, a principal problem was the establishment of a schedule that would minimize undercutting of the top bead. A number of trial welds were made using helium only to establish a weld setting that would produce test panels with an acceptable bead shape and quality. The only variables that were adjusted once the schedule was established were in voltage and amperage in which small changes were required to compensate for the variation caused by gas concentration changes. These changes were necessary to produce a weld with the proper penetration.

Step Eight

Prior to removal of the weldment panel from the chamber, the mass spectrometer was again checked for sensitivity with the calibrated gases. The panel was then removed from the chamber and fixture.

Step Nine

The fixture was cleaned by wiping with gauze dampened with methyl ethyl ketone prior to loading the next test panel.

Step Ten

The final steps in the weldment sequence was recording of data, visual examination of the welded test panel, and steel-stamping the identification code on the panel end.

RESULTS AND CONCLUSIONS

Following the preparation of the test weldments the samples were evaluated by radiographic, gravimetric porosity, and bend analysis as well as visual observation of general weld bead characteristics. The data was then computer processed and evaluated statistically.

Since time does not permit, the statistical treatment of data will not be discussed. This information is outlined in detail in the Boeing Document[1] Reference[1]. The results of the study are pictorially illustrated by Photo 11 through 16.

Photo 11 shows the metallographic analysis of welds prepared at low contamination levels. Photo 12 to 16 show the effects of contamination additions. As can be seen the addition of contamination provides a wide range of porosity depending on the type and level of the gas introduced.

Reference[1] Inert Gas Weldment Effects Study Phase I Report,
Boeing Document D2-23647-4 July 1, 1965

Photos 1 to 10:   TEST WELDMENT OPERATION
SEQUENCE

94
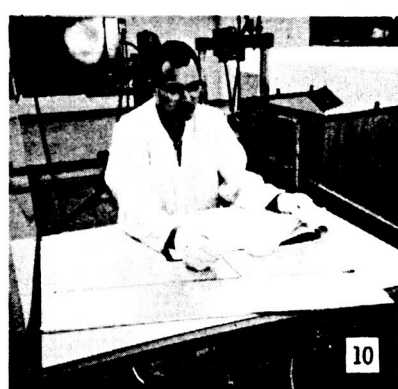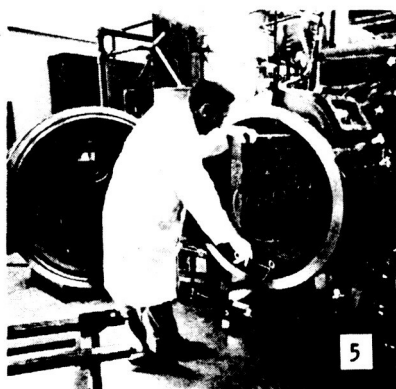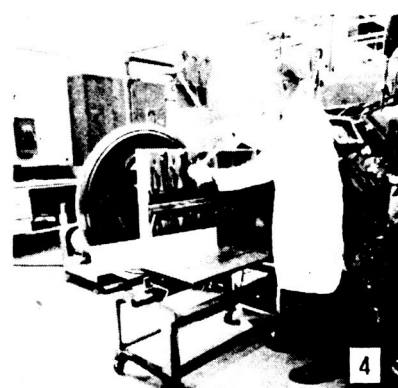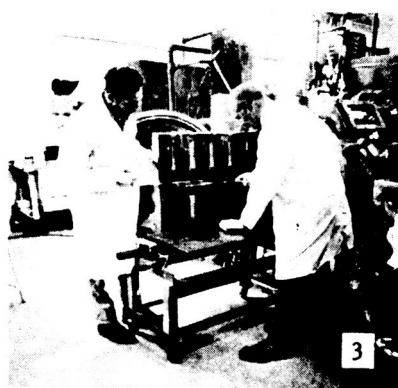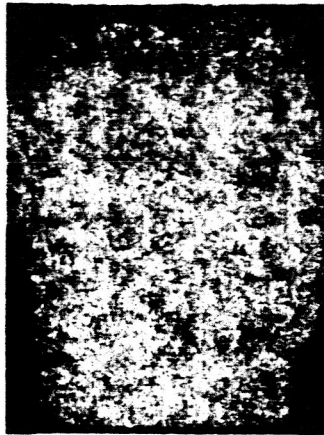
| | 2-07 | 3-07 | 2-02 |

Base Gas
< 50 H$_2$
< 50 N$_2$
< 5 O$_2$
< 5 H$_2$O

Base Gas
< 50 H$_2$
< 50 N$_2$
< 5 O$_2$
< 5 H$_2$O

Base Gas
< 50 H$_2$
< 50 N$_2$
< 5 O$_2$
< 5 H$_2$O

2-15

1-10

3-08
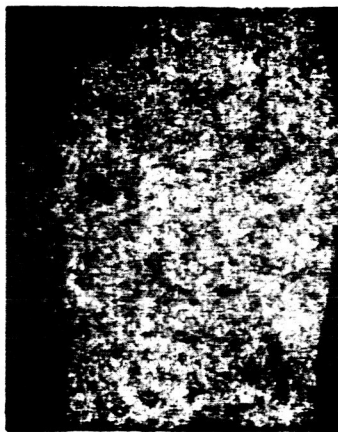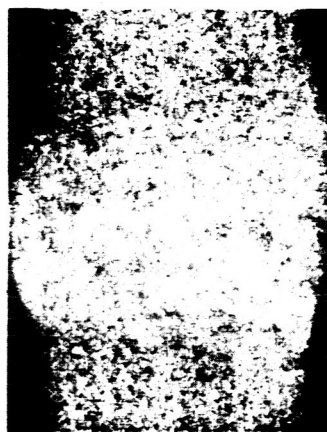
Base Gas
< 50 H$_2$
< 50 N$_2$
< 5 O$_2$
< 5 H$_2$O

Base Gas
< 50 H$_2$
< 50 N$_2$
< 5 O$_2$
< 5 H$_2$O
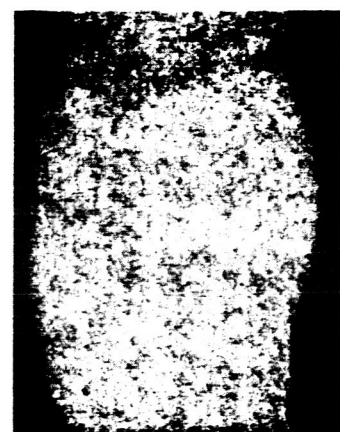
Base Gas
< 50 H$_2$
< 50 N$_2$
< 5 O$_2$
< 5 H$_2$O

Photo 11:   METALLOGRAPHIC PHOTOS

95

2-05

$H_2 = 16,800$
$O_2 = 5$
$N_2 = 50$
$H_2O = 5$
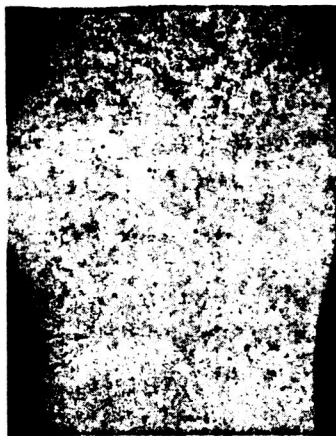
1-02

$O_2 = 5$
$H_2 = 860$
$N_2 = 50$
$H_2O = 5$
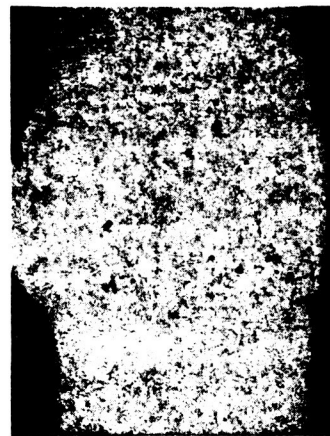
1-01

$O_2 = 90$
$H_2 = 1125$
$N_2 = 50$
$H_2O = 500$

2-09

$O_2 = 117$
$H_2 = 1000$
$N_2 = 50$
$H_2O = 100$

3-06

$O_2 = 500$
$H_2 = 1000$
$N_2 = 50$
$H_2O = 500$
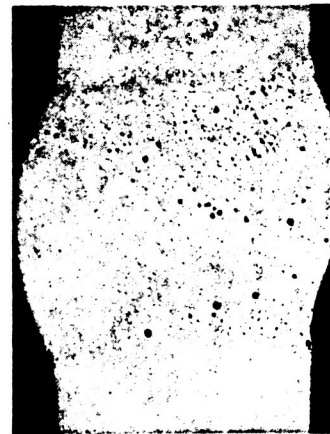
3-12

$O_2 = 100$
$H_2 = 1000$
$N_2 = 1000$
$H_2O = 500$

Photo 12: METALLOGRAPHIC PHOTOS (cont'd)

1-09	2-04	1-12
O_2 = 500	O_2 = 100	O_2 = 500
H_2 = 1000	H_2 = 1000	H_2 = 1000
N_2 = 50	N_2 = 1000	N_2 = 1000
H_2O = 100	H_2O = 100	H_2O = 100
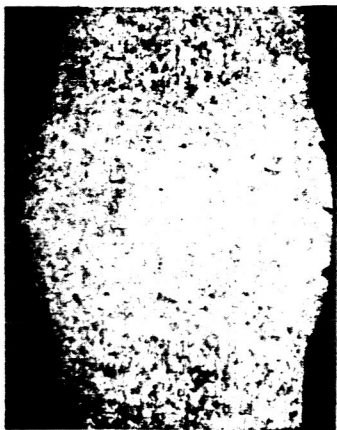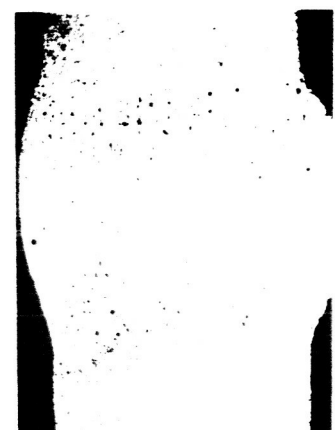
3-13	3-10	3-09
O_2 = 285	O_2 = 250	O_2 = 245
H_2 = 500	H_2 = 500	H_2 = 500
N_2 = 500	N_2 = 500	N_2 = 300
H_2O = 250	H_2O = 250	H_2O = 250

Photo 13. METALLOGRAPHIC PHOTOS (cont'd)

3-04

D_2 = 475
H_2 = 500
N_2 = 50
H_2O = 100

1-15

H_2O = 1000
H_2 = 50
N_2 = 30
O_2 = 5

2-08

H_2O = 500
N_2 = 50
H_2 = 50
O_2 = 5

3-11

O_2 = 105
H_2 = 100
N_2 = 50
H_2O = 500

Photo 14: METALLOGRAPHIC PHOTOS (cont'd)
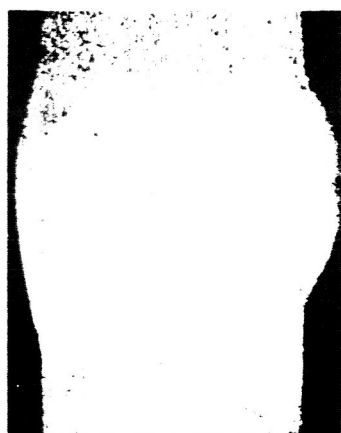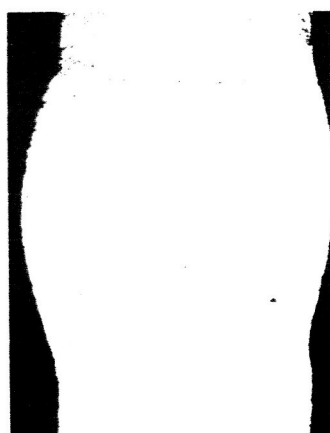
2-13	1-06	1-07
O_2 = 500	O_2 = 500	O_2 = 117
H_2 = 50	H_2 = 100	H_2 = 128
N_2 = 50	N_2 = 50	N_2 = 125
H_2O = 5	H_2O = 100	H_2O = 100

Photo 15: METALLOGRAPHIC PHOTOS (cont'd)

99

2-12

O_2 = 5
N_2 = 1000
H_2 = 50
H_2O = 5

2-16

O_2 = 100
H_2 = 160
N_2 = 1000
H_2O = 500

3-15

O_2 = 500
H_2 = 167
N_2 = 1000
H_2O = 500

2-16

O_2 = 100
H_2 = 160
N_2 = 1000
H_2O = 500

1-08

O_2 = 470
H_2 = 545
N_2 = 1330
H_2O = 250
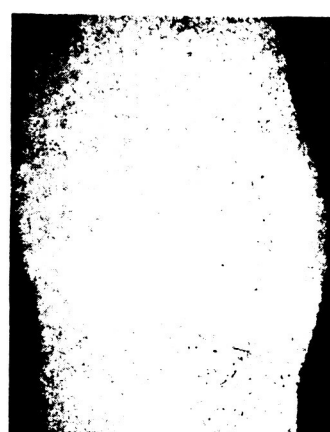
1-11

O_2 = 1000
H_2 = 50
N_2 = 50
H_2O = 5

Photo 16: METALLOGRAPHIC PHOTOS (cont'd)

100

In general, the statistical analysis showed that in almost all cases, porosity increases when hydrogen is increased. This is also generally true for water vapor; however, in some cases on increase in water vapor causes a decrease in porosity dependent on the levels of the other contaminants. An increase in oxygen may also cause an increase or decrease in porosity. For example, when studying the three-factor interaction between oxygen, hydrogen, and water vapor Table 1. (O_2, H_2, H_2O) for large porosity in the total weld, the following is noted: An increase in hydrogen causes an increase in porosity, except when oxygen is at the low level and water vapor is at the high level. An increase in water vapor causes an increase in porosity, except when oxygen is at the low level and hydrogen is at the high level. An increase in oxygen decreases porosity when hydrogen is at the high level and water vapor is at the low level, and when hydrogen is low and water vapor is high. However, an increase in oxygen when both hydrogen and water vapor are high increases porosity. A similar evaluation showed that increasing nitrogen can increase or decrease porosity, depending on the levels of the other contaminants.

The same type of effects were noted for the transverse shear strength (Bend Test) when studying the four-factor interaction: Increasing hydrogen decreases the shear strength in some cases and causes no change in others. Increasing water vapor or nitrogen can either decrease or increase shear strength. Increasing oxygen increases shear strength except when hydrogen is at the high level and nitrogen and water vapor are either both at the low level or both at the high level.

There were significant effects and interactions for most of the measures of weld quality evaluated; however, the effect on porosity appears to be the most important. While there were some significant effects and interactions determined from the bend test data, the size of these effects was small. Only when the contaminants were varied beyond the range covered by the factorial experiment were the effects large. For example, when hydrogen was increased to 16,800 ppm, a large decrease in the shear strength and increase in the bend angle were observed.
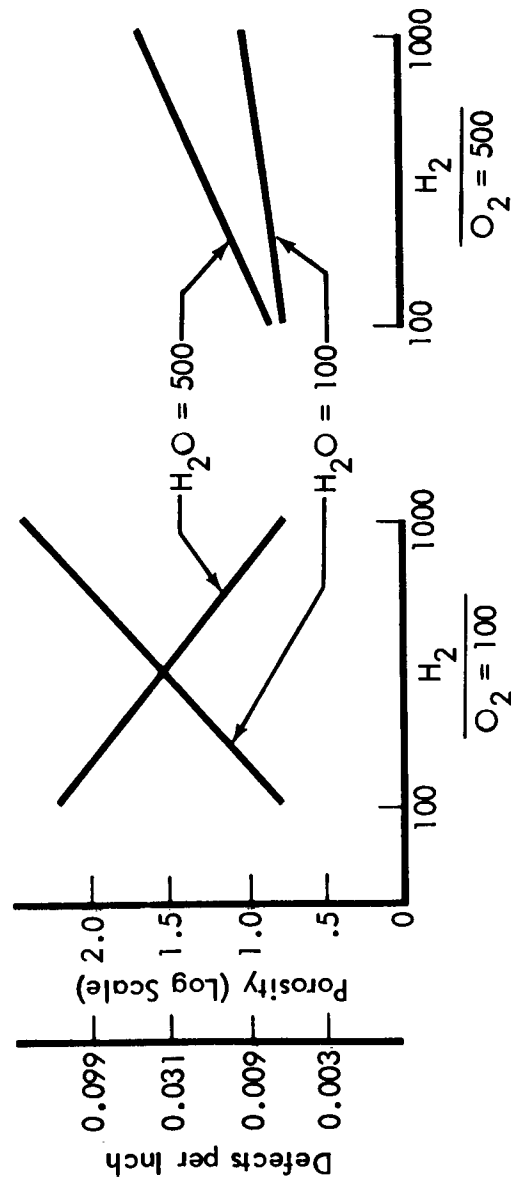
It was concluded as a result of this analysis that all contaminants studied have an effect on weld quality and that the effect of the contaminants is not independent. The fact that the mean of the weld quality responses did not coincide with the values at the center of the factorial design suggests the relationship between the contaminants and weld quality is nonlinear. To establish a valid relationship it was determined that all contaminants must be studied in the continuation quantitative phase and that more than two levels of each contaminant must be included in the experimental design. Review of the Phase I results indicates that the spacing of levels of the contamination for Phase II should be arithmetic rather than on a logarithmic scale.

FUTURE STUDIES

Since the initial objectives to establish a significant relationship between shielding gas contaminants and weldment quality was accomplished, a second

Table 1: POROSITY—TOTAL WELD, LARGE (TO 0.150)

Treatment Means –
Transformed Data

$O_2 \times H_2 \times H_2O$ Se = 0.559

	O_2	100		500	
H_2O	H_2	100	1000	100	1000
100		0.784	2.444	0.784	1.050
500		2.216	0.766	0.840	1.712

Porosity (Log Scale): 0, .5, 1.0, 1.5, 2.0

Defects per Inch: 0.003, 0.009, 0.031, 0.099

$\overline{O_2 = 100}$ H_2 (100 — 1000)

$\overline{O_2 = 500}$ H_2 (100 — 1000)

$H_2O = 500$

$H_2O = 100$

phase program was designed to determine a more quantitative relationship.

In the second phase of study we have attempted to design a program to yield data which can provide some common basis for relating shielding gas contamination as defined in this study to weld problems throughout industry. In order to accomplish this the following mathematical considerations have been postulated as an initial step toward defining the contamination variables in terms that can ultimately be related to other weld schedule parameters. For this purpose, a weldment quality level expressed as Q_L has been defined as the weld bead characteristics resulting from gas contamination at one fixed weld schedule. This quality level may be expressed in terms of porosity, bend ductility, fatigue life, or a combination of properties related to the gas contamination. The determination in Phase I that contamination is related to the quality of the weld allows the quality level (Q_L) to be expressed as a function of the contamination effect (C) as follows:

$$Q_L = F(C_1, C_2, C_3, ---C_n) \qquad (1)$$

Where C_1, C_2, C_3---C_n represents the contamination effects of contaminants 1, 2, 3, to n.

The contamination effect of a given contaminant (x) can be expressed in terms of the quantity of weld bead as:

$$C_x = \frac{R_x}{W_x} \qquad (2)$$

Where C_x = the contamination effect of contaminant (x)

R_x = the level of contamination

W_x = the quantity of the weld bead per unit inch affected

The level of contamination (R_x) is a function of the concentration and the flow rate of the gas. The quantity of weld bead (W_x) is a function of the energy input, filler metal addition, heat dissipation, travel speed, cooling effects of the gas, etc. In the special case where all variables remain constant except a single contaminant (x), Q_L would be related to C_x as follows:

$$Q_L = k\, C_x \qquad (3)$$

Where (k) is the proportionality constant relating the contamination level (C_x) to a quality level such as percent porosity. The study will be conducted at one weld schedule and the constant (k) for that schedule only will be determined. Since the quantity of the weld bead (W_x) is related to the contamination quality level (Q_L) (Equation 2), the Phase II program should provide an insight to the effects that changing other weld parameters will have on the properties of the weld at a constant contamination level.

In light of the test results and the theoretical considerations, Phase II was designed to quantitatively establish: (1) the level of porosity resulting from each specific concentration of contamination, (2) the concentration at which porosity begins to occur, (3) the levels of porosity resulting from the addition of mixed contamination, and (4) the mechanical relationships resulting from the contamination additions. In addition to the work previously scheduled, a preliminary survey will be made of the effects of contamination on the root surface of the weld bead only, to better simulate production conditions.

In the second phase of study the evaluation of samples will include radiographic, metallographic, fracture toughness, tensile, fatigue and gravimetric analysis.

In our opinion this program is a significant step in attaining higher weldment quality in 2219-T87 aluminum and three important results as related to gas contaminants are expected from this study as follows:

1. An increase in engineering flexibility in establishing structural design requirements to the desired porosity level, strength, ductility or fatigue life; and

2. To provide information necessary to control contamination levels to fabricate to the engineering requirements; and

3. To ultimately aid in attaining the major objective of higher reliability in aluminum weldments.

EFFECTS OF POROSITY ON MECHANICAL PROPERTIES

OF 2014 -T6 AND 2219-T87 ALUMINUM WELDS

Reference NAS 8-11335

REPORT OF PROGRESS

January 19, 1966

Edward J. Rupert

John F. Rudy

MARTIN MARIETTA CORPORATION
MARTIN COMPANY
WELDING RESEARCH AND DEVELOPMENT
DENVER, COLORADO

PRECEDING PAGE BLANK NOT FILMED.

EFFECTS OF POROSITY ON MECHANICAL PROPERTIES
OF 2014-T6 AND 2219-T87 ALUMINUM WELDS

I. INTRODUCTION

The objective of this program is to derive a working relationship between the mechanical properties of a weld and porosity within the weld. The final statement of this relationship will be in a form to enable intelligent acceptance or rejection (repair) of a given "irregular" weld, when the expected service loads are adequately defined. In essence, the objective is to establish an improved weld acceptance criteria.

The method for obtaining the data to meet these objectives is to produce a statistically significant number of defective welds, to classify these defects according to a system which has utility as a non-destructive tool in actual production welds, and to measure the mechanical properties of the classified welds. More specifically, the intent is to propose several systems of defect classification and to evaluate these systems by determining the relative ability of each to predict the mechanical properties.

In examining this methodology description it becomes apparent that the primary experimental challenge falls into three areas, (1) obtaining with a reasonable degree of predictability, desired levels of porosity in experimental welds, (2) deriving useful defect classification systems, and (3) obtaining mechanical property measures which are meaningful to the prediction of weld joint performance in real structures. A section to follow, Present Status, is sub-divided into these three subject areas.

II. EXPECTED FINAL STATEMENT

At the conclusion of this effort it is expected that weld acceptance criteria correlations will be provided over a wide range of spherical or gas bubble-like porosity for the following combinations: (1) 2014-T6 welded with 4043 filler wire and 2219-T87 welded with 2319 filler wire, (2) thicknesses of 1/4 and 3/4 inch plate, (3) flat, horizontal and vertical-up welding positions, and (4) in terms of static strength and ductility both longitudinal and transverse to the welding direction and transverse fatigue strength. It is not possible to predict at this time exactly what form the porosity classification systems will take, or which classification system shows the best ability to predict mechanical properties. However, the classification systems to be tested for their ability to predict will include (1) classification according to arbitrarily defined standards of degrees of "badness," (2) volume pore percentages per unit weld length, (3) and pore cross section percentages at the fusion line or bead edge as compared with similar pore percentages in the center one-third of the bead.

II. EXPECTED FINAL STATEMENT (Continued)

Since the porosity producing techniques which are being used produce primarily spherical porosity, such considerations as the presence of sharp corners will not be included in these classification systems. However, size distribution of porosity will be included.

It is expected, based on preliminary test data now available, that criteria for welds which see essentially a static load will be quite different than dynamic or fatigue loading weld acceptance criteria.

It will be recognized, in the final statement of acceptance criteria, that the alternative to accepting an irregularity as-is is to introduce a weld repair. Therefore, mechanical properties of defective welds will be compared with mechanical properties of repaired welds in addition to mechanical properties of original "perfect" welds. The basis for these comparisons have already been established for 2014-T6 in the forms shown in Figure 1, which illustrates the deterioration of transverse tensile strength with increasing number of repairs, and Figure 2, which compares as-repaired strengths with the strengths of the reasonably bad "P5" porosity level. P5 corresponds to a weld which contains a volume pore percent in the range 6 to 12.

In addition to the above comments pertaining to the direct objective of this program, statements will be provided concerning "side issues." For example, the techniques for obtaining porosity will provide an indication on the amount of contamination which can be tolerated. These toleration levels will differ for the two alloys, for the three welding positions, and for the two thicknesses. Also, the introduction of contaminants to the arc plasma results in electrical disturbance of the plasma and changing electrical characteristics. It may be possible to correlate backwards and to make useful statements which enable electrical measurements to be used as indications of the presence of contamination in production welds. In addition, it is noted that different types of contamination, for example, hydrogen or moisture in the arc atmosphere or hydrated coatings on the filler wire or base metal, result in different patterns and types of porosity. These data can be useful in solving production porosity problems by providing an indication of the contamination source which has caused the particular difficulty encountered.

III. FOLLOW ON EFFORT SUGGESTED BY THESE EXPERIMENTS

Since the "side effects" mentioned above are not part of the major objective of this program, conclusions involving these effects will not be firmly established at the completion of this program. Therefore, additional effort will be required to tie these suggested relationships down to firm statements. For example, the correlation between the type of porosity and the mechanism of contamination will require additional experimental activity, but could be quite practical and useful. Similarly, correlations between electrical measurements of the arc parameters and contamination level would be useful.

III. FOLLOW ON EFFORT SUGGESTED BY THESE EXPERIMENTS (Continued)

The major follow on effort which is suggested by this program is to expand the acceptance criteria which will be derived to include non-spherical porosity shapes. Welding fabricators generally have much more difficulty in predicting the expected mechanical property effect of non-spherical porosity, than in the assessment of gas porosity. Such designations as "porosity with tails" and dross or oxide inclusions require, in the present state of the criteria art, either a certified Witch Doctor or an overly conservative approach.

Another area of suggested follow on is repair techniques. If weld repairs could be performed with less damage to mechanical properties, then a more conservative weld acceptance criteria becomes a more practical approach to the problem of producing reliable hardware.

IV. PRESENT STATUS

A. Introduction of Porosity

For reasons of economy in performing these experiments, it is necessary that predictable levels of porosity be produced in each of the alloy-thickness-welding position combinations at a frequency along the weld seam which is sufficient to provide an adequate number of evaluation specimens. This precludes welding under "optimum" or simulated production conditions and taking the porosity which happens to occur. However, in introducing contamination intentionally, the necessity for producing a type of porosity which is representative of that found in production must be recognized. Also, the contamination which is introduced should, ideally, effect the mechanical properties only by way of the porosity which is introduced, and not by other contamination effects on the physical metallurgy of the weld bead. These considerations dictated that the contamination methods to be used should introduce hydrogen, since the greater part of the welding literature is in agreement that hydrogen is the important practical cause of aluminum welding porosity. In actual practice the source of hydrogen is moisture, which breaks down in the high-temperature arc plasma. Preliminary experiments investigated two routes for introduction of hydrogen and moisture to the weld puddle. The first was to contaminate the filler wire by various pre-weld anodizing and moisturizing treatments. The specific wire treatments evaluated have been reported in the previous program review, and included various times, bath temperatures, and current densities in anodizing treatments, and exposure to various temperature-humidity environments for various times. The general conclusion derived from these experiments was that filler wire contamination was an effective means of introducing porosity, but that the level of porosity to be obtained from a given filler wire treatment was not predictable. The porosity which was obtained tended more toward the dross or oxide inclusion

A. Introduction of Porosity (Continued)

geometry rather than the gas pore geometry, but could not be made to be really "bad" on a volume percentage basis. Thus, these porosity producing techniques were abandoned in favor of the more predictable results which have been obtained by metering hydrogen and/or moisture into the shield gas stream. However, the success of this technique in producing non-spherical porosity will be useful for follow on efforts in that direction.

The technique of metering contaminants into the shield gas provides predictable levels of porosity for a given level of contamination, and provides this level of porosity with a reasonably uniform distribution over the entire length of the two-foot weld panel. However, it has been found necessary to change the contamination levels for some material, thickness, and welding position. For example, porosity level No. 2 was obtained with the following shield gas compositions for each of the indicated welding conditions:

ALLOY		POSITION	CONTAMINANT
2014-T6,	1/4" THK	FLAT	5CFH Hydrogen
2014-T6,	1/4" THK	HORIZONTAL	25-30°F Dew Point
2219-T87,	1/4" THK	FLAT	5CFH Hydrogen
2219-T87,	1/4" THK	HORIZONTAL	2CFH Hydrogen
2014-T6,	3/4" THK	FLAT	-20°F Dew Pt.+ 5CFH Hydrogen
2219-T87,	3/4" THK	FLAT	-20°F Dew Pt.+ 5CFH Hydrogen

These required adjustments suggest several conclusions which can be stated at this time.

1. More contamination is required to produce porosity in flat welds than in horizontal welds. For example, moisture plus hydrogen is required in flat position welding if pores greater than 0.020 inches are to be obtained. By comparison, extensive porosity (up to level 4) can be obtained in horizontal welding by metered additions of moisture alone.

2. Porosity in flat welding is randomly distributed, whereas porosity in horizontal welding favors the upper edge of the bead.

3. Porosity is more difficult to obtain in 2219 than in 2014.

4. Porosity is more difficult to obtain in 3/4-inch thick welds than in 1/4-inch welds.

5. The ability of hydrogen to produce porosity seems to vary from tank to tank of hydrogen, suggesting that a contaminant in tank hydrogen plays a part in porosity formation.

A. <u>Introduction of Porosity</u> (Continued)

6. Hydrogen is a more effective porosity producer than moisture, but the combination of hydrogen plus moisture is most effective.

7. Porosity is more difficult to introduce in filler passes than in initial, or fusion passes.

8. Contaminated filler wire tends to produce angular or sharp-cornered voids, while shielding gas contamination tends to produce spherical or gas voids.

9. Moisture in shielding gas at less than -30°F Dew Point does not develop appreciable porosity as measured in two-foot long panel welds.

Several conclusions can also be presented concerning the "side effects:

10. Electrode configuration has been found to be a critical parameter in successful performance of horizontal welding.

11. Less filler wire, measured in inches of wire per inch of weld, is required as shielding gas contamination increases. This probably follows from changes in bead geometry as a function of gas composition.

12. Welding parameters, arc current and arc voltage, require adjustment as gas composition is changed. Generally, contaminated plasmas require higher arc voltage and lower arc current if the bead geometry is to be maintained as consistent as possible.

B. <u>Definition of Defect Classification Systems</u>

In the present status of the program, the system for classification of the degree of porosity has been primarily by comparison with a rough sequence of x-ray standards. Specimens are grouped prior to mechanical testing according to these standards, and analysis of the effects of porosity on mechanical properties have been performed in these terms. However, prior to testing each individual specimen is re-xrayed both straight-on, and by a double x-ray "parallax" system. This will enable re-evaluation of all mechanical property data in terms of the pore location criteria suggested in the introduction. In the final analysis, pores which are exposed on the fracture surface will also be classified and considered.

112

C. **Mechanical Property-Porosity Relationships**

Static tensile properties versus arbitrary standard levels of
porosity are plotted for several conditions in Figures 3 to 6.
The X-rays used as standards by arbitrary definition are as
shown in the slides. As pointed out, this is only a preliminary
classification system, but some conclusions can be presented.
In general, static strength and ductility do not fall off
appreciably until porosity gets fairly bad, by comparison with
generally accepted porosity standards in the industry. Transverse
weld strength is more sensitive to porosity than longitudinal weld
strength. Also, ductility as measured in the longitudinal specimen
does not appear to be overly sensitive to porosity level. Weld
strength of 2014-T6 is superior to 2219-T87, and does not appear to
be any more sensitive to the degree of porosity. However, longitudinal
weld ductility is greater for 2219. With both alloys, ductility
falls off more rapidly with increasing porosity when pulled in the
longitudinal direction.

Although the fatigue data are rather sketchy at this time, it is
appearent that porosity is much more potent in influencing fatigue
behavior that in inf uencing static tensile behavior.   For example,
life at 25 Ksi is 1,100,000; 24,000; 11,000; and only 2,000 respectively
for levels 0, 2, 3, and 4.

113

NUMBER OF REPAIR WELDS
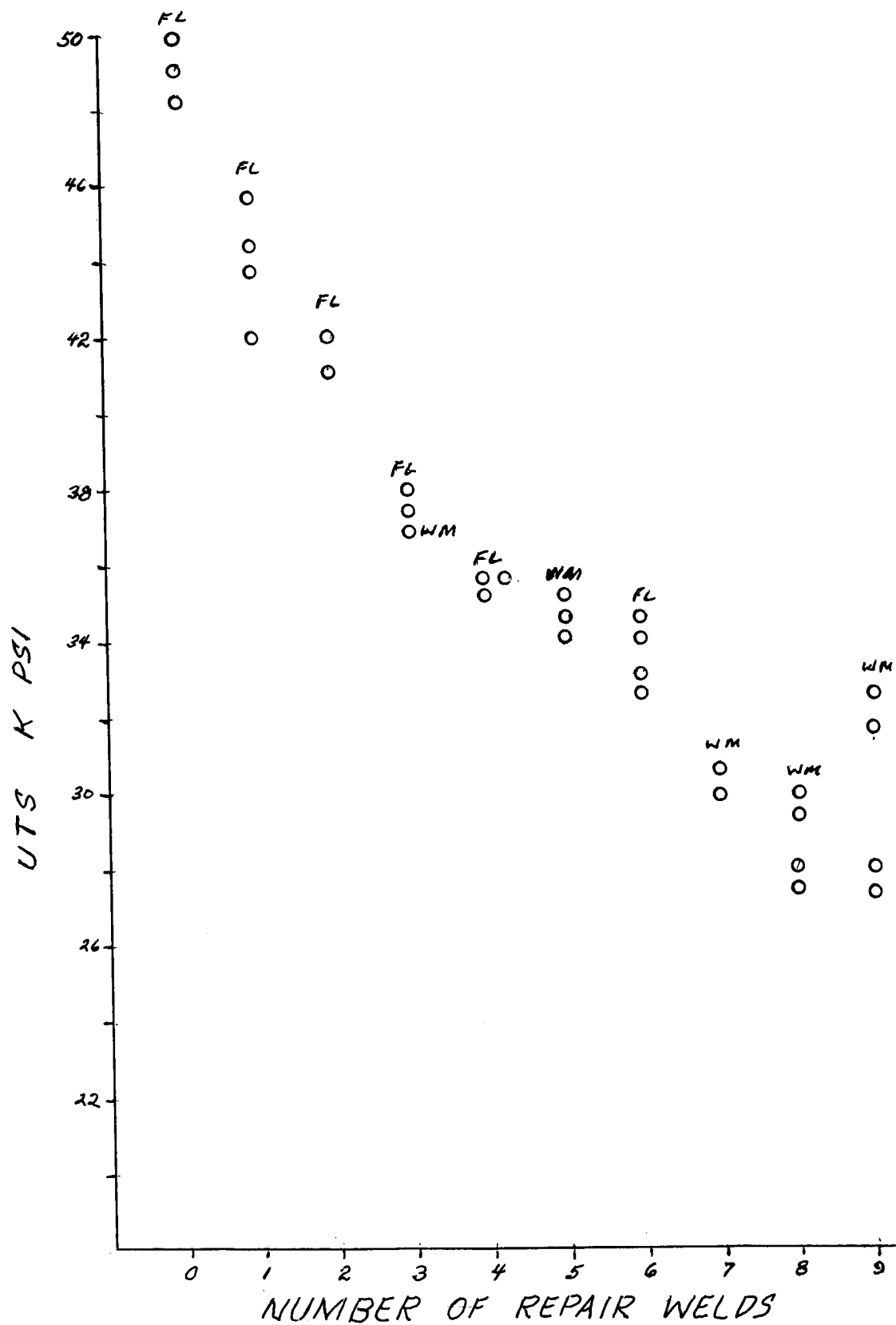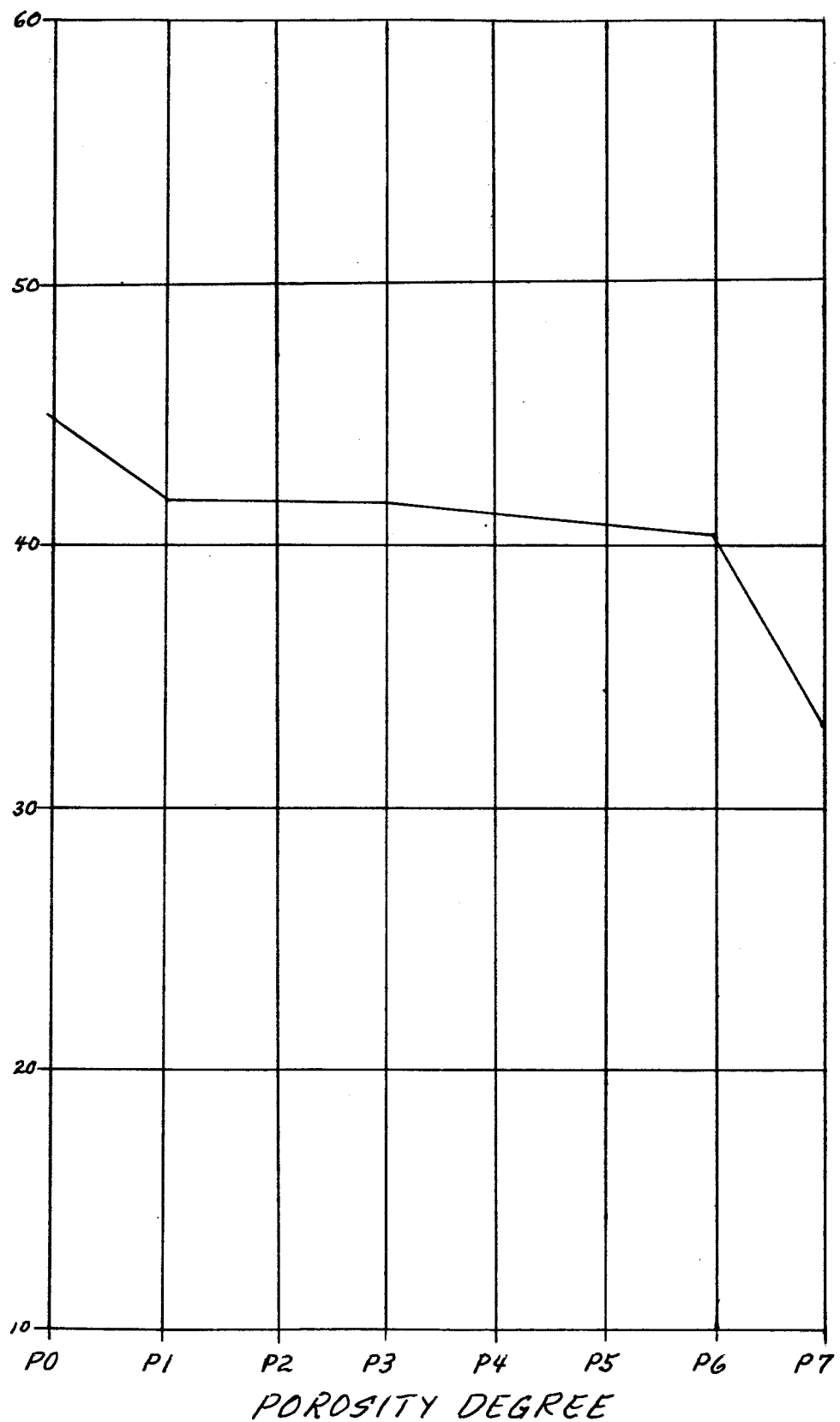
FIGURE 1

FIGURE 2 UTS AVERAGE
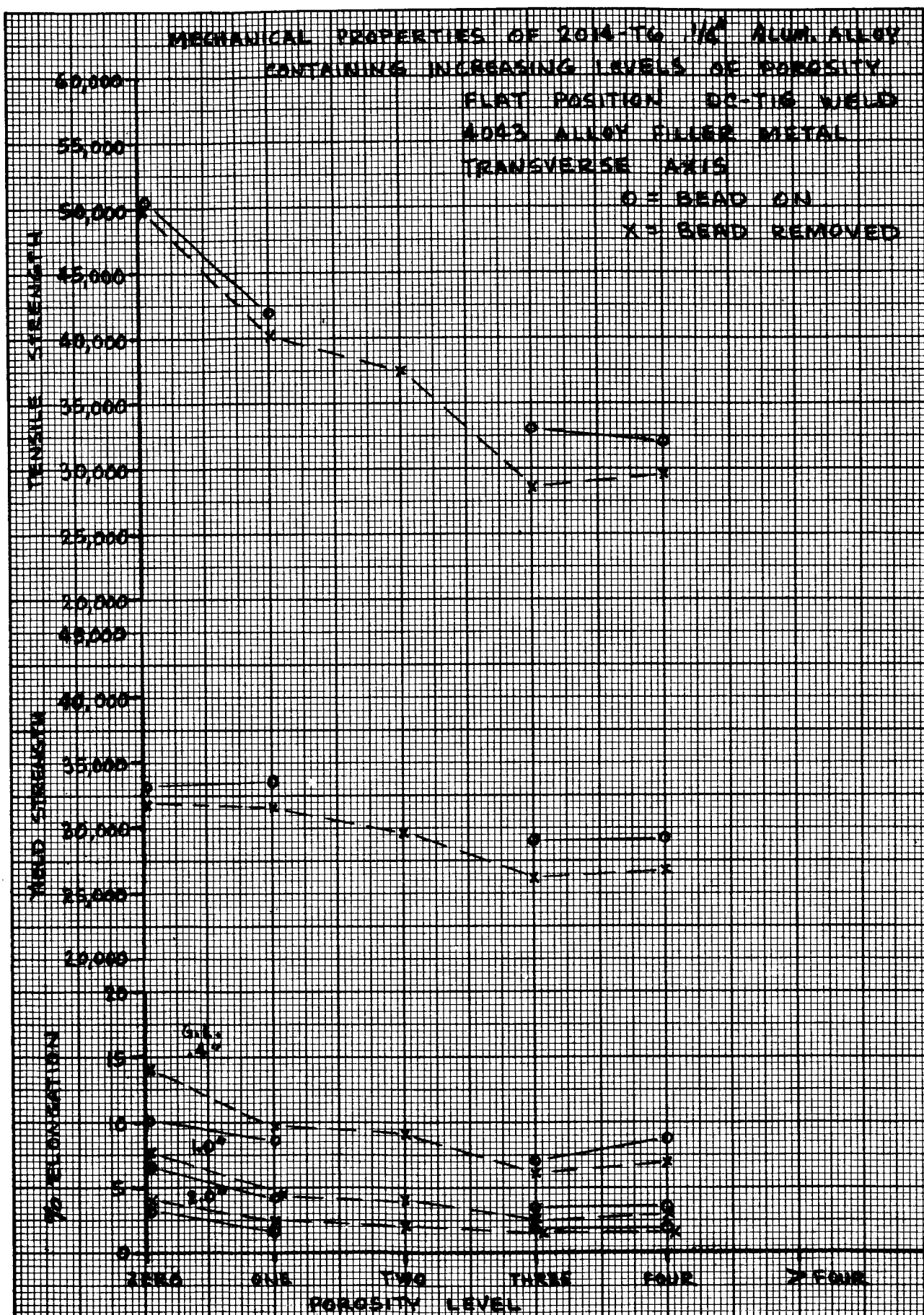
Figure 3
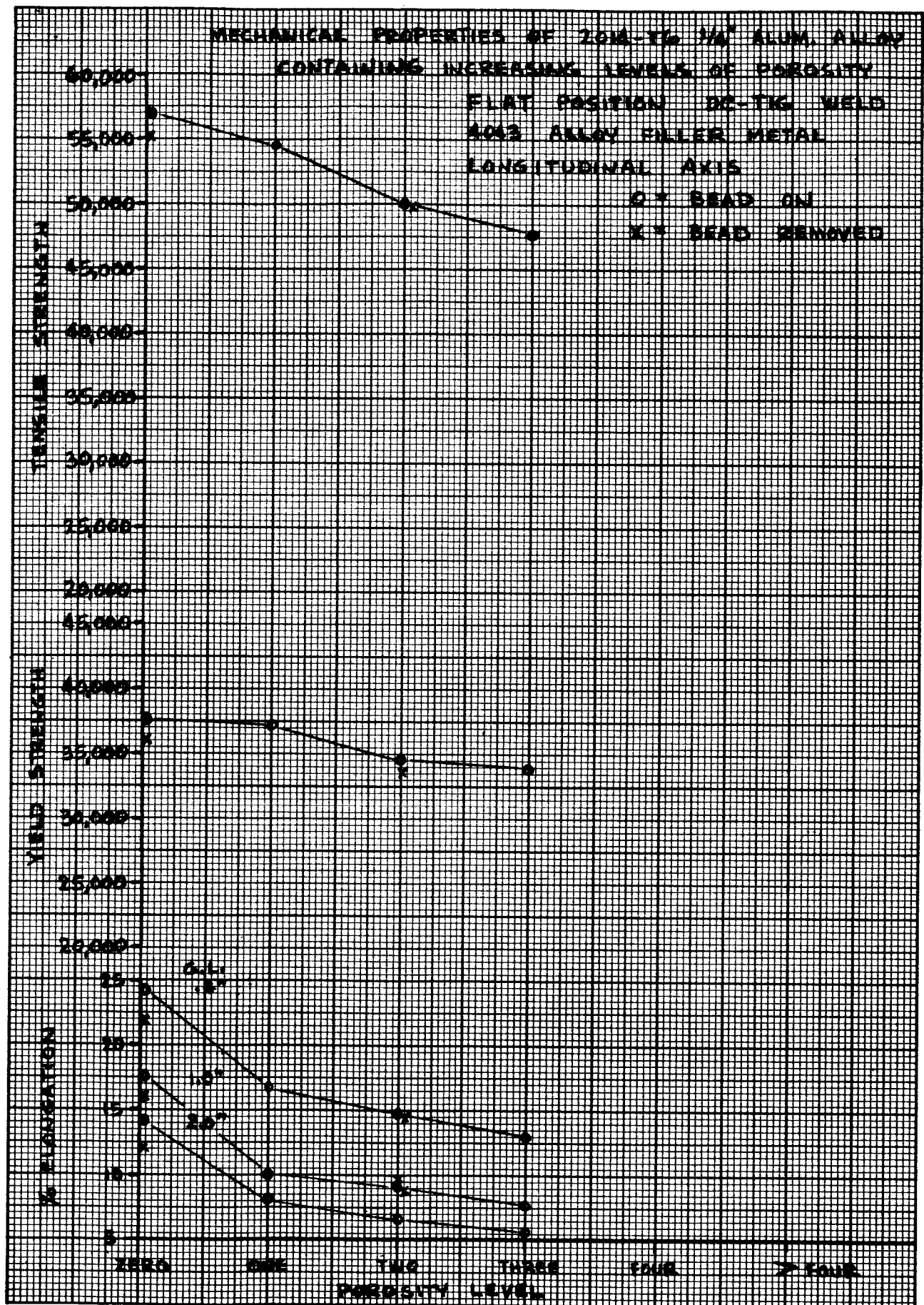
116

Figure 4

Figure 5

118

Figure 6

119

FIGURE 7

EFFECT OF POROSITY ON FATIGUE LIFE OF 5086-H31 3/16" DC TIG FLAT POSITION WELDED MATERIAL

LEGEND:

◇ — No contamination

◆ — Level 2 porosity
(50CFH hydrogen)

▲ — Level 3 porosity
(250CFH hydrogen +225°F
Dew Point)

⊕ — Level 4 porosity
(350CFH hydrogen +60°F
Dew Point)

NUMBER OF CYCLES TO FAILURE

10^3 10^4 10^5 10^6

STRESS, PSI

30,000
25,000
20,000
15,000
10,000
5,000

120
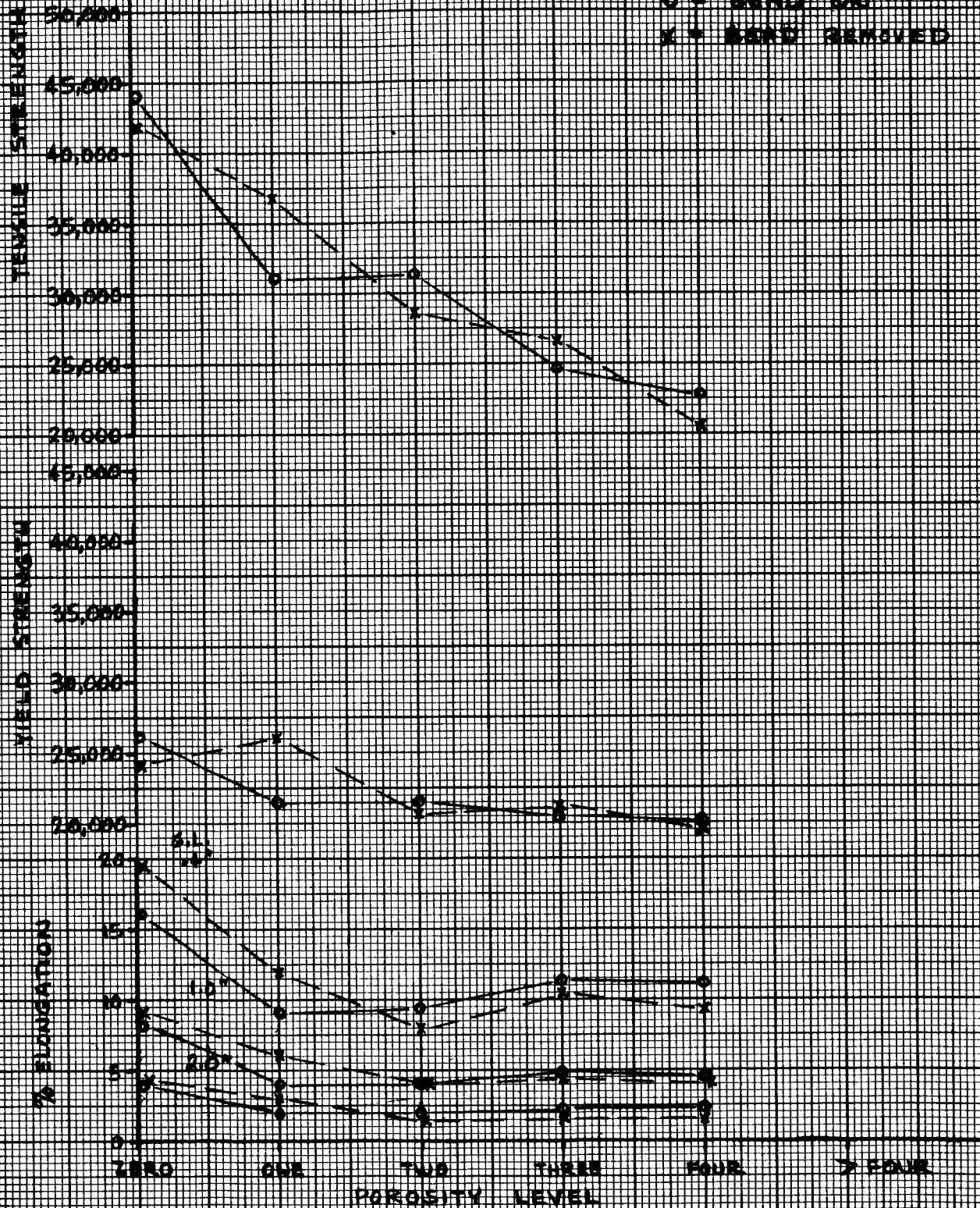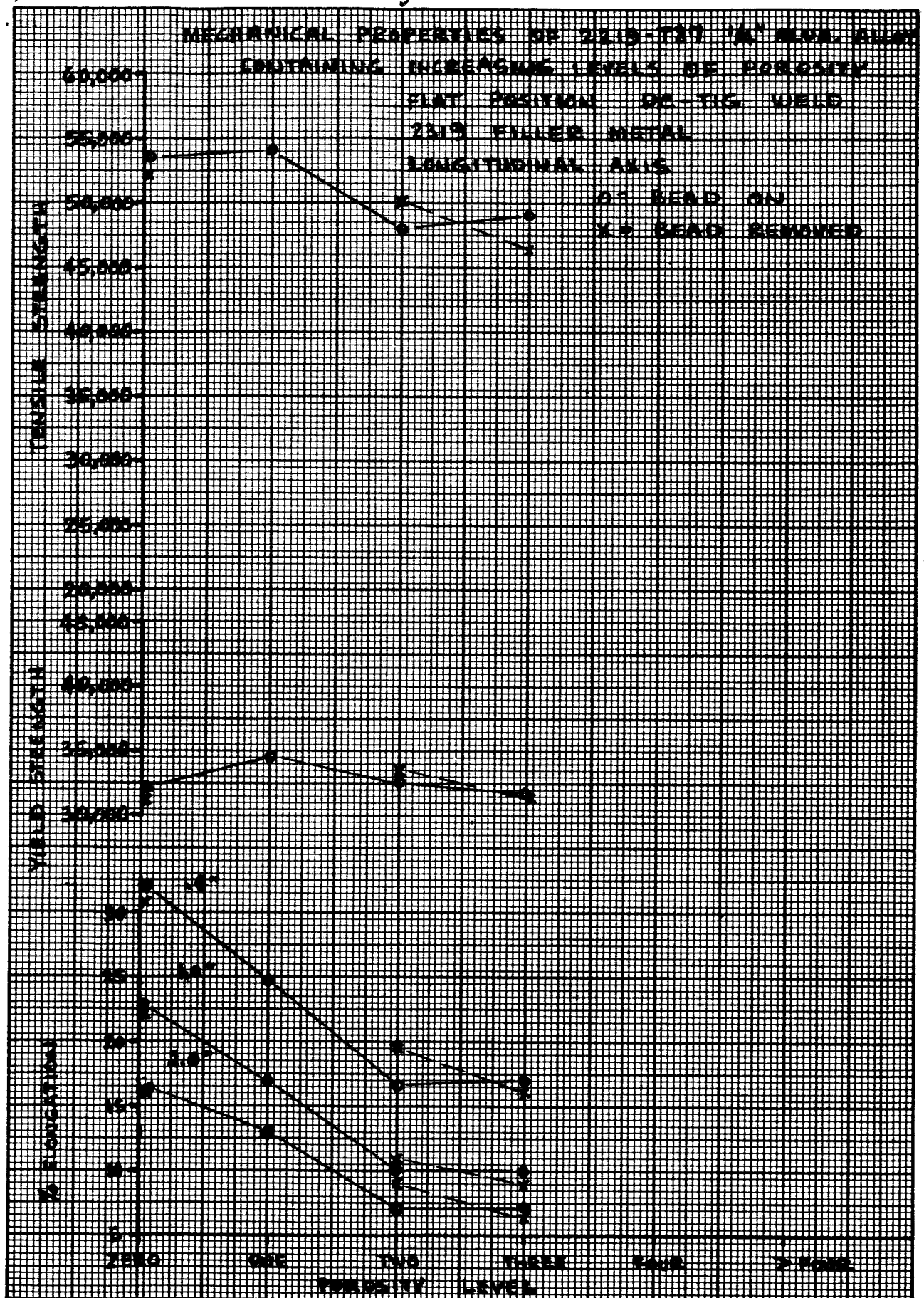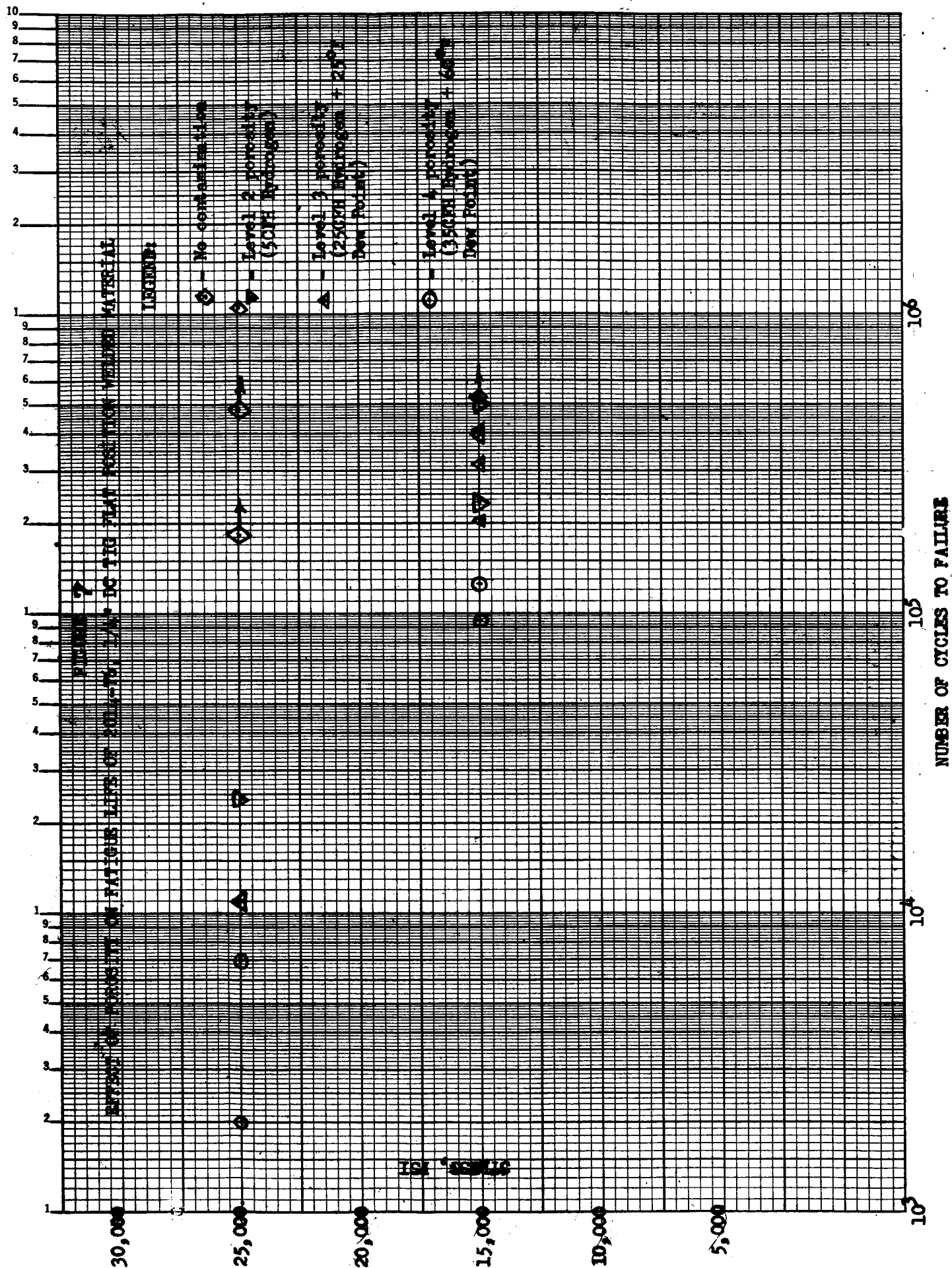
STATUS REPORT

on

A STUDY OF INERT-GAS WELDING PROCESS
TRANSFERABILITY OF SET-UP PARAMETERS
Contract NAS8-11435

to

ALUMINUM WELD DEVELOPMENT COMPLEX MEETING

GEORGE C. MARSHALL SPACE FLIGHT CENTER
NATIONAL AERONAUTICS AND SPACE ADMINISTRATION
Huntsville, Alabama

January 19, 1966

by

E. R. Seay

LOCKHEED-GEORGIA COMPANY
A Division of Lockheed Aircraft Corporation
Marietta, Georgia

MANUFACTURING RESEARCH

A STUDY OF INERT-GAS WELDING PROCESS
TRANSFERABILITY OF SET-UP PARAMETERS

PREFACE

This report is submitted by the Manufacturing Research Department of the Lockheed-
Georgia Company for presentation at the third NASA, R-ME-MW Weld Development Complex
Meeting. The investigation was conducted under contract NAS 8-11438 for the Manu-
facturing Engineering Division of Marshall Space Flight Center of the National
Aeronautics and Space Administration.

The welding portion of the program was carried out by the Manufacturing Research
Department 42-11. The radiographic inspection and evaluation was performed by
the Quality Standards and Test Laboratory, Department 58-12. The mechanical
evaluations were also carried out by the Quality Standards and Test Laboratory,
Department 58-12.

A STUDY OF INERT-GAS WELDING PROCESS
TRANSFERABILITY OF SET-UP PARAMETERS

Table of Contents

A STUDY OF INERT-GAS WELDING PROCESS
TRANSFERABILITY OF SET-UP PARAMETERS

List of Figures

* No Slide

A STUDY OF INERT-GAS WELDING PROCESS
TRANSFERABILITY OF SET-UP PARAMETERS

1. INTRODUCTION

This study of the inert-gas welding process is to determine and quantize the significance of the welding variables and to analyze the factors necessary for the successful transfer of weld settings which produce welds with similar characteristics.

Within the range of the investigation, the significance of each independent variable, and their interactions have been established for the primary responses of weld joint efficiency. The confidence limits for weld transfer have been established to be within acceptable manufacturing limits.

Conclusions from previous programs indicated several definite welding parameters that require considerable investigation if we are to be able to transfer with confidence from machine to machine and from facility to facility. To accomplish this, it has been necessary to first determine what the significant variables for each response are, and then determine the degree of control that we are able to maintain. This study is concerned with TIG and MIG welding in the horizontal position with the work insulated from the holding fixture to simulate the minimum tooling, tack-up welding technique. No hard tooling or back-up inert gas was used. The material used was 1/4", 2219-T87 and 3/4", 2219-T87 aluminum alloy. Square butt edge preparation was used for both the 1/4" and the 3/4" thickness for TIG. Square butt edge preparation was used on the 1/4" MIG weld test.

The welding programs were statistically designed so that the most meaningful data could be obtained and analyzed using computers.

A STUDY OF INERT-GAS WELDING PROCESS
TRANSFERABILITY OF SET-UP PARAMETERS

GMRI: 944
NAS 8-11435

TENSILE TEST SPECIMEN FOR
DETERMINING YIELD, ULTIMATE
AND ELONGATION.

SECTION A—A

LONGITUDINAL SECTION
SPECIMEN TO BE POLISHED
AND ETCHED FOR MACRO
EXAMINATION OF PEN —
TRATION AND WELD
QUALITY.

$X = 1"$ for 1/4
$1 \ 1/2"$ for 3/4

WELD DIRECTION

SECTION B—B

CROSS SECTION SPECIMEN
TO BE POLISHED AND ETCHED
FOR MACROGRAPHIC OR
MICROGRAPHIC EXAMINATION
OF THE WELD GEOMETRY

2"
2"
2"
10"
3"
1"

22" for 1/4 ℞
30" for 3/4 ℞

6" for 1/4 ℞
10" for 3/4 ℞

12" for 1/4 ℞
16" for 3/4 ℞
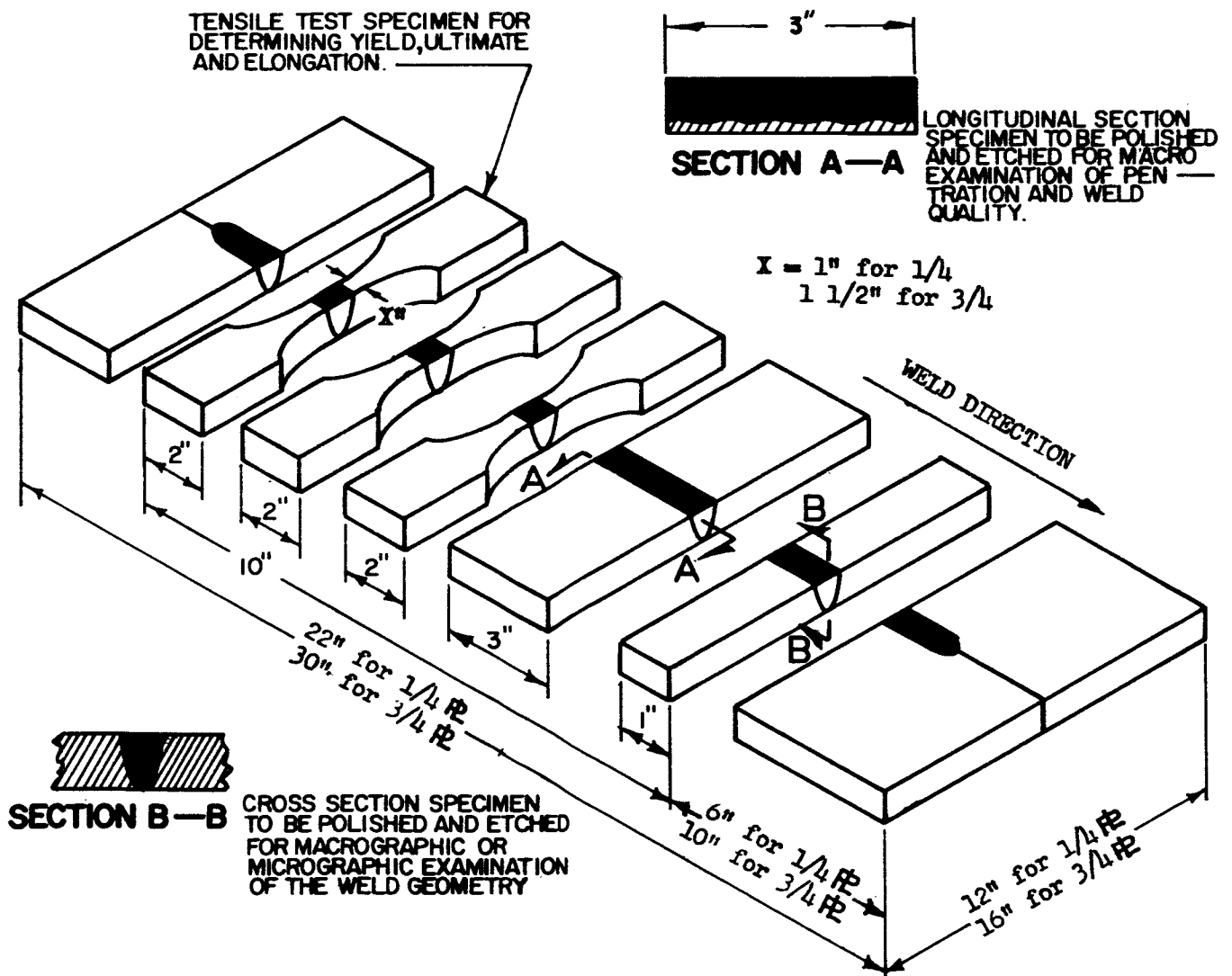
**WELD TEST SPECIMEN OF 1/4" AND 3/4" THICK 2219—T87
ALUMINUM ALLOY**

FIGURE 1 –

2. WELDING TEST PROCEDURE:

a. Facilities and Equipment

The welding units used in this project were as follows:

Welding Unit No. 1

Power	- Sciaky Model S-6 functional control 600 amperes DC welding power source.
Head	- Airco Model HME-E automatic head for the gas tungsten arc or the metallic inert arc welding system.
Carriage	- Lockheed developed all-position boom and carriage mounted on a Webb weld positioner. The carriage is controlled by a Servo-Tech tachometer feed-back governor.
Wire Feed	- Airco Model AHF-B feedrolls with Airco Model AHC-B feedback type governor control.
Instrumentation	- Texas Instrument "Servo/riter" 4 channel poten-tiometric recorder.

Welding Unit No. 2

Power	- Sciaky Model S-6 functional control 600 amperes welding power source.
Head	- Precision Sciaky (MIG - TIG) welding head with proximity head control.
Carriage	- Servo-Tech control system to operate a Lockheed designed carriage.
Wire Feed	- Airco AHC-B wire feed control with tachometer feedback governor.
Instrumentation	- Minneapolis-Honeywell "Electronic 17" four channel potentiometric recorder.

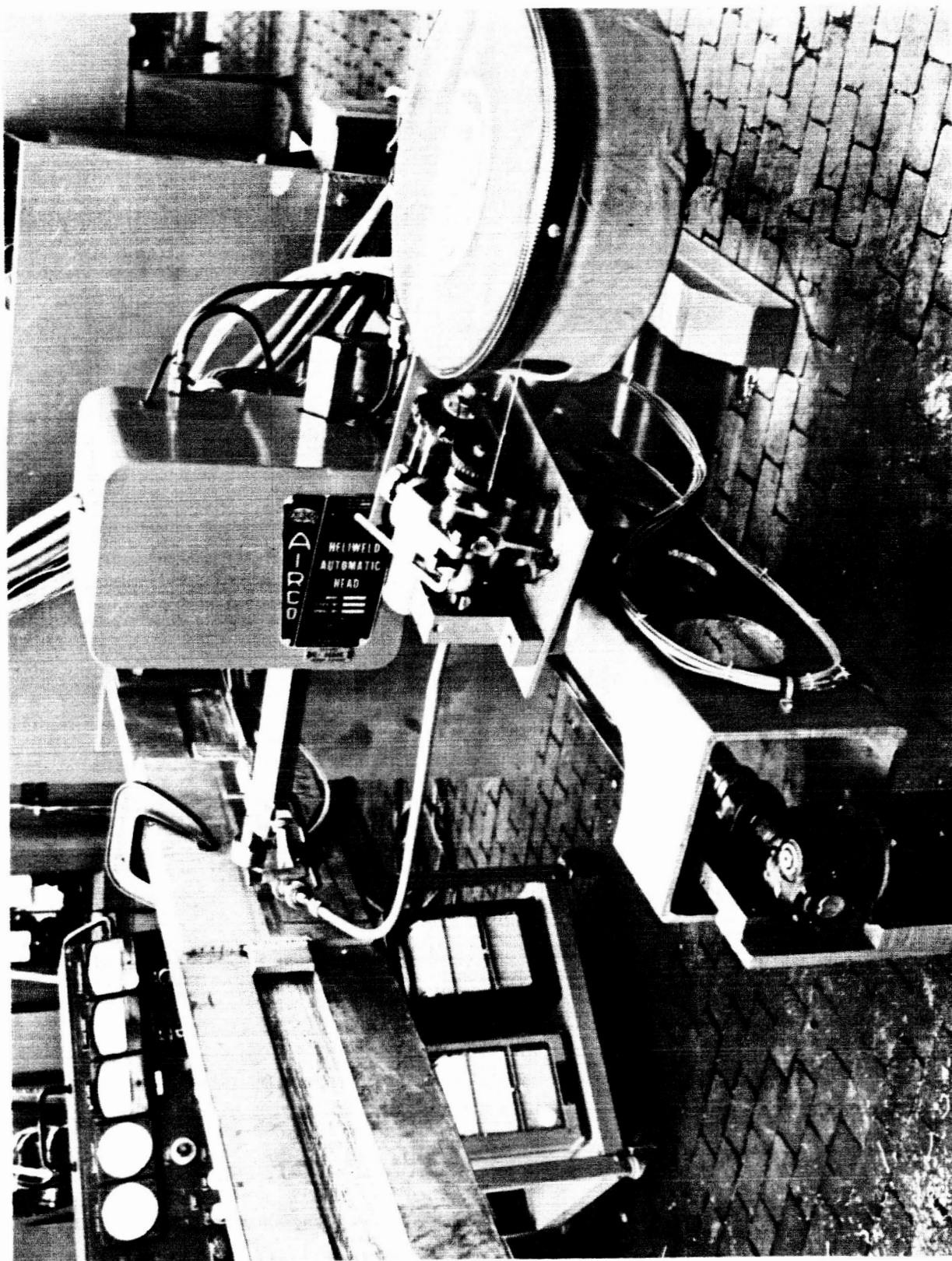FIGURE 2 - Weld Unit No. 1

A STUDY OF INERT-GAS WELDING PROCESS
TRANSFERABILITY OF SET-UP PARAMETERS

GMRI: 944
NAS 8-11435

FIGURE 3 -   Weld Unit No. 2
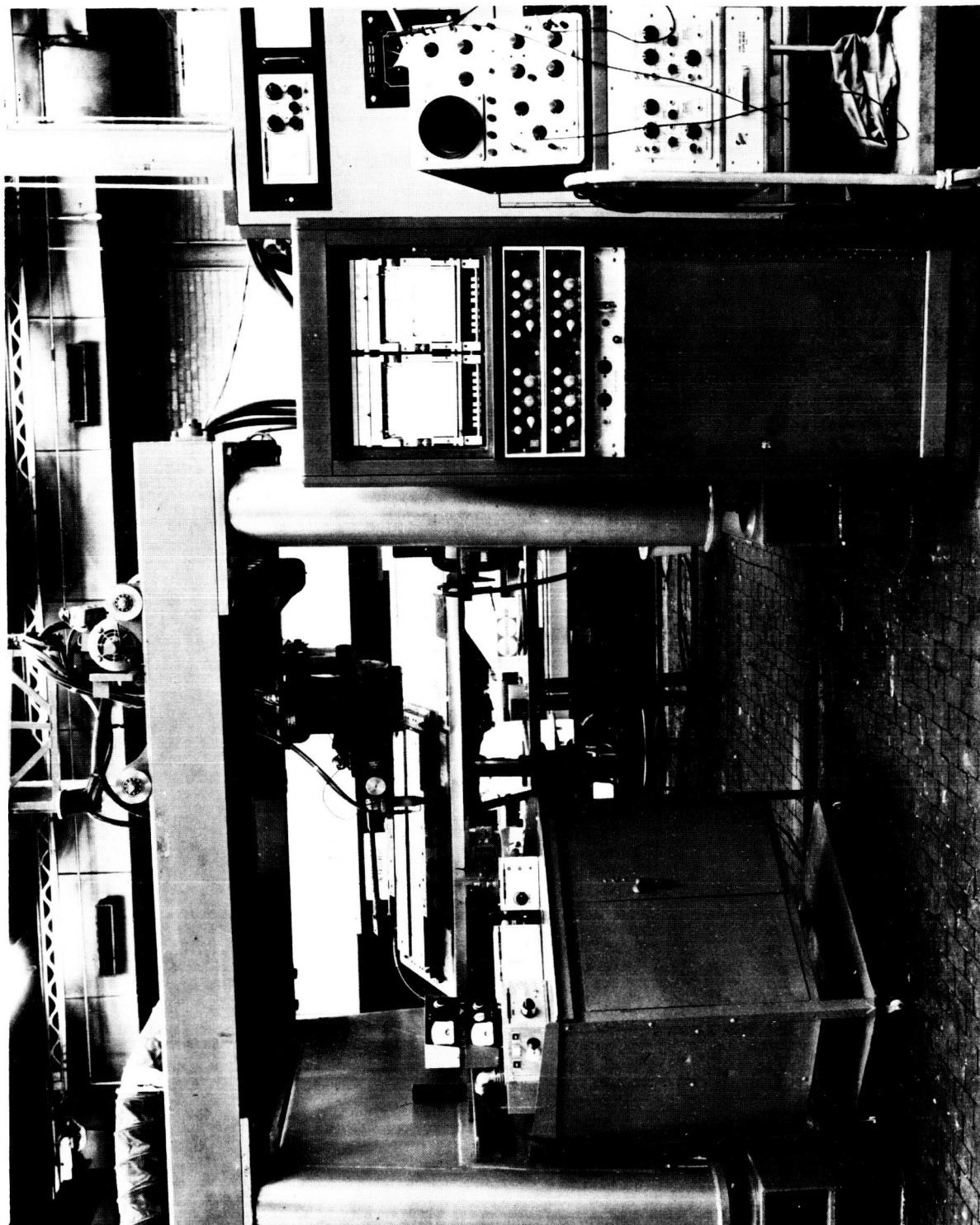
132

b. Instrumentation

Welding arc voltage is measured by potentiometric recorders. An adjustable range unit is used for suppression of 10 volts and for a chart span of 2 or 5 volts as required for the welding condition. The chart paper traveling at a speed of 6 inches per minute is ruled into 100 divisions making each division 0.02 or 0.05 volts. The instrument calibration accuracy is $\pm$ 0.30% of the span. Laboratory standard instruments, certified by the U. S. Bureau of Standards, are used for calibration checks.

Welding arc current was measured by potentiometric recorders. Normally a chart span of 5 millivolts is used and zero suppression as required. This gives a chart resolution of 0.5 amperes of welding current per chart division. A 500-ampere, 50-millivolt shunt calibrated at $\pm$ 0.5% was used. Laboratory standard instruments are used for calibration of the current measurement system.

A new system developed by Lockheed is used to continuously monitor the electrode proximity. This new system is independent of the arc voltage and is used to measure the electrode position by the potentiometric recorder on the same chart with the welding voltage. This system was used for all welds during this project.
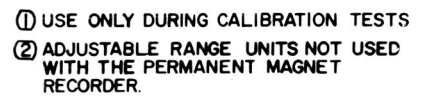
SCHEMATIC DIAGRAM OF INSTRUMENTATION SYSTEM

FIGURE 4 -

A STUDY OF INERT-GAS WELDING PROCESS
TRANSFERABILITY OF SET-UP PARAMETERS

GMRI: 944
NAS 8-11435

FIGURE 5 - Four Channel Potentiometric Recorder

c. Electrode Proximity Recording System

It is necessary to better understand the relationship between the welding
voltage or arc length control of the TIG process and the proximity of the
torch to the work. They system developed during this phase will contin-
uously record the head proximity and movement during the welding process.

The electrode proximity recording system uses an induction cartridge type
gage that is actuated by a bell crank responding to movements of the auto-
matic welding head, (see Figure 6).

The system uses a 5,000 cps power supply amplifier and a deviation in-
dicating meter. The system also includes a trace recording of these
signals during welding.

d. Temperature of the Weld Puddle

The relationship between the temperature of the weld puddle and the time
at temperature was studied. A method of taking a single point temperature
envelope measurement of the weld was devised. For this measurement a
thermocouple is attached to the back side in the center of the joint.

As shown on the temperature recorder trace, the maximum temperature (MT)
is indicated by the maximum point on the trace curve. The time at tem-
perature (TT) is measured directly off of the recording trace as a
function of chart speed. The total time as well as the area of the
temperature trace envelope was taken above the 450°F level. This tem-
perature was chosen as the probable beginning of metallurgical change.

A STUDY OF INERT-GAS WELDING PROCESS
TRANSFERABILITY OF SET-UP PARAMETERS

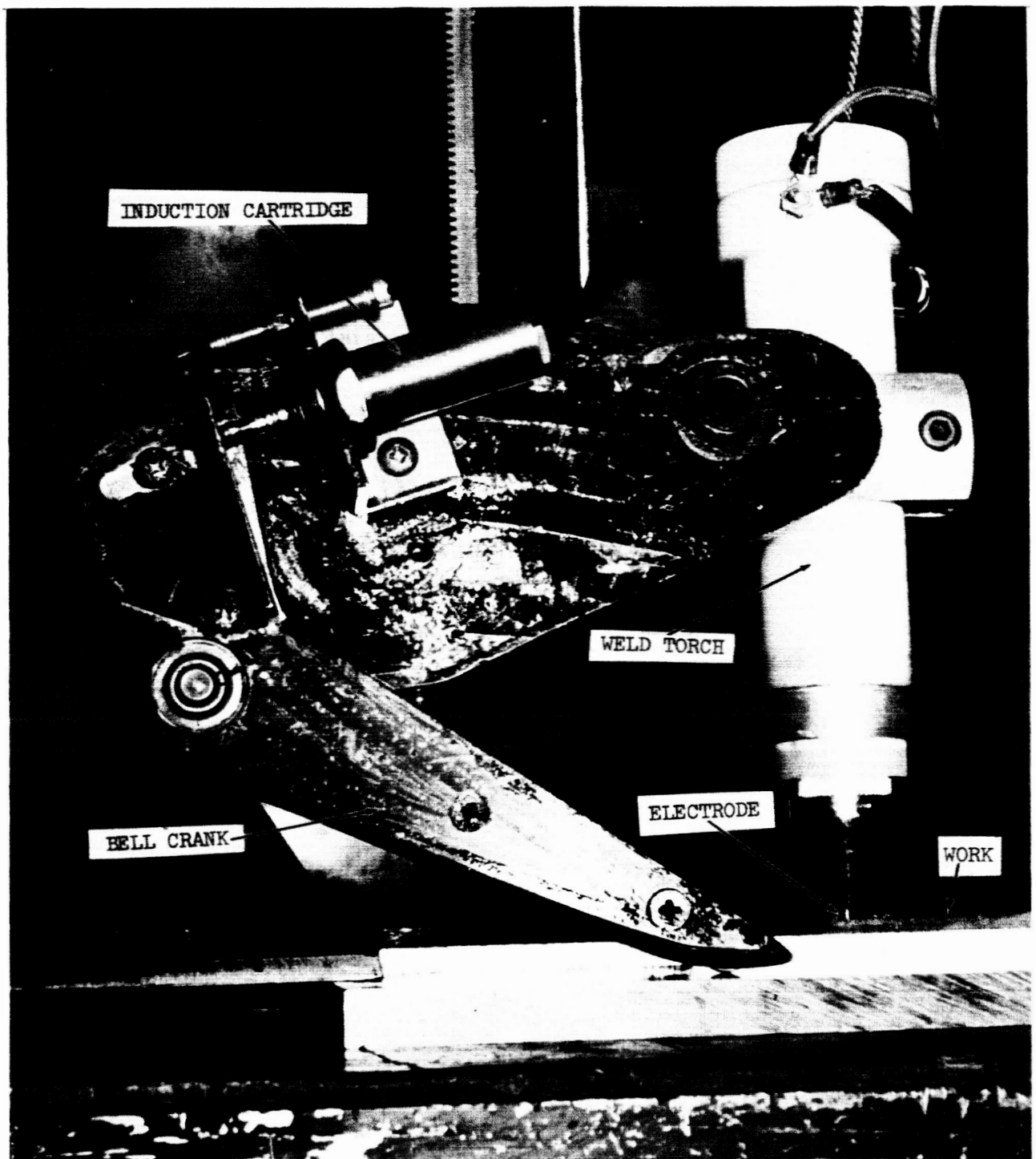FIGURE 6 –   Head Used for Recording Electrode Proximity to Work

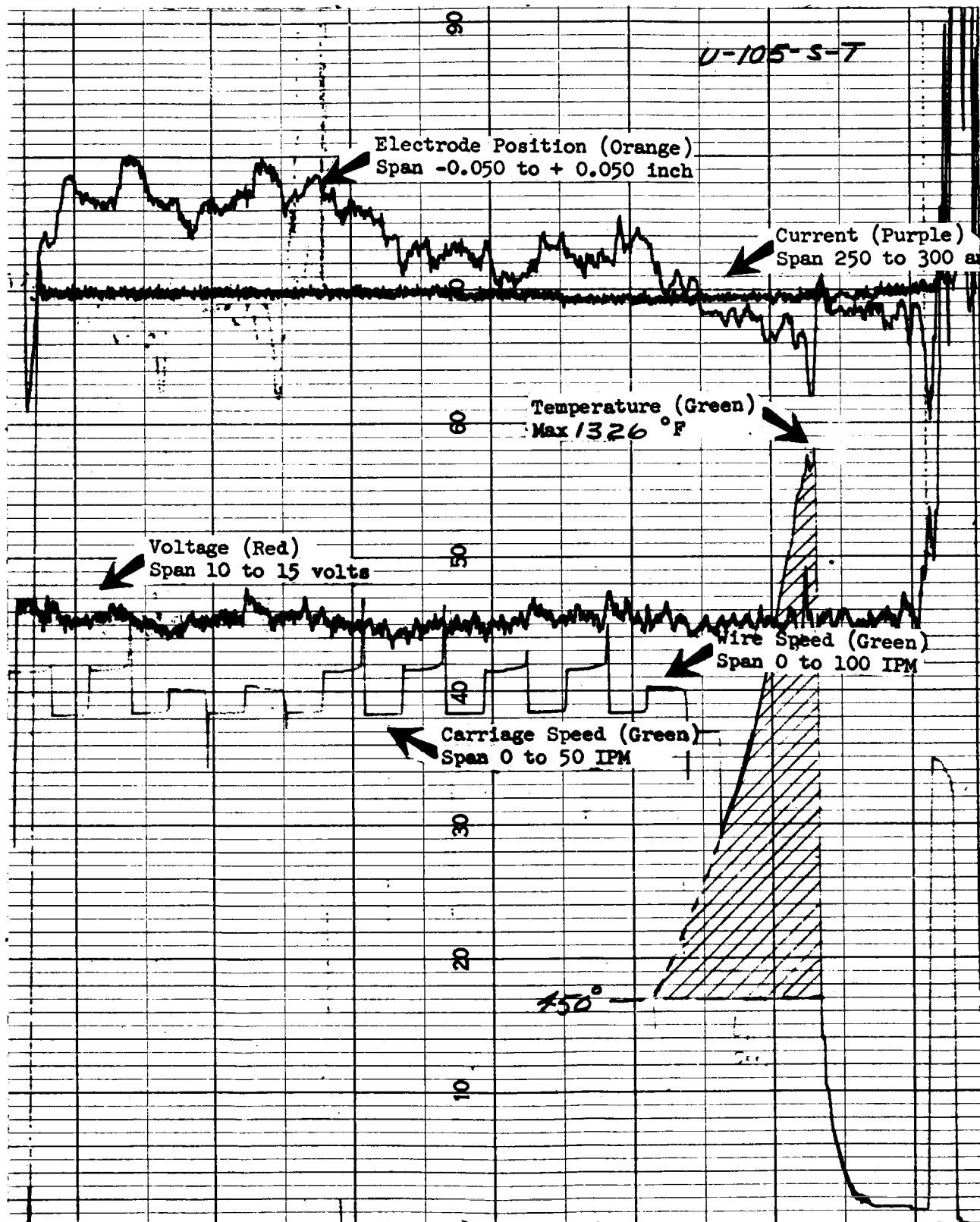FIGURE 7 - Temperature Recorder Trace

FIGURE 8 -

b. Porosity Grading System

Several methods of evaluating the weld porosity shown by an X-ray have been studied, but none produced a numerical system that may be used in the Lockheed Computer Programs. Therefore, a new method of grading this porosity was developed for this purpose. The new method utilizes a ten inch long plastic grid of 100 black and 100 transparent strips, .050 inch wide. The grid is placed over the X-ray film at the zone to be evaluated. With the strips perpendicular to the weld, only the ten inch length of weld from which the specimens are taken is graded. Each transparent strip showing porosity is counted. This count, from 1 to 100, is the data used in the computer program for evaluation.

3. WELDING PARAMETER CONTROL DEVELOPMENT:

a. TIG Welding Control Studies

During many tests, the electrode position was held constant. With this
condition the voltage was erratic and there was an erratic depth of
penetration. However, when the voltage was held constant with an auto-
matic voltage control head, the electrode position was erratic and equally
erratic penetration measurements resulted.

It was concluded that present automatic voltage head control or constant
electrode position control alone do not adequately maintain process control
of the welding arc and molten puddle. Another control system must be
applied to hold a constant electrode position (Ep) in addition to a
constant current (C), constant voltage (V), carriage travel speed (T),
and filler wire deposit rate (Wd).

The wire feed system presently used is reasonably accurate and reliable,
therefore, no attempt was made to couple this system to the other systems
influencing the welding arc process. All of the systems used, in various
ways, incorporated the other four welding variables. All of the systems
were designed to be regulated by equipment settings and still maintain process
control of the welding arc and the molten puddle. Cross coupled feed-back
controls are defined as controls used for measuring the response of one
variable and to simultaneously change the settings of another variable.
For example, a change in Ep causes a change in C. Self coupled feed-back
controls are defined as controls used to measure the response of a
variable and to adjust the controls of that same variable until the

140

WELDING PARAMETER CONTROL DEVELOPMENT: (Continued)

TIG Welding Control Studies (Continued)

response agrees with the desired set-point. For example, if Ep deviates

from the set-point, the error is measured on the recorder, amplified and

used to operate a servo system bringing Ep back to the set-point. The

basic difference in these two feed-back systems is the source of the

feed-back information. The cross-coupled system depends upon the response

of another variable caused by a change in the welding process, while the

self-coupled system is a direct measurement of the response, independent

of all other variables necessary to make up the welding process.

Six welding control systems have been examined with various results. The

first three systems have been evaluated and are considered inadequate for

accurate control of the welding process. Tests with the last three systems

indicate that they may be capable of maintaining process control of the

welding arc and the molten puddle. Further development will be required.

1. Automatic Voltage Control Head

    C - Self-coupled feed-back when using a function control power supply.

    V - Cross-coupled feed-back to adjust Ep.

    T - Self-coupled feed-back from a tachometer.

    Ep - No coupled feed-back, completely dependent upon the voltage
          control system.

Results:

Ep assumes any position and is allowed to wander if the voltage control

is satisfied. Although this system is in wide use it is considered

inadequate for accurate control of the welding process.

WELDING PARAMETER CONTROL DEVELOPMENT: (Continued)

TIG Welding Control Studies (Continued)

2. Automatic Electrode Position Control

C — Self-coupled feed-back when using a function control power supply.

V — No coupled feed-back, directly dependent upon Ep control system.

T — Self-coupled feed-back.

Ep — Self-coupled feed-back from sensing element to maintain constant position of the electrode in respect to the work surface.

Results:

Voltage wanders causing appreciable changes in penetration and geometry

of the melt zone.

3. Carriage Control Coupled to Electrode Position

C — Self-coupled feed-back.

V — Cross-coupled feed-back to adjustment of Ep to control voltage.

T — Cross-coupled feed-back directly coupled to Ep for speed control.

Ep — No coupled feed-back indirectly dependent upon voltage control system.

Results:

Wild fluctuations in carriage travel speed without changing other variables

in the welding process. This system was discarded.

WELDING PARAMETER CONTROL DEVELOPMENT: (Continued)

TIG Welding Control Studies (Continued)

4. Current Control Coupled to Electrode Position

C - Cross-coupled feed-back, directly coupled to Ep movements for control of current.

V - Cross-coupled feed-back for adjustment of Ep to control voltage.

T - Self-coupled feed-back.

Ep - No coupled feed-back, directly dependent upon voltage control system and will indirectly respond to change in current.

Results:

An evaluation of this system was made with the "classic" experiment and

the 3/4" central "composite" experiment.

5. Current Control Coupled to Voltage

C - Cross-coupled feed-back, directly coupled to voltage changes for control of the current.

V - No coupled feed-back, directly dependent upon Ep control system and will indirectly respond to a change in current.

T - Self-coupled feed-back.

Ep - Self-coupled feed-back.

Results:

Response of this system is dependent upon changes in the welding arc and

the molten puddle to control two weld variables. These changes are slow

and allow the equipment to "hunt". Evaluation of this system is incomplete.

WELDING PARAMETER CONTROL DEVELOPMENT: (Continued)

TIG Welding Control Studies (Continued)

6. Self-Coupled Feed-Back

C - Self-coupled by Silicon Control Rectifiers.

V - Self-coupled by a voltage regulator.

T - Self-coupled by tachometer.

Ep - Self-coupled by sensing element.

Results:

The function control constant current power supply senses a voltage change

to control the SCR and maintain a constant current. The system was not

compatible with the voltage regulator available. Evaluation of this system

is incomplete.

b. Electrode Position Alignment and Distance from Work

During the first test series of horizontal welds, the electrode was centered over the joint, however the cross section after welding clearly indicates that the melt zone is not symmetrical about the center line of the electrode. In fact, the point of maximum penetration is approximately 0.075 inch above the electrode center line. For several specimens having complete penetration all the joint was not covered by the melt zone. During all further welding of 1/4 inch thick material the electrode was centered 0.075 inch below the joint. Additional tests were conducted to further evaluate this phenomenon.

A possible explanation has been determined to explain the cause of the nonsymmetrical melt zone pattern of horizontal welds.

During the weld process, molten metal flows from the top of the arc cavity to the lower side. Thus the top plate is continuously exposed to the arc while the bottom plate is insulated by the molten metal. Also, the resistance of arc plasma is extremely low. When the arc is allowed to radiate there is very little inducement for the arc to go to the nearest point. These two conditions cause the melt pattern to be non-symmetrical about the electrode and will cause the point of deepest penetration to be above the centerline of the electrode. This distance above the electrode centerline seems to decrease with the depth of penetration. The type of melt obtained by the arc also will change this

Electrode Position Alignment and Distance from Work (Continued)

distance as noted in the 3/4 inch thick material. Tracings of welds U178ST

A&B and U158ST A&B are typical examples showing two different types of melts

and the change in location of the point of deepest penetration.

For all of the 3X photograph cross section tracings shown in this report,

the electrode was centered over the joint (dash line ending at the original

material surface). The electrode position and tip diameter are also shown

by the "U" shaped bracket.

Although some welds appear to overlap, the overlap is, in fact, intermittent

with some "gaps" of unfused material occurring along the length of the welds.

For several welds, U154ST for example, overlap was indicated by the cross

section, but the melt zone did not cover the joint. This condition cannot

be detected in the X-ray nor was it observed during the first 3X photo-

graphic examination of the cross section. This condition, however is very

apparent in the fracture surface of the tensile test specimen.

One source of erroneous data has been the nonsymmetrical melt zone. Close

examination of several tensile test fractures and the cross section re-

vealed that approximately .100 inch of the joint was not fused by the

melt zone. Consequently, the tensile strength data from these 3/4 inch

thick specimens were low.

CROSS-SECTION OF $\frac{1}{4}$-INCH WELD
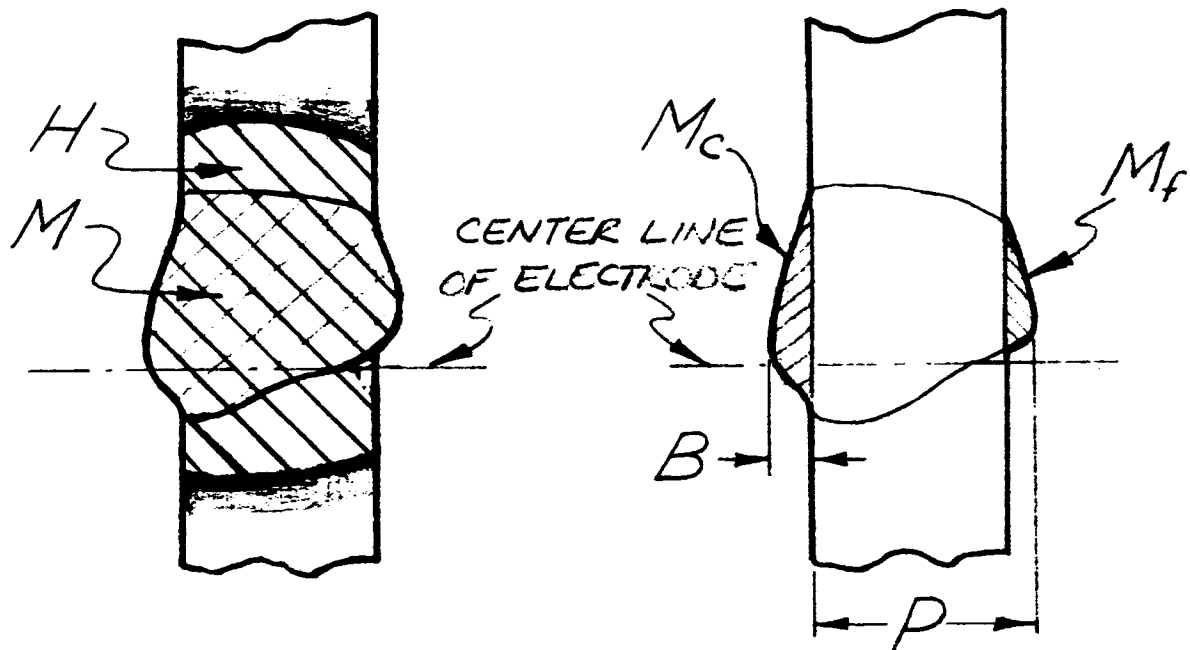
H — CROSS-SECTION, HEAT-AFFECTED AREA.

M — CROSS-SECTION, TOTAL MELT AREA.

M_c — CROSS-SECTION, AREA OF CROWN.

M_f — CROSS-SECTION, AREA OF FALL-THROUGH.

B — HEIGHT OF CROWN.

P — PENETRATION OF MELT ZONE FROM PART SURFACE.

FIGURE 9 –

Electrode Position Alignment and Distance from Work   (Continued)

Another phenomenon observed during this series of tests that required
additional investigation was the relationship of the electrode position
and depth of penetration. Several specimens had considerably deeper pene-
tration on one side than on the other. The welds on each side were set up
with identical weld parameters and examination of recordings confirmed that
setups were accurately established. In several cases the second weld had
less penetration than the first weld. However, in additional tests, the
reverse was indicated. In these welds, the electrode position was noted
to be deeper in the welds with less penetration. The electrode position
for these welds was controlled by the automatic head to maintain a constant
arc voltage regardless of the electrode position. In every case the arc
voltage recordings were stable and accurately controlled at the correct
settings.

There is considerable evidence from previous experience indicating that a
deep electrode position is associated with deep penetration. However, the
evidence obtained during this project has indicated that the electrode
position variation recorded for any given weld setting (voltage, current,
travel speed) using automatic voltage control is an indication of vari-
ations in penetration. The deeper electrode positions result in less
weld melt penetration.

<u>Electrode Position Alignment and Distance from Work</u> (Continued)

It may be concluded that; (1) with a given welding setup and with automatic voltage control the deeper electrode position indicates a hemispherical arc cavity has developed and will result in a reduction of penetration, and (2) penetration due to changes in electrode position were as great as the changes caused by the classic parameters.

c. <u>Inert Gas Flowmeter</u>

A calibration check of the flowmeters currently used indicated a 200% error. The regulators and flowmeters were immediately discarded and a two stage regulator was installed with a more accurate flowmeter.

d. <u>Torch Resistance Variation</u>

The electrical resistance of the welding torch can cause errors in the welding set-up parameters. A method of measuring the error was developed which utilizes a tungsten electrode with one end silver soldered to a copper block and the other end inserted in the welding torch. A current simulating the welding arc is passed through the torch, electrode and copper block. Four potentiometric recorders are used to record the voltage drop through the torch, electrode and the total drop through both the torch and the electrode. The fourth recorder is used to measure the simulated welding current. Using Ohm's law the resistance of the torch may be computed from these recordings. Data taken by this method shows a wide variation and an inconsistancy in electrical resistance of the welding torches tested. This variation can cause variation in the welding set-up parameters.

Torch Resistance Variation (Continued)

This problem was eliminated by designing and building a high current, low

and consistent resistance torch. This Gelac torch was used throughout the

program.

e. Shielding Gas Contamination

The analysis of the helium shielding gas indicated that 19 of the 20

cylinders would be classified as low contamination. The gas contamination

of one cylinder exceeded the capability of the measuring equipment. Eight-

teen cylinders were deliberately contaminated with ambient air and were

used for the high and medium levels of shielding gas contamination during

the various weld test.

f. Welding Test Program

During the test program, "Significance of the Variables and Transferability",

there were three separate statistically designed weld experiments con-

ducted and many separate data points established covering 1/4" and 3/4"

2219-T87 aluminum. The data has been divided into several data sets for

analysis of the variables versus the important responses such as weld

joint performance, penetration and radiographic quality.

The original variables were chosen as the most probable having any

significant influence on the strength and quality of the weld joint and

the control of the welding process.

A STUDY OF INERT-GAS WELDING PROCESS
TRANSFERABILITY OF SET-UP PARAMETERS

Welding Test Program   (Continued)

Since the electrode position (Ep) is now recognized to be another welding set-up parameter that must be controlled in order to predict the weld penetration, it was added to the regression analysis computer program as an input variable. The equations now produced for predicting ultimate strength (Ftu), yield strength (Fty), area of melt zone (M), area of heat affected zone (H), and penetration (P), are much more accurate than previous equations in which Ep was not employed as an input variable.

The experiments using 1/4", 2219 TIG process data are divided into two data sets. The first data set treats weld back bead temperature as an independent variable, along with current, voltage, weld travel speed, shielding gas purity, temperature of the weldment, electrode position and electrode tip diameter. By this treatment the relationship between weld bead temperature and ultimate strength could be analyzed. In the second 1/4" data set, weld bead temperature is treated as response or dependent variable.

The 3/4" data has been divided into four data sets. The first consists of a one-sixteenth fractionally replicated factorial design at two levels, in which current, voltage, weld travel speed, wire deposit, gas purity, gas flow, temperature of the weldment, electrode position, and electrode tip diameter were treated as independent variables.

A STUDY OF INERT-GAS WELDING PROCESS
TRANSFERABILITY OF SET-UP PARAMETERS

Welding Test Program (Continued)

The second 3/4" data set consists of a central composite rotatable design,
which treats current, voltage, travel, wire deposit, weldment temperature,
and electrode position as independent variables.

The third 3/4" data set consists of welds treating current, voltage, weld
travel, and electrode position as independent variables. This data set is
to determine the confidence limits when only these four basic variables
are evaluated.

The fourth data set is a composit of all data on 3/4" TIG.

Computer Analysis

Each data set was fitted to a polynomial of up to ten variables by the method
of least squares. This analysis was accomplished by using an I.B.M. 7094
step-wise multiple regression program with variable transformation.

An "F" level may be chosen so that only significant variables are included
in the final regression to any desired level of confidence. Each equation
was developed for a 90% or 95% confidence level.

A STUDY OF INERT-GAS WELDING PROCESS
TRANSFERABILITY OF SET-UP PARAMETERS

GMRI: 944
NAS 8-11435

WELD SEQUENCE	C	V	T	Wd	GP	Gf	°F	J	D
1	L	L	L	H	L	H	L	L	H
2	H	L	L	H	L	H	H	H	L
3	M	M	M	M	M	M	M	M	M
4	L	L	L	L	H	H	L	H	L
5	L	H	L	L	H	L	L	L	H
6	L	L	H	H	H	L	L	H	H
7	H	L	L	L	H	H	H	L	H
8	L	H	H	L	L	H	L	H	H
9	H	H	L	H	L	L	H	L	H
10	M	M	M	M	M	M	M	M	M
11	L	H	L	H	H	H	H	H	H
12	L	H	H	L	H	L	H	H	L
13	H	L	L	L	L	L	L	L	L
14	L	L	L	H	H	L	H	L	L
15	L	H	L	L	L	H	H	L	L
16	H	H	H	H	L	L	L	H	L
17	L	H	H	H	L	L	H	L	H
18	L	L	L	L	L	L	L	L	L
19	L	L	H	L	H	H	H	L	H
20	M	M	M	M	M	M	M	M	M
21	H	H	H	L	L	H	H	L	L
22	H	H	L	H	H	H	L	L	L
23	L	H	H	H	H	H	L	L	L
24	H	L	H	L	L	L	H	H	H
25	L	L	H	H	L	H	H	H	L
26	M	M	M	M	M	M	M	M	M
27	L	L	H	L	L	L	L	L	L
28	H	H	H	L	H	L	L	L	H
29	H	L	H	H	L	H	L	L	H
30	H	L	H	H	H	L	H	L	L
31	L	L	L	L	L	L	H	H	H
32	H	L	L	H	H	L	L	H	H
33	H	L	L	H	H	L	H	H	L
34	H	L	H	L	H	H	L	H	L
35	L	L	L	H	H	L	L	H	L
36	H	H	L	L	L	H	L	H	H

FIGURE 10 – Experimental Design 1/4" Data Sets 1 & 2, and
3/4" Data Set 1

TUNGSTEN ARC WELD 2219 – T87 ALLOY
3/4" THICK   DATA SET 1

	CODE LETTER	HIGH	MEDIUM	LOW	UNITS FOR COMPUTER
ARC CURRENT	C	4.40	4.20	4.00	AMP/100
ARC VOLTAGE	V	11.5	11.35	11.2	VOLTS
TRAVEL SPEED	T	10	9	8	I.P.M.
WIRE DEPOSIT/IN. OF WELD	Wd	.3835	.1817	0	IN^3 x 100/IN.
GAS PURITY	GP	1.50	0.90	0.30	PPM /100
GAS FLOW	G_f	1.25	1.00	0.75	scfh/100
INDICATED FLOW		1.54	1.21	.88	
WORK TEMPERATURE	°F	1.50	1.13	.75	°F/100
JOINT GAP	J	.020	.010	0	INCH
ELECTRODE TIP DIAMETER	D	.135	.122	.108	INCH

FIGURE 11 –

4. REGRESSION ANALYSIS SUMMARY

The IBM 7094 computer print-out of the multiple step-wise regression analysis is presented in summary form for each problem.

For example; the analysis sheet for 3/4", Data Set 1, Ftu vs. Weld Set-up (Table 27) shows that variation of ultimate strength is analyzed with respect to the independent welding variables of current, voltage, wire deposit, gas purity, temperature of the weldment, electrode position and electrode tip diameter.

There were 35 data points in this experiment as indicated by the "number of data" notation. An "F" level was chosen to insure, with at least a 90% probability, that any variable entered into the regression equation is valid.

The standard error (standard deviation) of Y, is used to determine the confidence interval or confidence limits of the predicted Ftu. In the problem in this example the standard error is 4.6187. The predicted value for Ftu is computed from the regression equation.

$$Ftu = -.41018 \text{ (V.T.)} + 2.00715 \text{ (GP. °F)}$$
$$+733.384 \text{ (Ep. D)} +78.09681$$

If   Voltage (V) = 11.5 volts
Travel (T) = 8.0 I.P.M.
Gas Purity (GP) = 10 parts/million
Temperature of Weldment (°F) = 75°F
Electrode position above work (Ep) = .040"
Electrode Tip Diameter (D) = .1215"

Then   Ftu = 44.226 KSI is predicted.

This is shown in the Ftu table for this problem.

REGRESSION ANALYSIS SUMMARY (Continued)

The confidence limits for a predicted value of Ftu of 44.226 is calculated

as follows:

Confidence limits = $44.226 \pm S (t)$

Where "t" is obtained from the "t" distribution table for a particular con-

fidence level. The "Z" is chosen for the confidence level desired such as

90%, 95%.

For 90% confidence level the lower confidence limit = 44.226 - 4.6187 (1.28)

$$= 44.23 - 5.91$$

$$= 38.32$$

At the 95% confidence level the lower confidence limit = 44.226 - 4.6187 (1.65)

$$= 44.23 - 7.52$$

$$= 36.66$$

At 99% confidence level the lower confidence limit = 44.226 - 4.6187 (2.34)

$$= 44.23 - 10.76$$

$$= 33.47$$

This implies for instance that for the 90% confidence limit, there is a 90%

probability that all welds, made at these settings and under the same con-

ditions will have an ultimate strength above 38.32 KSI.

The coefficient of determination, which is the square of the multiple

correlation coefficient, in this example is 74%. This indicates that the

regression equation accounts for 74 percent of the variation observed in

the response, Ftu. The variation not accounted for in the equations may be

due to significant variable not included in the test, experimental error, or

an incorrect assumption of the mathematical model.

REGRESSION ANALYSIS SUMMARY   (Continued)

The sum of the partial derivatives of each of the variables presented in the
regression are presented in the regression analysis summary sheet. The solution
of any one of the derivatives shows, in terms of the units used in the welding
process, the effect of varying that variable. This is a good way to evaluate
the significance of that variable as related to our ability to control that
variable. This may be presented in tables and graphs for the important re-
sponses such as ultimate strength and penetration.

Note that only the terms containing a change in the weld parameter remain in
the equation. If there is no change in the other parameters, the derivative
is zero and the term drops out.

The Beta coefficient for each term in the regression indicates the order of
statistical significance of the variables with no units involved.

It is understood that the variable that is the most significant statistically
may not be the most important or most significant variable from the standpoint
of control of the process. For example a variable that is of low statistical
significance may be the variable of most concern if that variable is out of
control.

A STUDY OF INERT-GAS WELDING PROCESS
TRANSFERABILITY OF SET-UP PARAMETERS

STEPWISE REGRESSION
Ftu vs. C, V, T, Wd, Gp, Gf, °F, Ep, D
3/4" 2219 TIG Horizontal

NO. OF DATA	35
NO. OF VARIABLES	55
WEIGHTED DEGREES OF FREEDOM	35.00
F LEVEL TO ENTER VARIABLE	4.130 - 95%
F LEVEL TO REMOVE VARIABLE	4.130 - 95%

F LEVEL	5.1019
STD. ERROR OF Y	4.6187
MULTIPLE CORRELATION COEFFICIENT	0.86120
COEFFICIENT OF DETERMINATION	74%

VARIABLE	COEFFICIENT	STD. ERROR
(V·T) Voltage·Travel	- .41018	.07189
(Gp·°F) Gas Purity·°F	2.00715	.88862
(Ep·D) Elect.Position·Tip Diam	733.38416	184.69308

CONSTANT = 78.09681

$$Ftu = -.41018(V \cdot T) + 2.00715(Gp \cdot °F) + 733.3842(Ep \cdot D) + 78.09681$$

$$\begin{aligned}
dFtu = &-.41018(V)dT \\
&-.41018(T)dV \\
&+2.00715(°F)dGp \\
&+2.00715(Gp)d°F \\
&+733.3842(Ep)dD \\
&+733.3842(D)dEp
\end{aligned}$$

CONFIDENCE LIMITS FOR CONFIDENCE LEVELS OF:

90% >Ftu - 5.91
95% >Ftu - 7.57
99% >Ftu - 10.76

FIGURE 12 - Regression Analysis Summary Sheet
3/4" Data Set 1

A STUDY OF INERT-GAS WELDING PROCESS
TRANSFERABILITY OF SET-UP PARAMETERS

a. Data Set Number 1, (3/4")

Design

The experimental design for Data Set Number 1, (3/4") was a 1/16 replicate, fractional factorial design with control points added for quadratic analysis.

These experiments were run using the constant current, voltage control, TIG, welding system with nine independent variables and eleven dependent variables. The joints were double welded with one weld from each side.

The independent variables are:

1. Current   (C)

2. Voltage   (V)

3. Travel Speed   (T)

4. Wire Deposit   (Wd)

5. Gas Purity   (GP)

6. Gas Flow   (GF)

7. Weldment Temperature   (°F)

8. Joint Gap   (J)

9. Tungsten Tip Diameter   (D)

The responses are:

1. Ultimate Strength   (Ftu)

2. Yield Strength   (Fty)

3. Elongation   (E)

A STUDY OF INERT-GAS WELDING PROCESS
TRANSFERABILITY OF SET-UP PARAMETERS

Data Set Number 1, (3/4") Continued

    4. Melt Area (Section)   (M)

    5. Melt Crown (Section)   (Mc)

    6. Penetration Overlap (Section) (Q)

    7. Heat Effected Area (Section) (H)

    8. Penetration (one weld)   (P)

    9. Weld Bead Buildup (Section) (B)

  10. Electrode Position   (P)

  11. Porosity (X-Ray)   (X)

Preliminary analysis of this data indicated that Joint Gap was not a significant variable, therefore it was not entered in subsequent data sets. The electrode position data was entered for computer regression analysis as an independent variable.

Results

Ftu

The analysis of the data indicates that the variables represented in the regression equation account for 74% of the variation in ultimate strength.

At the 90% confidence level the confidence limit is: Calculated Ftu- 5.91KSI.

Data Set Number 1, (3/4") Continued

The variables in order of statistical significance are:

1. Voltage x Travel Speed

2. Electrode Position x Tungsten Tip Diameter

3. Gas Purity x Weldment Temperature

Delta "T"

With all other variables held constant, an increase in travel speed causes a decrease in ultimate strength. The amount of this decrease is dependent upon the level of the voltage. The higher the voltage, the greater the decrease in ultimate strength.

Delta "V"

With all other variables held constant, an increase in voltage causes a decrease in ultimate strength. The higher the travel speed, the greater the strength loss caused by increasing voltage.

Delta "GP"

With all other variables held constant, an increase in gas impurity causes an increase in ultimate strength. The amount of increase is dependent upon the temperature of the weldment. The higher weldment temperatures result in the greatest gain in strength.

Delta "EP"

With all other variables held constant, an increase in electrode distance from the work results in a slight increase in ultimate strength, the greater the Electrode Tip Diameter, the greater the increase in strength.

Data Set Number 1, (3/4") Continued

Ultimate Strength Tables

The table of Ultimate Strength versus a range of the values of the variables appearing in the regression indicates that the best strength combination occurs where voltage is at the low end of the range of the experiment (11.5 volts), travel is low (8.0 ipm), gas impurity is high (160 ppm), weldment temperature is high (150°F), electrode position is high (+ 0.040"), and electrode tip diameter is high (0.1350").

This table predicts strength values for weld variable combinations that are beyond the normal range of the welding process control system. This is caused by entering electrode position as an independent variable. This was done in order to analyze the significance of the variables and their relationship to one another, therefore the equation is not intended for weld setting optimizing.

Penetration

The analysis of this data indicates that 83% of the variation observed in this experiment is accounted for by the variables in the regression equations.

The variables controlling penetration in order of their statistical significance are:

1. Current x Electrode Position

2. Voltage x Travel Speed

3. Current

4. Electrode Tip Diameter

5. Gas Purity x Weldment Temperature

Data Set Number 1, (3/4") Continued

Delta "C"

With all other variables held constant, a change of +10 amperes will cause an increase in penetration of about 0.0125" dependent upon the electrode position. The greatest penetration will occur at the greatest electrode to work distance.

Delta "T"

With all other variables held constant, an increase of one inch per minute travel speed will cause a decrease of about .030" in penetration. The exact change in penetration is dependent upon the voltage. The higher voltages result in a greater loss of penetration.

Delta "°F"

With all other variables held constant, an increase in weldment temperature will result in an increase in penetration. The amount of the penetration increase is dependent upon the gas purity. The greater the contamination, the greater will be the increase in penetration.

$$\triangle T @ \ V \quad = \quad \triangle FTU$$

1.00000	11.55000	-4.73758
1.00000	11.65000	-4.77860
1.00000	11.75000	-4.81961
1.00000	11.85000	-4.86063
1.00000	11.95000	-4.90165
1.00000	12.05000	-4.94267

FIGURE 13 - Delta Ultimate Strength vs.
Delta Significant Variables
3/4" Data Set 1

A STUDY OF INERT-GAS WELDING PROCESS
TRANSFERABILITY OF SET-UP PARAMETERS

$$\Delta V \ @ \ T \ = \ \Delta F_{tu}$$

0.10000	8.00000	-0.32814
0.10000	9.00000	-0.36916
0.10000	10.00000	-0.41018

FIGURE 13a - Delta Ultimate Strength vs.
Delta Significant Variables
3/4" Data Set 1

$$\Delta GP @ \, ^\circ F \quad = \quad \Delta Ftu$$

0.20000	0.75000		0.30107
0.20000	1.00000		0.40143
0.20000	1.25000		0.50179
0.20000	1.50000		0.60211

FIGURE 13b - Delta Ultimate Strength vs.
        Delta Significant Variables
        3/4" Data Set 1

$$\triangle °F @ GP = \triangle FTU$$

0.25000	0.10000		0.05018
0.25000	0.30000		0.15054
0.25000	0.50000		0.25089
0.25000	0.70000		0.35125
0.25000	0.90000		0.45161
0.25000	1.10000		0.55197
0.25000	1.30000		0.65232
0.25000	1.50000		0.75268

FIGURE 13c - Delta Ultimate Strength vs.
Delta Significant Variables
3/4" Data Set 1

167

A STUDY OF INERT-GAS WELDING PROCESS
TRANSFERABILITY OF SET-UP PARAMETERS

STEPWISE REGRESSION
P vs. C, V, T, Wd, Gp, Gf, °F, Ep, D ·
3/4" 2219 TIG Horizontal

NO. OF DATA	·70
NO. OF VARIABLES	55
WEIGHTED DEGREES OF FREEDOM	70.00
F LEVEL TO ENTER VARIABLE	3.990 - 95%
F LEVEL TO REMOVE VARIABLE	3.990 - 95%

F LEVEL	4.9308
STD. ERROR OF Y	0.0289
MULTIPLE CORRELATION COEFFICIENT	0.91267
COEFFICIENT OF DETERMINATION	83%

VARIABLE	COEFFICIENT	STD. ERROR
(C)Current	.13391	.02163
(C·Ep)Current·Elect. Position	.27289	.02982
(V·T) Voltage·Travel	- .00256	.00034
(Gp·°F)Gas Purity·°F	.00912	.00411
(D^2)Tip Diam^2	-5.36202	1.26815

CONSTANT = .18704

$$P = .13391(C) +.27289(C·Ep) -.00256(V·T) +.00912(Gp·°F) -5.36202(D^2) +.18704$$

$$dP = .13391dC +.27289EpdC$$
$$+.27289CdEp$$
$$-.00256VdT$$
$$-.00256TdV$$
$$+.00912Gpd°F$$
$$+.00912°FdGp$$
$$-2(5.36202)DdD$$

CONFIDENCE LIMITS FOR CONFIDENCE LEVELS OF:

90% = ±0.04740
95% = ±0.05664
99% = ±0.07439

FIGURE 14 - Regression Analysis Summary Sheet
3/4" Data Set 1

$$\triangle C @ EP = \triangle P$$

0.10000	-0.09000	0.01093
0.10000	-0.08000	0.01121
0.10000	-0.07000	0.01148
0.10000	-0.06000	0.01175
0.10000	-0.05000	0.01203
0.10000	-0.04000	0.01230
0.10000	-0.03000	0.01257
0.10000	-0.02000	0.01285
0.10000	-0.01000	0.01312
0.10000	0.0	0.01339
0.10000	0.01000	0.01366
0.10000	0.02000	0.01394
0.10000	0.03000	0.01421
0.10000	0.04000	0.01448

FIGURE 15 – Delta Penetration vs.
Delta Significant Variables

$$\Delta P @ C = \Delta P$$

0.01000	4.00000	0.01092
0.01000	4.10000	0.01119
0.01000	4.20000	0.01146
0.01000	4.30000	0.01173
0.01000	4.40000	0.01201

FIGURE 15a – Delta Penetration vs.
Delta Significant Variables

A STUDY OF INERT-GAS WELDING PROCESS
TRANSFERABILITY OF SET-UP PARAMETERS

$$\Delta T @ V \quad = \quad \Delta P$$

1.00000	11.55000	-0.02957
1.00000	11.65000	-0.02982
1.00000	11.75000	-0.03008
1.00000	11.85000	-0.03034
1.00000	11.95000	-0.03059
1.00000	12.05000	-0.03085

FIGURE 15b - Delta Penetration vs.
Delta Significant Variables

b. Data Set Number 2 and 3, (3/4")

Design

A central composite rotable designed experiment was selected from
Experimental Designs by Cochran and Cox, page 371. Five weld set-up
parameters were applied to the experimental design and control system
No. 4 (voltage-proximity-current) was used for welds No. 305 through
359. Data taken was analyzed by use of the 3314.001 Gelac Computer
Program.

Control system No. 4 depends upon an automatic voltage control head to
maintain a constant voltage movement of the head. A proportional control
of the current is mechanically attached to the electrode position recorder.
Through this coupling system head movement also adjusts the current. This
current adjustment stabilizes the head movement and results in a more stable
welding process.

In Data Set Number 2 and 3, the following variables were entered for
computer analysis as independent variables:

1. Current   (C)

2. Voltage   (V)

3. Travel Speed   (T)

4. Wire Deposit   (Wd)

5. Temperature of the Weldment   (°F)

6. Electrode Position   (Ep)

EXPERIMENT DESIGN (contd).

RUN Nº	V	C	T	W	°F	V	C	T	W	°F
317	-2	0	0	0	0	11.2	420	6.5	14	150°
318	-1	1	-1	1	1	11.4	430	6.0	16	175°
319/320	0	0	0	-2	0	11.6	420	6.5	10	150°
321	0	0	0	0	-2	11.6	420	6.5	14	100°
322	1	1	-1	1	-1	11.8	430	6.0	16	125°
323	0	0	2	0	0	11.6	420	7.5	14	150°
324	1	-1	1	1	-1	11.8	410	7.0	16	125°
325	0	0	0	2	0	11.6	420	6.5	18	150°
326	0	0	-2	0	0	11.6	420	5.5	14	150°
327	1	1	1	1	1	11.8	430	7.0	16	175°
328	2	0	0	0	0	12.0	420	6.5	14	150°
329	-1	-1	1	1	1	11.4	410	7.0	16	175°
330	-1	1	1	1	-1	11.4	430	7.0	16	125°
331	0	0	0	0	2	11.6	420	6.5	14	200°
332	0	2	0	0	c	11.6	440	6.5	14	150°
333	0	-2	0	0	0	11.6	400	6.5	14	150°

FIGURE 16 -   Experimental Design 3/4" Data Sets 2 & 3

A STUDY OF INERT-GAS WELDING PROCESS
TRANSFERABILITY OF SET-UP PARAMETERS

Data Set Number 2 and 3, (3/4") Continued

Data Set No. 2 consists of 13 data points for the evaluation of ultimate strength, yield strength, and elongation.

Data Set No. 3 consists of 121 data points for the evaluation of weld geometry.

Results   Data Set Number 2

Ftu

The regression for ultimate strength derived from this data accounts for 43% of the variation in ultimate strength.

At the 95% confidence level, the only variable entering the regression is voltage. The confidence limit for a confidence level of 90% is - 0.103 KSI ultimate strength.

Examination of the data indicates that there was very little variation in ultimate strength and only 43% of that variation accounted for.

Further experimentation will be necessary to properly evaluate the variables that are significant for a variation in ultimate strength when using the "voltage controlling electrode position controlling current" system.

Data Set Number 2 and 3, (3/4") Continued

Results   Data Set Number 3

Penetration

The regression equation derived from the computer analysis of Data Set
No. 3 includes the following variables in order of their statistical
significance:

1. Voltage

2. Current x Voltage

3. Weld Travel Speed

The variables in the regression equation account for 76% of the variation
in penetration. At 90% confidence level, the confidence limits are plus
and minus 0.019".

Delta Voltage

With all other variables held constant, an increase of 0.10 volts would
cause an increase in penetration of approximately 0.00495". The variation
in penetration is dependent upon the current level. The higher the current
the greater the increase in penetration caused by an increase in voltage.

Delta "T"

With all other variables held constant, an increase in travel speed of
1.0" per minute, will cause a decrease in penetration of approximately
-0.100". The amount of variation caused by a change in travel speed
becomes greater as the travel speed decreases.

c. Electrode Position vs. Penetration

Design

In order to evaluate the significance of the electrode position a short, 2 level, "classic" experiment was designed in which voltage, current, and weld travel speed were varied one at a time. This was done so that the variation in the electrode position and penetration could be isolated without a computer analysis.

A second object of this experiment was to evaluate the TIG welding control system where voltage controls the electrode position and the electrode position is coupled to the current control. This current stabilizes the weld torch movement and results in a more stable welding process.

Results

The trace recordings taken of voltage and current while testing this control system show that there is about twice as much deviation in these variables as compared with the conventional TIG voltage control system. At the same time there is much less deviation in the resulting electrode position.

This resulted in a welding system that is much more stable than voltage control TIG. Welds can be made at extreme combinations of voltage, current and weld travel without loss of control of the process.

Electrode Position vs. Penetration (Continued)

This system does not control penetration in the sense that the value of

penetration is predicted and dialed into the control, but it does tend

to stabilize the penetration at whatever level is established by the

combination of significant variables.

d. Data Set Number 4, (3/4")

2219 Horizontal Weld Number 153 through 359

This data set consists of a composite of all of the 3/4" TIG welds. This

represents equipment, control system, as well as weld setting changes.

This data also includes all of the experimental designs used.

Results

Penetration

The regression equation derived from the computer analysis of the com-

posite of all 3/4" TIG, horizontal welds consisting of 266 data points

includes the following variables in order of statistical significance.

1. Current x Travel

2. Travel x Travel

3. Current

4. Electrode Position x Electrode Position

5. Gas Purity x Electrode Position

6. Current x Voltage

7. Travel Speed x Gas Purity

Data Set Number 4, (3/4") Continued

The variables in the regression account for 75% of the variation observed

in penetration. At the 90% confidence level the confidence limits are

plus and minus 0.0565".

Delta "T"

With all other variables held constant, an increase in travel speed of

1 inch per minute will cause a decrease in penetration. The amount of

this penetration decrease is dependent upon the operating level of the

current, travel speed, and the purity of the gas. The decrease in pene-

tration caused by an increase of 1 inch/minute in travel speed is predicted

to be as high as -0.083" at slow travel speeds.

Delta "C"

With all other variables held constant, an increase in current of 10

amperes is predicted to cause an increase in penetration of up to + 0.023"

at the slower travel speeds. In addition to travel speed, the variation

caused by current is dependent upon voltage.

Delta "Ep"

With all other variables held constant, an increase in the electrode position

(out from the weldment) of 0.010" will cause an increase in penetration

when the electrode tip is below the surface and a decrease in penetration

when the electrode position is above the surface. The change in pene-

tration can range from + 0.15" to -0.009", depending upon the gas purity

and electrode position.

$$P = .46622(C) +.00456(C \cdot V) -.04721(C \cdot T) +.00951(T^2) +.00192(T \cdot Gp)$$
$$+.67682(Gp \cdot Ep) -12.31961(Ep^2) -.76923$$

C	V	T	Gp	Ep	P
4.0000	11.0000	6.0000	0.1000	-0.0200	0.50048
4.0000	11.0000	6.0000	0.1000	0.0100	0.50620
4.0000	11.0000	6.0000	0.1000	0.0400	0.48976
4.0000	11.0000	6.0000	0.8000	-0.0200	0.49907
4.0000	11.0000	6.0000	0.8000	0.0100	0.51901
4.0000	11.0000	6.0000	0.8000	0.0400	0.51677
4.0000	11.0000	6.0000	1.5000	-0.0200	0.49766
4.0000	11.0000	6.0000	1.5000	0.0100	0.53181
4.0000	11.0000	6.0000	1.5000	0.0400	0.54379
4.0000	11.0000	8.0000	0.1000	-0.0200	0.38946
4.0000	11.0000	8.0000	0.1000	0.0100	0.39519
4.0000	11.0000	8.0000	0.1000	0.0400	0.37874
4.0000	11.0000	8.0000	0.8000	-0.0200	0.39074
4.0000	11.0000	8.0000	0.8000	0.0100	0.41068
4.0000	11.0000	8.0000	0.8000	0.0400	0.40844
4.0000	11.0000	8.0000	1.5000	-0.0200	0.39202
4.0000	11.0000	8.0000	1.5000	0.0100	0.42617
4.0000	11.0000	8.0000	1.5000	0.0400	0.43815
4.0000	11.0000	10.0000	0.1000	-0.0200	0.35453
4.0000	11.0000	10.0000	0.1000	0.0100	0.36025
4.0000	11.0000	10.0000	0.1000	0.0400	0.34380
4.0000	11.0000	10.0000	0.8000	-0.0200	0.35849
4.0000	11.0000	10.0000	0.8000	0.0100	0.37843
4.0000	11.0000	10.0000	0.8000	0.0400	0.37620
4.0000	11.0000	10.0000	1.5000	-0.0200	0.36246
4.0000	11.0000	10.0000	1.5000	0.0100	0.39661
4.0000	11.0000	10.0000	1.5000	0.0400	0.40859
4.0000	11.5000	6.0000	0.1000	-0.0200	0.5°°°°
4.0000	11.5000	6.0000	0.1000	0.0100	0.5°.°2
4.0000	11.5000	6.0000	0.1000	0.0400	0.49888
4.0000	11.5000	6.0000	0.8000	-0.0200	0.50819
4.0000	11.5000	6.0000	0.8000	0.0100	0.52813
4.0000	11.5000	6.0000	0.8000	0.0400	0.52589
4.0000	11.5000	6.0000	1.5000	-0.0200	0.50678
4.0000	11.5000	6.0000	1.5000	0.0100	0.54093
4.0000	11.5000	6.0000	1.5000	0.0400	0.55291
4.0000	11.5000	8.0000	0.1000	-0.0200	0.39858
4.0000	11.5000	8.0000	0.1000	0.0100	0.40431
4.0000	11.5000	8.0000	0.1000	0.0400	0.38786
4.0000	11.5000	8.0000	0.8000	-0.0200	0.39986
4.0000	11.5000	8.0000	0.8000	0.0100	0.41980
4.0000	11.5000	8.0000	0.8000	0.0400	0.41756
4.0000	11.5000	8.0000	1.5000	-0.0200	0.40114

FIGURE 17 - Penetration
3/4" Data Set 4

A STUDY OF·INERT-GAS WELDING PROCESS
TRANSFERABILITY OF SET-UP PARAMETERS

4.0000	11.5000	8.0000	1.5000	0.0100	0.43529
4.0000	11.5000	8.0000	1.5000	0.0400	0.44727
4.0000	11.5000	10.0000	0.1000	-0.0200	0.36365
4.0000	11.5000	10.0000	0.1000	0.0100	0.36937
4.0000	11.5000	10.0000	0.1000	0.0400	0.35292
4.0000	11.5000	10.0000	0.8000	-0.0200	0.36761
4.0000	11.5000	10.0000	0.8000	0.0100	0.38755
4.0000	11.5000	10.0000	0.8000	0.0400	0.38532
4.0000	11.5000	10.0000	1.5000	-0.0200	0.37158
4.0000	11.5000	10.0000	1.5000	0.0100	0.40573
4.0000	11.5000	10.0000	1.5000	0.0400	0.41771
4.0000	12.0000	6.0000	0.1000	-0.0200	0.51872
4.0000	12.0000	6.0000	0.1000	0.0100	0.52444
4.0000	12.0000	6.0000	0.1000	0.0400	0.50800
4.0000	12.0000	6.0000	0.8000	-0.0200	0.51731
4.0000	12.0000	6.0000	0.8000	0.0100	0.53725
4.0000	12.0000	6.0000	0.8000	0.0400	0.53501
4.0000	12.0000	6.0000	1.5000	-0.0200	0.51590
4.0000	12.0000	6.0000	1.5000	0.0100	0.55005
4.0000	12.0000	6.0000	1.5000	0.0400	0.56203
4.0000	12.0000	8.0000	0.1000	-0.0200	0.40770
4.0000	12.0000	8.0000	0.1000	0.0100	0.41343
4.0000	12.0000	8.0000	0.1000	0.0400	0.39698
4.0000	12.0000	8.0000	0.8000	-0.0200	0.40898
4.0000	12.0000	8.0000	0.8000	0.0100	0.42892
4.0000	12.0000	8.0000	0.8000	0.0400	0.42668
4.0000	12.0000	8.0000	1.5000	-0.0200	0.41026
4.0000	12.0000	8.0000	1.5000	0.0100	0.44441
4.0000	12.0000	8.0000	1.5000	0.0400	0.45639
4.0000	12.0000	10.0000	0.1000	-0.0200	0.37277
4.0000	12.0000	10.0000	0.1000	0.0100	0.37849
4.0000	12.0000	10.0000	0.1000	0.0400	0.36204
4.0000	12.0000	10.0000	0.8000	-0.0200	0.37673
4.0000	12.0000	10.0000	0.8000	0.0100	0.39667
4.0000	12.0000	10.0000	0.8000	0.0400	0.39444
4.0000	12.0000	10.0000	1.5000	-0.0200	0.38070
4.0000	12.0000	10.0000	1.5000	0.0100	0.41485
4.0000	12.0000	10.0000	1.5000	0.0400	0.42683
4.2000	11.0000	6.0000	0.1000	-0.0200	0.54710
4.2000	11.0000	6.0000	0.1000	0.0100	0.55283
4.2000	11.0000	6.0000	0.1000	0.0400	0.53638
4.2000	11.0000	6.0000	0.8000	-0.0200	0.54569

FIGURE 17a - Penetration
3/4" Data Set 4

4.2000	11.0000	6.0000	0.8000	0.0100	0.56563
4.2000	11.0000	6.0000	0.8000	0.0400	0.56339
4.2000	11.0000	6.0000	1.5000	-0.0200	0.54428
4.2000	11.0000	6.0000	1.5000	0.0100	0.57843
4.2000	11.0000	6.0000	1.5000	0.0400	0.59041
4.2000	11.0000	8.0000	0.1000	-0.0200	0.41720
4.2000	11.0000	8.0000	0.1000	0.0100	0.42293
4.2000	11.0000	8.0000	0.1000	0.0400	0.40648
4.2000	11.0000	8.0000	0.8000	-0.0200	0.41848
4.2000	11.0000	8.0000	0.8000	0.0100	0.43842
4.2000	11.0000	8.0000	0.8000	0.0400	0.43618
4.2000	11.0000	8.0000	1.5000	-0.0200	0.41976
4.2000	11.0000	8.0000	1.5000	0.0100	0.45391
4.2000	11.0000	8.0000	1.5000	0.0400	0.46589
4.2000	11.0000	10.0000	0.1000	-0.0200	0.36338
4.2000	11.0000	10.0000	0.1000	0.0100	0.36911
4.2000	11.0000	10.0000	0.1000	0.0400	0.35266
4.2000	11.0000	10.0000	0.8000	-0.0200	0.36735
4.2000	11.0000	10.0000	0.8000	0.0100	0.38729
4.2000	11.0000	10.0000	0.8000	0.0400	0.38505
4.2000	11.0000	10.0000	1.5000	-0.0200	0.37131
4.2000	11.0000	10.0000	1.5000	0.0100	0.40546
4.2000	11.0000	10.0000	1.5000	0.0400	0.41744
4.2000	11.5000	6.0000	0.1000	-0.0200	0.55668
4.2000	11.5000	6.0000	0.1000	0.0100	0.56240
4.2000	11.5000	6.0000	0.1000	0.0400	0.54595
4.2000	11.5000	6.0000	0.8000	-0.0200	0.55527
4.2000	11.5000	6.0000	0.8000	0.0100	0.57521
4.2000	11.5000	6.0000	0.8000	0.0400	0.57297
4.2000	11.5000	6.0000	1.5000	-0.0200	0.55385
4.2000	11.5000	6.0000	1.5000	0.0100	0.58801
4.2000	11.5000	6.0000	1.5000	0.0400	0.59999
4.2000	11.5000	8.0000	0.1000	-0.0200	0.42678
4.2000	11.5000	8.0000	0.1000	0.0100	0.43250
4.2000	11.5000	8.0000	0.1000	0.0400	0.41606
4.2000	11.5000	8.0000	0.8000	-0.0200	0.42805
4.2000	11.5000	8.0000	0.8000	0.0100	0.44799
4.2000	11.5000	8.0000	0.8000	0.0400	0.44576
4.2000	11.5000	8.0000	1.5000	-0.0200	0.42933
4.2000	11.5000	8.0000	1.5000	0.0100	0.46348
4.2000	11.5000	8.0000	1.5000	0.0400	0.47540
4.2000	11.5000	10.0000	0.1000	-0.0200	0.37296

FIGURE 17b - Penetration
3/4" Data Set 4

TUNGSTEN ARC WELD
2219 - T87 Alloy
¼" Thick, (Single Weld)

	Code Letter	High	Medium	Low	Units for Computer
Arc Current	C	2.85	2.73	2.60	Amp/ 100
Arc Voltage	V	12.75	12.5	12.25	Volts
Travel Speed	T	23	21	19	Ipm
Wire Deposit/In. of Weld	Wd	1.228	.955	.682	$In.^3 x$ 100/In.
Gas Purity	Gp	1.50	.90	.30	Ppm/100
Gas Flow	Gf	1.25	1.00	.75	scfh/100
Indicated Flow		1.54	1.21	.88	
Work Temperature	°F	1.50	1.13	.75	°F/100
Joint Gap	J	.020	.010	0	In.
Electrode Tip Diameter	D	.125	.108	.090	In.

FIGURE 18 -   Weld Parameters
¼" Data Set 1 and 2

A STUDY OF INERT-GAS WELDING PROCESS
TRANSFERABILITY OF SET-UP PARAMETERS

STEPWISE REGRESSION
Ftu vs. C, V, T, Gp, °F, D, Ep, MT, TT, AT
$\frac{1}{4}$" 2219 TIG Horizontal

NO. OF DATA	29
NO. OF VARIABLES	66
WEIGHTED DEGREES OF FREEDOM	29.00
F LEVEL TO ENTER VARIABLE	2.89 - 90%
F LEVEL TO REMOVE VARIABLE	2.89 - 90%

F LEVEL	4.0432
STD. ERROR OF Y	2.2419
MULTIPLE CORRELATION COEFFICIENT	0.97103
COEFFICIENT OF DETERMINATION	94%

VARIABLE		COEFFICIENT	STD. ERROR
(C)........	Current	-141.84611	44.40096
(C·T)......	Current·Travel	9.52253	1.92407
(C·D)......	Current·Tip Diameter	-366.98919	182.51091
(T)........	Travel	- 24.87564	5.32856
(T·D)......	Travel·Tip Diameter	- 40.75639	13.23178
(D^2).......	Tip Diameter$^{(2)}$	8086.81989	2563.56616
(D·MT).....	Tip Diam·Max Temp	4.83399	1.79849

CONSTANT = 495.61423

$$Ftu = -141.84611(C) +9.52253(C·T) -366.98919(C·D)$$
$$-24.87564(T) -40.75639(T·D) +8086.81989(D^2)$$
$$+4.83399(D·MT) +495.61423$$

$$dFtu = -141.84611dC +9.52253TdC -366.98919DdC$$
$$-24.8756dT +9.52253CdT -40.75639DdT$$
$$+2(8086.81989)DdD -366.98919CdD$$
$$+4.83399MTdD -40.75639TdD$$
$$+4.83399DdMT$$

CONFIDENCE LIMITS FOR CONFIDENCE LEVELS OF:
90% >Ftu - 2.93   95% >Ftu - 3.81   99% >Ftu - 5.61

FIGURE 19 - Regression Analysis Summary Sheet
$\frac{1}{4}$" Data Set 1

e. **TIG Data Set 1 and 2, (1/4")**

Summary

Design

The experimental design for data set number 1 and 2 (1/4") is a 1/16
replicate fractional factorial design with central points added for
quadratic analysis.

These experiments were run using the constant current, voltage control,
TIG, control system with nine independent variables and fourteen de-
pendent variables or responses.

The independent variables are:

1.	Current	(C)
2.	Voltage	(V)
3.	Travel Speed	(T)
4.	Wire Deposit	(Wd)
5.	Gas Purity	(Gp)
6.	Gas Flow	(Gf)
7.	Weldment Temperature	(°F)
8.	Joint Gap	(J)
9.	Tungsten Tip Diameter	(D)

The responses are:

1.	Ultimate Strength	(Ftu)
2.	Yield Strength	(Fty)
3.	Elongation	(E)
4.	Melt Area (Section)	(M)
5.	Melt Crown Area (Section)	(Mc)

TIG Data Set 1 and 2, (1/4") Continued

6.	Melt Fall through Area (Section)	(Mf)
7.	Heat Effected Area (Section)	(H)
8.	Penetration	(P)
9.	Build Up (Weld Bead)	(B)
10.	Electrode Position (From Work Surface)	(Ep)
11.	Porosity (X-ray)	(X)
12.	Max. Temperature of Back Bead	(Mt)
13.	Time above 450°F (Back Bead)	(Tt)
14.	Area under Temperature Curve above 450°F	(At)

Preliminary examination and analysis of the data indicated that for the
range of joint gap evaluated there was no significant variation in the
responses that could be attributed to joint gap. Therefore, joint gap
was not entered in subsequent data sets.

In 1/4" data set 1, electrode position (Ep), maximum temperature (Mt),
time temperature exceeded 450°F (Tt), and area under the temperature
curve (At) were entered in the regression analysis as additional in-
dependent variables.

Results, Data Set 1

Ftu

The analysis of this data indicates that the variables expressed in the
regression equation account for 94% of the variation observed in Ftu.
At the 90% confidence level, the confidence limit is calculated

A STUDY OF INERT-GAS WELDING PROCESS
TRANSFERABILITY OF SET-UP PARAMETERS

TIG Data Set 1 and 2, (1/4") Continued

Ftu -2.93 KSI. The variables represented are listed in the order of statistical significance as follows with the product of two variables indicating significant interaction.

1. Current x Travel Speed

2. Travel Speed

3. Tungsten Tip Diameter

4. Current x Tungsten Tip Diameter

5. Current

6. Travel Speed x Tungsten Tip Diameter

7. Tungsten Tip Diameter x Maximum Temperature of Back Bead.

Change in Current (Delta C)

With all other variables held constant, a⁺change in current will cause a corresponding⁺change in ultimate tensile strength (Ftu). The exact amount of the resulting change is dependent upon the values of the interacting variables, welding current and travel speed.

Delta "T"

With all other variables held constant, a⁺change in travel speed will cause a corresponding⁺change in Ftu. The exact amount of the change is dependent upon the values of the interacting variables; welding current and tungsten tip diameter.

TIG Data Set 1 and 2, (1/4") Continued

Delta "D"

With all other variables held constant, a change in the tungsten tip
diameter will cause a corresponding change in Ftu. The exact amount
of the change depends on the current, travel speed, maximum temperature,
and tungsten tip diameter involved. The smaller the initial tip diameter
the more significant a change becomes.

Time - Temperature

The time at temperature over 450°F, the maximum temperature, and the
area under the temperature curve about 450°F, were entered for computer
regression analysis as independent variables to study their relationship
to the ultimate strength. The resulting regression at the 90% confidence
level accounted for only 34% of the variation in Ftu. Maximum temperature
was the only significant variable. At the 90% confidence level the con-
fidence limit was calculated; Ftu -8.9 (KSI).

X-Ray

The analysis of the data and the regression for X-Ray or porosity in-
dicates that the variables in the data set account for only 23% of the
variation in porosity at the 90% confidence level.

The variables presented in the regression are listed in order of
statistical significance.

        Gas purity x area under temperature curve

        Gas purity x time at temperature above 450°F

A STUDY OF INERT-GAS WELDING PROCESS
TRANSFERABILITY OF SET-UP PARAMETERS

TIG Data Set 1 and 2, (1/4") Continued

An increase in shielding gas impurity causes an increase in porosity depending upon the area under the time-temperature curve. The greater the area the greater the increase in porosity. At the same time, the greater the maximum temperature, the greater the porosity increase.

$$\Delta C \ @ \ T \ @ \ D \quad = \quad \Delta FTU$$

	ΔC	@ T	@ D		ΔFTU
	0.1000	20.0000	0.0900		1.5570
	0.1000	20.0000	0.1000		1.1000
	0.1000	20.0000	0.1100		1.0000
	0.1000	20.0000	0.1200		0.6500
	0.1000	20.0000	0.1300		0.0800
	0.1000	21.0000	0.0900		0.5000
	0.1000	21.0000	0.1000		2.1100
7	0.1000	21.0000	0.1100		1.7750
	0.1000	21.0000	0.1200		1.4000
6	0.1000	21.0000	0.1300		1.0410
	0.1000	22.0000	0.0900		3.4600
5	0.1000	22.0000	0.1000		3.0050
	0.1000	22.0000	0.1100		2.7200
4	0.1000	22.0000	0.1200		2.3600
	0.1000	22.0000	0.1300		1.0900
3	0.1000	23.0000	0.0900		4.4100
	0.1000	23.0000	0.1000		4.0400
2	0.1000	23.0000	0.1100		3.6000
	0.1000	23.0000	0.1200		3.3100
A	0.1000	23.0000	0.1300		2.9000

FIGURE 20 – Delta Ultimate Strength vs.
Delta Significant Variables

$$\Delta T \ @ \ C \ @ \ D \ = \ \Delta FTU$$

ΔT	C	D	ΔFTU
1.00000	2.60000	0.09000	-3.78514
1.00000	2.60000	0.10000	-4.19272
1.00000	2.60000	0.11000	-4.60026
1.00000	2.60000	0.12000	-5.00783
1.00000	2.60000	0.13000	-5.41539
1.00000	2.70000	0.09000	-2.83288
1.00000	2.70000	0.10000	-3.24045
1.00000	2.70000	0.11000	-3.64801
1.00000	2.70000	0.12000	-4.05557
1.00000	2.70000	0.13000	-4.46314
1.00000	2.80000	0.09000	-1.88063
1.00000	2.80000	0.10000	-2.28819
1.00000	2.80000	0.11000	-2.69575
1.00000	2.80000	0.12000	-3.10332
1.00000	2.80000	0.13000	-3.51088
1.00000	2.90000	0.09000	-0.92839
1.00000	2.90000	0.10000	-1.33595
1.00000	2.90000	0.11000	-1.74351
1.00000	2.90000	0.12000	-2.15108
1.00000	2.90000	0.13000	-2.55864

FIGURE 20a – Delta Ultimate Strength vs.
Delta Significant Variables

A STUDY OF INERT-GAS WELDING PROCESS
TRANSFERABILITY OF SET-UP PARAMETERS

$$\Delta D \ @ \ C \ @ \ T \ @ \ MT \ @ \ D \ = \ \Delta FTU$$

ΔD	C	T	MT	D	ΔFTU
.02000	2.50000	20.00000	5.00000	0.00000	-5.60336
.02000	2.60000	20.00000	5.00000	0.11000	0.77600
.02000	2.60000	20.00000	10.00000	0.00000	-5.30654
.02000	2.60000	20.00000	10.00000	0.11000	1.16207
.02000	2.60000	20.00000	14.00000	0.00000	-4.91002
.02000	2.60000	20.00000	14.00000	0.11000	1.54053
.02000	2.60000	21.00000	5.00000	0.00000	-5.59040
.02000	2.60000	21.00000	5.00000	0.11000	0.03903
.02000	2.60000	21.00000	10.00000	0.00000	-5.12177
.02000	2.60000	21.00000	10.00000	0.11000	0.34760
.02000	2.60000	21.00000	14.00000	0.00000	-5.73505
.02000	2.60000	21.00000	14.00000	0.11000	0.73441
.02000	2.60000	22.00000	6.00000	0.00000	-7.32360
.02000	2.60000	22.00000	5.00000	0.11000	0.25477
.02000	2.60000	22.00000	10.00000	0.00000	-6.03600
.02000	2.60000	22.00000	10.00000	0.11000	0.46715
.02000	2.60000	22.00000	14.00000	0.00000	-5.55033
.02000	2.60000	22.00000	14.00000	0.11000	0.03073
.02000	2.70000	20.00000	5.00000	0.50000	-5.42733
.02000	2.70000	20.00000	5.00000	0.11000	0.04237
.02000	2.70000	20.00000	10.00000	0.00000	-5.04600
.02000	2.70000	20.00000	10.00000	0.11000	0.42800
.02000	2.70000	20.00000	14.00000	0.00000	-5.65700
.02000	2.70000	20.00000	14.00000	0.11000	0.03557
.02000	2.70000	21.00000	5.00000	0.00000	-7.24245
.02000	2.70000	21.00000	5.00000	0.11000	0.77200
.02000	2.70000	21.00000	10.00000	0.00000	-5.05573
.02000	2.70000	21.00000	10.00000	0.11000	0.39028
.02000	2.70000	21.00000	14.00000	0.00000	-5.46001
.02000	2.70000	21.00000	14.00000	0.11000	0.03044
.02000	2.70000	22.00000	5.00000	0.00000	-8.05750
.02000	2.70000	22.00000	5.00000	0.11000	-1.50033
.02000	2.70000	22.00000	10.00000	0.00000	-7.57007
.02000	2.70000	22.00000	10.00000	0.11000	-1.20143
.02000	2.70000	22.00000	14.00000	0.00000	-7.28415
.02000	2.70000	22.00000	14.00000	0.11000	-0.91470

FIGURE 20b - Delta Ultimate Strength vs.
Delta Significant Variables

5. Transfer Weld Summary

The first four data sets were developed using Welding Unit No. 1. This
unit was used with conventional voltage control during the welding for the
1/4" data set 1 and 2 and during the welding for 3/4" data set 1.

Replicates of several of the weld settings used in 3/4" data set 1 were
transferred to 3/4" data set 2. Data set 2 was run using Welding Unit No.
1 with the control modified to the configuration of control system No. 4
which is with voltage controlling electrode position and electrode position
controlling current. These welds were transferred successfully with vari-
ation in weld strength and geometry well within the 90% confidence limit
range.

Further transfer experimentation was conducted by transferring from Welding
Unit No. 1 with "voltage-proximity - current" control to Welding Unit No. 2
with "voltage-proximity" control.

Difficulty was encountered during these experiments with several weld
parameter combinations. It was found that some weld parameters that produce
very stable and controllable welds when using "voltage-proximity - current"
control, produced unstable and uncontrollable welds when transferred to the
"voltage" control system. Transfers from the "voltage" control system to
the "voltage-proximity - current" system is accomplished with no difficulty
from a stability and control standpoint.

Transfer:Weld Summary (continued)

The transfer weld data, Weld No. T-1 through T-20 are replicates of Weld No. 305 through 316, and Weld No. 334 through 339 from 3/4" data Set No. 2.

The average penetration observed from Weld No. T-1, T-20 was .564".
The standard deviation for this data was 0.05 which gives 90% confidence limits of 0.482" to 0.646". All of the replicates of this weld setting run in Welding Unit No. 1 were within these limits.

The solution of the regression equation from 3/4" data Set No. 4, using the same weld parameter settings as used in the T-1 through T-20 series, gives a predicted penetration of 0.531". The 90% confidence limits for this equation give limits of from 0.475" to 0.5883". The transfer weld penetrations are well within these limits.

The average ultimate tensile strength produced by the transfer welds T-1, T-20, was 40.89 KSI. When these settings were transferred back to Welding Unit No. 1, Weld No. 334-339, the ultimate strength was 42.94 KSI. This is well within the 90% confidence limits of the T-1, T-20 data set.

CONCLUSIONS:

The tables and charts, along with the regression analysis summary sheets to be presented in the final report provide, at a glance, many more conclusions about the relationship of the variables than is practical to present in abstract. Therefore, only the major contributions are presented here.

CONCLUSIONS: (continued)

It is concluded that:

1. Data Analysis

   With statistically designed experiments, computer reduction and analysis of
   data it is possible to quickly solve problems and explore the relationships
   of the variables far beyond our capability using "conventional" techniques.

   One set of raw welding data may be used in different combinations with
   computer analysis to simulate many additional welding experiments and equip-
   ment modifications.

2. TIG Penetration

   Within the range of the data, the variables that account for a majority of
   the variation in weld penetration are:

   > Travel Speed
   >
   > Current
   >
   > Tungsten Tip Diameter
   >
   > Electrode Position

   Weld travel speed becomes very critical to penetration control at low speeds.
   Electrode position control is least critical when operating approximately at
   the weldment surface and becomes significantly critical when operating above
   or below the surface.

   Electrode tip diameter becomes increasingly critical as the diameter decreases.

   When using the "Voltage-Proximity-Current" TIG, control system, weld travel
   speed is the variable of greatest significance.

194

CONCLUSIONS: (continued)

3. TIG Ultimate Strength

Within the range of the data, the variables that account for a majority of

the variation in Ultimate Strength are:

Tungsten Tip Diameter

Current

Weld Travel Speed

Tungsten tip diameter becomes critical at small diameters.

4. TIG Porosity

Within the range of the data, the variables that account for variations in

porosity are:

Inert-Gas Purity

Time-Temperature Function

Although these variables are the only ones entering the regression at the

90% confidence level, they account for only a small percentage of the vari-

ation in porosity. The predominant porosity variables are not identified.

5. Transferability, TIG

In order to transfer the following conditions must be met:

a. Good instrumentation must be provided for the basic four TIG welding

variables of (1) Current, (2) Travel Speed, (3) Electrode Position, and

(4) Voltage, in order of importance.

The instrumentation should be high resolution, calibrated equipment,

preferably trace recording type.

CONCLUSIONS: (continued)

b. The static variables, gas purity and tungsten tip diameter must be
   maintained constant.

Where the conditions above are met, along with duplicate conditions of weld
joint preparation, tooling and welding position, duplicate trace recordings
indicate duplicate welds.

A change of the welding control system from one system to another may pre-
clude the ability to successfully transfer a weld setting. For example,
settings that are stable and satisfactory when welding with the conventional
"voltage" control system can be transferred to the "Voltage-Proximity-
Current" system but the opposite is not always possible. However duplicate
trace recordings of the four dynamic variables indicates duplicate welds
regardless of system change.

An accumulation of variation in the minor static variables such as wire
deposit rate, gas flow, gas purity, etc., will cause significant variation
in the resulting welds. Wire deposit volume normally is not a critical
variable, however, the angle and position of entry into the weld puddle is
extremely sensitive. The filler wire angle and position of entry must be
duplicated in order to duplicate welds.

RECOMMENDATIONS:

It is recommended that:

1. Additional development programs be conducted to determine the significance of the tooling and welding position variable on the weld joint performance responses.

2. A program be initiated for the development and improvement of TIG welding control system so that the basic dynamic TIG parameters of current, voltage, and electrode position may be controlled and set independently.

SECTION VI

PRECEDING PAGE BLANK NOT FILMED.

DEVELOPMENT OF CONTROLS FOR
TIME-TEMPERATURE CHARACTERISTICS
IN ALUMINUM WELDMENTS

CONTRACT No. NAS8-11930
Control No. DCN1-5-30-12723-01

Prepared For

The Third Symposium
on Welding Studies

January 19, 1966

At

George C. Marshall Space Flight Center
National Aeronautics and Space Administration
Huntsville, Alabama

By

HARVEY ENGINEERING LABORATORIES
for Research & Development
a division of
HARVEY ALUMINUM (Incorporated)
19200 South Western Avenue
Torrance, California

Copy No._____

NOTICE - Preliminary Report

This report contains information which is of a preliminary nature and is subject to correction or modification upon the collection and evaluation of additional data.

FOREWORD

The work covered by this report has been sponsored by National Aeronautics and Space Administration under Contract No. NAS8-11930 issued by Marshal Space Flight Center.

The principal investigators for this work have been D. Q. Cole and A. E. Bennet under the direction of L. W. Davis and the Contracting Officer's Technical Representative at NASA is Frank Jackson.

PRECEDING PAGE BLANK NOT FILMED.

TABLE OF CONTENTS

ABSTRACT

This report contains a summary of accomplishments during the first nine months of an eighteen month program to develop methods, tooling concepts, and processes to control the time-temperature characteristics in the weld and heat affected zone, in order to improve tensile properties and reduce porosity in aluminum weldments.

A literature survey, conducted during the first four months, revealed that although a considerable amount of work has been done to control heat input, there has been little documented experimental work on controlling thermal patterns by heat extraction. This program proposes to investigate means of producing and controlling optimum thermal patterns by balancing heat input and heat extraction through use of cryogenic liquids and auxiliary heat sources if required.

Although only very preliminary data have been obtained during the four months since the beginning of experimental work, there are strong indications that the technical concepts of the program are sound and that it will be possible to accomplish the objectives of the program. Initial tests indicate that increased tensile properties and reduced porosity in weldments in 5/16-inch and 1/2-inch 2014-T6 plate have resulted

205

from shortening the time-temperature cycles and controlling the solidification pattern by using liquid CO_2 as a chilling agent during welding.

Future work will include verification of the preliminary data, extension of this work to weldments in 2219-T87 plate, and establishment of optimum thermal patterns for weldments in both materials by devising additional means of adjusting and controlling the balance between heat input and heat extraction.

I. Program Objectives

The objective of this program is to develop methods, tooling concepts, and processes to control the time-temperature characteristics in the weld and heat affected zone, in order to improve tensile properties and reduce porosity in aluminum weldments.

The need for this work has been brought about by the increasing requirement for higher strength-weight ratio and for greater reliability of weldments in aerospace vehicles, in particular the aluminum components for the Saturn V. These weldments have had a high incidence of porosity. Improved joint efficiencies are, of course, extremely desirable to meet the stringent design requirements.

A secondary objective of this program is to advance the state-of-the-art by developing control methods which will aid the welder in consistently producing better welds in all materials.

II. Technical Approach

A. Increase Quench Rate

The copper bearing heat treatable aluminum alloys are strengthened by controlled precipitation of intermetallic compounds from the solid solution by aging. These precipitates must be finely divided and uniformly dispersed in order to

accomplish strengthening. This condition is attained by a sensitive time-temperature relationship. Unless the proper relationship is maintained throughout all stages of fabrication, a soft matrix and/or brittle planes of weakness will result. Welding produces an adverse time-temperature history in that the high temperatures can produce coalesence of grain refining and strengthening elements, and slow cooling produces overaging. Slow cooling near the melting point also produces excessively large grain growth which can result in additional loss of strength by forming planes of weakness.

Also, unless conditions are such that gases can escape through the molten liquid, slow cooling through the melting range can result in gross porosity (usually lineal), while fast cooling may produce fine scattered porosity which may not be detrimental.

The use of chill bars has long been used to achieve quenching during welding. While this method is perhaps adequate for welds in non-critical structure, it has three distinct advantages: (1) non-uniform contact between the chill bars and the work piece can cause erratic chilling with resultant hot and cold spots along the length of the weld; (2) the degree of chilling is not easily adjustable to the variety of materials, thicknesses, configurations, etc; and (3) "hard" tooling cannot always be used.

208

Some efforts to control weld chilling by selection of special chill bar materials, such as titanium, and insulator type materials, have indicated some promise in overcoming erratic chilling but are subject to the other limitations and produce only a limited degree of heat extraction.

The concept currently being utilized for this program is to produce chilling by impingement of a cryogenic liquid on the weldment during welding. This method appears to hold promise for overcoming the major disadvantages of "hard" tooling for chilling, and it is expected that by properly selecting the cryogenic liquid and setup for applying it during welding, the required increase in chill rate can be achieved.

B. **Alter Solidification Pattern**

It has long been the practice in aluminum casting to reduce gross porosity by effecting chilling in such a manner that the casting solidifies from the bottom up and as nearly unidirectionally as possible.

Application of this practice to welding should also result in reduced porosity in aluminum weldments. It is, therefore, expected that proper application of chilling by means of cryogenic liquids, with or without the use of auxiliary heat sources, will reduce porosity in aluminum weldments.

III. <u>Program Outline</u>

A. <u>General</u>

The program is divided into two phases. The first consisted of a survey of literature and industry. The work on this survey was performed over a period of four months and was completed in August 1965. The second phase consists of the experimental work which has been in progress for approximately five months and is scheduled to be completed in September 1966.

IV. <u>Literature Reviewed</u>

The purpose of the survey was to obtain information which might be helpful in the performance of this program, by avoiding duplication of effort and/or by supplementing the original program concept.

Current abstract bulletins published by the National Aeronautics and Space Administration (STAR) and by the Defense Documentation Center (TAB) were checked for reports of work pertinent to fusion welding of aluminum, and significant reports were acquired for review.

A similar survey was made of applicable technical books and periodicals, including those of the American Welding Society, the American Society of Metals and the American Institute of Mining and Metallurgical Engineers. Particular emphasis was devoted to issues of the Welding Journal published during the past ten years.

Sixty-three reports were selected for review and were classified under three general subject areas according to their principal interest to this program: (1) Time-Temperature Studies, (2) Heat Flow During Welding, and (3) General Welding Techniques.

No reported or unreported work was found which would indicate that any part of this program is a duplication of effort. A considerable amount of information was obtained which will facilitate the experimental portion of the program, particularly that work pertaining to heat transfer analysis and specific welding techniques currently in use for fabricating aerospace structures by welding the particular materials involved.

V. Organizations Contacted

Those organizations and individuals who were considered to be involved in work related to this program were contacted for personal interview or for interview by telephone. The cooperation was excellent, and in some cases special data were furnished and tours of plant facilities arranged. In general, a great deal of interest was expressed in this program.

It appears that at the present time, no specific work is in progress to develop data in addition to that already reported in the literature for development of time-temperature controls or theoretical heat flow information for welding of aluminum alloys.

However, in some work recently completed by Frankford Arsenal it was determined that three significant trends were noted in the microstructure which indicate the merit of the use of super-chilling during welding of aluminum: (1) the amount of microporosity was substantially lessened, (2) the width of the zone of grain boundary melting at the interface was reduced appreciably, and (3) a finer grained cast structure was obtained.

All of this work was performed on 0.090" thick 2014 and 2024 aluminum alloys. In one set of experiments the chill bars (both top and bottom) were cooled with brine at -45°F. In a second set, for which data has been published recently, the chill bars were cooled with liquid nitrogen. In each case, welding was performed after the parts to be welded reached a selected temperature, -30°F and 250°F, respectively. Difficulty with condensation of moisture on the parts was overcome by enclosing the part in a flexible bag containing dry argon or helium.

A large amount of work has been done and is currently in progress to improve the quality of weldments in aerospace components fabricated from aluminum. Although only a few specific studies have apparently been conducted on a laboratory basis for determining the effect of time-temperature on properties of weldments, a good many of the process controls adopted for shop welding are aimed in the direction of controlling thermal patterns.

VI. Experimental Program

A. General

The experimental program consists of two essential steps. The first is to establish realistic target thermal patterns designed to improve the weld properties. The second will be to devise and test various means of providing the temperature controls through heat input studies and studies to determine the effectiveness of heat extraction by cryogenic liquids. For these studies, plate in two thicknesses (1/2-inch and 5/16-inch) in each of two alloys (2014-T6 and 2219-T87) will be used. Tensile properties of the 2014-T6 material are shown in the following table:

Figure 1

2014-T6 Parent Metal Tensile Properties

Material	Grain Direction	Yield Strength (psi)	Ultimate Strength (psi)	Elongation in 1" (%)
5/16" 2014-T6	Long.	64,800	69,900	15.0
5/16" 2014-T6	Trans.	64,000	70,900	15.0
1/2" 2014-T6	Long.	62,400	68,100	14.0
1/2" 2014-T6	Trans.	60,900	69,200	11.7

Welding will be performed in the horizontal position by the semi-automatic TIG process, using direct current straight polarity, on square butt joint preparation, with 2319 filler

wire and helium shielding gas. It is contemplated that various cryogenic liquids and auxiliary heat sources will be used to alter thermal patterns during welding. Tensile tests and hardness surveys will be used to correlate mechanical properties with thermal pattern.

B. **Modification of Equipment**

Existing equipment was modified as shown in the following photograph (Figure 2) for welding test panels from one side in the horizontal position. The basic equipment consists of a Miller Model 600/1200 power supply, a Miller high frequency unit, a Berkley Davis side beam and carriage system, an Airco TIG welding torch and wire feed system with mounting brackets, a fixture for 12" x 48" weld panels, a cryogenic jet spray system and suitable brackets and attachments for mounting radiometers.

C. **Instrumentation**

As shown in the following sketch (Figure 3) the instrumentation for monitoring welding process variables and thermal patterns in the weld panels consists of Weston ammeter and voltmeter, an optical tachometer, a Leeds & Northrup 12-channel temperature recorder with thermocouples, an Airco helium flowmeter, an Airco filler wire speed regulator, a Tektronic oscilloscope, and infrared radiation thermometers.
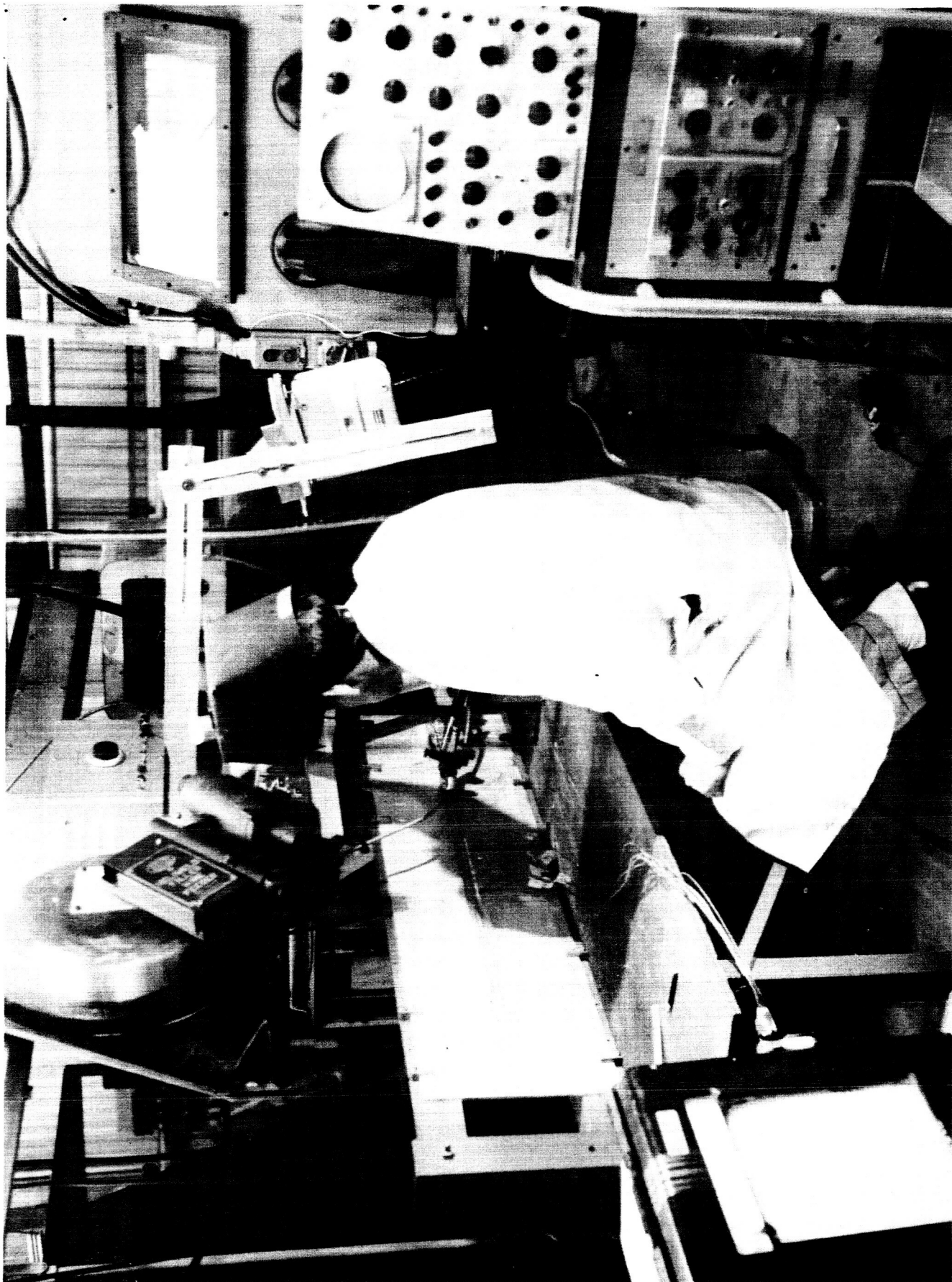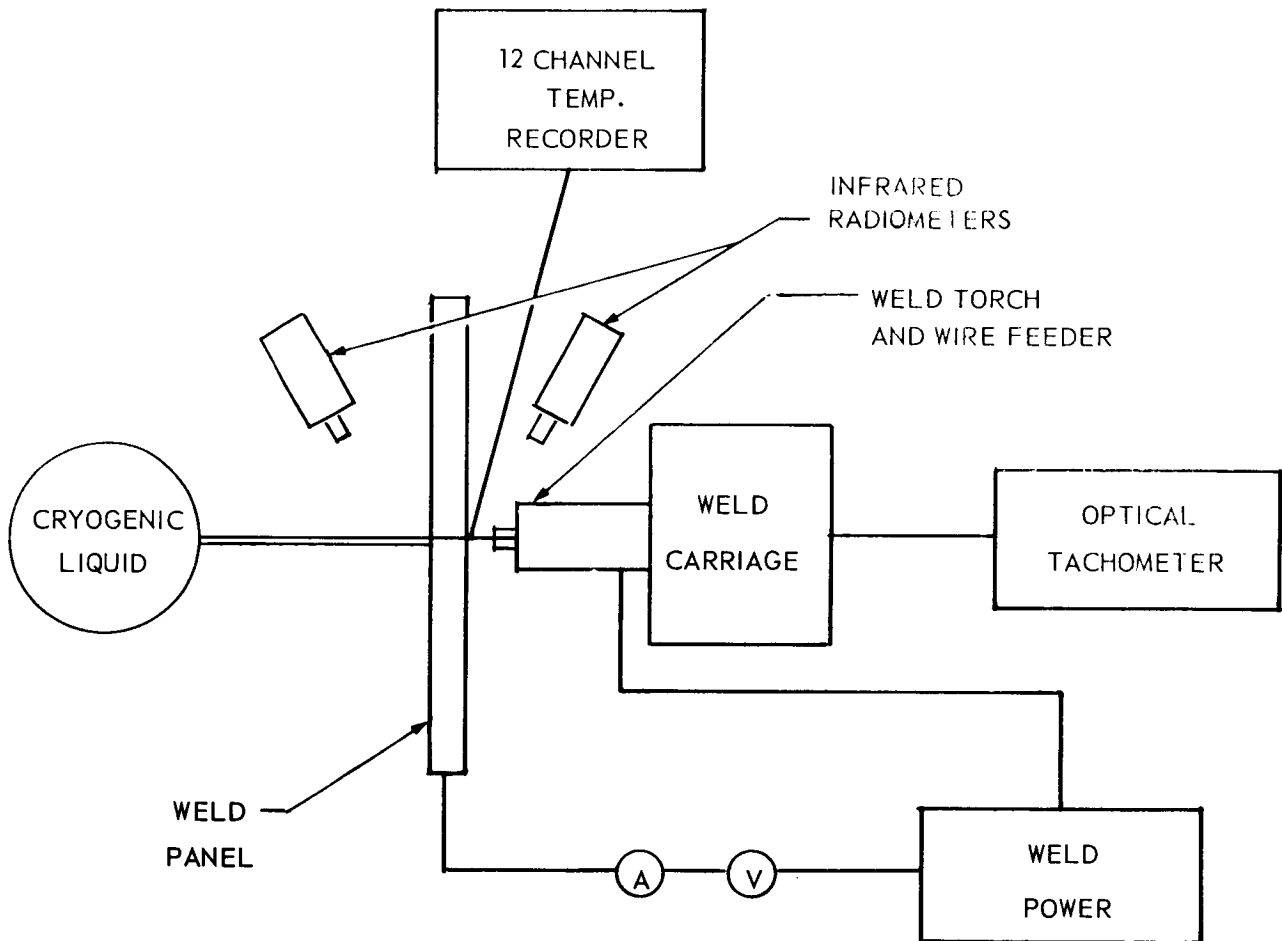
Figure 2

215

Figure 3.

SKETCH OF EXPERIMENTAL SETUP

D. Reference Weldments

In order to establish reference data to which future experimental welding will be compared, weldments in each of the aluminum plate materials are to be fabricated under monitored conditions without the use of chilling. The thermal pattern data in connection with the mechanical and metallurgical characteristics of these weldments will be used as the starting point for alteration of thermal patterns to improve the properties.

E. Preliminary Check-out of Cryogenic System

Preliminary trials of the liquid CO_2 system shown in the following sketch (Figure 4) indicate that more than adequate chilling effects can be obtained on the back side of the weld. A 250 lb. container with flexible delivery tube and a variety of nozzles with orifice sizes from 0.008" to 0.032" are available for subsequent modifications.

Figure 4.

Jet Arrangement No. 1:

Weld Torch

Backing Material

½" | ½" | ½"

Jet (.024" orifice)

Jet (.014" orifice)

Liquid CO_2 Source
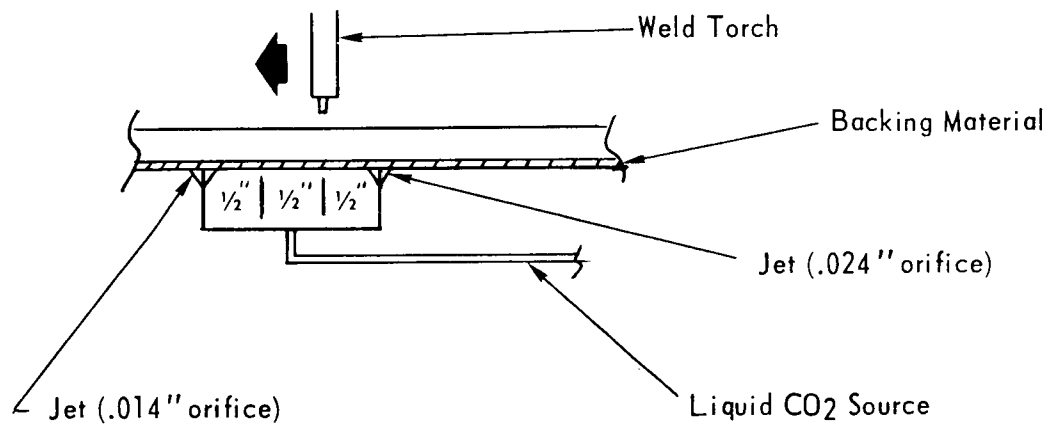
Backing Material No. 1: Adhesive glass tape over
non-adhesive glass tape.

VII. Preliminary Data

A. Weld Schedules

Using the weld setup and jet arrangement shown in the previous sketches, welding schedules were developed and heat input calculated for the penetration passes in 5/16" and 1/2" plate as shown in the following table:

Figure 5

Weld Panel Number	Thickness (inches)	Chilled	Weld Parameters	Heat Input (BTU/in.)
1A1	5/16	no	250 amps 14 volts 9.0 ipm	22.2
1EC1	5/16	yes	235 amps 16 volts 6.9 ipm	31.1
1F2	1/2	no	300 amps 16 volts 7.5 ipm	36.4
1DC3	1/2	yes	310 amps 15 volts 6.0 ipm	44.1

It is realized that these schedules may not be optimum, and are subject to modification as experimental work continues. Welds in the 1/2" thicknesses were made without filler wire. Those in the 5/16" thicknesses were made with the addition of 2319 filler wire in a subsequent weld pass.
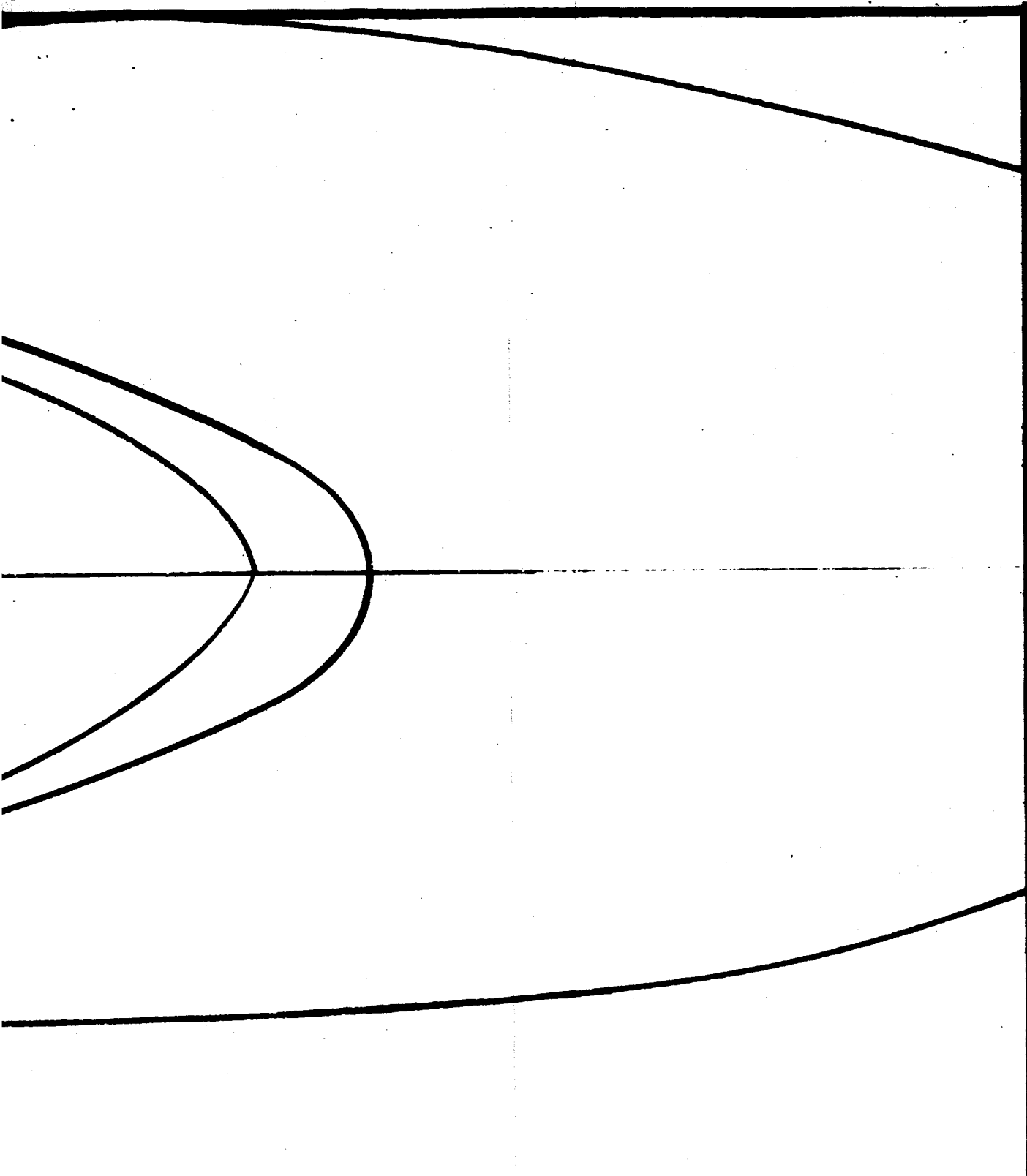
CHILLED, 1/2" 2014-T6, PENETRATION PASS

,NO CHILLING, 1/2" 2014-T6, PENETRATION PASS

ATTERN   FULL SCALE

224

THERMAL CYCLE CURVES FOR A TYPICAL
SINGLE POINT ON THE WELD CENTERLINE
DURING THE WELDING OPERATION

Time at Temperatures above 500F:

Unchilled: 48 sec.

CO_2 Chilled: 32 sec.

Quench Rate 750F to 500F:

Unchilled: 15.5F/sec.
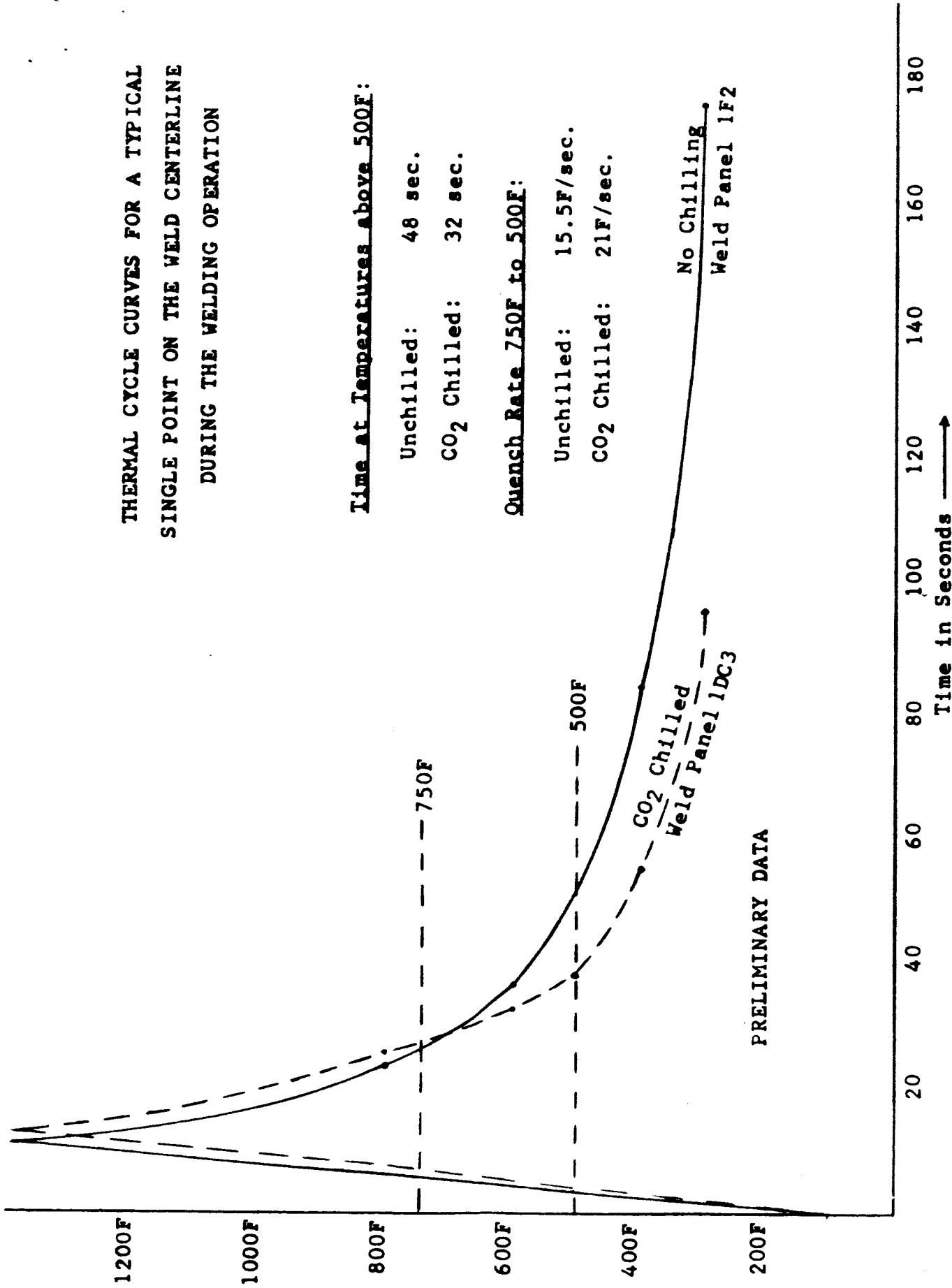
CO_2 Chilled: 21F/sec.

No Chilling
Weld Panel 1F2

750F

500F

CO_2 Chilled
Weld Panel $1DC_3$

PRELIMINARY DATA

1200F
1000F
800F
600F
400F
200F

20   40   60   80   100   120   140   160   180

Time in Seconds ➔

FIGURE 11   EFFECT OF LIQUID CO_2 CHILLING ON TIME-TEMPERATURE CURVES DURING
WELDING OF 1/2" 2014-T6 ALUMINUM PLATE

225

jet arrangements in combination with minimal heat input, a quench
rate closer to the theoretical required for maximum properties
can be achieved (100°F/sec).

Figures 12 - 14, inclusive, show similar data for welds in
5/16" plate. The effect of chilling is even more pronounced in
the thinner material, as the same jet arrangement was used as
for the thicker material; i.e., more chilling was available per
unit of metal than for the 1/2" plate.

C. Radiographic Inspection

All welds contained some degree of porosity. Those made
by one penetration pass without the addition of filler wire
(1F2 and 1DC3) contained relatively small amounts of fine
scattered porosity. The two welds made by one penetration
pass and one filler pass (1A1 and 1EC1) contained substantial
amounts of large porosity. Of this group, the unchilled weld
(1A1) exhibited 60% more porosity than the chilled weld (1EC1).
A large amount of this porosity in the unchilled weld was
lineal, while the porosity in the chilled was essentially
scattered.

Results of preliminary X-ray examination and tensile test
fracture studies indicate that chilling the back side of the
weld with liquid CO_2 effects some reduction in gross porosity.
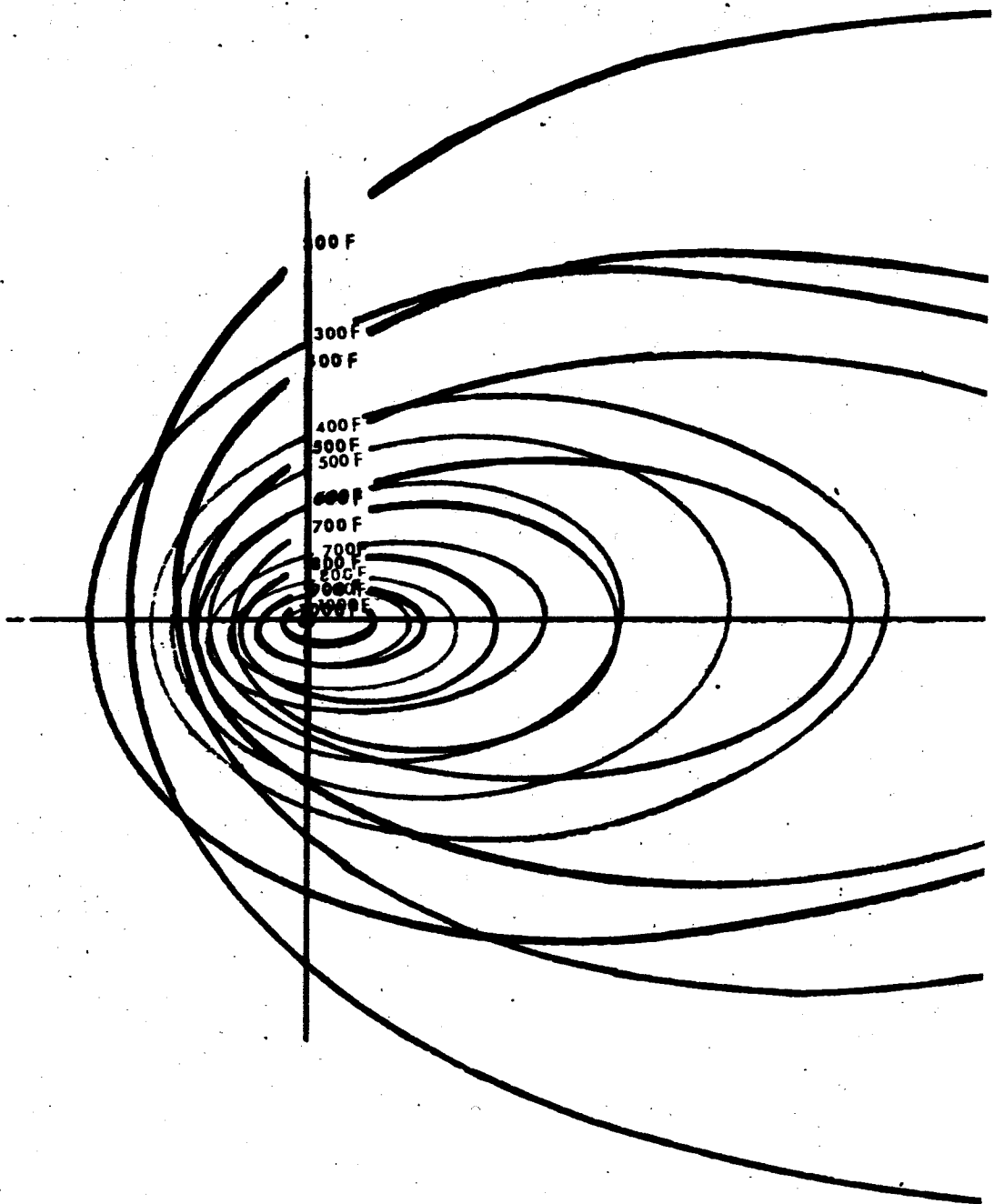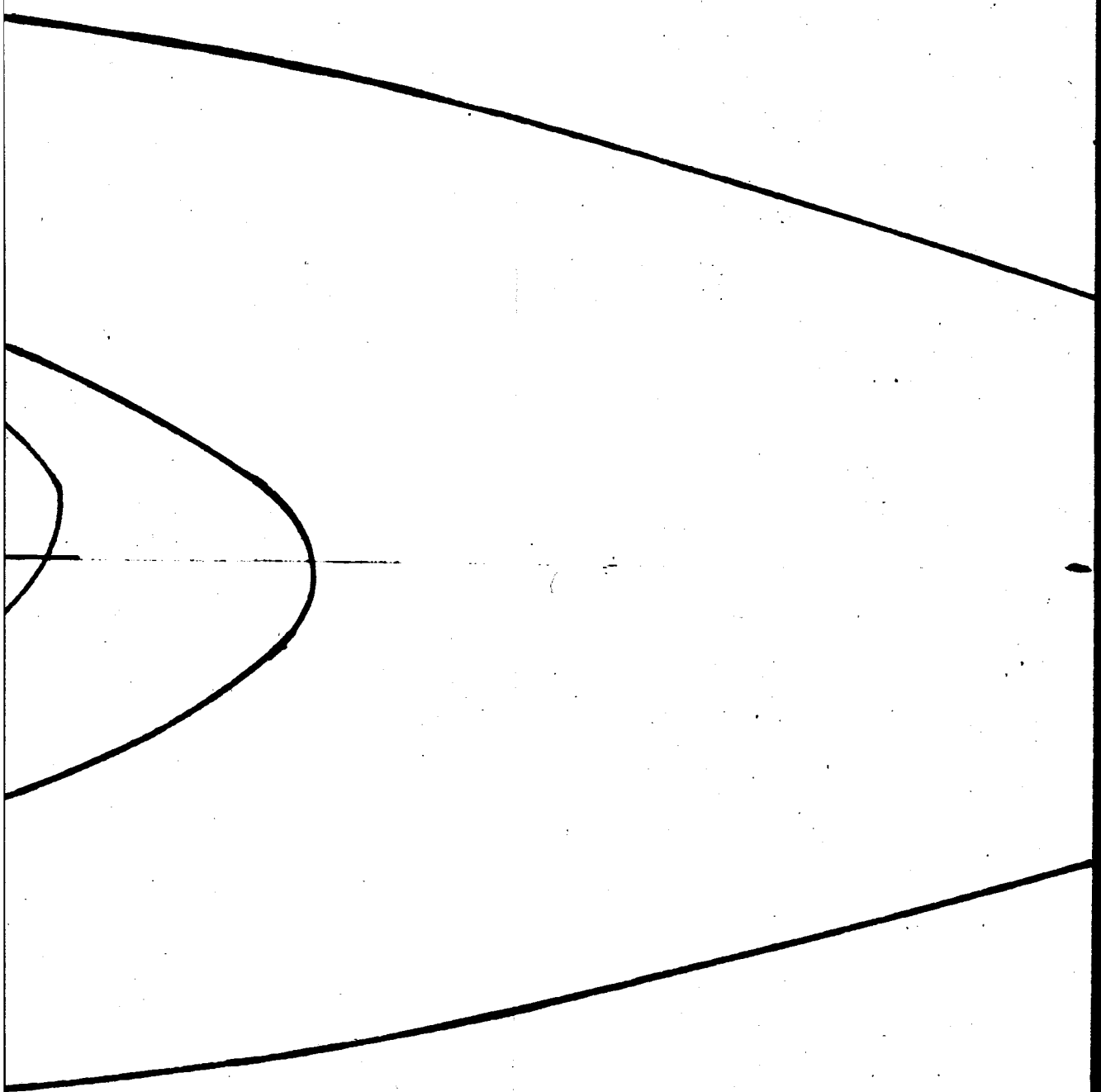For welds in 5/16" 2014-T6 plate, the average porosity for all

226

FIGURE 12. THERMAL PATTERN FOI

FIGURE 13 THERMAL PATTERN FOR V

227

CHILLING, 5/16" 2014-T6, PENETRATION PASS.

CHILLED, 5/16" 2014-T6 PENETRATION PASS.

ERN

FULL SCALE

228

THERMAL CYCLE CURVES FOR A TYPICAL
SINGLE POINT ON THE WELD CENTERLINE
DURING THE WELDING OPERATION

Time at Temperatures above 500F:

Unchilled: 42 sec.

CO_2 Chilled: 27 sec.

Quench Rate 750F to 500F:

Unchilled: 10F/sec.

CO_2 Chilled: 25F/sec.

No Chilling
Weld Panel 1Al

750F

500F

CO_2 Chilled
Weld Panel 1EC1

PRELIMINARY DATA

1200F

1000F

800F

600F

400F

200F

10   20   30   40   50   60   70   80   90
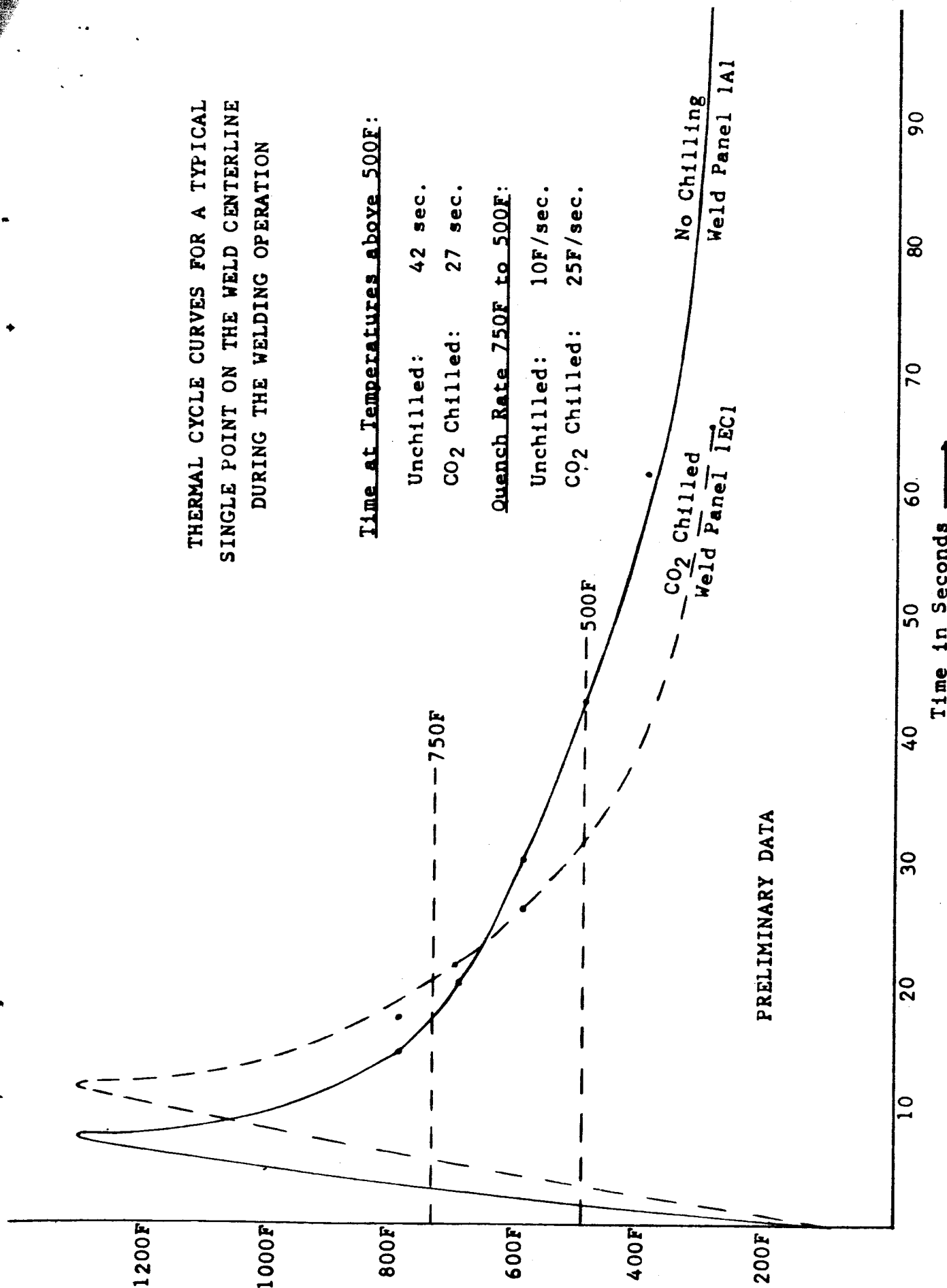
Time in Seconds ──▶

FIGURE 14 - EFFECT OF LIQUID CO_2 CHILLING ON TIME-TEMPERATURE CURVES DURING
WELDING OF 5/16" 2014-T6 ALUMINUM PLATE

specimens from the unchilled weld panel was 5%, while the average porosity for all specimens from the chilled weld panel was 2%, indicating that chilling reduced the amount of this porosity by a factor of more than two.

For specimens from the 1/2" plates, welded without the addition of filler, X-ray results and fracture studies indicated less than 1% porosity in both chilled and unchilled welds.

Gross lineal porosity appears to be associated with the addition of filler wire. The causes for fine scattered porosity have not yet been determined. In both instances, the causes must be investigated and corrected before the effect of chilling on eliminating or reducing porosity and improving weld properties can be properly evaluated.

While these results cannot be considered conclusive, and indicate the need for further refinement of general welding techniques, there appears to be sufficient evidence of improvement to warrant further development of the current concept.

D. Metallurgical Examination

Examination of the structure of the welds by macrosection indicated that chilling substantially reduces the extent of the heat affected zone and also reduces grain size as shown in the two following illustrations (Figures 15 and 16).
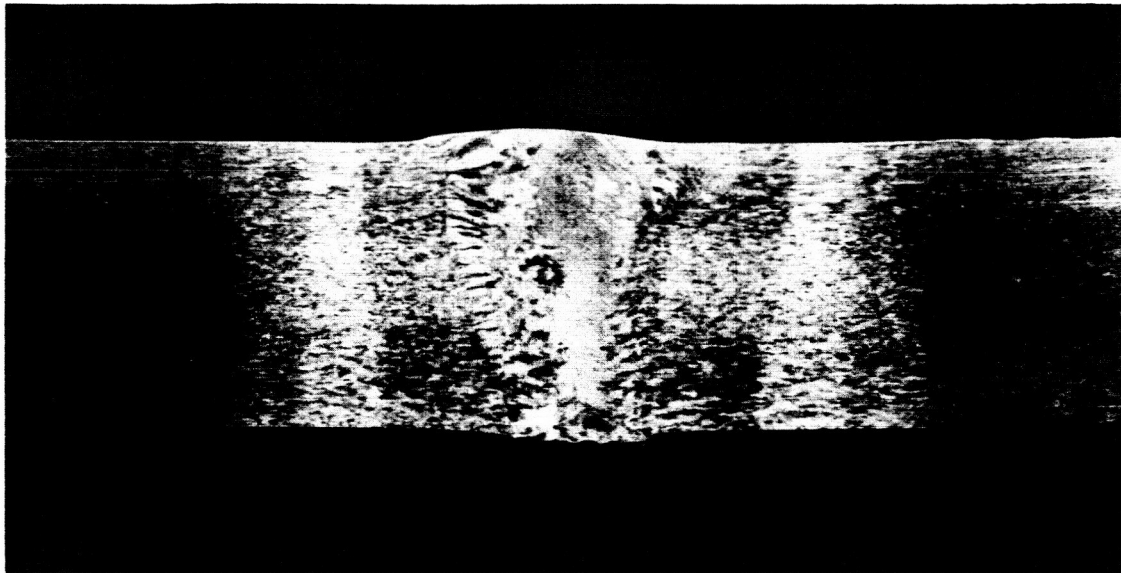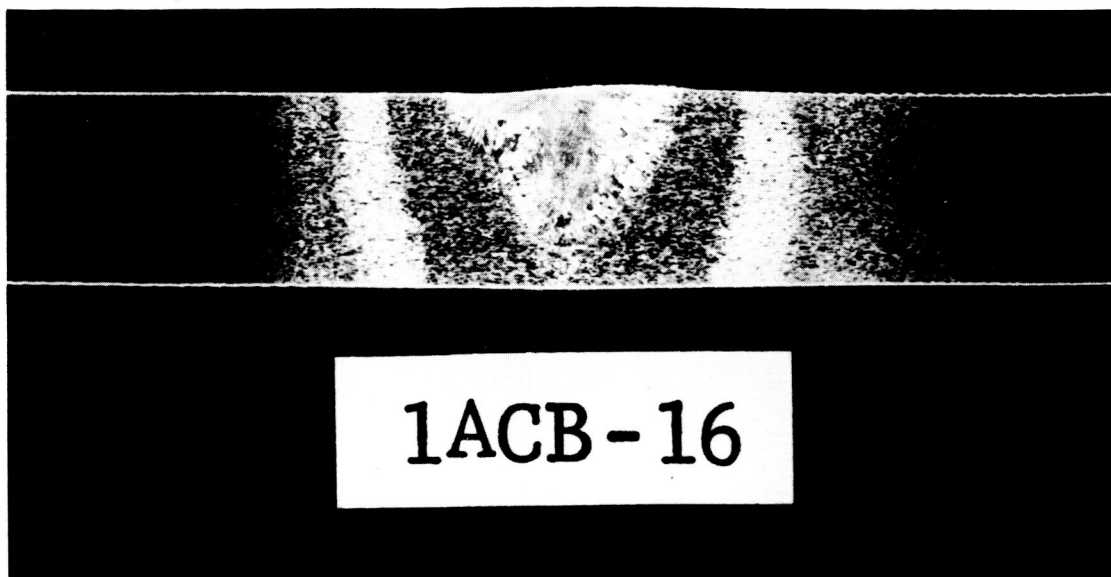
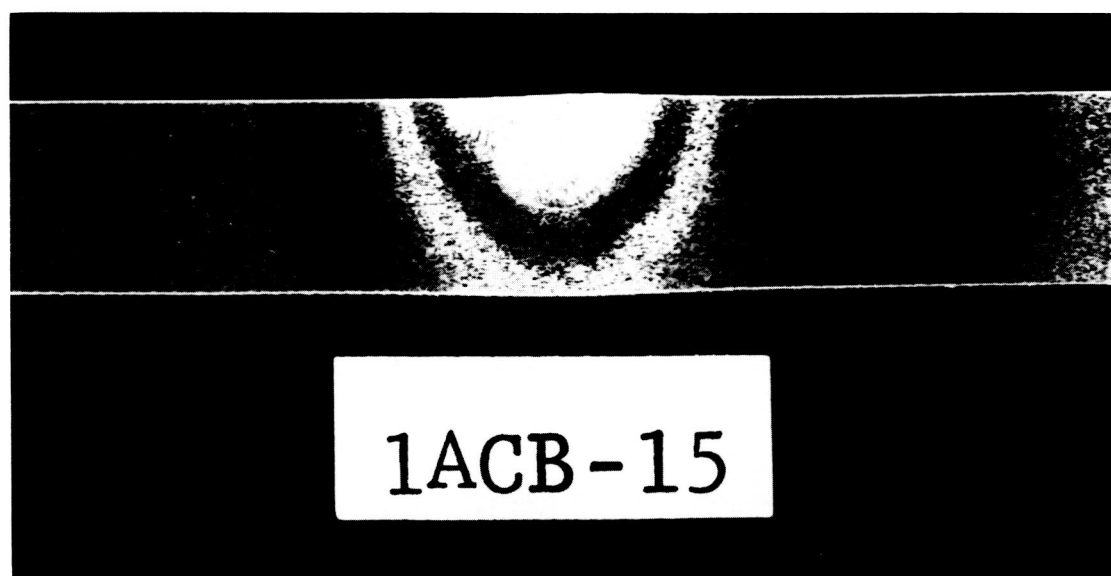**MACROSECTION OF WELD**
PANEL 1F2, 1/2", 2014, NO FILLER
NO CHILLING
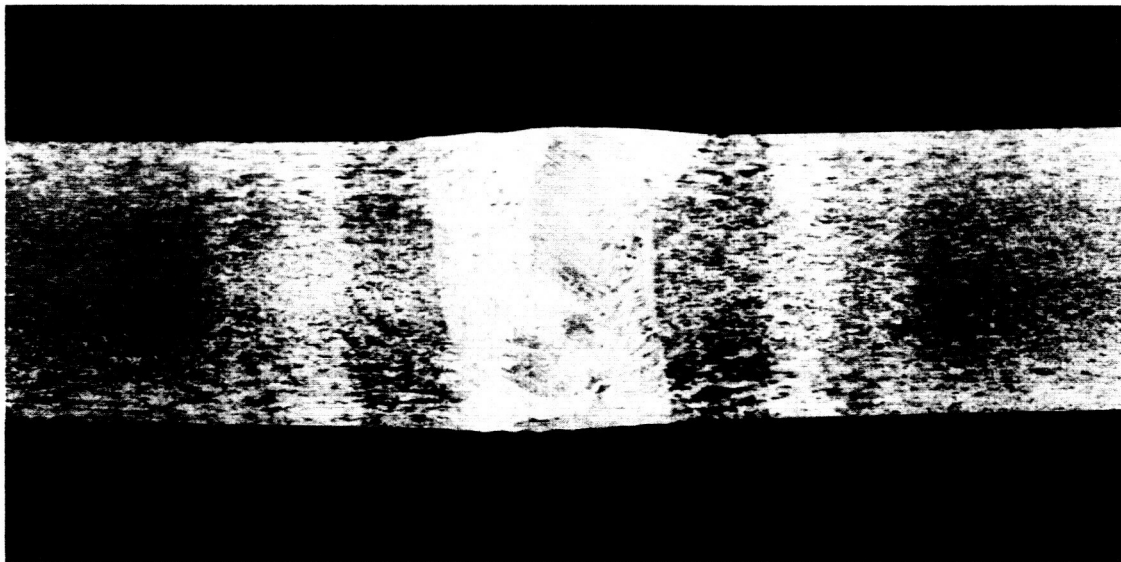
MACROSECTION OF WELD
PANEL 1DC3, 1/2" 2014, NO FILLER
CO_2 CHILLED

Figure 15

NO CHILLING

CO$_2$ CHILLED

Figure 16

In Figure 15, macrosections of two welds in 1/2" plate of 2014 alloy are shown. The thermal pattern for these welds was shown in Figure 11. It will be noted that the size and orientation of grains in the weld bead has been considerably improved by chilling in spite of the fact that the fit-up between the plates was not as good and a wider weld bead was required. It will also be seen that the heat affected zone is narrower when chilling is employed.

In Figure 16, two bead on plate welds in 1/2" plate are shown in which the heat input was the same in both cases. Again, it will be seen that the grains in the weld bead are smaller and differently oriented and that the heat affected zones are considerably more narrow in the chilled weld.

E. **Tensile Tests**

1. **Weld Specimens**

Location of specimens for tensile testing was selected from the X-ray films so that representative porous and non-porous areas were included. All specimens were 12 inches long with the weld bead transverse and centered in a 1" x 7" reduced section (the weld line being parallel to the direction of rolling). Six specimens were prepared for each weld panel, three with the weld bead intact and three with the weld bead flush with the parent metal.

2. Weld Tests

The following table (Figure 17) shows averages of tensile test results for specimens from welded panels in 5/16" and 1/2" 2014-T6 plate.

Figure 17

Comparison of Tensile Properties of Unchilled Welds
and Welds Chilled by Liquid CO_2 in 2014-T6 Plate
(Preliminary Data)

Specimen	Test	Tensile Properties		
		Unchilled	Chilled	Improvement
5/16" Bead on	Yield (psi)	27,900	30,300	8.6%
	Ultimate (psi)	42,100	45,500	8.1%
	% Elongation in 2"	5.0	7.0	20.0%
1/2" Bead on	Yield (psi)	27,500	31,500	14.5%
	Ultimate (psi)	45,300	47,600	5.8%
	% Elongation in 2"	5.5	6.0	9.1%

All tests were performed at room temperature. In order to evaluate the effect of chilling on tensile properties, it was necessary to select tests for specimens which contained less than 1% porosity in the fractured area so that the effect of porosity would not mask the effect of metallurgical changes. It was further necessary to limit these specimens to comparable groups, which again narrowed the selection.

It appears that there are improvements in tensile strength ranging from approximately 5% to 14% for welds chilled by CO_2

over unchilled welds, with corresponding increases in elonga-
tion. Although the observed improvement is based on limited
data, it is believed that there is some justification for
optimism as the tests were randomized by the fact that two
thicknesses were welded, thus averaging out variables which
might not have been precisely controlled.

3. Infrared Radiation Thermometer Evaluation

Attempts to quantitatively interpret the signal from
a line scanning infrared radiometer with respect to tempera-
ture of specific points on the weld panel during welding were
unsuccessful. On the basis of work performed to date, it is
felt that a great amount of additional effort and costly
supplementation would be required to utilize effectively the
line scanner as a monitor for thermal patterns during welding.
Single point radiometers appear to offer more promise; and
therefore, it is expected that efforts in the near future
will be confined to this type.

VIII. Future Work

It is expected that during the remainder of the program means of producing and controlling optimum thermal patterns for the materials under consideration will be developed (Figure 18)

Figure 18

Devise and Test Means of Controlling Thermal Patterns

Optimum Time-Temperature Cycles

    Minimal heat input control
    Auxiliary chilling devices

Optimum Solidification Patterns

    Auxiliary chilling devices
    Auxiliary heating devices

Additional cryogenic liquids (nitrogen, argon, and possibly helium) will be investigated; various jet arrangements, positions, and orifices will be tried; and, if necessary, auxiliary heat sources will be used to obtain the desired time-temperature cycles and solidification patterns.

IX. Conclusions

Based on this preliminary data, it appears that it will be possible to achieve the goal of the program to improve the tensile properties and reduce porosity by refinement and supplementation of present concepts for controlling the thermal pattern during welding. Tensile results indicate an improvement in strength of 5 to 14% with increases in elongation of up to 20%. Chilling apparently reduced gross porosity in welds made with filler wire by a factor of more than two.

SECTION VII

RELATIONSHIPS BETWEEN WELD QUALITY AND NON-VACUUM ELECTRON BEAM WELDING PROCEDURES

N66 35573

F. D. Seaman

Westinghouse Electric Corporation
Astronuclear Laboratory

ABSTRACT

Critical procedure details for non-vacuum electron beam welds have been identified and related to such qualities as undercut, bead width, contour and porosity. Welds that are consistant with actual quality standards have been produced. The strength of one-side one-pass welds produced exceeds the reported strength of TIG welds. Work has been accomplished on .250 inch 2219-T37 and is being continued to include .5 inch 2219-T37 and T87.

PRECEDING PAGE BLANK NOT FILMED.

INTRODUCTION

During 1964 Westinghouse engineers had completed a systems engineering study aimed at developing an electron beam welder specifically for the demanding conditions of non-vacuum welding. This approach not only freed the electron beam process from the confinement of a vacuum chamber but also provided the gun with some of the flexibility of an automatic TIG welding head.* Further, limited tests indicated that the unit might show a number of advantages over conventional arc processes (i.e., lower distortion, less heat input, higher welding speeds, etc.)**

On June 15, 1965 a contract between NASA (Manufacturing Engineering Laboratory) and the Westinghouse Electric Corporation was initiated. Phase I of this contract is a welding engineering study. Phase II required the construction of a light weight, portable non-vacuum electron beam welding head, manipulator and enclosure. The Phase II effort is progressing satisfactorily, but is not within the scope of this paper and will not be discussed further.

The objective of the Phase I welding portion of the program was to demonstrate in Task C the practical capabilities of the 15 KVA portable, light weight, versatile non-vacuum electron beam welding unit (XWEB 15121) by applying it to materials and thicknesses characteristic of existing space hardware and inspecting the welds according to actual hardware standards - as opposed to the generalized in-house study that had preceeded this contract. In order to meet the above objectives it was necessary to complete two preliminary experimental programs using an available 10 KVA laboratory welder and translate the findings of these programs to the demonstration of the welding capabilities of the 15 KVA unit.

Task A (10 KVA Laboratory Welder) - An existing Westinghouse 10 KVA non-vacuum electron beam welder was applied to the study of the relationship between welding procedure details and the achievement of the radiographic quality established in ABMA-PD-R-27A, Class 2 (and other standards as set forth in ABMA-PD-W-45).

---

* J. Lempert, J. Lowry, F. Seaman, C. Williams, "A Compact Non-Vacuum Electron Beam Welder" Proceedings of Electron and Laser Beam Symposium, 1965, p. 393.

** F. Seaman, J. Lempert, J. Lowry, C. Williams, "Joining 2219 Aluminum Alloy with the Westinghouse Non-Vacuum Electron Beam Welder" 9th National Symposium "Joining of Metals for Aerospace", Society of Aerospace Materials & Process Engineers, Nov., 1965.

Task B (10 KVA Laboratory Welder) - The above relationships were applied to the 10 KVA welder to permit the development of optimum as-welded mechanical properties.

Task C (15 KVA XWEB 15121) - Utilizing the 15 KVA XWEB 15121 portable, non-vacuum electron beam welder (to be built under Phase II) as government furnished equipment, scale up the information obtained in Tasks A and B to weld thicknesses of 0.5 in. (or, if possible, greater).

PROGRAM STATUS AND SCOPE OF THIS PAPER

At the present, Phase I Task A has been largely completed and thus is discussed in some detail - though the results must be considered tentative until all testing is finished. Task B has been started and only gross data can be presented. An analysis of variance will be used to determine which data represents significant findings and therefore would be eligible to appear in the final program report. Task C has not been started therefore is not included. In order to present the data the report has been divided according to the above tasks into:

Part I - Task A
Part II - Task B

EQUIPMENT

The 10 KVA laboratory unit on which welding tests covered by this paper were conducted is shown in Figure 1. This welder (unlike the XWEB 15121 unit being built in Phase II of this contract) is a stationary device designed to test development components. It is mounted in a lead cabinet having a lead glass window in the access door to permit viewing of the weld Referring to the photograph, the cylinder at the top of the gun house an oil-insulated section designed to permit the use of high voltage cables as a means of feeding power to the gun. The section of the unit marked by the Westinghouse trade mark Ⓦ is the acceleration chamber which houses the cathode assembly. The electron beam is accelerated and electrostatically focused in this region using voltages up to 150 KV. The magnetic lens may be observed directly below. The exit orifice of the gun is housed in a cylindrical lead enclosure and can be observed in the
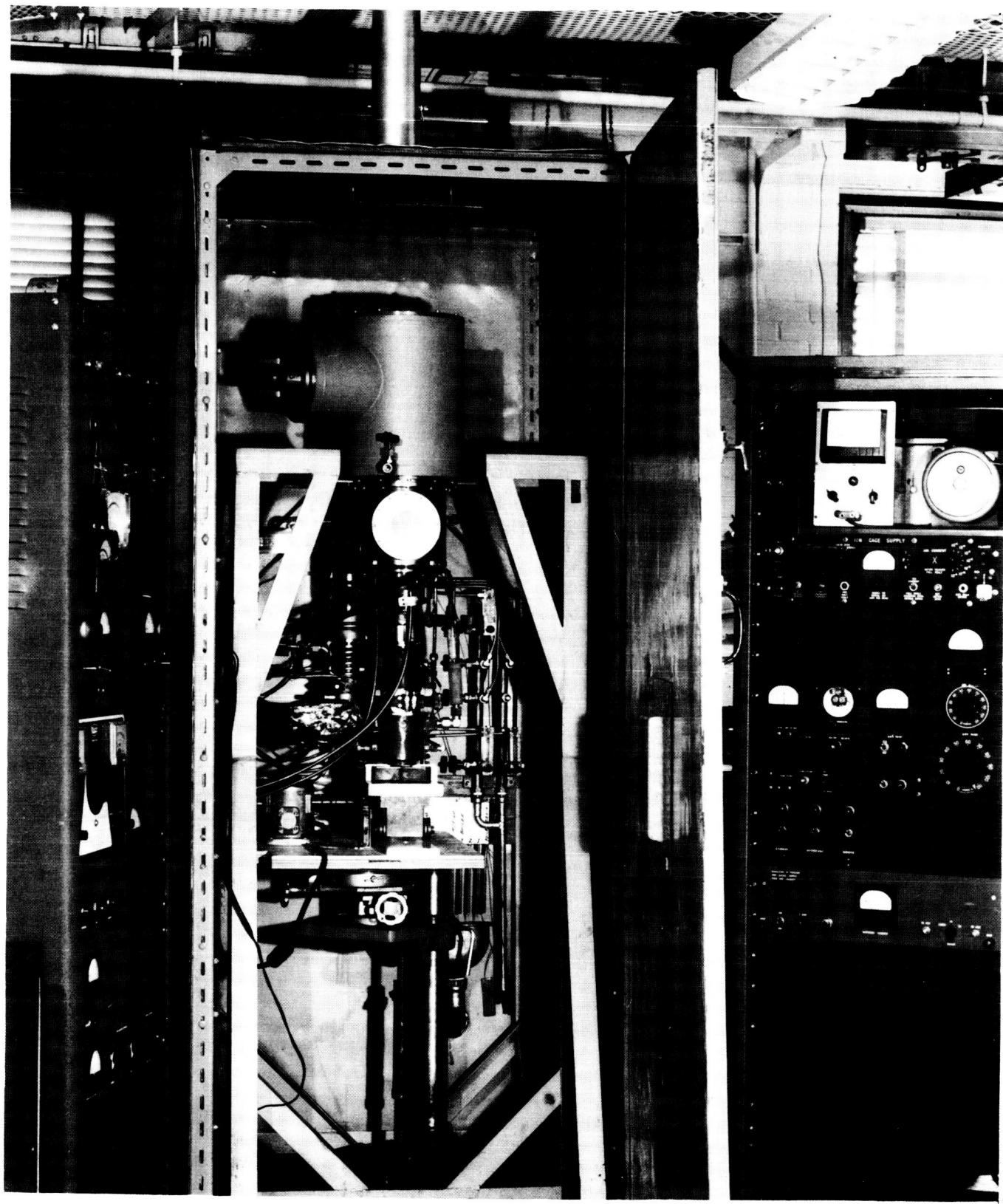
Westinghouse 10 KVA Laboratory Welder Used for Tasks A and B (Phase I)
FIGURE 1

center of the picture immediately above a rack and pinion-driven cart situated directly underneath the gun.

Electrons are released from the cathode of the gun and focused through differentially pumped orifices by a combination of electrostatic and electromagnetic electron optical systems. A positive pressure is applied at a special gas protection orifice which is located just below the exit orifice of the gun producing the flow of gas to the work area which directs particulate matter and vapor away from the nozzle. This orifice protection system minimizes contamination of the vacuum system. The use of the protective gas nozzle also permits control of the atomic number of the gas which is pumped into the vacuum system.

The stainless steel fixture (essentially parallel plane surfaces spaced about 1/2 inch from the center line of the weld) is placed on the power-driven cart directly underneath the gun. Using the adjustable table below the cart the work can be moved vertically through the nominal working range of the process (1/4" - 1/2" gun-to-work piece spacing).

MATERIAL

Material for the program was 2219 aluminum alloy furnished in the T37 condition. The nominal chemical analysis was as follows:

Typical	Si	Fe	Cu	Mn	Mg	Zn	Ti	V	Zr	Other Total
Percent (maximum unless otherwise stated)	.20	.30	5.8/6.8	.20/.40	.02	.10	.02/.01	.05/.15	.10/.25	.15

The mechanical properties of each of the 48" x 96" sheets from which test panels were cut have been determined* are as follows:

TENSILE STRENGTH AVERAGES

Thickness (Inches)	Ultimate (psi)		Yield (psi)		Elongation (%)	
	Longitudinal	Transverse	Longitudinal	Transverse	Longitudinal	Transverse
.250	66,160	66,560	52,500	50,670	15.9	14.4
.354	69,310	69,450	57,120	55,590	14.2	--

* NASA-MSFC - Manufacturing Engineering Division Request No. 83.

PART I   TASK A

USE OF A 10 KVA WELDER TO STUDY BASIC RELATIONSHIPS BETWEEN PROCEDURE DETAILS AND WELD QUALITY

In Task A the existing, demountable 10 KVA welder (Figure 1) was applied to study the relationships between welding procedures details and the achievement of weld quality. Four hundred welds were prepared and analyzed. This welding was accomplished in five experimental series. The experimental design and the findings of each series are discussed under a separate heading in the following sections:

Section A-1: Covers the relationship of procedure details such as power, speed, focus (lens current), gun-workpiece distance to the physical features of the weld. These features include contour of the upper surface, underbead drop-through and penetration.

Section A-2: Deals with various means for controlling porosity.

SECTION A-1
RELATIONSHIP BETWEEN PHYSICAL FEATURES OF A NON-VACUUM ELECTRON BEAM WELD AND MACHINE SETTINGS

INTRODUCTION

A four factor experiment was designed to establish the relationship between the physical features of the weld and machine settings using the following controlled variables (or factors):

Power (A):   2 levels were tested (both at 140 KV)

$$3.6 \text{ Kw}$$
$$6.0 \text{ Kw}$$

Gun - Work Piece Distance D_T (B):   3 levels were investigated

$$D_T = 3/8"$$
$$D_T = 7/16"$$
$$D_T = 1/2"$$

Process Speed (C):   3 levels for physical data

B/M = Bench Mark (i.e., maximum speed to produce full penetration for a given process)

85% B/M = Bench Mark speed minus 15-20% of Bench Mark

70% B/M = Bench Mark speed minus 30-40% of Bench Mark

Lens Current I_L (D): 3 levels – values vary with power level

High: Maximum lens current usable without distorting beam so that it overheats gun.

Low: Minimum lens current usable without distorting beam so that it overheats gun.

Medium: Lens current midway between high and low value for the particular power level.

Four response variables were measured. Three of these variables involved the physical dimensions of the cross section of the weld and were utilized to draw a deductive picture of the behavior of the welding process (particularly the manner in which heat energy was applied to the weldment). Additionally, such dimensions as undercut have a direct bearing on weld quality standards. The three physical variables were:

W_B – Width of the underbead.

T_B – Contour of the top of the weld bead (+ indicates crown; – indicates undercut).

U_B – Contour of the underbead (in terms of extension below the lower surface of the plate).

Porosity was also chosen as a response variable because of its direct relationship to weld quality standards. Furthermore, porosity serves as a telltale relating to thermal conditions in the weld and environmental conditions around the weld. The relationship between machine settings and porosity are discussed in Part I Task A Section A2.

In order to determine the influence of accelerating voltage a supplementary series of tests was run at 110 KV and 3.6 KW (actually 3.7 KW). Only one working distance was

evaluated. The results of this series are shown in Tables I-S (for "supplementary"), II-S, III-S, and IV-S.

The values of the individual response variables were subjected to an analysis of variance* in order to determine if any of the observed effects were significant. The results of the analysis are presented as Tables I-IV. Significance, based on 95% confidence, is indicated by the value of the "F-Ratio" in the right hand column. If this value is over the value listed in the following table the effect (i.e., A, B, C, or D), or the interaction between effects (A x B, A x D, etc.), is significant. When significance was indicated for any of the two factor interactions the F ratio was not calculated for the individual main effect.

F Ratio Values Indicative of Significance

1 and 28 Degrees of Freedom – 4.20

2 and 28 Degrees of Freedom – 3.34

4 and 28 Degrees of Freedom – 2.71

While the experiment was designed to detect 3 and 4 factor interactions none were found to be significant and the variance from these interactions was included in the residual.

In all of the welds produced to establish how machine settings or other mechanical procedure details influence the undercut, drop through and other qualities of the weld the following procedural elements were held constant (except when specifically noted).

1.   Test Specimen: All material discussed under section A-1 is .250 inch thick 2219 aluminum described under "Materials". Four inch strip was sheared from 48" x 96" plates. These strips were in turn sheared to six inch lengths.

2.   Type of Weld: Three welds were made in each panel at - each at a different lens current (Figure 2). Welds were produced in the bead-through-plate mode so that variations in joint fit up did not obscure the relationships under study.

3.   Tooling: Stainless steel support blocks were used. These were spaced one inch apart to minimize their effect on the observations.

---

* Davies, O.L., "Design and Analysis of Industrial Experiments", Hafner Publishing Company, New York City, New York

TABLE I

WIDTH AT BOTTOM (W_B)

ANALYSIS OF VARIANCE

Source of Variation		Degrees of Freedom	Sums of Squares	Mean Squares	F – Ratio
Power	(A)	1	17244.91	17244.91	
Distance	(B)	2	32150.93	16075.47	
Speed	(C)	2	111067.59	55533.80	19.4**
Lens Current	(D)	2	45584.26	22792.13	7.95**
A x B		2	19006.47	9503.24	3.32*
A x C		2	706.48	353.24	–
A x D		2	15400.92	7700.46	–
B x C		4	12424.07	3106.02	–
B x D		4	19124.07	4781.02	–
C x D		4	4857.41	1214.35	–
Residual (3 and 4 factor interactions)		28	80229.65	2865.35	
TOTAL		53	357796.76		

 * Significant at 95% Level
** Significant at 99% Level

Mean Values for Significant Effects

Grand Mean 168.8

$S = .054$
$2S = .108$

Power	Distance 3/8	7/16	1/2
25 ma	194.4	233.3	132.2
43 ma	167.8	147.8	137.2

Speed	
15/40	226.4
17.5/50	164.4
20/60	115.5

Lens	Current
H	127.8
M	187.2
L	191.4

TABLE II

UNDERBEAD CONTOUR (U_B)

ANALYSIS OF VARIANCE

Source of Variation		Degrees of Freedom	Sums of Squares	Mean Squares	F-Ratio
Power	(A)	1	492.02	492.02	
Distance	(B)	2	2414.78	1207.39	
Speed	(C)	2	3744.78	1872.39	
Lens Current	(D)	2	2671.44	1335.72	11.3 **
A x B		2	2265.14	1132.57	9.57**
A x C		2	588.48	294.24	--
A x D		2	485.15	242.58	--
B x C		4	2465.11	616.28	5.21**
B x D		4	270.11	67.53	--
C x D		4	415.11	103.78	--
Residual (3 and 4 factor interactions)		28	3313.38	118.33	
TOTAL		53	19125.50		

* Significant at 95% Level
** Significant at 99% Level

Mean Values for Significant Effects

Grand Mean   37.2

S = .010
2S = .020

Power	Distance 3/8	7/16	1/2
25 ma	38.8	42.2	21.3
43 ma	52.8	30.0	37.8

Speed	Distance 3/8	7/16	1/2
15/40	55.8	55.0	29.2
17.5/50	40.8	33.3	41.2
20/60	40.8	20.0	18.3

Lens Current	
H	27.2
M	42.3
L	41.9

TABLE III

UPPER SURFACE CONTOUR

ANALYSIS OF VARIANCE

Source of Variation		Degrees of Freedom	Sums of Squares	Mean Squares	F–Ratio
Power	(A)	1	1420.91	1420.91	
Distance	(B)	2	1009.60	504.80	
Speed	(C)	2	4127.26	2063.63	32.9 **
Lens Current	(D)	2	942.93	471.46	
A x B		2	514.70	257.35	4.11*
A x C		2	11.26	5.63	--
A x D		2	463.59	231.79	3.70*
B x C		4	553.18	138.29	--
B x D		4	309.84	77.46	--
C x D		4	430.85	107.71	--
Residual (3 and 4 factors interactions)		28	1754.42	62.66	
TOTAL		53	11538.54		

* Significant at 95% Level
** Significant at 99% Level

Mean Values for Significant Effects

Grand Mean -9.91 $S = .008$
                          $2S = .016$

Power	Distance		
	3/8	7/16	1/2
25 ma	-15.0	-21.3	-8.8
43 ma	-12.1	- 3.3	1.1

Power	Lens Current		
	H	M	L
25 ma	-5.2	-18.8	-21.0
43 ma	-2.8	- 7.1	- 4.4

Speed	
15/40	-21.5
17.5/50	- 7.8
20/60	- 0.4

TABLE IV

POROSITY

ANALYSIS OF VARIANCE

Source of Variation		Degrees of Freedom	Sums of Squares	Mean Squares	F - Ratio
Power	(A)	1	3884.52	3884.52	
Distance	(B)	2	222.11	111.06	3.59*
Speed	(C)	2	2133.44	1066.72	
Lens Current	(D)	2	364.00	182.00	
A x B		2	200.70	100.35	--
A x C		2	1128.04	564.02	18.27**
A x D		2	574.37	287.19	9.30**
B x C		4	211.45	52.86	--
B x D		4	113.89	28.47	--
C x D		4	121.33	30.31	--
Residual (3 and 4 factor interactions)		28	864.25	30.87	
TOTAL		53	9818.00		

* Significant at 95% Level
** Significant at 99% Level

Mean Values for Significant Effects

Grand Mean   113.3

S = 55
2S = 110

Power	Speed		
	15/40	17.5/50	20/60
25 ma	13.3	15.6	56.7
43 ma	62.2	205.6	326.7

Power	Lens Current		
	H	M	L
25 ma	36.7	32.2	16.7
43 ma	116.7	227.8	250.0

Distance

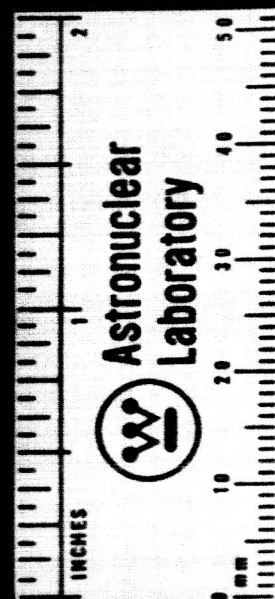|	
3/8	90.0
7 16	110.1
1 2	139.4

RESULTS OF SECTION A-1 EXPERIMENTATION

The following paragraphs cover the findings from the portion of the program concerned with the relationship between machine settings (plus gun – workpiece spacings) and the physical shape of the weld (i.e., contour, undercut width, etc.).

Penetration of a non-vacuum electron beam weld thermal energy input into the non-vacuum electron beam weld bead, such as those shown in Figure 2, can be divided into two parts (at least). First the concentrated electron beam penetrates the surface of the metal forming what has been described as a high pressure plasma in a cavity within the workpiece. The lower portion of the optimized non-vacuum electron beam weld consists of a narrow fusion zone similar to that associated with the hard-vacuum processes. This zone is a manifestation of the electron beam mode of heat input. Inelastic scattering of the emitted beam undoubtedly heats the surface of the workpiece creating the broad upper portion of the weld. Although the concentrated heat input of the beam emanates from the heart of the workpiece, thermal diffusivity can at lower speeds occur to some degree from either the scatter-source or cavity source. Thus process speed determines how much thermal diffusivity dominates the procedure.
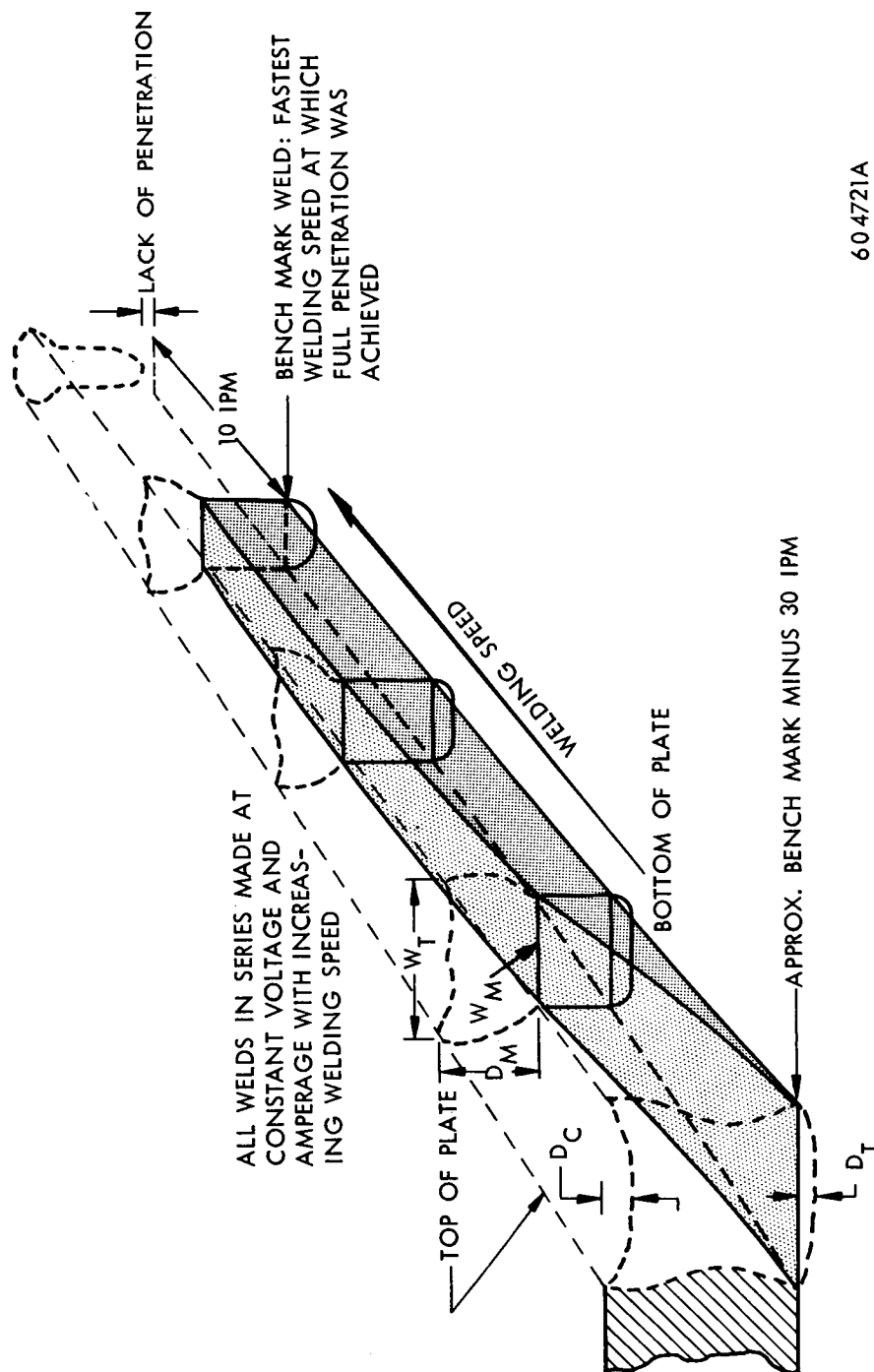
Figure 3 illustrates the increasing domination of diffusivity as speed decreased for a given set of parameters. During these experiments this progressive change in fusion zone cross section was recorded for power levels as low as 3.6 KW (where the highest process speed was 20-25 ipm) and as high as 9 KW (where the highest process speed was about 110-130 ipm).

Bench Mark Welds: Since the number of power levels were to be studied and related, the fastest weld speed at which penetration was observed for any given series of settings was termed the "bench mark" (Figure 3) weld about which the following observations can be made.

1. The bench mark (B/M) represents the lowest heat input obtainable for a one-side one-pass weld.

2. The weld cross section contour (as evidenced by weld bead width for example) of the bench mark weld at 3.6 KW is not greatly different than that at 7.8 KW if working distance and focus are held constant. The heat (K_i/in) input related to

Typical Test Series
FIGURE 2

255

LACK OF PENETRATION

10 IPM

BENCH MARK WELD: FASTEST WELDING SPEED AT WHICH FULL PENETRATION WAS ACHIEVED

WELDING SPEED

ALL WELDS IN SERIES MADE AT CONSTANT VOLTAGE AND AMPERAGE WITH INCREAS- ING WELDING SPEED

W_T

W_M

D_M

TOP OF PLATE

D_C

BOTTOM OF PLATE

APPROX. BENCH MARK MINUS 30 IPM

D_T

604721A

DEVELOPMENT OF WELD CROSS SECTION WITH INCREASING SPEED

FIGURE 3

256

bench mark welds at either 3.6 KW or 6 KW is about the same (7.2 - 6 K_i/in. respectively).

3. There is a limited range of speed below bench mark (extended downward to about 85% of bench mark speed) where welds in .250 inch material did not exhibit a significant change in fused zone cross section. Whether there is any disadvantage to utilizing this range becomes a matter relating to loss of mechanical properties and is the subject of Task B. As far as weld appearance goes it appears that either the 3.6 KW process or the 6 KW process has a $^+_-$ 7-1/2 inch per minute tolerance for speed on .250 inch thick material. In order to make the best use of available data all process speeds were stated in terms of a percentage of the bench mark speed for that process. Conventionally tests were run at 85% and 70% of bench mark and at the bench mark.

4. The following bench mark values were adopted for this program from observations made during the initial experiment:

3.6 KW process	20- 25 ipm
6.0 KW process	60 ipm
7.8 KW process	90-100 ipm (from subsequent tests)
9.0 KW process	above 110 ipm

Other publications* have indicated a relationship between power, accelerating voltage and the depth of fusion into a thick block. In butt welding it was felt to be of practical value to observe if greater power or accelerating voltage could form a full penetration joint at higher speeds or with lower thermal energy. It was also felt that other procedure details might influence the bench mark. Figure 4 graphically displays the various bench marks that were determined. Possibly the increments of working distance and speed were too coarse to detect their effect but an explainable trend does not show in the data. The higher power beam

---

*Meir, J. W., "Recent Developments in Non-Vacuum Electron Beam Welding" Presented at International Conference on Electronic Ion Beam Technology, Toronto, Canada, May 1964.

(6 KW) seemed most effected when the workpiece was near the gun. The lower power beam had an erratic effect near the gun but a more distinct trend became evident as the workpiece moved away.
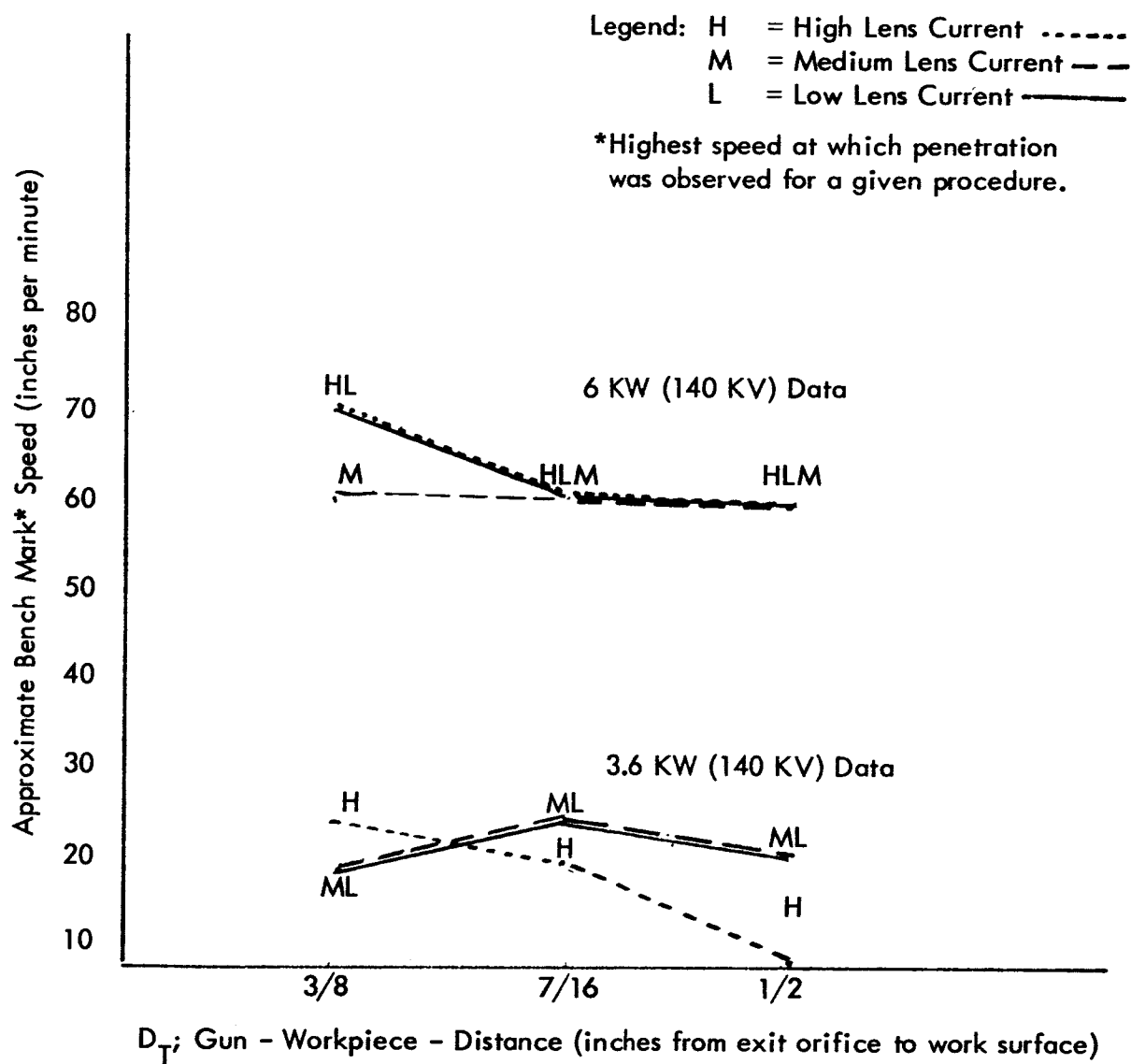
EFFECT OF WORKING DISTANCE, POWER, AND LENS CURRENT ON BENCH MARK SPEED

FIGURE 4

FACTORS EFFECTING UNDERBEAD WIDTH

Each of the variables A, B, C, and D is significant with regard to its ability to change the width of the underbead with A and B interacting and C and D appearing as main effects power. As speed was increased the mean value of the underbead width was reduced about 50% as shown in Figure 5 (a single curve can be used since the A x C, B x C, and C x D interactions are not significant). Lens current can also be considered in the same fashion and its effect can be seen in Figure 6. Changing lens current from low to medium resulted in little reduction in underbead width. The use of a high lens current apparently imparts a distinct "V" shape to the weld and underbead width is reduced by approximately 50%.

The significance of the A x B interaction in Table I suggests that the influence of working distance (D_T) depends upon the power level. The mean values for underbead width shown in Figure 7 indicate that it is the lower (3.6 KW) power setting at which working distance increases in importance as far as its effect on underbead is concerned.

Since the values investigated approximate boundary conditions for a practical process, it would appear that control of speed deserves a high priority in establishing process reliability where full penetration (as evidenced by an adequate, uniform underbead) is used as a criterion of quality.

The lack of a significant interaction between working distance and lens current (B x D) suggests that the factors which control the width of the bottom of the weld are independent of current density or focal point since these phenomenon presumably do change as distance and lens current are changed.

FACTORS EFFECTING UNDERBEAD CONTOUR

Each of the variables A, B, C, and D is significant with regard to its ability to influence the distance that the underbead extends below the plate according to Table II.

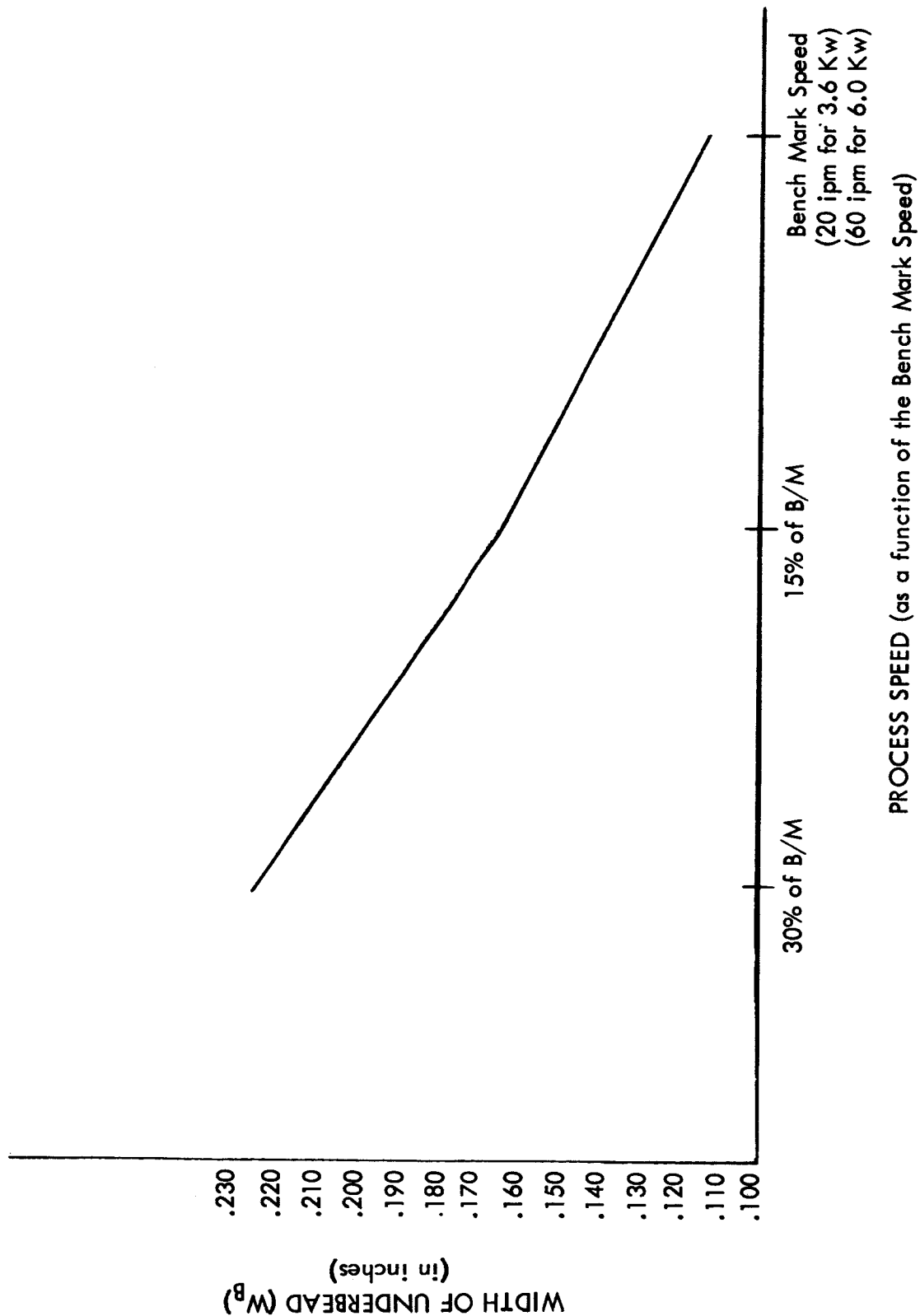PROCESS SPEED (as a function of the Bench Mark Speed)

FIGURE 5

UNDERBEAD WIDTH - COMPOSITE EFFECT OF SPEED AT TWO POWER LEVELS
THREE WORKING DISTANCES AND THREE LENS CURRENT SETTINGS
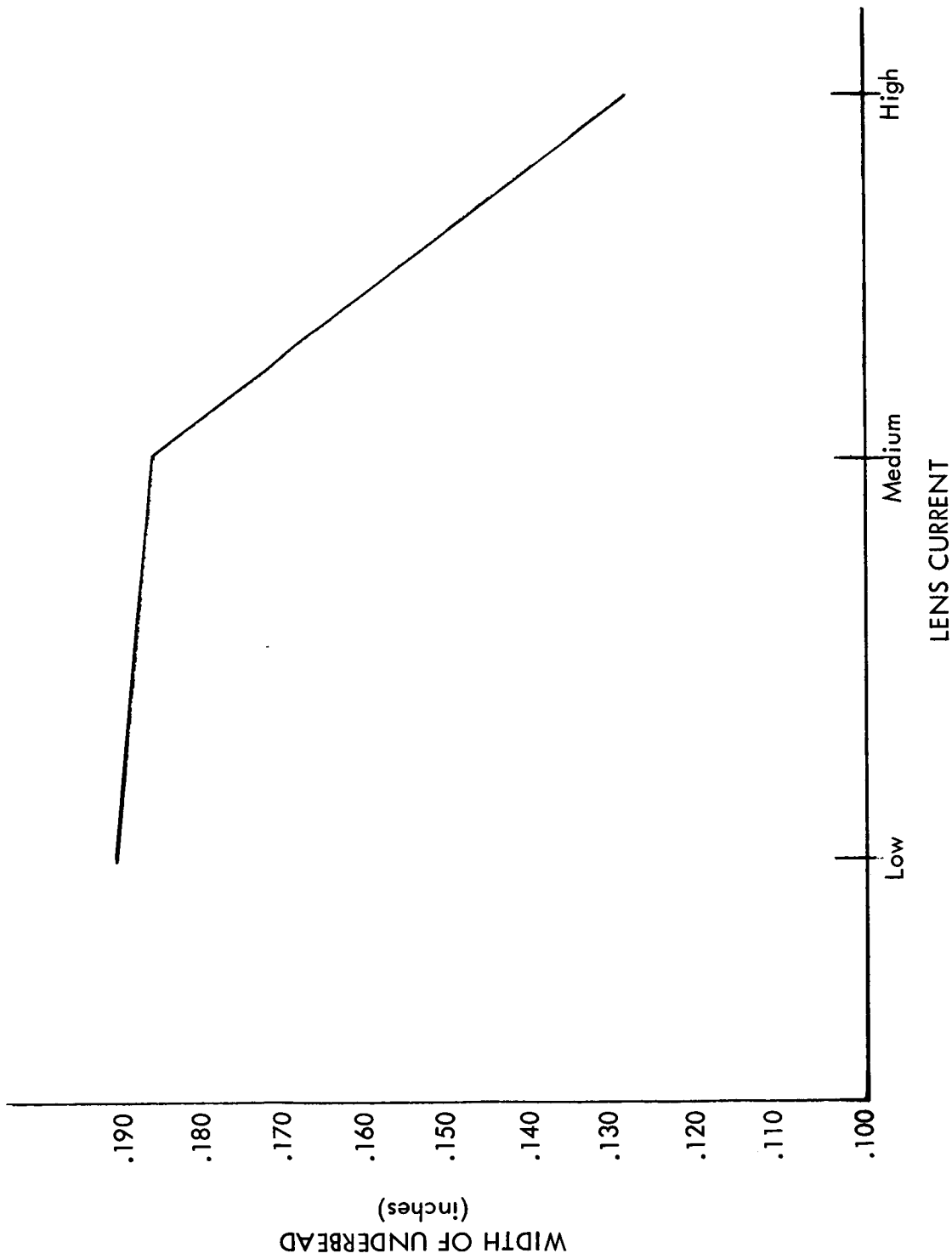
FIGURE 6

UNDERBEAD WIDTH – COMPOSITE EFFECT OF LENS CURRENT AT THREE SPEEDS
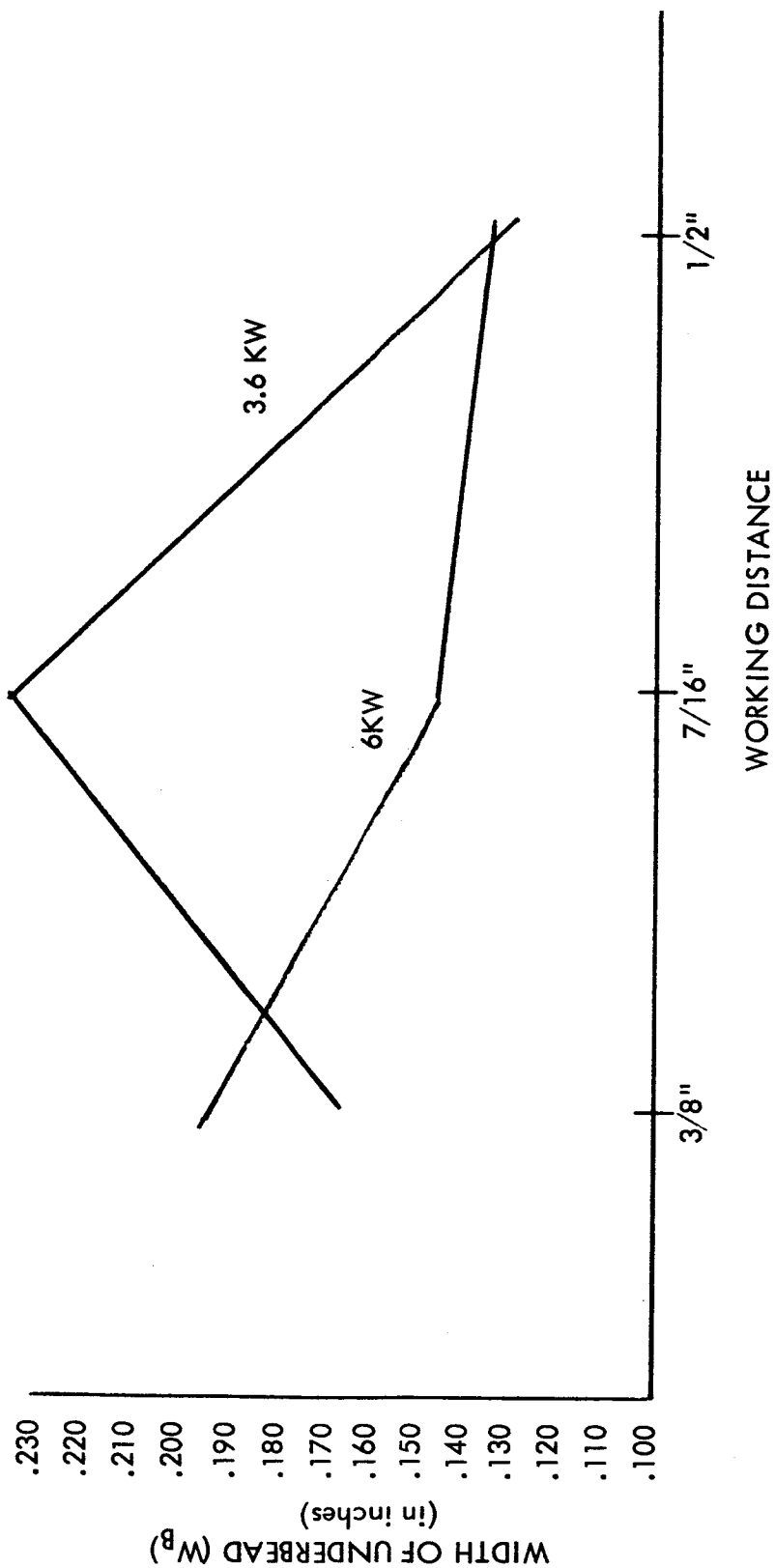THREE WORKING DISTANCES AND TWO POWER LEVELS

WORKING DISTANCE

FIGURE 7

WORKING DISTANCE - EFFECT AT TWO LEVELS OF POWER

Power (A), working distance (B), and speed (C) are all involved in two factor interactions which are discussed below. Lens current appears to operate independently, Figure 8, and suggests that high lens current (i.e., a beam that is focused nearer the gun) produces the least underbead drop through.

Increasing the working distance (Figure 9) from 3/8" to 1/2" decreases the amount of drop through. The lower power produces the least drop through at both distances. At the intermediate distance of 7/16" the effect is not as easily described. The drop through for the high power process is less than at either 3/8" or 1/2" and is greatest for the low power series, exceeding either 3/8" or 1/2".

When the effect of working distance is established with respect to its interaction with the three speeds (Figure 10) that were investigated, the trend toward reduced drop through with increasing working distance is once more evident at the highest (bench mark) and lowest (bench mark – 30% bench mark) speeds. At the intermediate speed working distance does not appear to have a consistent effect.

FACTORS EFFECTING SURFACE CONTOUR

The control of undercut is a function of each of the variables as noted in Table III. Increasing speed limits the tendency of the metal to drop out of the joint – presumably because the volume of metal that is molten for any significant period of time is minimized by the smaller weld puddle associated with faster welding process. The effect is not severe. Even when speed is reduced 15% the undercut is only .0078 inch. This value is below the confidence level of the experiment and is less than 10% of the metal thickness (a value generally used to denote unacceptable undercut). The results are shown in Figure 11.

The effect of the significant two-factor interaction involving lens current and working distance at the two power levels is shown in Figures 12 and 13. Lens Current has a significant effect when the process is operating at low power. Moving the point of focus toward or
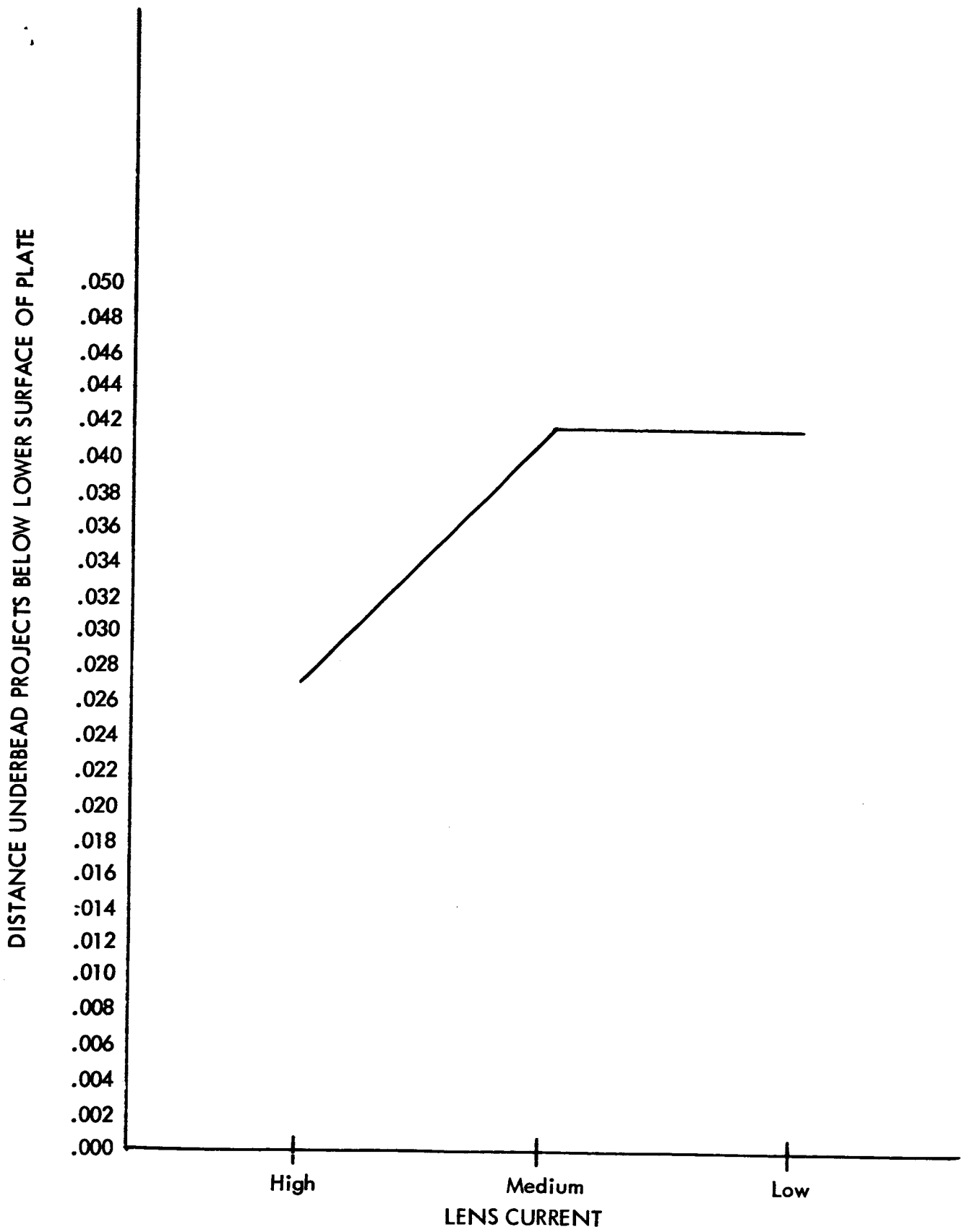
FIGURE 8

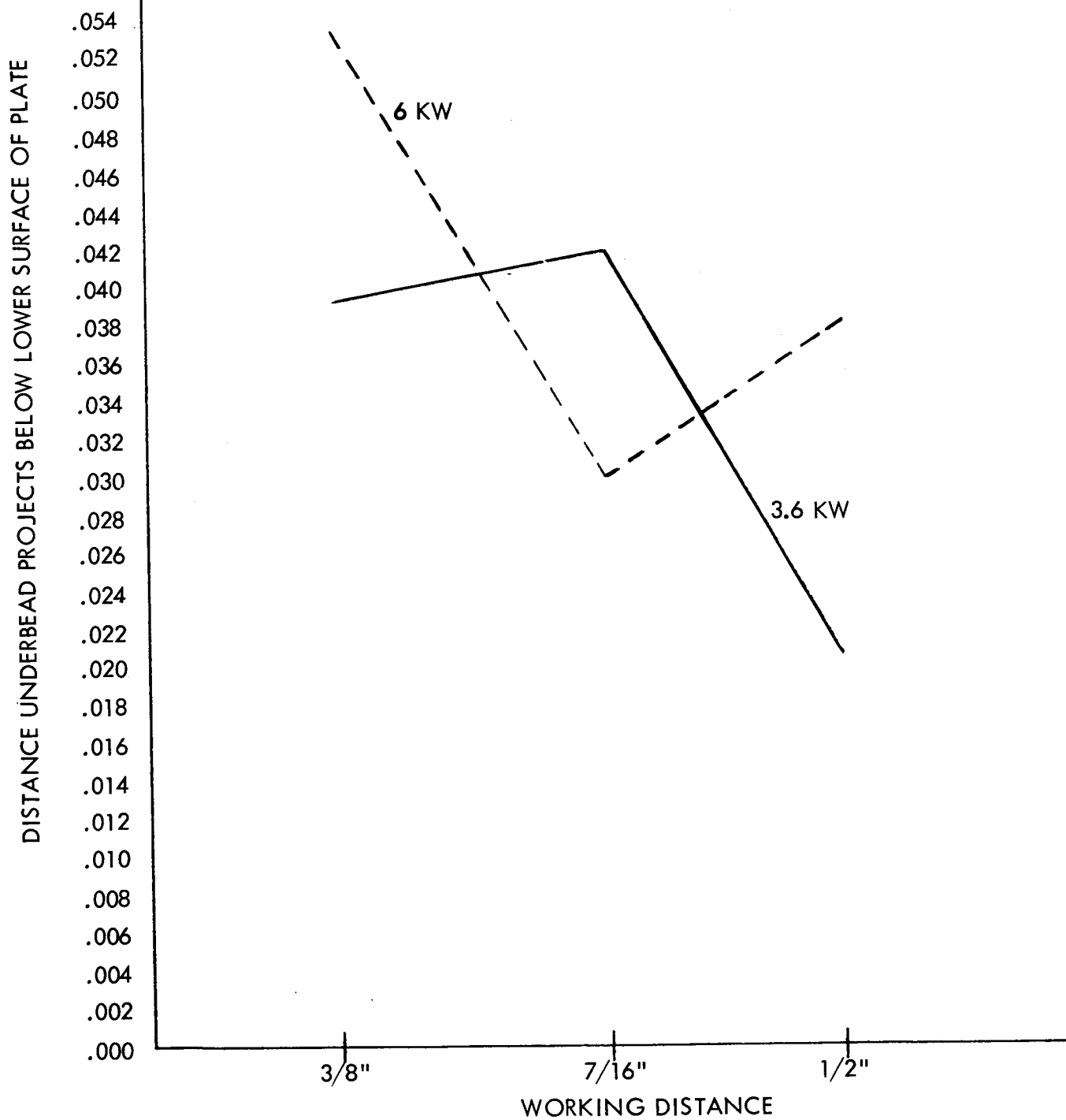COMPOSITE EFFECT OF LENS CURRENT ON UNDERBEAD CONTOUR

FIGURE 9

THE EFFECT OF WORKING DISTANCE ON UNDERBEAD CONTOUR
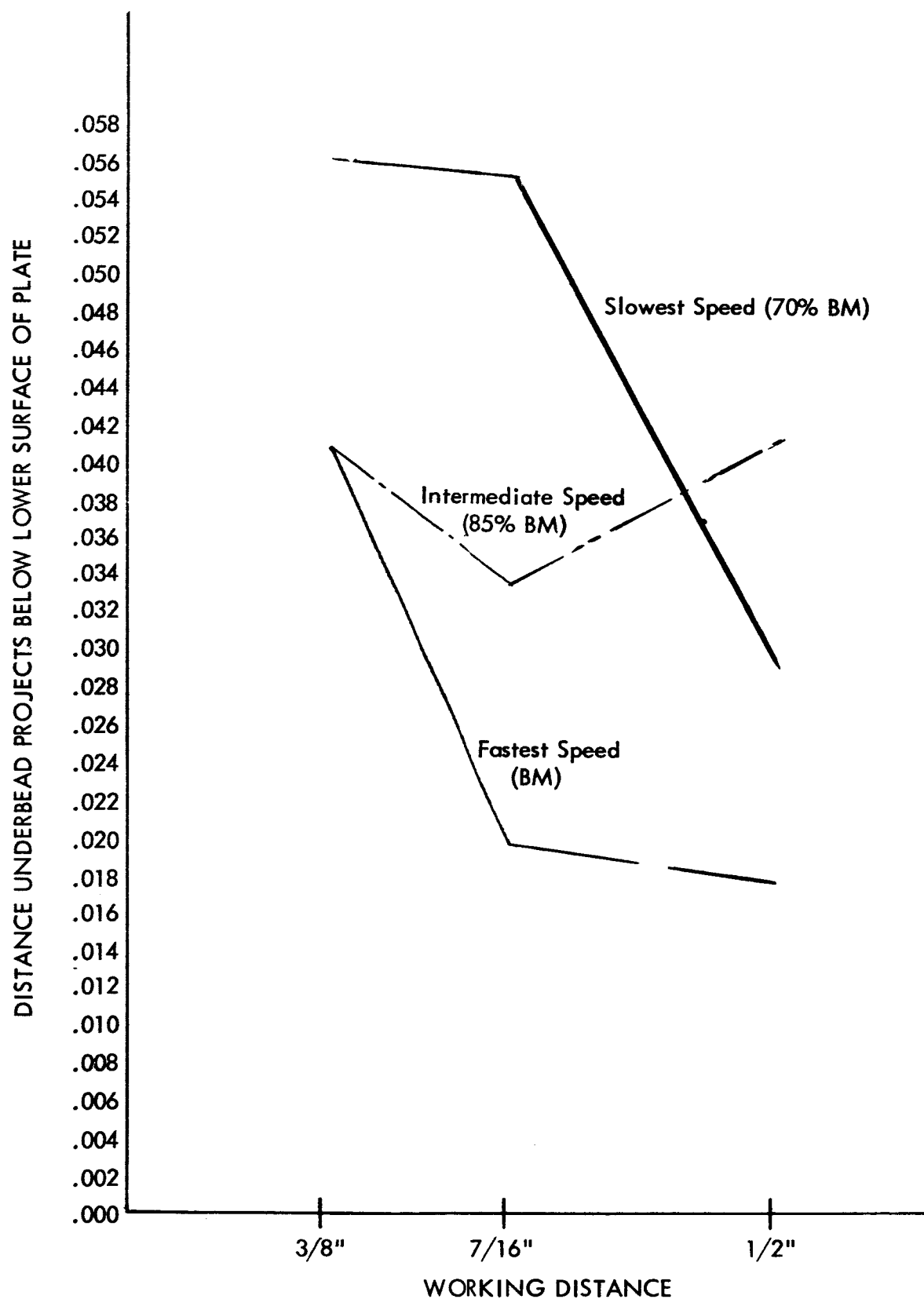AT TWO POWER LEVELS

FIGURE 10

EFFECT OF WORKING DISTANCE AT BENCH MARK SPEED
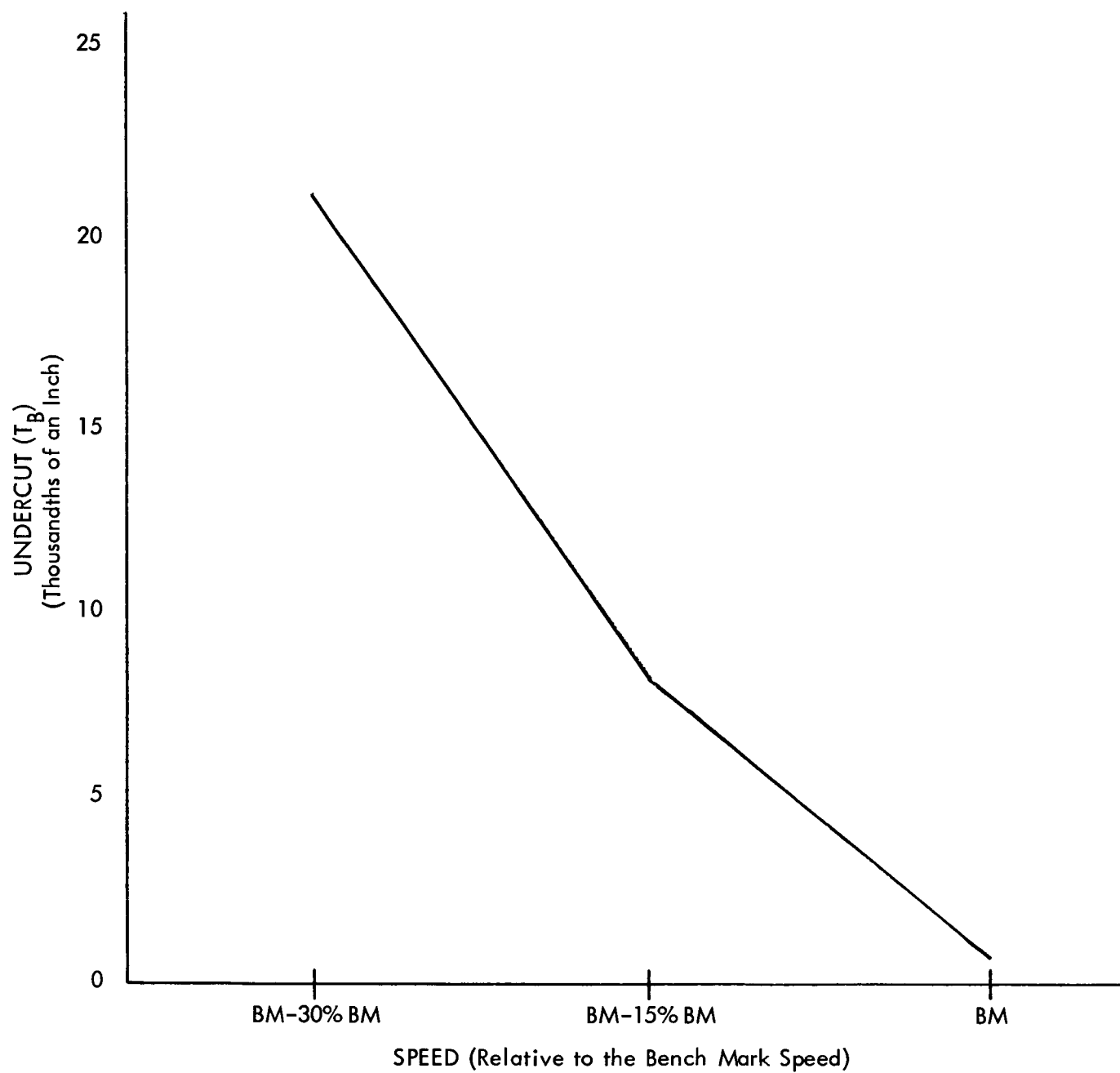AND AT TWO LOWER SPEEDS

267

FIGURE 11

SPEED – COMPOSITE EFFECT AT TWO POWER LEVELS, THREE LENS CURRENTS
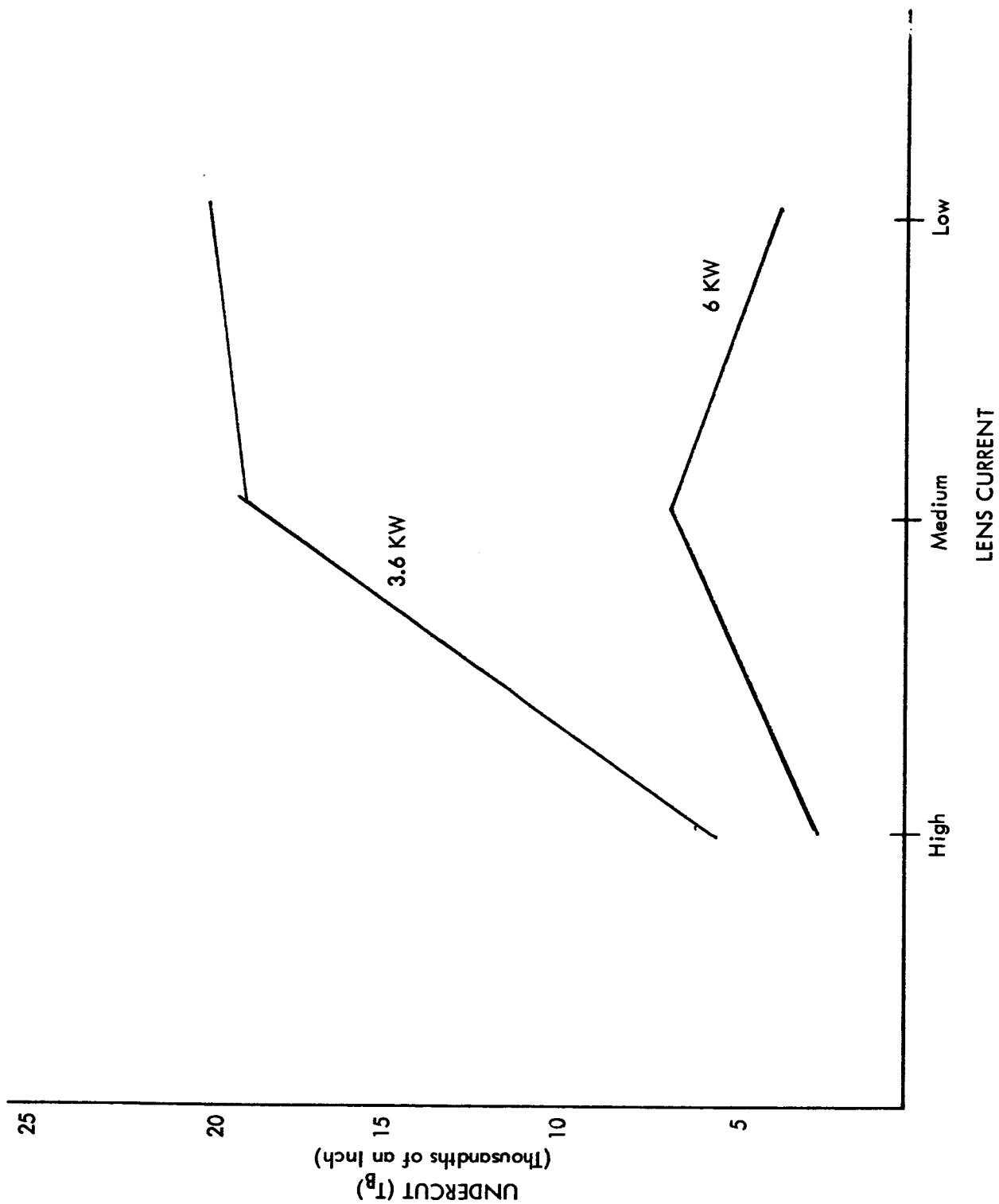AND THREE WORKING DISTANCES

FIGURE 12

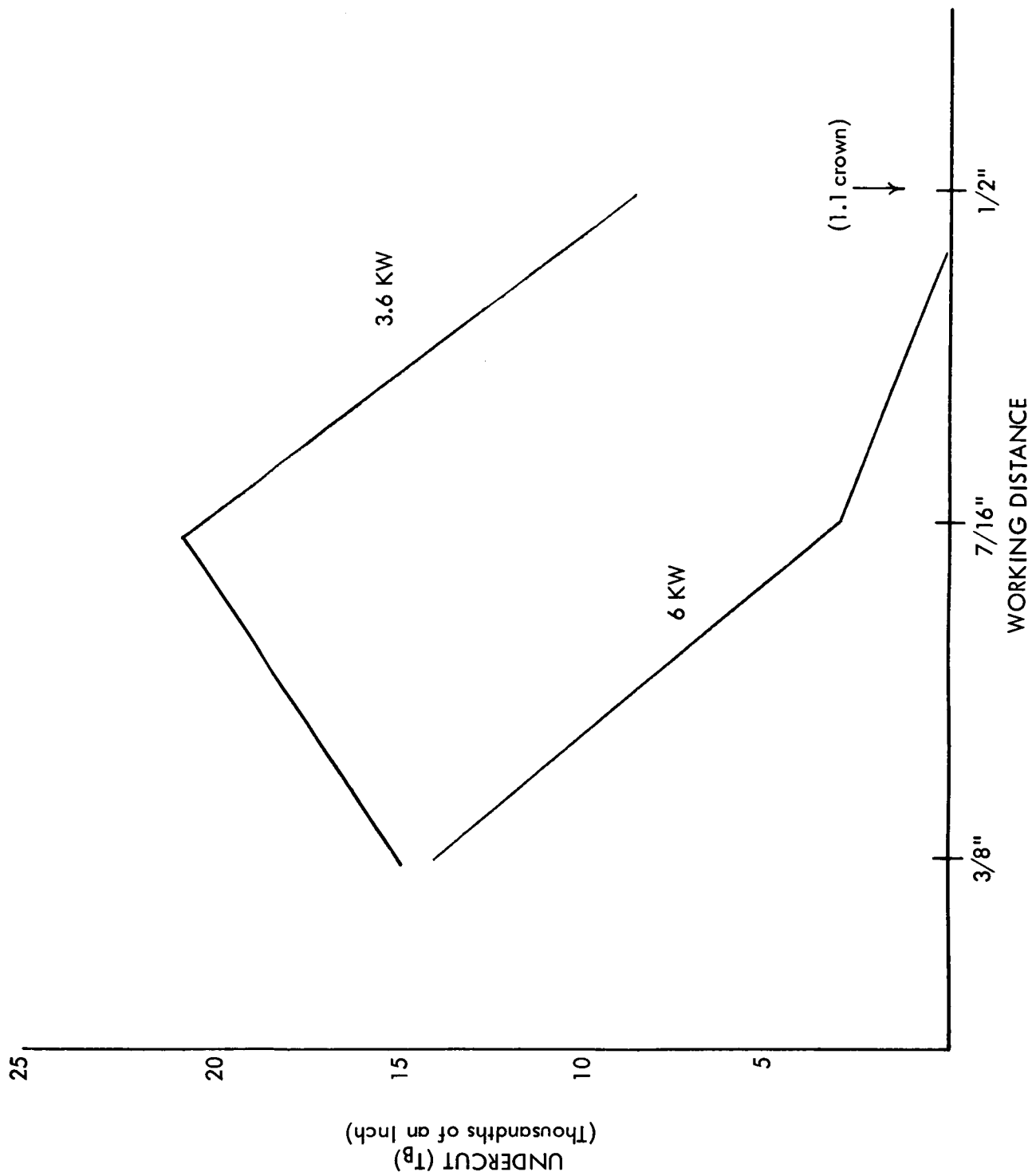EFFECT OF LENS CURRENT AT TWO POWER LEVELS

UNDERCUT (T_B)
(Thousandths of an Inch)

25
20
15
10
5

3.6 KW

6 KW

(1.1 crown)

3/8"
7/16"
1/2"

WORKING DISTANCE

FIGURE 13

EFFECT OF WORKING DISTANCE AT TWO POWER LEVELS

TABLE I-S (110 KV)

WIDTH AT BOTTOM

ANALYSIS OF VARIANCE

Source of Variation		Degrees of Freedom	Sums of Squares	Mean Squares	F – Ratio[1]
Accelerating Voltage	(A)	1	48.35	48.35	--
Speed	(C)	2	213.70	106.85	3.73*
Lens Current	(D)	2	77.70	38.85	--
A x C		2	50.02	25.01	--
A x C		2	61.69	30.84	--
C x D		4	119.54	29.89	--
Residual (A x C x D)		4	130.57	32.64	--
TOTAL		17	701.57		

* 95% Confidence Level

[1] Tests are made from use of residual variance of previous study. Residual variance of 2865 with 28 degrees of freedom.

Mean Values for Significant Effects

Grand Mean   178.1

Grand Mean of Previous Study   168.8

Speed
15/20	226.7
17.5/25	150.8
20/30	156.7

TABLE II-S (110 KV)

POROSITY

ANALYSIS OF VARIANCE

Source of Variation		Degrees of Freedom	Sums of Squares	Mean Squares	F – Ratio[1]
Accelerating Voltage	(A)	1	122.72	122.72	
Speed	(C)	2	241.00	120.50	
Lens Current	(D)	2	33.33	16.66	--
A x C		2	236.78	118.39	3.84*
A x D		2	8.45	4.22	--
C x D		4	156.67	39.17	--
Residual (A x C x D)		4 —	9.55	2.39	--
TOTAL		17	808.50		

* 95% Confidence Level

[1] Tests are made from use of residual variance of previous study. Residual variance of 3087 with 28 degrees of freedom.

Mean Values for Significant Effects

Grand Mean   55.0

Grand Mean of Previous Study   113.3

Speed	Accelerating Voltage	
	140-25	110-28
15/20	23.3	40.0
17.5/25	33.3	20.0
20/30	30.0	183.3

TABLE III-S (110 KV)

UNDERBEAD CONTOUR

ANALYSIS OF VARIANCE

Source of Variation		Degrees of Freedom	Sums of Squares	Mean Squares	F – Ratio[1]
Accelerating Voltage	(A)	1	868	868	7.36*
Speed	(C)	2	853	426	3.61*
Lens Current	(D)	2	486	243	--
A x C		2	103	52	--
A x D		2	453	226	--
C x D		4	481	120	--
Residual (A x C x D)		4	513	128	--
TOTAL		17	3757		

* 95% Confidence Level

[1] Tests are made from use of residual variance of previous study. Residual variance of 118 with 28 degrees of freedom.

Mean Values for Significant Effects

Grand Mean   31.9

Grand Mean of Previous Study   37.2

Accelerating Voltage	
140-25	38.9
110-28	25.0

Speed	
15/20	41.7
17.5/25	27.5
20/30	26.7

TABLE IV-S·(110 KV)

UPPER SURFACE CONTOUR
ANALYSIS OF VARIANCE

Source of Variation		Degrees of Freedom	Sums of Squares	Mean Squares	F – Ratio[1]
Accelerating Voltage	(A)	1	313	313	4.97*
Speed	(C)	2	1059	530	8.41**
Lens Current	(D)	2	402	201	--
A x C		2	208	104	--
A x D		2	401	200	--
C x D		4	429	107	--
Residual (A x C x D)		4	629	157	--
TOTAL		17	3441		

* 95% Confidence Level
** 99% Confidence Level

[1]Tests are made from use of residual variance of previous study. Residual variance of 63 with 28 degrees of freedom.

Mean Values for Significant Effects

Grand Mean   -10.8

Grand Mean of Previous Study   -9.9

Accelerating Voltage	
140-25	-15.0
110-28	- 6.7

Speed	
15/20	-21.7
17.5/25	- 5.0
20/30	- 5.8

into the work increases undercut. As noted back in Table II, drop-through of the underbead is effected in the same manner by lens current. No significant lens current effect was observed with the high power process.

An increase from the closest to the furthest working distance reduces undercut. However, as was the case for the underbead contour, the intermediate point of the low power process shows a reverse trend.

INFLUENCE OF REDUCTION IN ACCELERATING VOLTAGE FROM 140 KV TO 110 KV

The results shown in Tables I-S through IV-S show what happens when the accelerating voltage of the 3.6 KW process is reduced from 140 KV to 110 KV.

Underbead Width: Changing the accelerating voltage per se did not influence bottom width but the influence of speed is significant and appears to be more drastic than was the case when the accelerating voltage was 140 KV. The absence of any effect of accelerating voltage on a dimension such as underbead width that logically can be considered to be penetration sensitive might appear to be an anomaly. However, the data on Table I also indicated that underbead was not sensitive to factors affecting current density or focus and accelerating voltage would fall into the same category.

Porosity: There appears to be little difference in the two accelerating voltages at lower speeds. The failure of the auxiliary shield during the 110 KV bench mark series and its replacement by an unimproved shield may explain the severe porosity encountered at the lower KV value. The 140 KV - 3.6 KW series was run with a shield that had been modified to provide improved shielding around the orifice so that no comparison can be drawn with assurance.

Underbead Contour: Lowering the accelerating voltage reduced underbead drop through. There appears to be an anology between penetration into a block and underbead drop through.

275

<u>Upper Surface Contour</u>:   The behavior of the upper surface parallels that of the underbead as accelerating voltage is reduced.

As a general comment, it appears that the lack of significance of the lens current and virtual absence of two-factor interactions suggests that the low accelerating voltage reduces the sensitivity (and perhaps flexibility) of the process. Possibly there are optical effects in force at 110 KV that offset any influence that lens current or any of the two-factor interactions that were observed at 140 KV might otherwise exist.

Once again, as noted in 140 KV welds, changes which intensify and sharpen the beam (i.e., focus) cause metal to be displaced vertically but do not narrow or widen the weld. Underbead width is narrowed or widened by what goes on inside the workpiece not by what goes on inside the gun.

DISCUSSION OF SECTION I-A RESULTS

The results of Task A Series A may be viewed in two ways. First, they provide guidance for the adjustment of procedure details during the optimization of a welding procedure for future applications. Second, the trends described in Figures 5 through 13 can be considered, deductively, to present a picture of the various phenomenon that take place during the progressive fusion and solidificate of a joint in an assembly that is being welded by the non-vacuum electron beam process.

With regard to the various thermal phenomena that operate during welding, there is a strong suggestion that some thermal focus phenomena exists outside of the welder and inside of the workpiece. This "point" can be made more diffuse and/or moved toward the top and bottom of the weld by manipulating procedure details. Its location determines the cross sectional shape of the molten pool that forms the fusion zone. The shape of the molten pool, and perhaps other factors, in turn controls underbead drop through and undercut. The width of the process that produces the molten pool alone seems to control underbead

width. Short or long focal positions do not effect it. Thus with this tentative picture the welding engineer can exert a control over these characteristics to suit a particular application.

RELATIONSHIP BETWEEN POROSITY AND PROCEDURE DETAILS

INTRODUCTION

Control of porosity is essential to the application of this process to aerospace hardware. Such control, in conventional welding processes, places constraints on nearly every feature of the welding procedure and the nature of these constraints must be determined before any procedure can be optimized.

The major culprit insofar as gas porosity in aluminum is concerned is generally conceded to be hydrogen. Hydrogen is quite soluable as nacent H^+ in molten aluminum. The hydrogen in the metal will be rejected in the form of porosity as the metal freezes. The welding engineer must consider three aspects of the porosity problem at all times.

1. Source of the hydrogen.
2. Mechanisms that govern the entrance of the hydrogen into the metal and rejection from the metal in the form of gas nuclei.
3. Growth and floatation (on entrapment as detectable porosity) of the gas nuclei.

The most direct method for reducing porosity appeared to lie within the technology associated with shielding. Improved shielding (with efficient cleaning) minimizes the amount of H^+ available to the melt.

Therefore, the major experiment was designed to improve the shielding and in a subsequent series of trials (not statistically desianed experiments) some cleaning variations were investigated.

Radiography was accomplished using the following procedure:

KV = 100   Time = 65 seconds

Ma = 3.5   Film = Kodak M

Distance = 48"   Sensitivity = 2-2T

The film was then read using a 7X glass equipped with scale that could be read to .005 inch. Because the trailing shield tends to pull air into its gas flow when it overhangs the ends of the weld, readings were confined to the center 1-1/2 inches of the four-inch long weld.

RESULTS OF SECTION A-2 EXPERIMENTATION

The following paragraphs cover the findings from that portion of the program concerned with the radiographic quality of welds as it applied to porosity.

ROLE OF MACHINE SETTINGS IN SUPPRESSING POROSITY

All test plates from the factorial experiment described in the previous section were subjected to x-ray examination. The diameter of each indication that could be observed at 7X was recorded and placed in one of the following catagories.

Range (inches)	Nominal Diameter (inches)	Volume (inches x 10^{-9})
.007 - .015	.005	60
.007 - .015	.010	500
.015 - .025	.020	4,000
.025 - .050	.040	32,000

Thus the information on the film was made amenable to an analysis of variance. Such analysis was carried out using pore diameter and pore volume. The results are discussed in the following paragraphs.

Each of the variables A, B, C, and D is significant with regard to its ability to influence the amount of porosity in the weld. Power level, in general, and speed at high power levels appear (Figure 14) to have the greatest effects. Both would be expected to exert this effect through such phenomena as freezing rate and thermal gradient. The effect of the two factors, lens current and working distance, which might be expected to influence current density is much less.
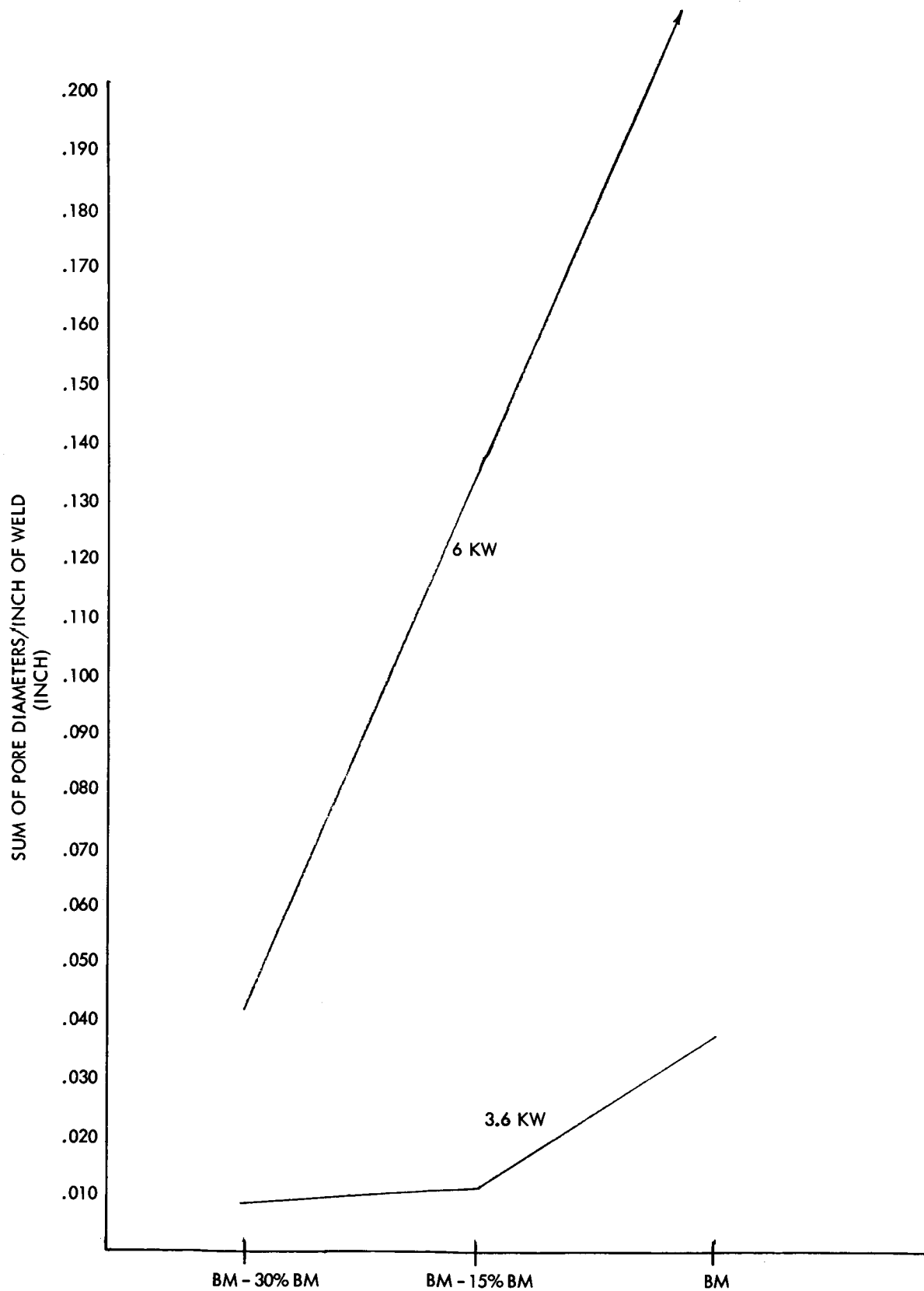
FIGURE 14
EFFECT OF SPEED ON POROSITY AT TWO POWER LEVELS

Only working distance (B) appears to operate independently (Figure 15). It should be noted that increasing working distance also resulted in an increase in the gap between the inert gas shield and the surface being shielded (from 1/16" to 9/16" approximately) which may have contributed to the porosity.

The effect of lens current on porosity is involved in an interaction with power levels. Figure 16 indicates an insensitivity (or slight suppression of porosity) at the 3.6 KW power levels as lens current is changed from high to low. As the lens current is decreased at 6 KW, porosity increases sharply.

Most notable in both Figure 14 and Figure 16 is the tremendous effect of power.

EFFECT OF SHIELD CONFIGURATION ON POROSITY (SERIES B)

The shields used for all tests described previously (experimentally identified as Series A) were constructed as an accessory to the existing 10 KVA welder. Under these circumstances sealing around the nozzle of the welder was not very effective. The shields overheated at their midpoint. This destroyed the seal by causing a lengthwise bow. In addition to the bowing problem, severe oxidation of the diffuser material (steel wool and screen) necessitated frequent changes of the shield so that the experimental variance was high in Series A. Since Series B was primarily concerned with porosity as a function of shield configuration, the nozzle was redesigned to accept mounting plates for the various shield test configurations – a "test bed" which could be tightly sealed to the welder. This test bed was cooled to assure its dimensional stability during tests. Shield configurations that provided a simple, easily studied, gas curtain around the beam, were built up from modular components. These were fastened to the test bed with solder. Thus a modification in length or width could be accomplished in a few hours. A bottom view of an outer perimeter and filler – gas manifold soldered on the cooled mounting plate is shown in Figure 17.

Experimental Design: Several features of shield configuration were to be evaluated.
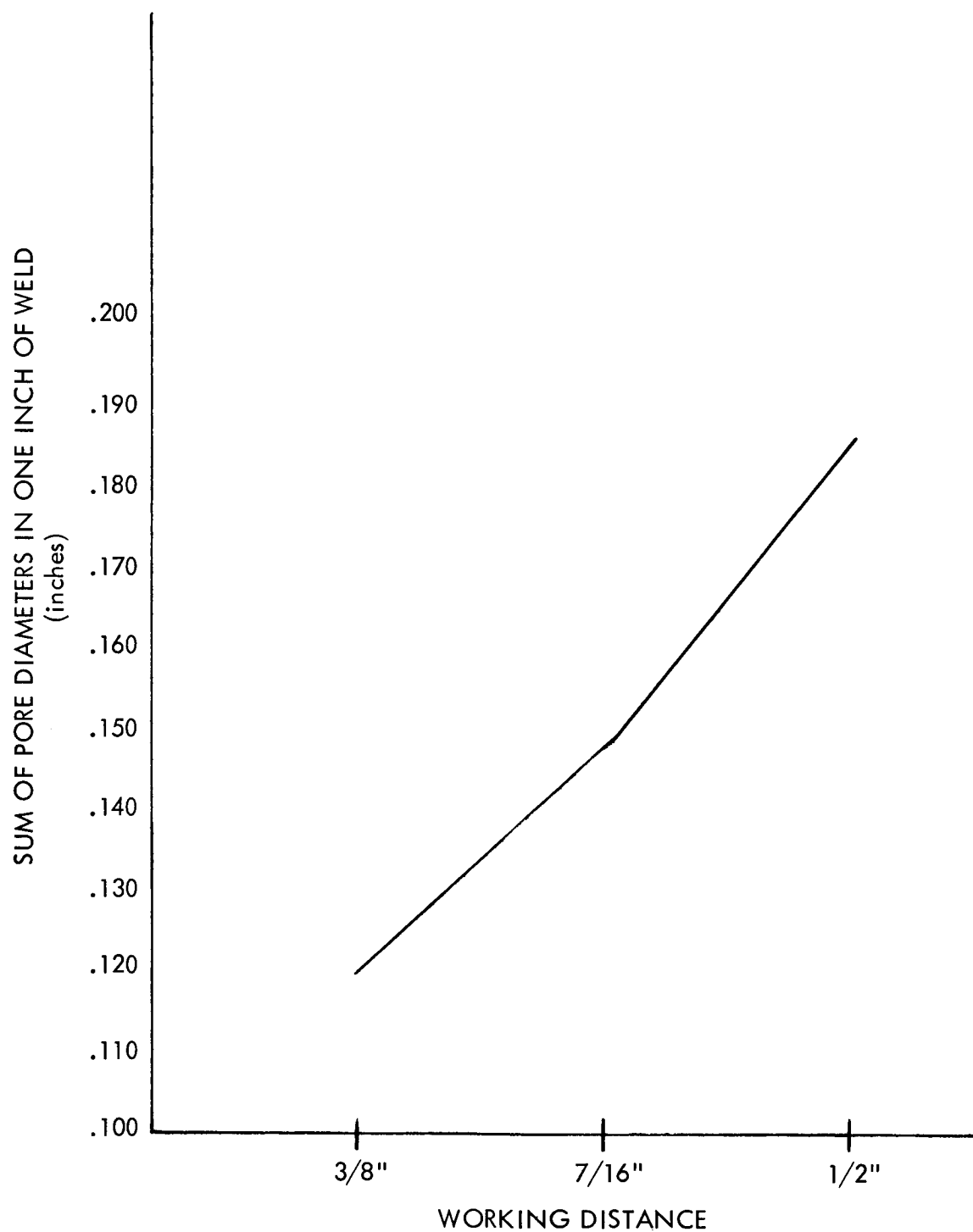
FIGURE   15

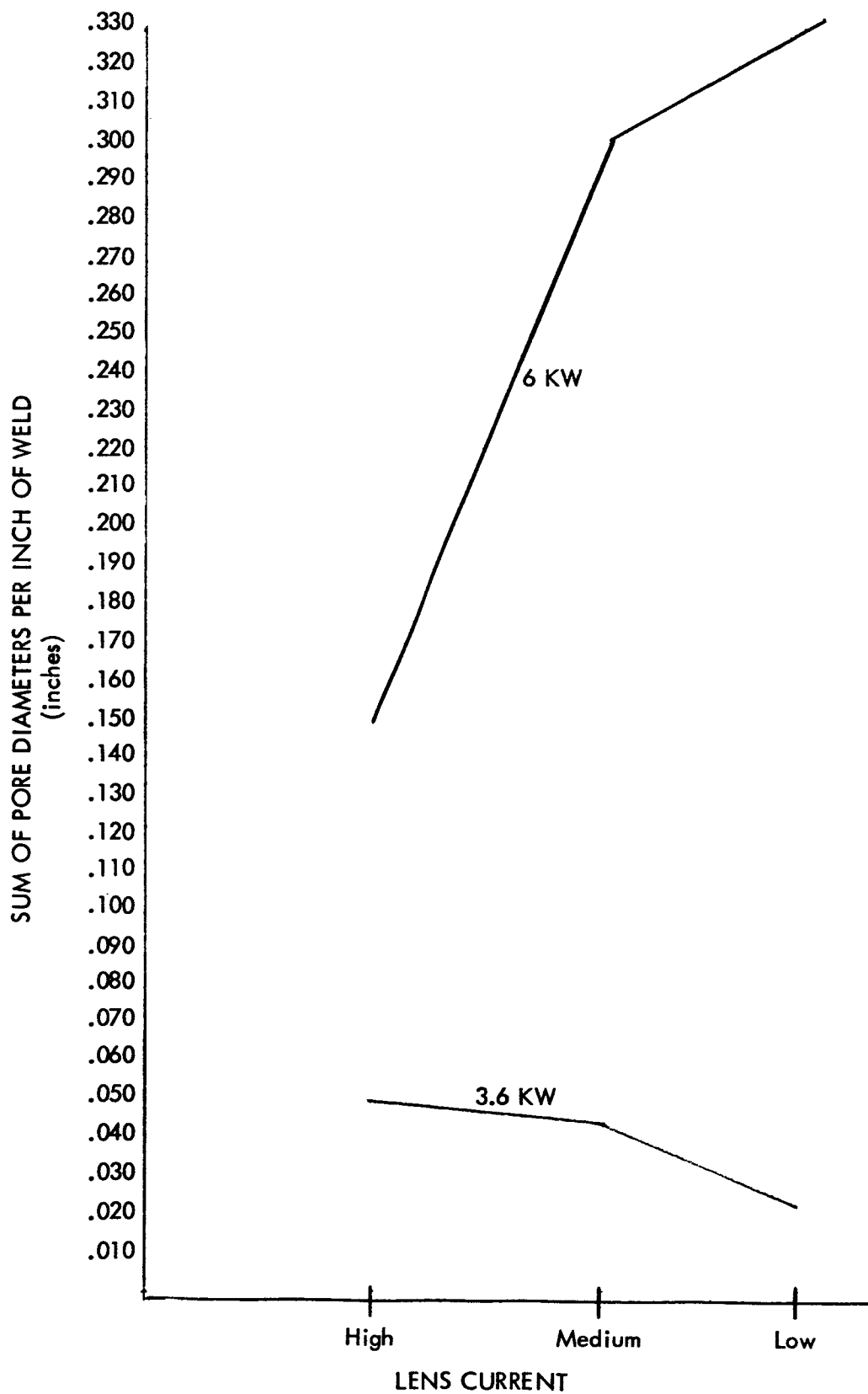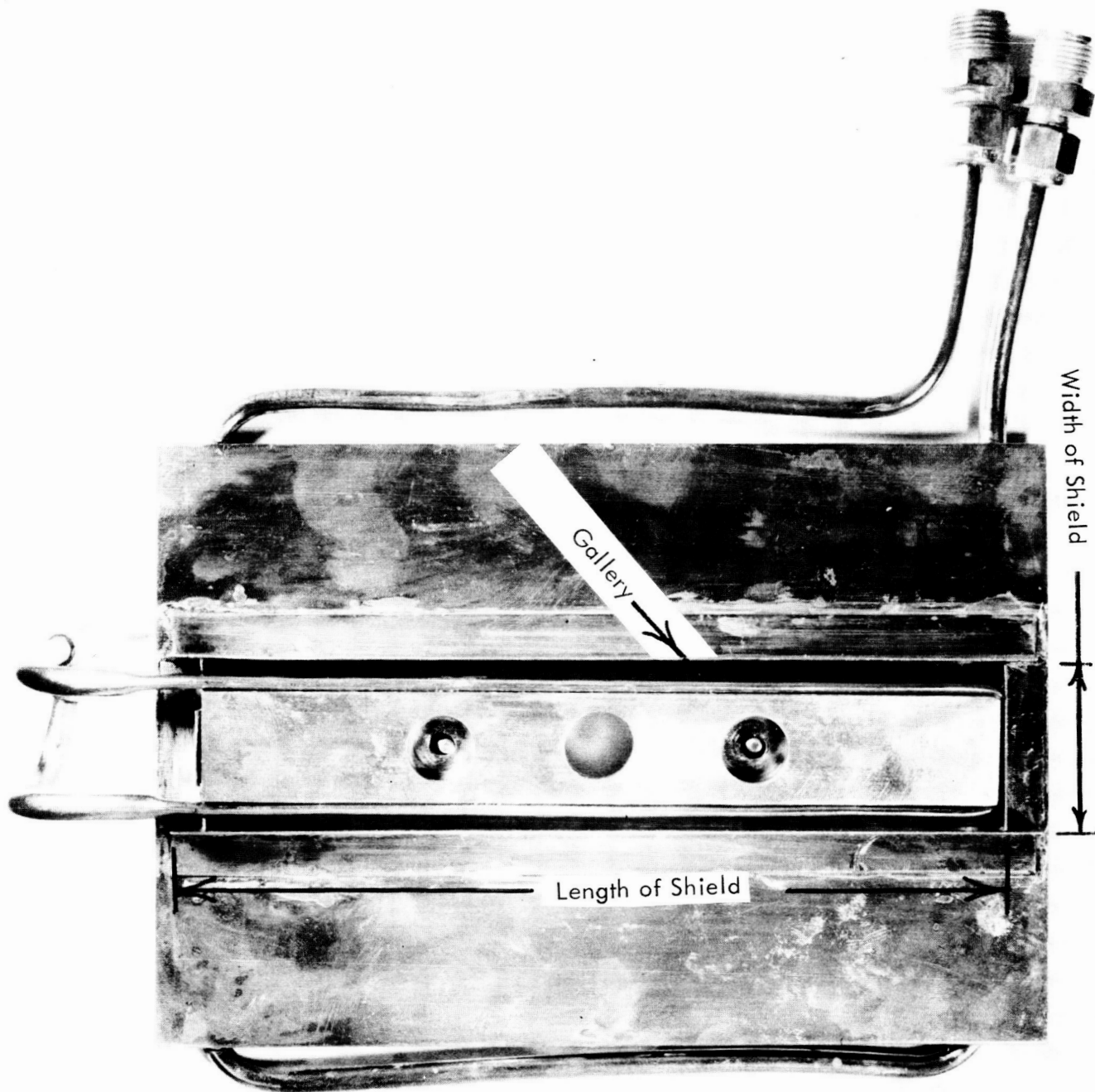COMPOSITE EFFECT OF WORKING DISTANCE ON POROSITY

FIGURE 16

EFFECT OF LENS CURRENT ON POROSITY

283

Assembled Gas Curtain Test Shield
(Bottom View)
FIGURE 17

These were:

> Length of Shield: 2 levels
>
> Width of Shield: 2 levels
>
> Volume of chambers (gallery) into which gas was introduced: 2 levels
>
> Level of gas flow (for one type of gas): 2 levels

The total number of tests was reduced to 32 through the use of a 1/4 factorial design.

Effect of Shield Configuration: Only the distance that the manifold pipes were spaced apart (shield width) was shown to be a significant factor in controlling porosity (Figure 18). The extending of the shield ahead and behind the beam caused no significant effect when an analysis of variance was applied. The volume of the gallery chamber into which the gas was introduced prior to being directed onto the surface had no effect on porosity.

EFFECT OF THE ADDITION OF A DIFFUSER AND DISCUSSION OF THE ROLE OF OTHER PROCEDURE VARIABLES ON POROSITY

Qualitative observations of the influence of variables ranging from speed to post cleaning procedures on the formation of porosity emphasize need for strict attention to a multitude of details. In this section some of the effects of details such as the addition of a diffuser in the filler block and other procedure variables will be discussed. Actual radiographs will be used to illustrate the findings. As the Task A program approached a point where optimum procedures had to be selected in order to proceed with Task B, no single parameter such as pore volume could be relied upon alone to relate weld quality to existing specifications.

Figure 19 illustrates the severe porosity that can occur in bench mark welds at relatively high power levels (6 KW) when cleaning and shielding are marginal as was the case in Series A of Task A. Simply reducing the power to 3.6 KW under the same shielding conditions accomplished the improvement illustrated in Figure 20. The responsible phenomena would appear to relate to freezing rate or other factors that control the growth of porosity.
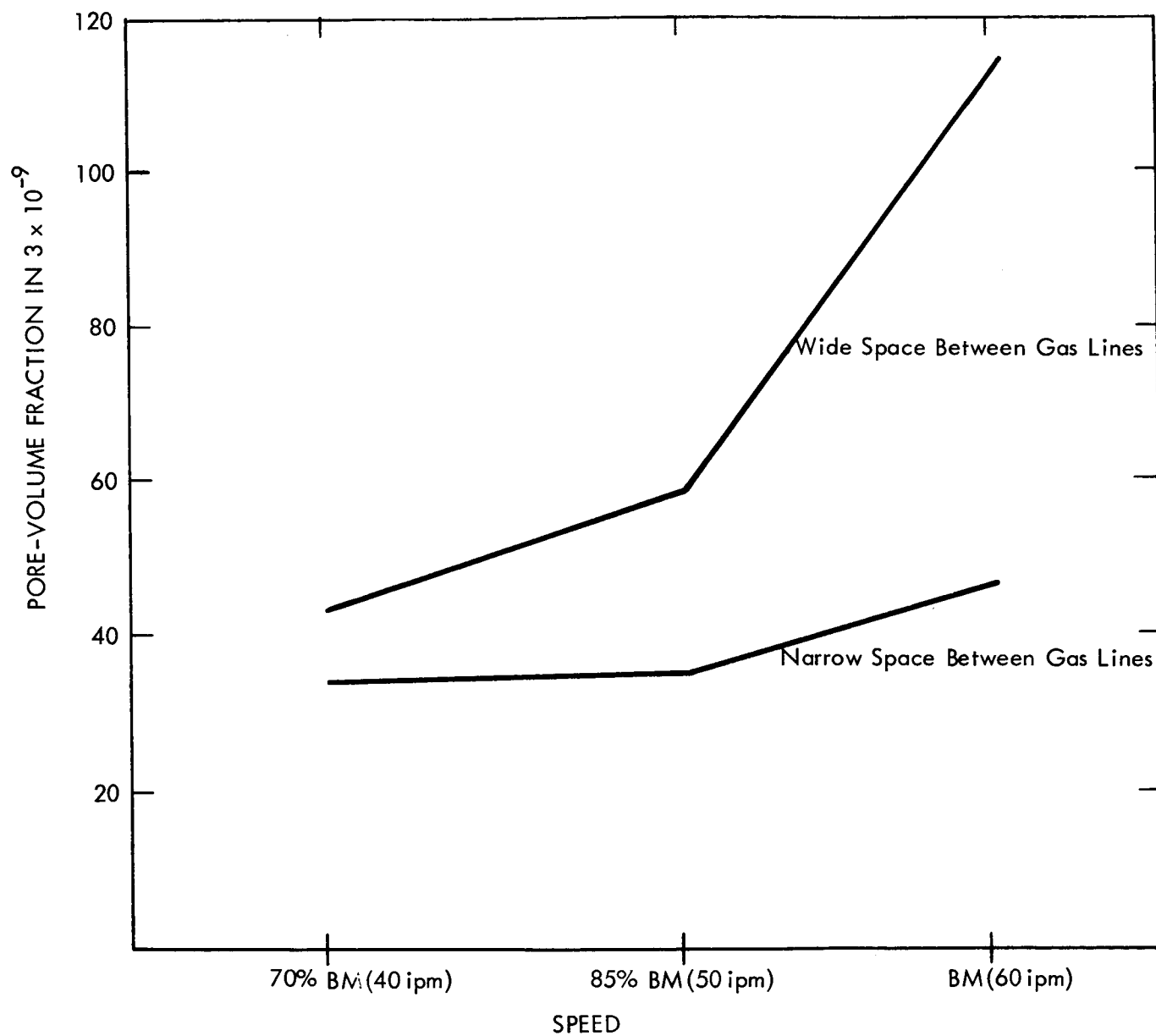
FACTORS CAUSING CHANGE IN POROSITY LEVEL FOR A 6 KW WELDING PROCESS

FIGURE 18
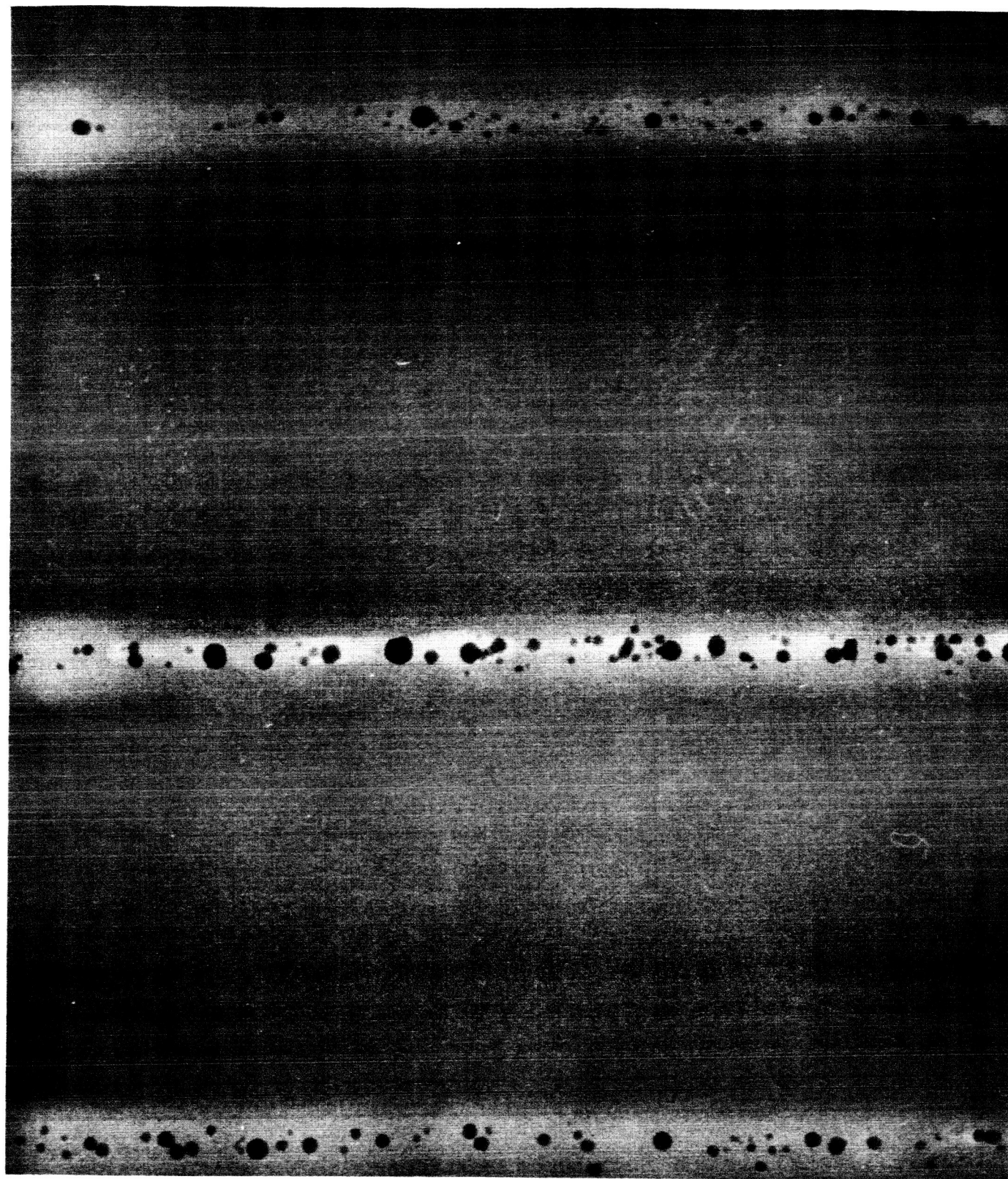
Radiographic Survey of Early Specimens with Non-Optimum Shielding and Cleaning Shows
Severe Porosity for High Speed (60-70 ipm), High Power (6 KW) Procedure

2X   Top-to-Bottom; Short, Long, Medium Focus   Welds 88-90

FIGURE 19
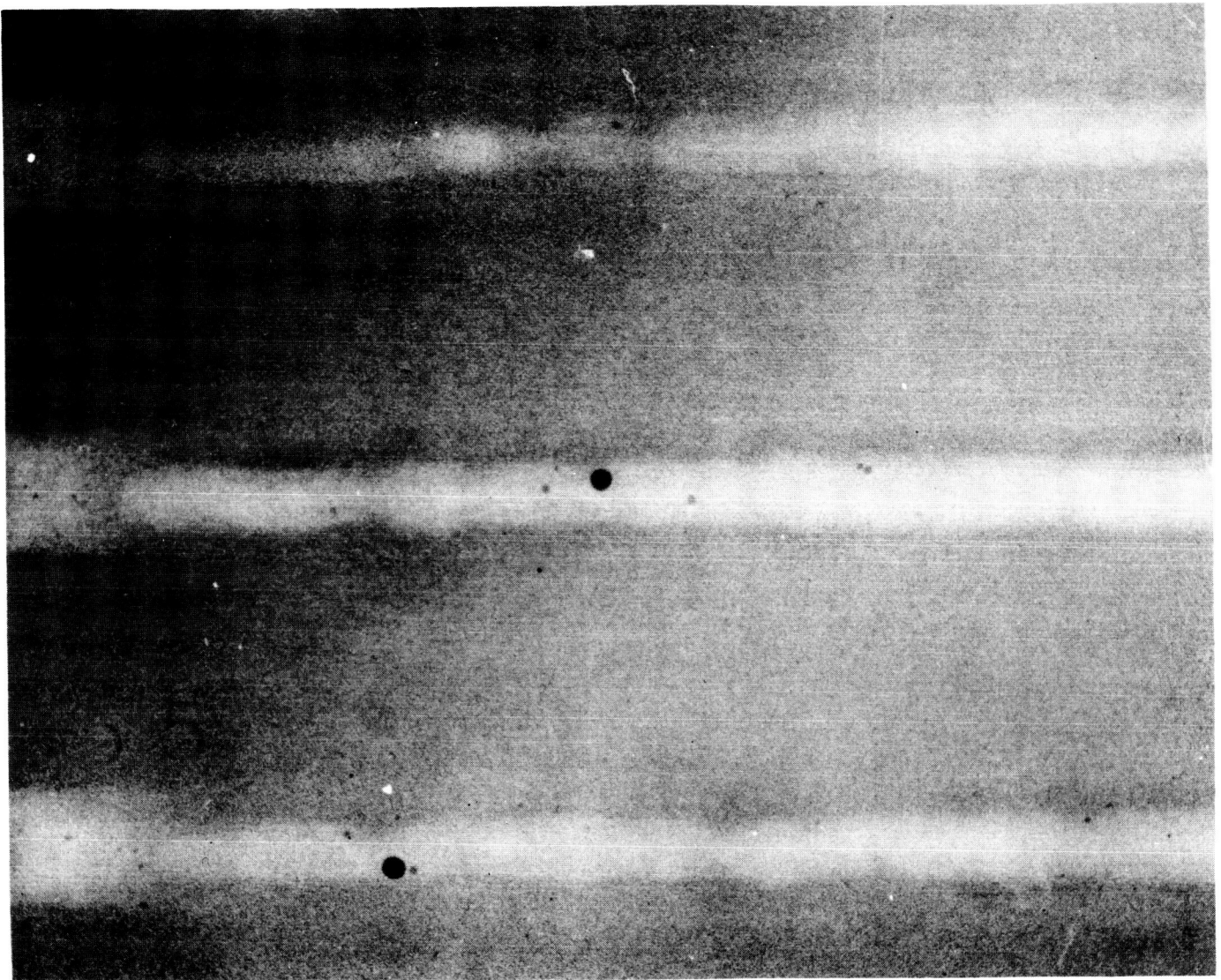
3.6 KW Procedure Produces Only Moderate Porosity in Spite of Non-Optimized Shielding and Cleaning Practices

| 2.25X | Top-to-Bottom; Short, Long, Medium Focus | Welds 53-5 |

FIGURE 20
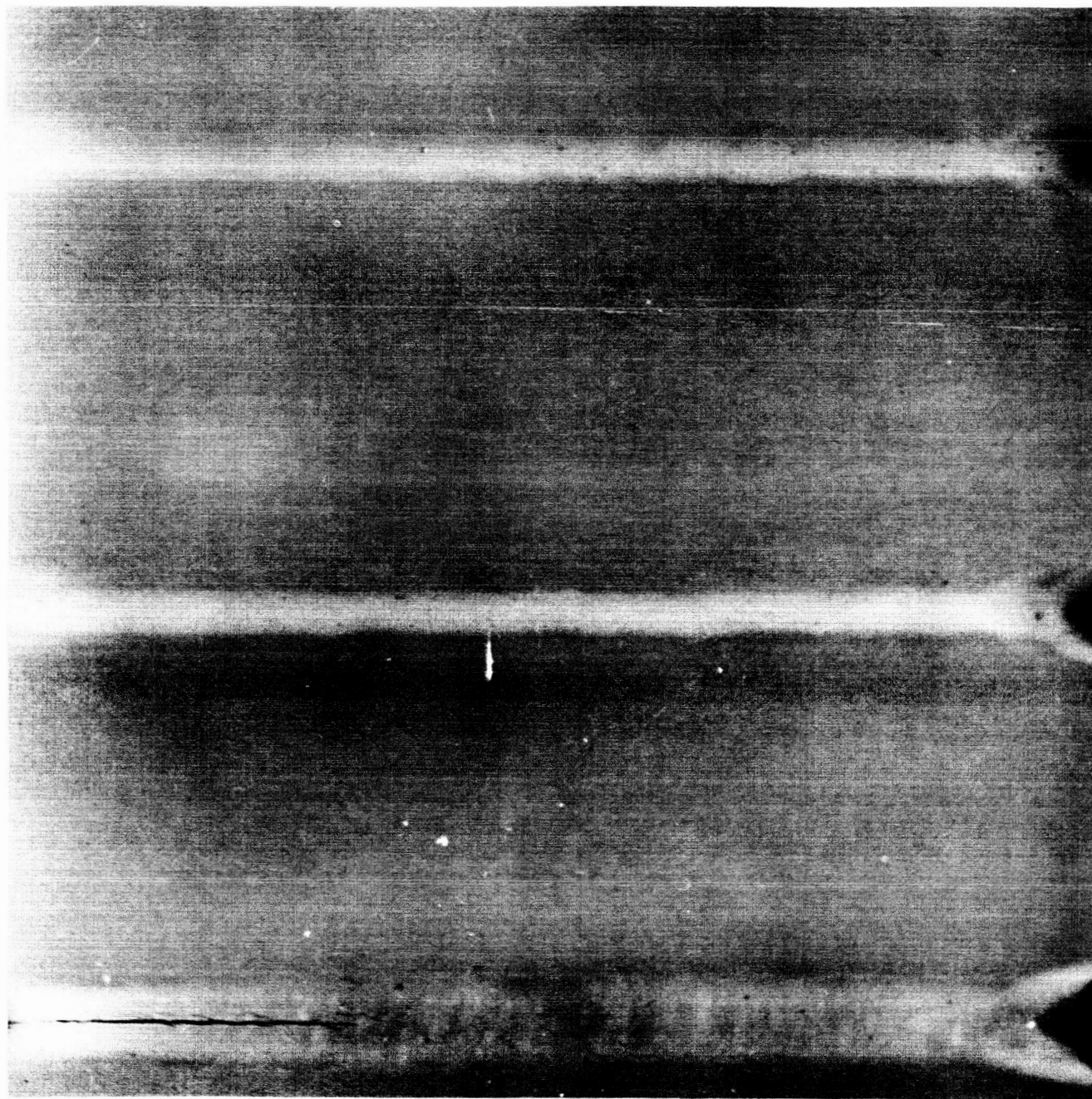
Optimum Shield Configuration (Closely Spaced Gas Manifolds) Reduces Porosity from 6 KW
Welding Procedure to Feasible Level
2X   Top-to-Bottom; 60 ipm (BM); 50 ipm; 40 ipm   Welds 166-8
FIGURE 21
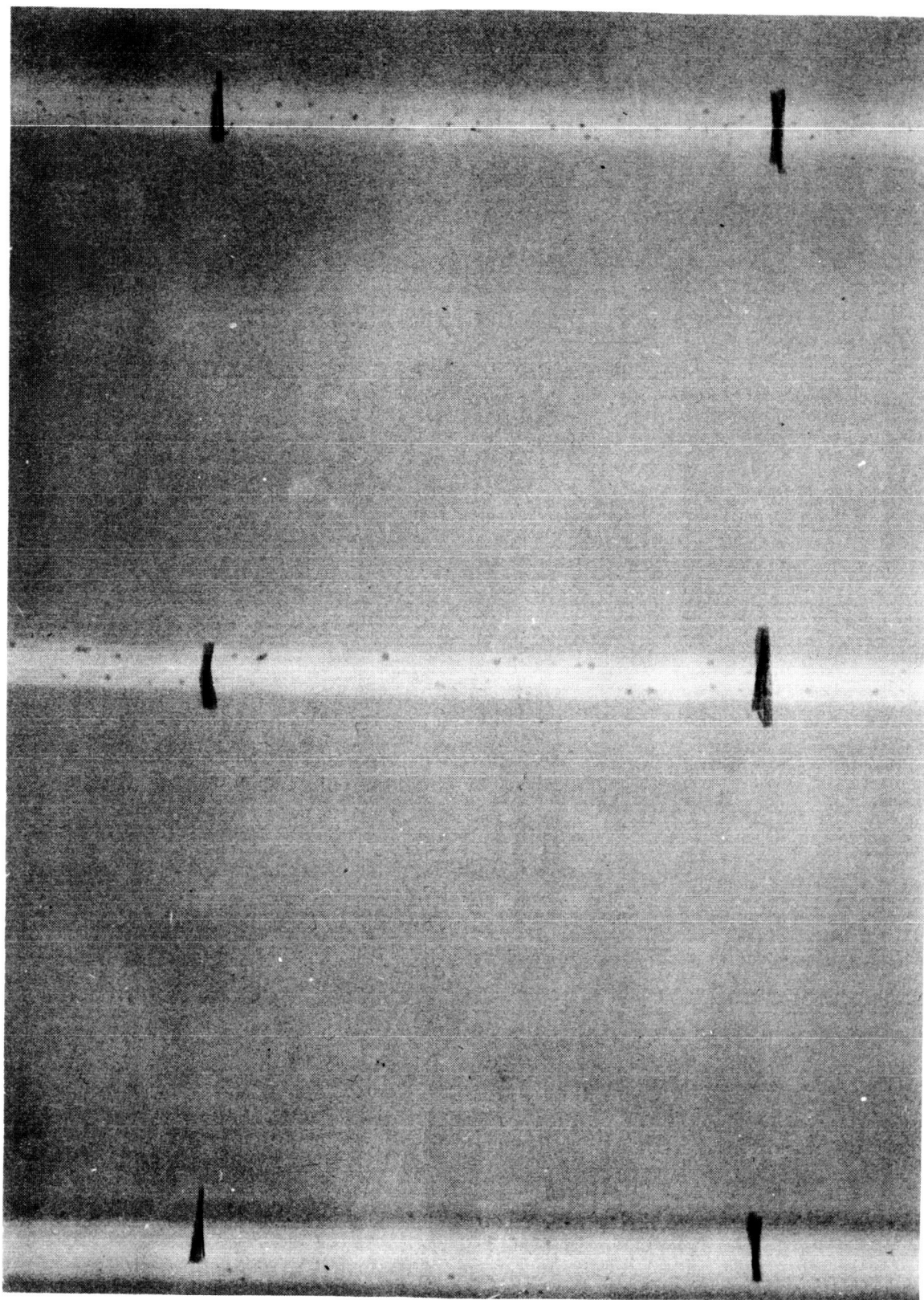
Porosity Level Obtained Using Shield Which Incorporates Both Diffuser and an Optimum Gas
Manifold Configuration
2X   Top-to-Bottom; 60 ipm (BM); 50 ipm; 40 ipm   Welds 254-6
                                           FIGURE 22
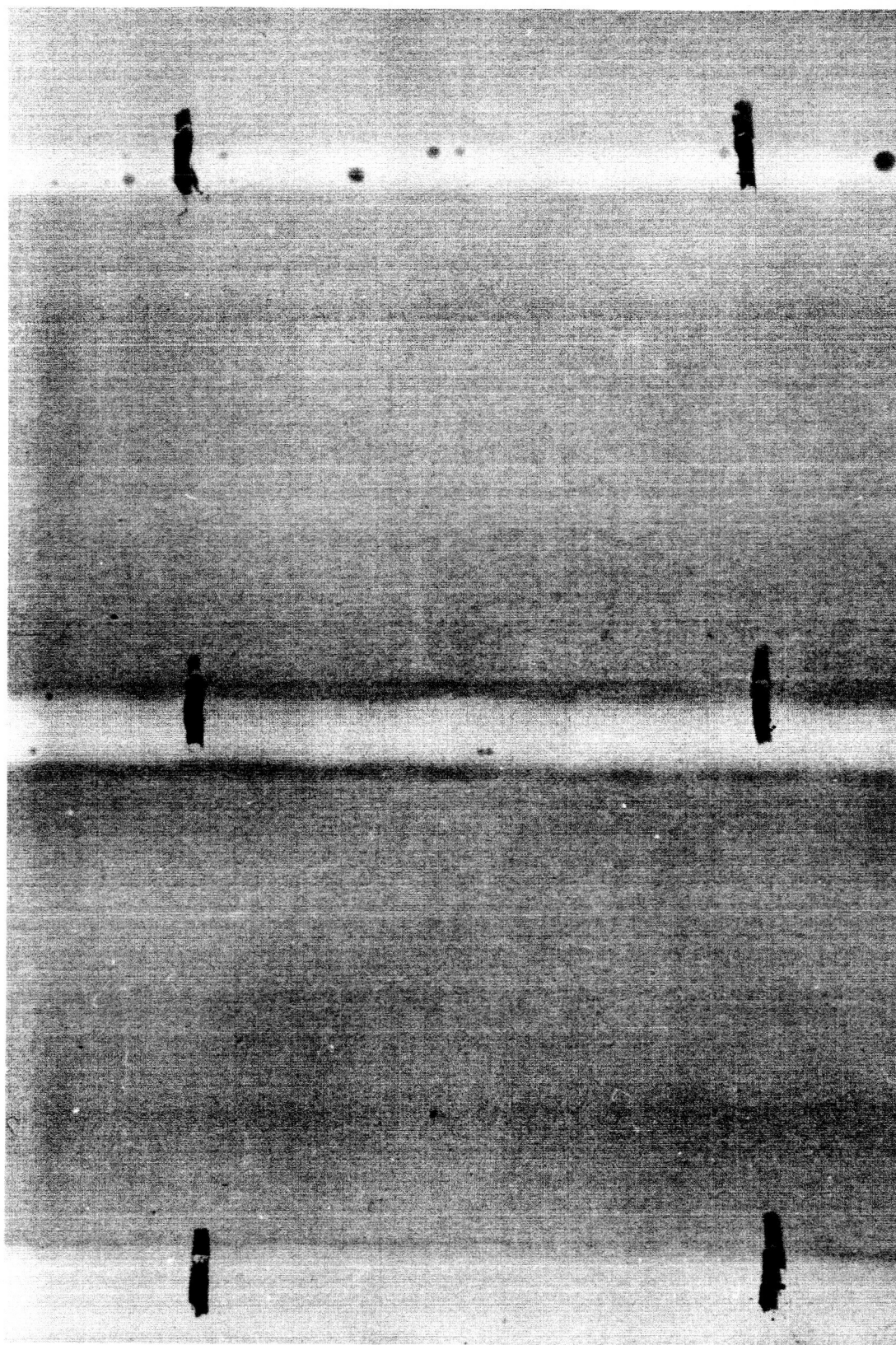
Porosity Level Obtained Using Optimized Shield, Diffuser and Chemical, (instead of Mechanical)
Cleaning Plus an Underbead Shield

2X   Top-to-Bottom; 60 ipm (BM); 50 ipm; 40 ipm   Welds 297-9

FIGURE 23

Note that the more "V" shaped weld formed when a high lens current was used (upper weld) appears somewhat less porous, reinforcing the role of freezing rate and direction as they relate to pore growth and floatation.

The quantitative observation that moving the parallel inert gas manifolds toward the center line resulted in an improvement, is qualitatively illustrated in Figure 21 (though the weld procedure is comparable to the first 6 KW illustration). The improvement resulting when the manifolds were moved together suggests a thermal turbulence in the volume of gas surrounding the beam and weld. When the manifolds were far apart the parallel streams of inert gas failed to meet above the path of the weld. Under these circumstances an open corridor existed ahead of and behind the beam impingement area. Down this corridor air could be drawn into the turbulent volume about the intensely hot welding zone. When the manifolds moved together the parallel streams met ahead and behind the weld so that all gas drawn by convection into the weld zone was furnished by these inert gas streams. Placing a diffuser between the manifolds (i.e., in the corridor) simply reduced reliance upon the meeting of the streams and assured a supply of inert gas directly ahead of the process. The improvement resulting from the diffuser particularly at the bench mark speed is illustrated in Figure 22. A review of the cleaning (mechanical) on this plate indicates removal of less than .001 inch total from both sides – this would not now be considered adequate cleaning. Additionally alcohol was used after cleaning. This practice has been discontinued.

At this point in the optimization effort, blanketing of the weld area apparently was rather effective because the substitution of argon (with its high cross section for electrons) for helium severely altered the penetrating qualities of the process. Thus it was felt that the shield was working and the search for sources of porosity was switched to other areas from which hydrogen might emanate. An analysis of two test coupons from Series B indicated less than .3 ppm H_2 so that the base metal was not believed to be unduly effecting porosity – particularly the bench mark speed porosity.

Chemical cleaning did not decrease the volume of porosity but appeared to change the nature of the porosity by increasing its size (Figure 23). It may be that chemically

cleaning once and then producing the high speed weld may have very effectively dried the plate so that succeeding welds on the same plate were always somewhat less exposed to moisture. Additionally alcohol was not used on chemically cleaned welds. Both of these changes from the original mechanical cleaning procedure would reduce sources of H_2 and tend to produce a more favorable picture of chemical cleaning than might be the actual case.

Underbead shielding added to either cleaning methods improved the appearance of the underbead and produced the welds shown in Figure 24. These are among the most acceptable welds even though their numerical rating was not significantly different than those observed for welds without underbead shielding. Underbead protection (20 cfh of helium) also reduced or eliminated an "abrasive" surface condition that had been observed on some underbeads. This condition was sometimes linked with undue porosity in slow welds.

DISCUSSION OF SECTION A-2 RESULTS

DISCUSSION

While the several remedies tried above produced welds that could be accepted under actual specifications such as ABMA-PD-R-27A it should be noted that the greatest degree of acceptability was achieved in welds made at speeds representing 85% of the bench mark speed (about 50-60 ipm for 6 KW). On the other hand bench mark welds (60-75 ipm) exhibited marked increases in porosity. According to Sapperstein and Pollock* the inter-mediate speeds should have been rapid enough to minimize porosity while the fatest speed should have exhibited even less tendency toward porosity. It would be desirable to eliminate this apparent anomaly thus permitting the speed of the optimized non-vacuum electron beam welding process to correspond with the potential maximum speed of the process.

---

*Sapperstein, Z. P. and Pollock, D. D., "Porosity Formation and Solidification Phenomena" Minutes – Aluminum Welding Symposium, July 1964, p. 99.
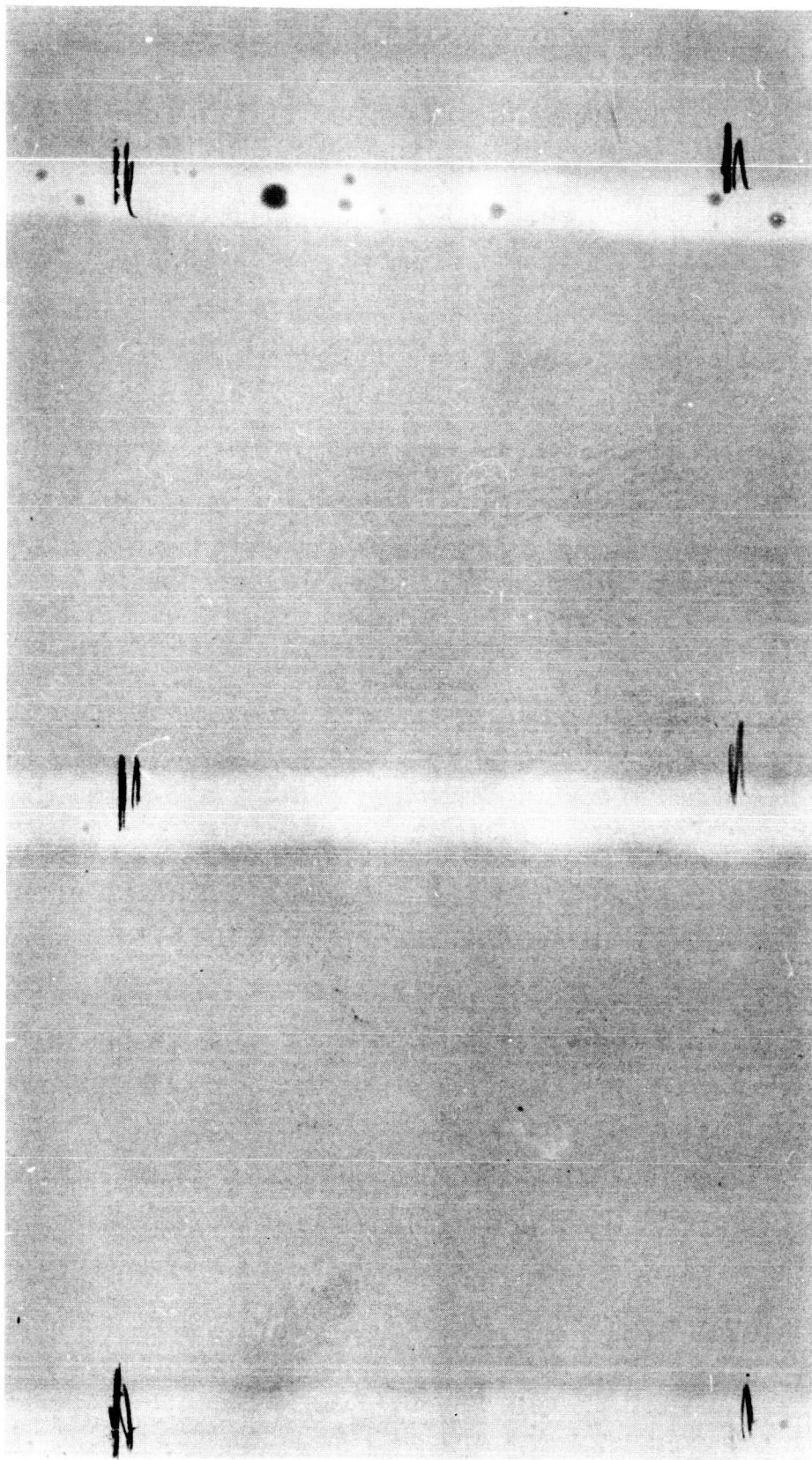
Porosity Level Obtained Using Optimized Shield Diffuser, Mechanical Cleaning and Underbead
Shielding

2X   Top-to-Bottom; 60 ipm (BM); 50 ipm; 40 ipm   Welds 273-5
                                FIGURE 24

PART II TASK B

USE OF THE 10 KVA WELDER TO OPTIMIZE
AS-WELDED MECHANICAL PROPERTIES

Recognizing the constraints imposed by the relationships developed in Task A, two series of tests have been completed on material in the -T37 condition. The tests are in the process of being repeated on -T87 material. These tests are:

Series A - One-side, one-pass welds

1. 6 KW (140 KV) Procedure (BM; 85% BM; 70% BM)

2. 3.6 KW Procedure (BM; 85% BM; 70% BM)

(a) 140 KV accelerating voltage

(b) 110 KV accelerating voltage

Series B - Minimum Thermal Cycle Welds (two-side, one-pass welds made at 120 ipm)

Since Task B is aimed at sorting out effects, the number of side effects has been minimized by using the bead-through-plate approach. Plates were scraped to remove .003 inch of material and no further cleaning applied (i.e., the use of alcohol was discontinued). Tensile testing was accomplished on ASTM-E-8 Figure 7 specimens. The root reinforcement was removed from a few specimens as noted (no significant crown was observed). The testing rate was set so that the .2% offset yield (as determined by a strain gage on a calibration sample) was reached in 60 seconds. This is equivalent to a crosshead rate of .001 inch per minute.

RESULTS: ONE-SIDE - ONE-PASS WELDS (-T37)

Only ultimate strengths were available for this paper, and these were limited to T37 base material. The Series A (one-side one-pass) welds are shown on Figure 25 super imposed on specific points of data presented for other processes and related to a general relationship

ONE-SIDE, ONE-PASS WELDS (.250 inch 2219-T37)
FIGURE 25
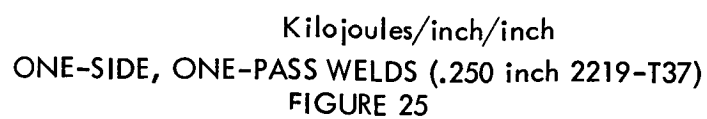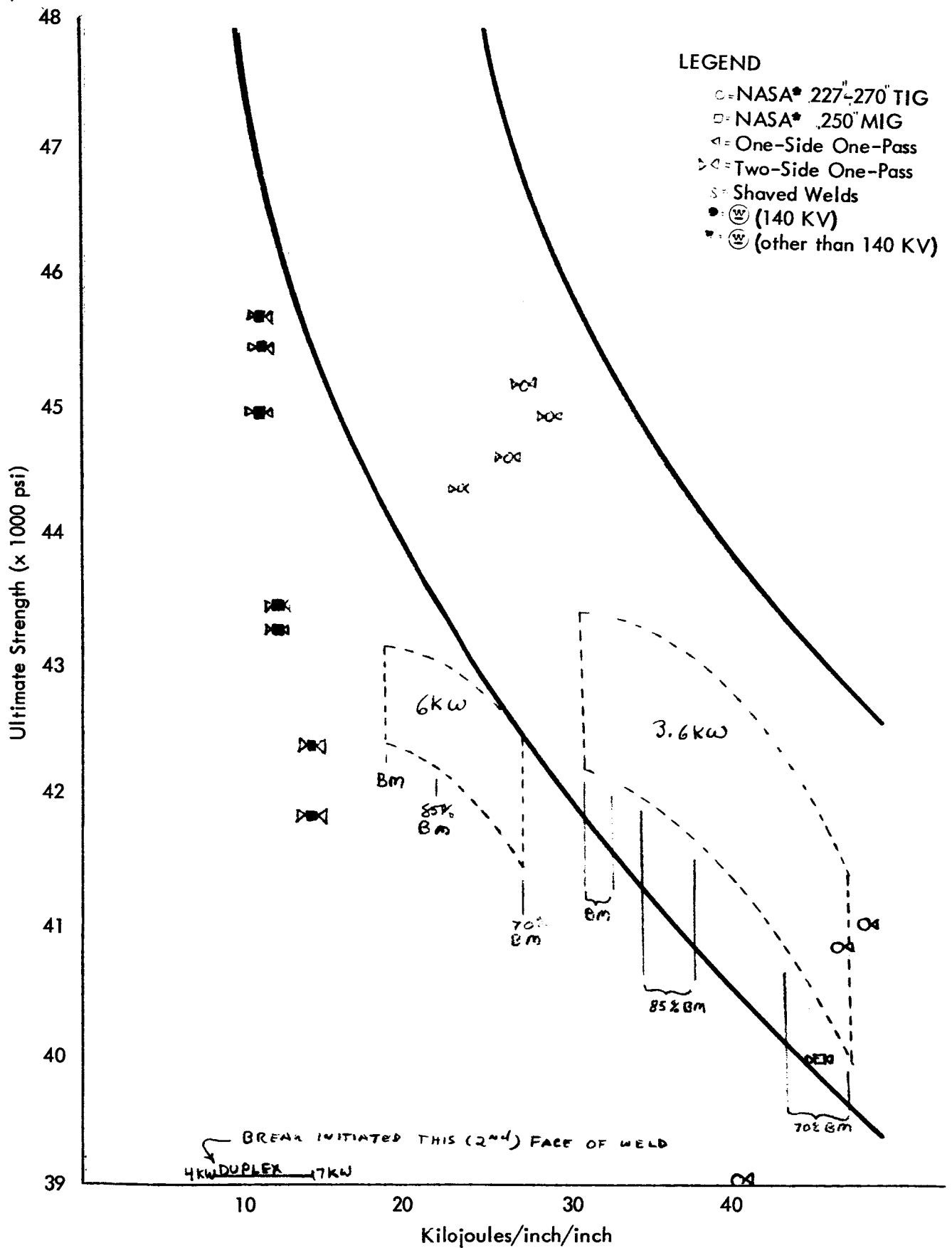
MINIMUM HEAT INPUT WELDS (120 ipm – two-side x one-pass – .225 2219-T37)

FIGURE 26

297

(between strength and heat input) and has been suggested* by other investigators.

The bench mark and 85% bench mark non-vacuum electron beam welds were stronger than either the one-side one-pass TIG joints or the two-side one-pass MIG. joints (reported in the reference*) for either the 3.6 KW or 6 KW procedure. In fact, there is little difference in strength between the welds produced by the 3.6 KW or 6 KW processes. This observation is more easily verified from Figure 26 where the relative positions of the two groups of data has been shown in a less detailed manner than in Figure 25.

RESULTS: TWO SIDE - ONE PASS (-T37)

The strongest of the two-side one-pass welds (5 KW each side) coincides with the lowest energy input (10 K_i /in/in) and also the highest radiographic quality. Apparently slight increases in power result in considerable loss of strength when the two-side procedure is applied. Some of the loss may have come from increased porosity.** Usually high speed processes are not as sensitive to procedure changes so, tentatively, the cause of the degradation seems to be related to the use of opposing weld beads of excessive penetration. The behavior of the duplex weld wherein a low power (4 KW) pass placed against the toe of a 7 KW pass failed first suggests that placing a second weld near the underside of an over penetrated first weld is undesirable.

Moving the workpiece from 1/2" to 1/4" below the beam exit (Figure 27) reduced bead widths and increased penetration:

Power (KW)	Penetration (inches) $D_T = 1/2"$	$D_T = 1/4"$	Bead Width (inches) $D_T = 1/2"$	$D_T = 1/4"$
4.5	.090	.145	(.207)	.185
5.0	.115	.150	.218	.195
6.0	.160	.175	.233	.200

However there did not seem to be any effect on weld strength even though the increased penetration permitted welds to be made at heat input rates as low as 9 K_i/in/in.

---

* "Minutes of Aluminum Welding Symposium", NASA-MSFC/ME, July 1964, p. 153

** Since the one-side one-pass weld will not be used for Task C it has not been optimized and is used here only to permit study of high welding speeds with the 10 KVA equipment.
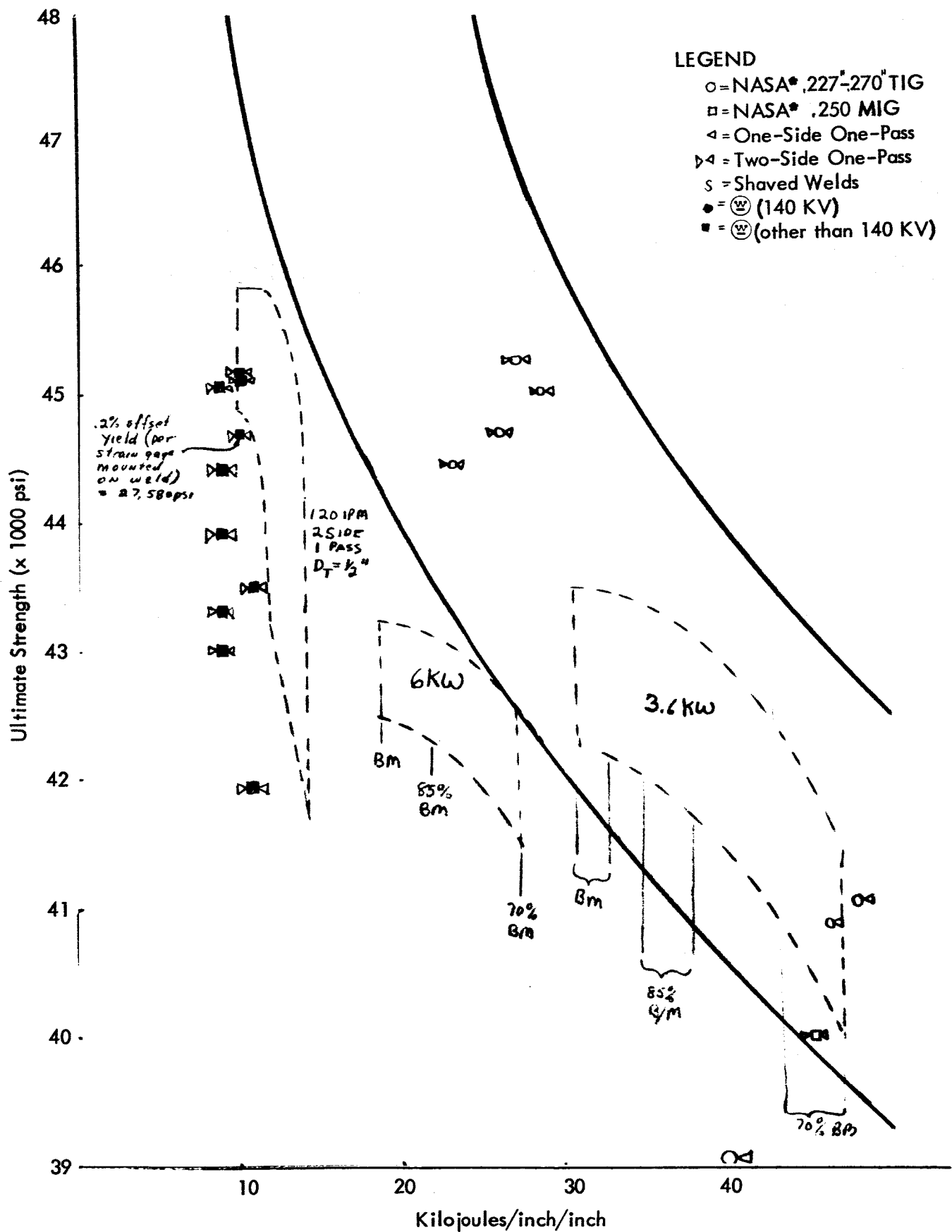
MINIMUM HEAT INPUT WELDS (120 ipm – two-side x one-pass – .225 2219-T37)

FIGURE 27

299

SUMMARY

Prior to the initiation of the present contract it appeared that the Model XWEB 15121 welder permitted the electron beam welding process to be freed from the constraints imposed by the vacuum environment. Further the Model XWEB 15121 had also been freed from its adjunct stationary pumps and power supply (so that the gun could be brought to the workpiece if necessary).

Each step of the Phase I experimental welding programs has thus far served to illustrate and demonstrate the practical applicability of non-vacuum welding in terms of actual quality standards.

1.   At the conclusion of the first section of the experimental program the machine settings that must be controlled in a detailed welding procedure were clearly identified.

2.   The relationship of these settings to the physical characteristics of a weld (undercut, width, contour, etc.) was defined for the ranges and intervals studied and these have been quantitatively set forth for at least one thickness of aluminum.

3.   At the conclusion of the Task A, the influence of practical procedure details and shielding methods on porosity in welds was studied. Welds that appear to meet radiographic soundness criteria were produced in at least one thickness of aluminum.

4.   Combining the procedure detail necessary for achievement of an acceptable set of physical characteristics with the details required to achieve radiographic soundness in the third step of the program (Task B) produced weld strengths in one-side, one-pass welds that exceed the strength of one-side one-pass welds produced by TIG in the .250 inch thickness of aluminum.

5.   Using present best shielding and cleaning techniques, porosity increases with increasing speed. Thus the power and speed of the optimum process (though it is producing attractive welds and about three times faster than conventional processes) do not coincide with the maximum available from the equipment.

RECOMMENDATIONS FOR FURTHER STUDY

The relationship between power-speed-porosity is anomolous when compared to work carried out by other investigators. This suggests that a careful study of the factors causing voids be accomplished under conditions where such factors as surface and atmospheric contamination can be carefully controlled. A better understanding of the formation of porosity under these high speed welding conditions would assist in utilizing the maximum capabilities of the process and provide information that might extend our present understanding of porosity formed in all open arc processes.

SECTION VIII

Authors: Peter J. Tkac
            Project Engineer
            Lear Siegler, Inc.
            Power Equipment Division
            Box 6719
            Cleveland, Ohio   44101

            Louis J. Lawson
            Chief Project Engineer, Electronics
            Lear Siegler, Inc.
            Power Equipment Division
            Box 6719
            Cleveland, Ohio   44101

N66 35574

Abstract

The flexibility afforded by a portable induction brazing system for
metallic tubing used in aerospace applications has been enhanced by the
recent development of a compact, lightweight VLF power supply operating
in the 3 to 15 Kcps region. The principles of induction brazing are
discussed in this paper along with a consideration of the effects of fre-
quency and tube geometry on depth of current penetration and thermal
efficiency. The application of the new brazing power supply with both
existing and anticipated brazing tools is described along with predicted
improvements in induction brazing equipment.

Introduction

The extensive application of metal tubing to missile liquid propellant and
hydraulic systems has created a need for a safe method of tube repair. The
repair of tubing on a missile is facilitated by lightweight equipment which
can be readily transported to the location of the fault. This is particu-
larly true if the missile is erected on the launch pad. In this case, the
equipment should be light enough to be hand-carried. The majority of tub-
ing repairs are accomplished by cutting away the defective portion of
tubing and brazing a new section in its place. The conventional open-flame
method of brazing in this application is both difficult and hazardous. It
is difficult since there is a good chance that the repair must be made in a
congested area. The hazard results from the possibility of fire damage to
surrounding cables or components as well as the proximity of flammable or
explosive substances. Thus, in order to effect a successful tube repairing
procedure, the repairing system must be flameless, light in weight, usable
in congested areas, and most important, capable of producing a reliable
brazing joint. All of these characteristics point to the use of induction
brazing as a means of repairing metal tubing. Using solid state electronics
the power supplies for induction brazing can be built small enough to be
hand-carried. Induction brazing tools are presently available to fit in
reasonably congested areas. With continued design effort these brazing
heads can be made smaller. In addition, there is no flame associated with
induction heating.

Principles of Induction Brazing

At this point it is worthwhile to discuss induction heating and the conditions that are necessary in order to induction heat effectively. The basic elements required for induction heating are an electric coil and the material to be heated. A cross-section of an induction coil and a piece of metal tubing is shown in Figure 1. Alternating current flows in the induction coil and causes a changing electromagnetic field to exist around the coil. If a conductor offers a complete path for the flow of current, the induced electromagnetic field causes current to flow in the path. Work is being done when the current overcomes the resistance of the path; this work appears as heat. It is this heat that makes induction brazing possible.

As alternating current flows in the conductor path a skin effect phenomenon occurs. Skin effect is the reduction of current density from the surface to the interior of a conductor carrying alternator current. Since it is the flow of current in a conductor that causes heat, and the current density decreases from the exterior to the interior of the conductor, the heat generated by the current will also decrease in the same proportion. This effect is very important in brazing tubing, since it is desirable to heat uniformly throughout the thickness of the tubing. For non-magnetic materials the depth of heat penetration is a function of the electrical resistivity of the conductor and the frequency of current. Mathematically this is expressed as follows:

$$t = 1.98 \sqrt{\frac{\rho}{\mu f}} \qquad (1)$$

where:

t = depth of penetration in inches

ρ = electrical resistivity in microhm centimeters

μ = relative permeability

f = frequency in cps

Figure 2 shows the plot of depth of current penetration versus frequency for stainless steel material. In the case of hollow tube brazing it is desirable to have a depth of penetration that is equal to the thickness of the tubing. Thus, the tubing will be heated uniformly throughout its thickness and a better brazing joint may be attained. If the depth of penetration is much greater than the thickness of material, high magnetizing forces are required to deliver power to the material. This is undesirable since the efficiency is low and excessive heating of the brazing tool results. Figures 3 and 4 show the power that is delivered to 2.0 inch and .25 inch diameter stainless steel tubing as the frequency is varied from 1 Kcps to 50 Kcps. From these curves the frequency at which the delivered power starts dropping off is easily determined.

If the depth of penetration is equal to or greater than the tube thickness for a non-magnetic material, the cylinder can be analyzed as though it were a short-circuited, single-turn secondary of an air-core transformer. The power delivered to the tube under these conditions can be expressed mathematically as follows:

$$P = \frac{5.15 \, f^2 t d^2 \rho H^2 \times 10^{-9}}{\rho^2 + 1.6 \, t^2 d^2 f^2 \times 10^{-2}} \qquad (2)$$

where

P = power density in watts per square inch

f = frequency cycles per second

t = tube thickness in inches

d = tube diameter in inches

ρ = resistivity in microhm-centimeters

H = peak magnetizing force in oersteds

The peak magnetizing force, H , can be expressed as:

$$H = 0.7 \, N I \qquad (3)$$

where

N = pitch of the coil in turns per inch

I = current in the coil in amperes rms.

Figures 5 and 6 show the relationship of current into the coil versus power into stainless steel tubing of 2.0 inch and 0.25 inch diameter. For these curves the frequency was held constant at 10 Kcps. Once the power into the tubing is determined the theoretical temperature rise (assuming no heat losses) of the tubing can be determined. The temperature rise of stainless steel tubing versus power input is shown in Figures 7 and 8 for 2.0 inch and 0.25 inch diameters. The temperature rise of the tubing can be expressed mathematically as:

$$P = 1056 \, M c \, \Delta T \qquad (4)$$

where

P = power input in watts per second

M = pounds of material heated

c = specific heat of material

ΔT = temperature rise in °F. per second

Using equations (1) through (4) all the information is available to predict the power input, the correct operating frequency and the expected temperature rise of the metal tubing. With this information the induction brazing tool and the power supply to drive the tool can be designed.

Induction brazing tools are available to braze metal tubing from 1/4 inch to 2-1/2 inch sizes. These tools consist of split coils which can be opened and slipped over a section of tubing. Because of the high currents flowing through the induction coil, these tools must be cooled while operating.

Description of Induction Brazing Power Supply

The power supply is a 7.5 KW unit which has an adjustable frequency range from 3 Kcps to 15 Kcps. The block diagram of the unit is shown in Figure 9. A description of the functions of the power supply system as shown in Figure 9 will follow.

Rectifier	-	A standard, full-wave, 3 phase, bridge type rectifier. The output is 300 VDC at 30 amps.
D.C. Power Supply	-	Provides outputs at 28 VDC, 10 VDC, 5 VDC and -10 VDC to supply power for the control circuitry.
Oscillator	-	A unijunction oscillator which is capable of frequency adjustment from 3 Kcps to 15 Kcps.
Voltage Control	-	Consists of an operational amplifier and two pulse binary counters which control the duty cycle of the output. The rms output voltage is proportional to the percent of duty-cycle.
Driver	-	A transistorized push-pull amplifier which provides the base drive for the power transistors.
Power Bridge	-	Consists of three power transistorized bridges. Thyristors (SCR's) are used to prevent short circuits due to slow turn-offs of power transistors. The power bridge can continuously deliver 30 amps at 300 V at frequencies up to 15 Kcps.
Tank Circuit	-	The tank circuit consists of a capacitor - tuned transformer circuit. The tapped output transformer matches the tool impedance to the power supply thus providing high current at low voltage to the brazing tool. The values of capacitance and the transformer ratio are chosen to tune the load to unity power factor. The tank circuit has a 15 KVA continuous rating.
Load	-	Consists of an induction heating coil (brazing tool) and the material to be heated.

The unit has short circuit protection which will turn the system off within five microseconds if the current in the power semiconductors exceeds their rated values. Preset timers are used to cycle the pre-purge (inert gas), the power on and the post-purge (inert gas) cycles.

Power Factor Correction

The power factor presented by the induction brazer to the power supply is approximately 20 percent. This means that only one fifth of the KVA going into the load is doing work. Thus, it is impractical to design a power supply without employing power factor correction. A parallel tuning capacitor is used in the Lear Siegler, Inc. induction brazing system to linearize the load seen by the power supply. Oil-filled paper power factor

correcting capacitors for operation at 15 Kcps at a level of 15 KVA weigh approximately 40 pounds. If a capacitor bank is to be provided to tune the several brazing tools throughout the frequency range, the weight of the paper capacitors will become prohibitive.

One of the new innovations to the induction brazing system resulting from the present development contract is the use of poly-carbonate dielectric capacitors to replace the bulky oil-filled paper capacitors. The weight of poly-carbonate capacitors to handle 15 KVAR at 15,000 cps is approximately 3 pounds. This represents a significant reduction over the conventional paper capacitors. The use of poly-carbonate capacitors make a power factor correction capacitor bank feasible for use in a portable system.

As a result of unity power factor tuning, the rating of the power supply can be reduced 5 to 1 and still deliver the same power to the tool. The use of poly-carbonate tuning capacitors has reduced the weight of the capacitors by a factor of 13.

Lightweight Output Transformer

The output transformer for the induction brazing application should have the transformer secondary designed for low voltage but extremely high current (approximately 800 amperes). In order to reduce I^2R loss, large diameter copper wire must be used. In the induction brazing application, this problem is compounded due to skin effect on a conductor at high frequencies. At 15 Kcps the impedance of a copper wire is much higher than its d.c. resistance.

In order to reduce secondary I^2R losses, the conductor should have a thin cross-section. In the application of the output transformer, a unique coil design was used. This coil is shown in Figure 10. With this design it can be seen that the transformer winding consists of a center conductor within an outer conductor separated by a ceramic insulator. Thus, the center conductor acts as the primary winding and the outer conductor acts as the secondary. This coil design provides three advantages:

1. It conserves space; it can be used with a minimum window area in the transformer core.

2. It provides a secondary that is thin walled, but has a large volume of copper.

3. There is extremely low flux leakage between the primary and the secondary of the transformer.

These coils can be stacked on a C core and interconnected to arrive at the transformer step-down ratio required. It is estimated that a saving in transformer weight by a factor of approximately 2 to 1 results from the use of this technique.

Conclusions

The successful design of a fully practical, lightweight portable induction brazing system has resulted from a direct confrontation of the problems which have previously made such a unit impractical. The solution of the power factor correction problem by application of the latest components and techniques has made the concept of portability feasible. In particular, the use of polycarbonate dielectric capacitors along with a unique type of output transformer in the tuned load circuit has resulted in system weight reductions by a factor of 2.

The principal design objective of the solid state power supply development program was achievement of the desired output power over the required frequency range and limiting total hardware weight to permit portability. In future developments, two design changes can be made which will reduce the weight of this package by more than 50%. The first change is the incorporation of airborne packaging techniques. At present steel cabinets are used in which only 33% of the volume is utilized for the power supply components. Thus, the unit is larger and heavier than necessary.
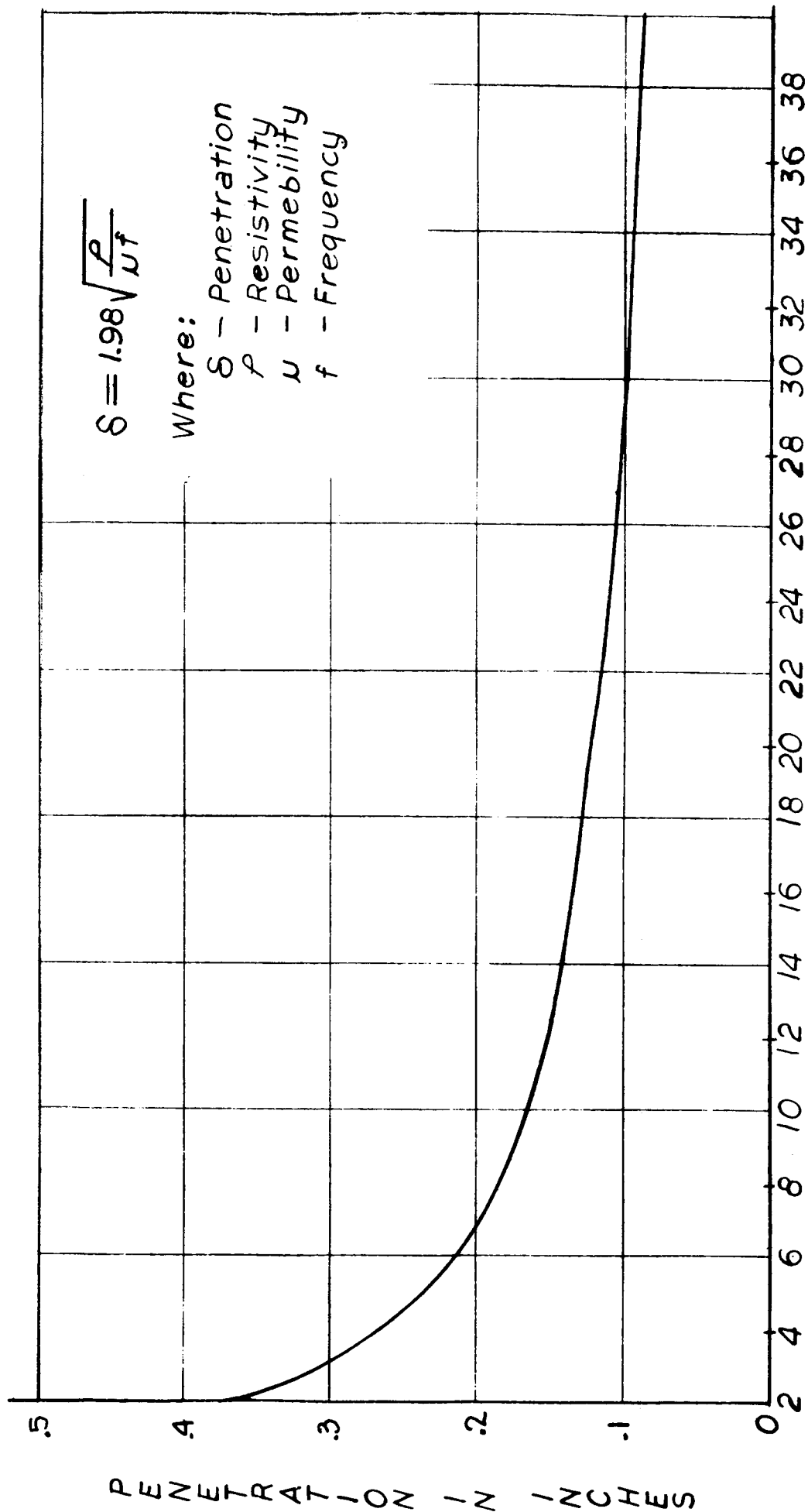
The second item which would reduce weight considerably is the modification of the power stage design to incorporate thyristors (SCR's) as switching elements. At present, the power bridge consists of 12 power transistors and 12 power diodes along with four thyristors for short circuit protection. All these components require heat sinks which add significantly to system weight. In addition to the reduction in power state devices, the six two amp driver circuits, which are needed to drive the power transistors, can be eliminated. Thus, the thyristor power bridge implementation would result in a considerable weight reduction.

The development model of the 7.5 KW brazing power supply including controls, power stages, and tank circuit weighs approximately 300 pounds with a volume of about seven cubic feet. This size and weight is significantly below that of a conventional brazing power supply. The next generation of equipment can be reduced to a total weight below 100 pounds and a maximum volume of 2.0 cubic feet by the use of the latest packaging techniques and thyristors in the power stages.
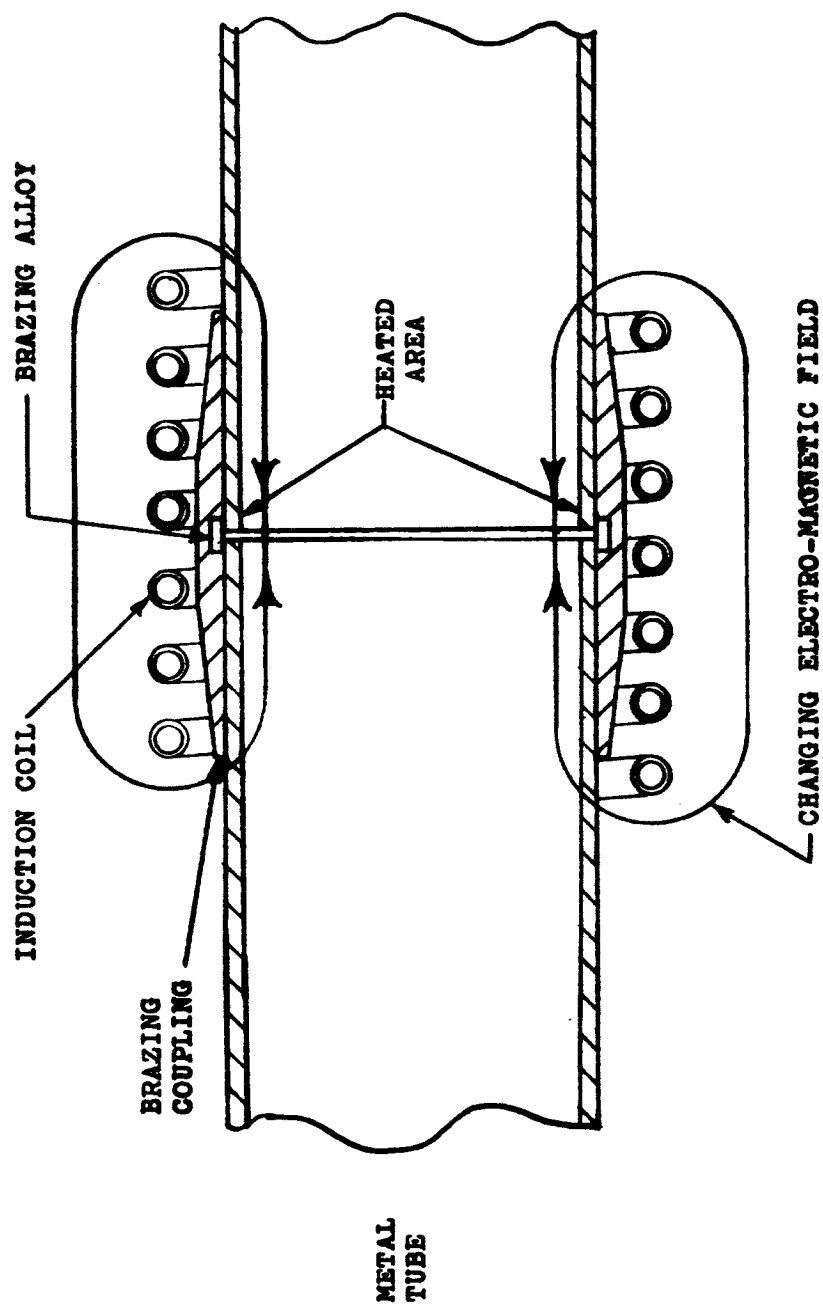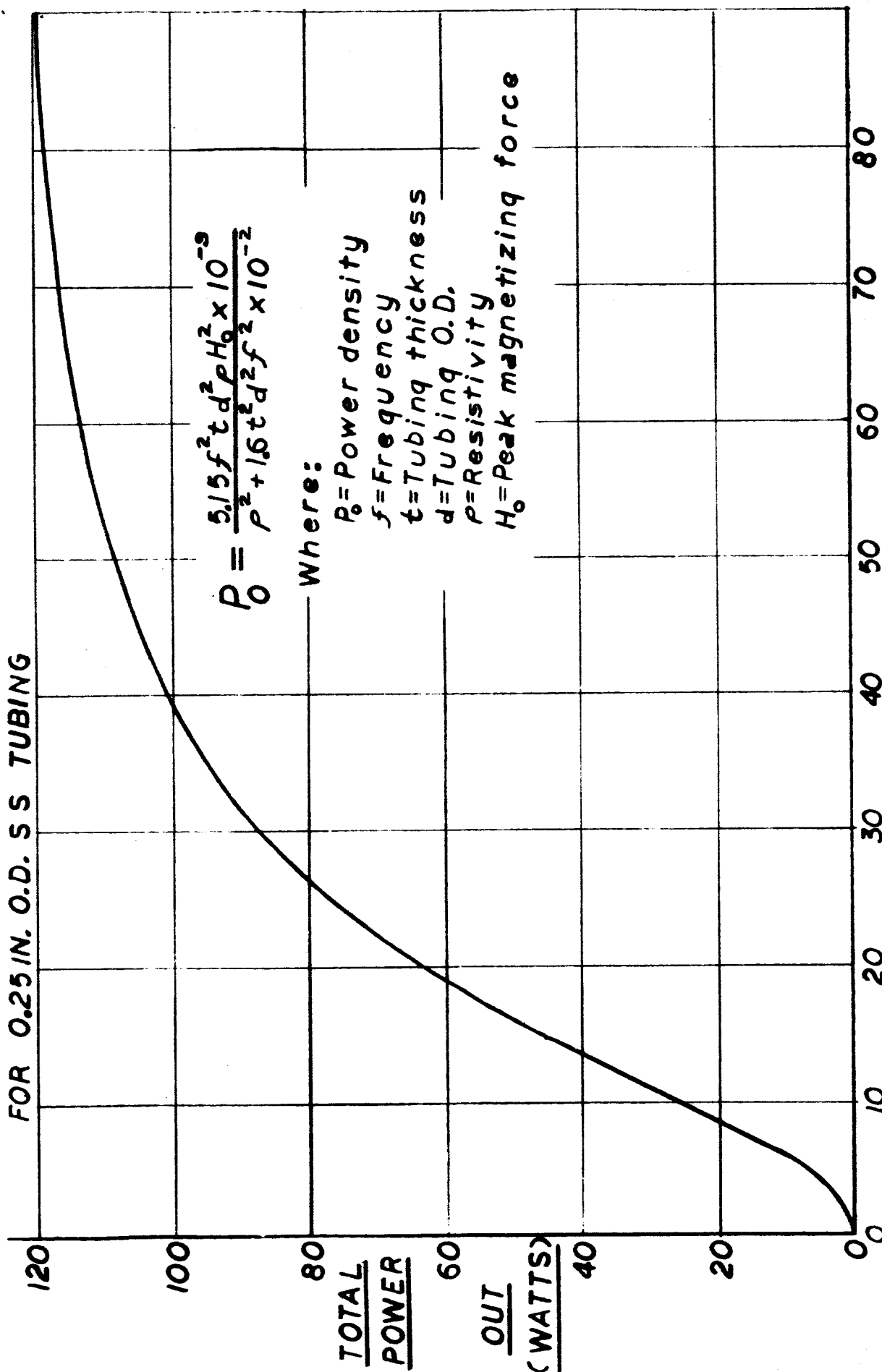
INDUCTION BRAZING

FIGURE 1

DEPTH OF PENETRATION VS FREQUENCY
FOR STAINLESS STEEL TUBING

$$\delta = 1.98\sqrt{\frac{\rho}{\mu f}}$$

Where:

δ – Penetration
ρ – Resistivity
μ – Permebility
f – Frequency

FREQUENCY IN KCPS

FIGURE 2

PENETRATION IN INCHES

OUTPUT POWER VS. FREQUENCY

FOR 0.25 IN. O.D. S.S. TUBING

$$P_0 = \frac{5.15 f^2 t d \rho H_0^2 \times 10^{-9}}{\rho^2 + 16 t^2 d^2 f^2 \times 10^{-2}}$$

Where:

P_0 = Power density
f = Frequency
t = Tubing thickness
d = Tubing O.D.
ρ = Resistivity
H_0 = Peak magnetizing force

FREQUENCY IN KILOCYCLES

FIGURE 3

313

OUTPUT POWER VS. FREQUENCY

FOR 2.0 IN. O.D. S.S. TUBING

FREQUENCY IN KILOCYCLES

TOTAL POWER OUT (WATTS)
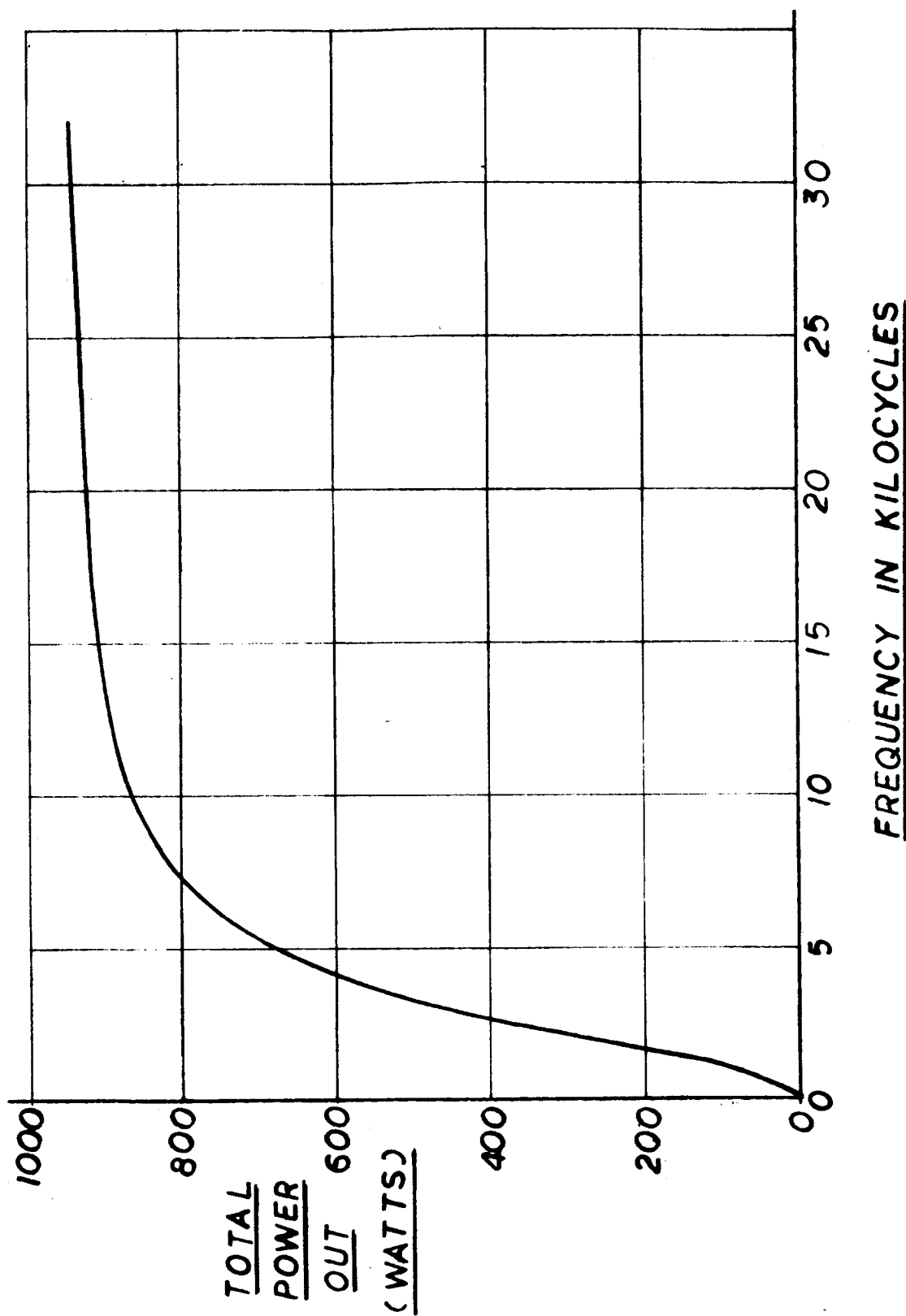
FIGURE 4

OUTPUT POWER VS INPUT CURRENT

FOR 2.0 INCH O.D. S.S. TUBING

$$P_o = \frac{2.52 \, t^2 + d^2 \rho N^2 I \times 10^{-9}}{\rho^2 + 1.6 \, t^2 d^2 f^2 \times 10^{-2}}$$

Where:
- P_o — Power Density
- f — Frequency
- t — Tubing Thickness
- d — Tubing O.D.
- ρ — Resistivity
- N — Coil Turns per Inch
- I — Coil Amps

POWER OUT IN WATTS

120 100 80 60 40 20 0

0 100 200 300 400 500 600 700 800
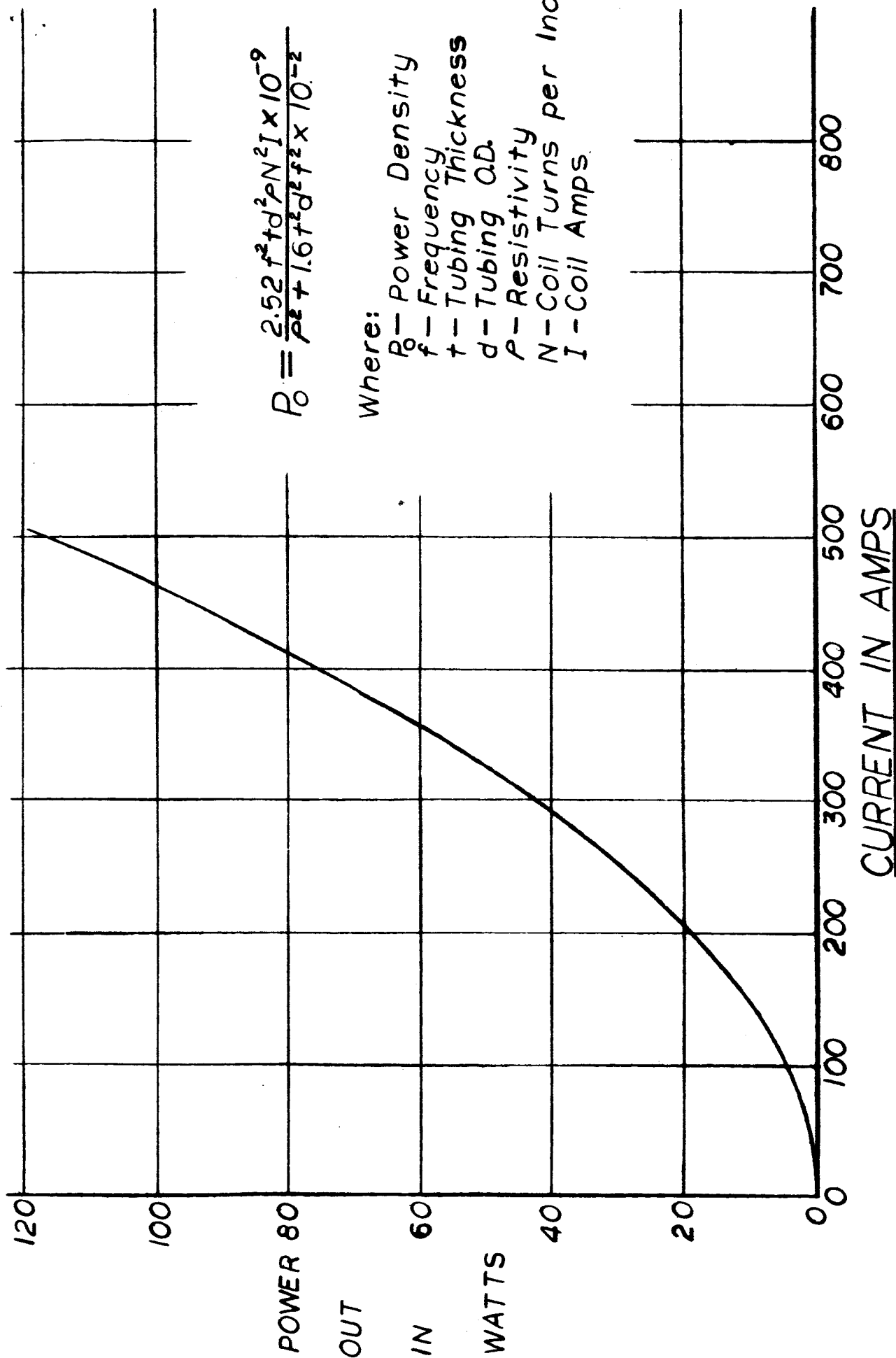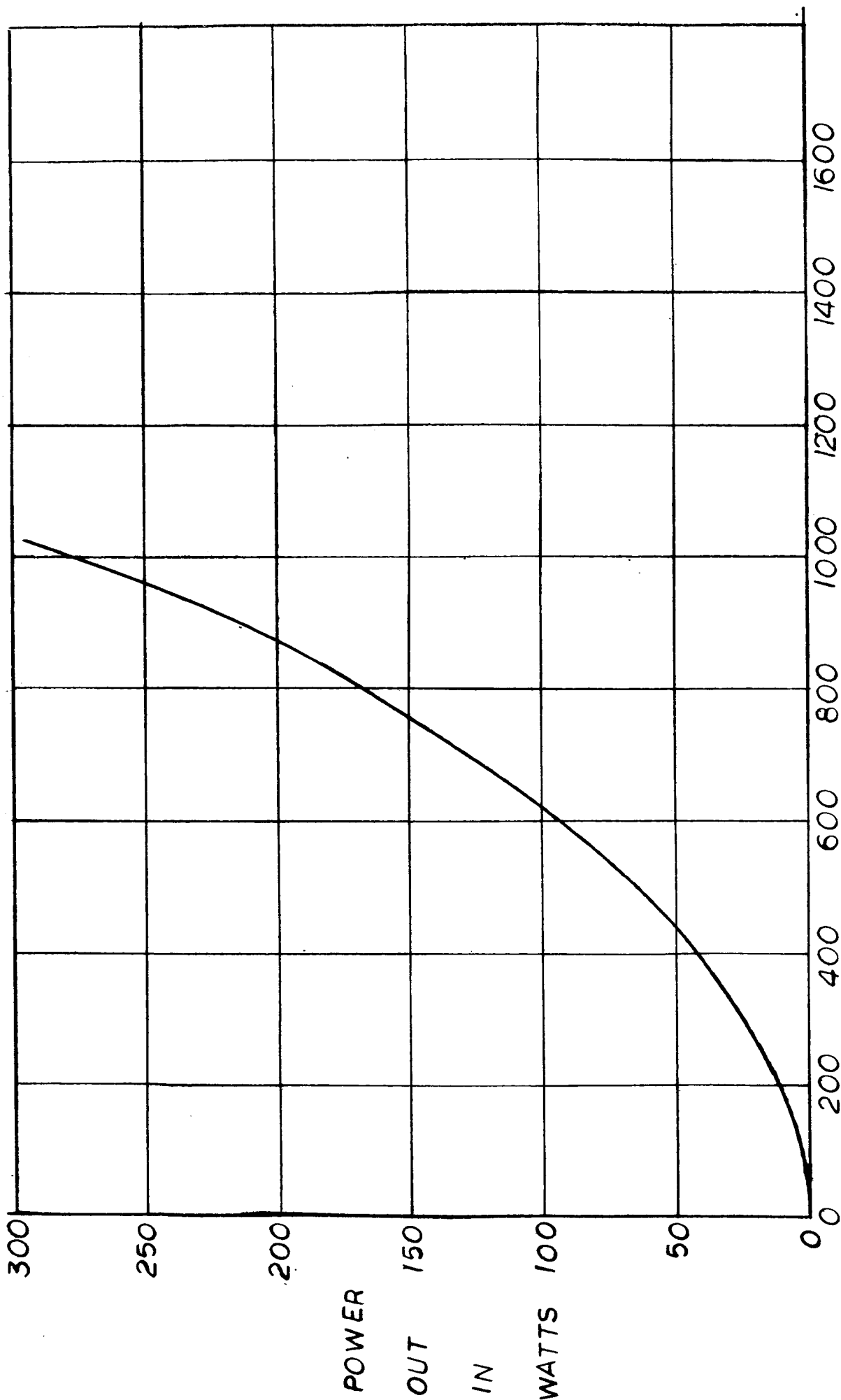
CURRENT IN AMPS

FIGURE 5

OUTPUT POWER VS INPUT CURRENT
FOR 0.25 INCH O.D. S.S. TUBING

CURRENT IN AMPS

FIGURE 6

POWER OUT IN WATTS
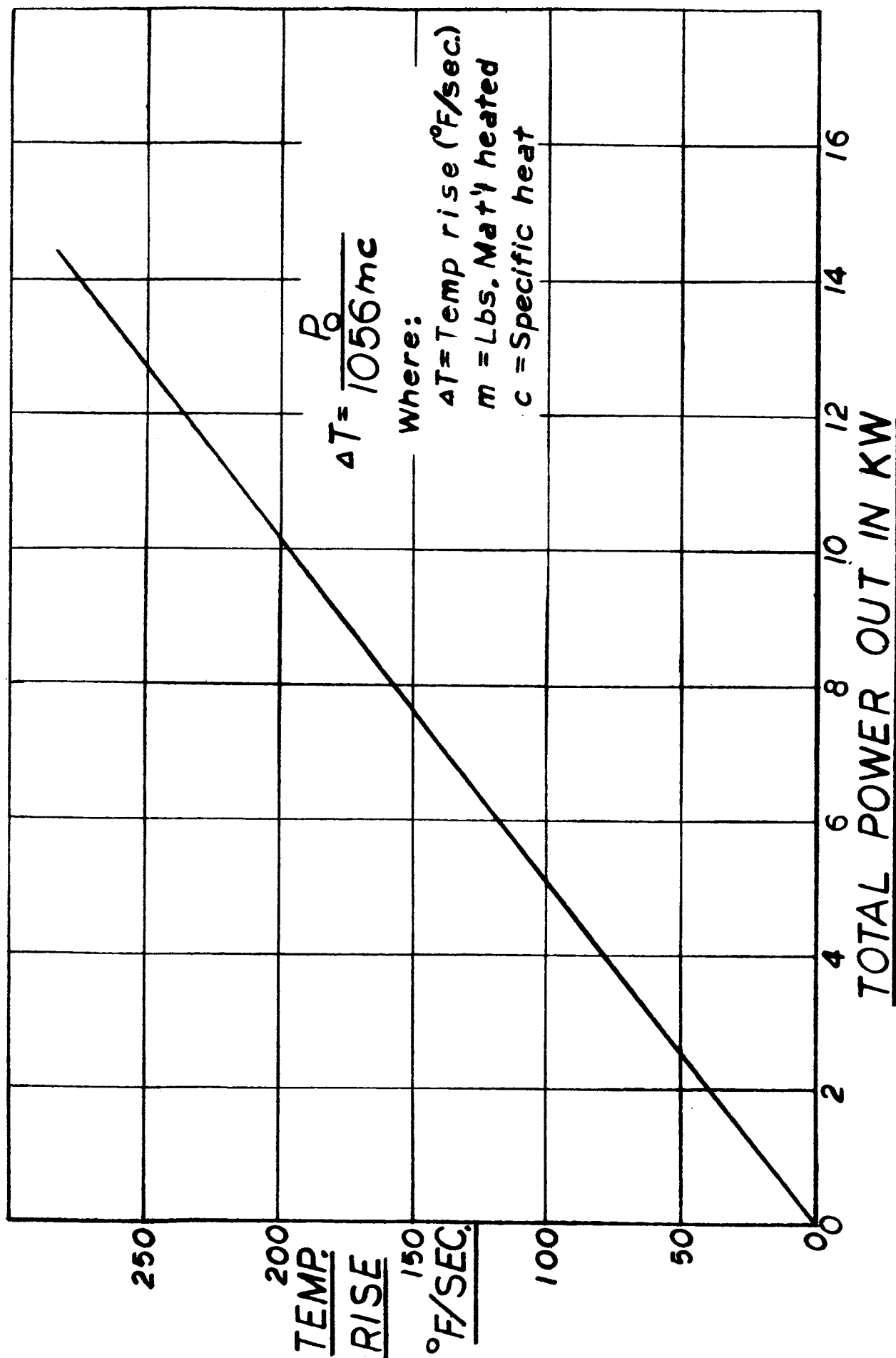
TEMPERATURE RISE VS POWER OUTPUT
FOR 2.0 INCH O.D. S.S. TUBING

$$\Delta T = \frac{P_o}{1056mc}$$

Where:

ΔT = Temp rise (°F/sec.)
m = Lbs. Mat'l heated
c = Specific heat

TEMP. RISE °F/SEC.

250
200
150
100
50
0

TOTAL POWER OUT IN KW

0   2   4   6   8   10   12   14   16

FIGURE 7

TEMPERATURE RISE Vs. POWER OUTPUT
FOR 0.25 O.D S S TUBING

FIGURE 8

TOTAL POWER OUT IN KW

TEMP. RISE °F/SEC.
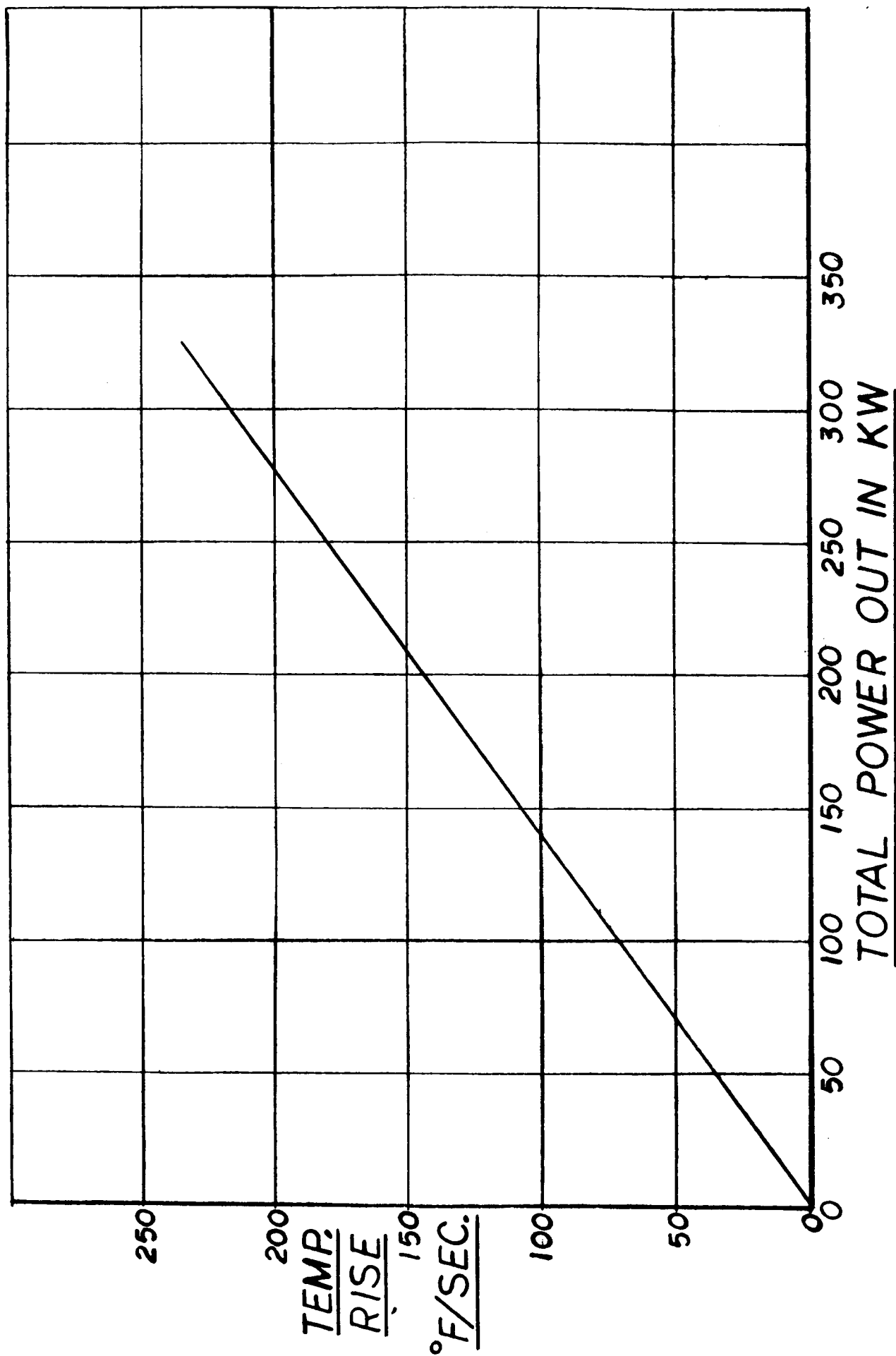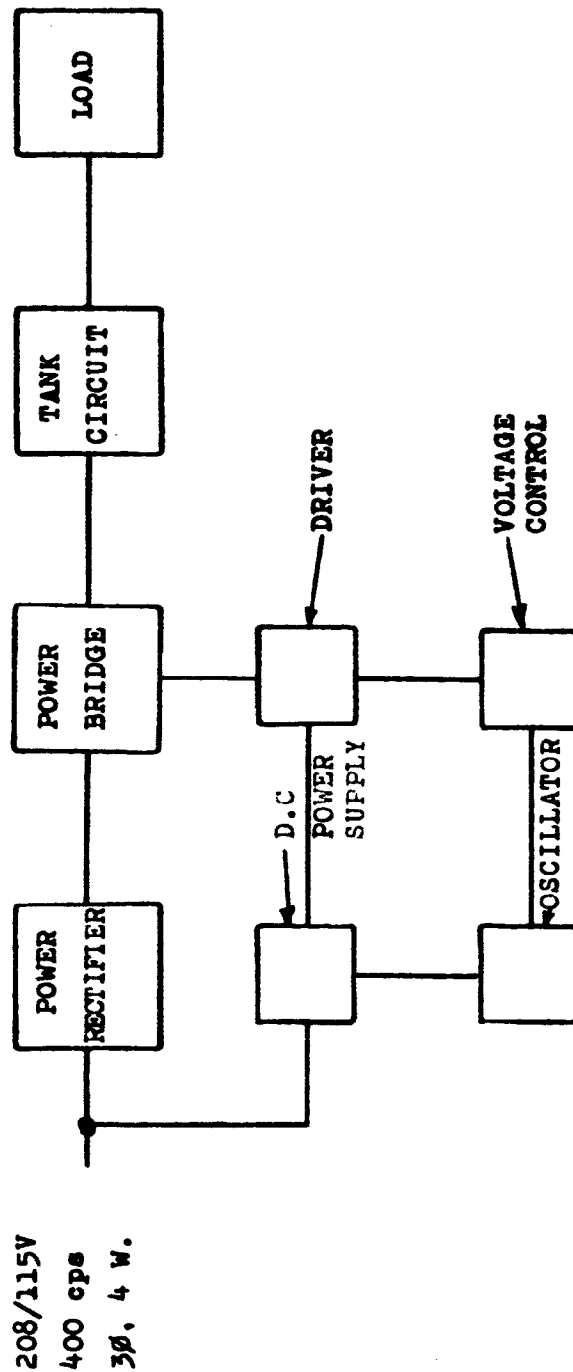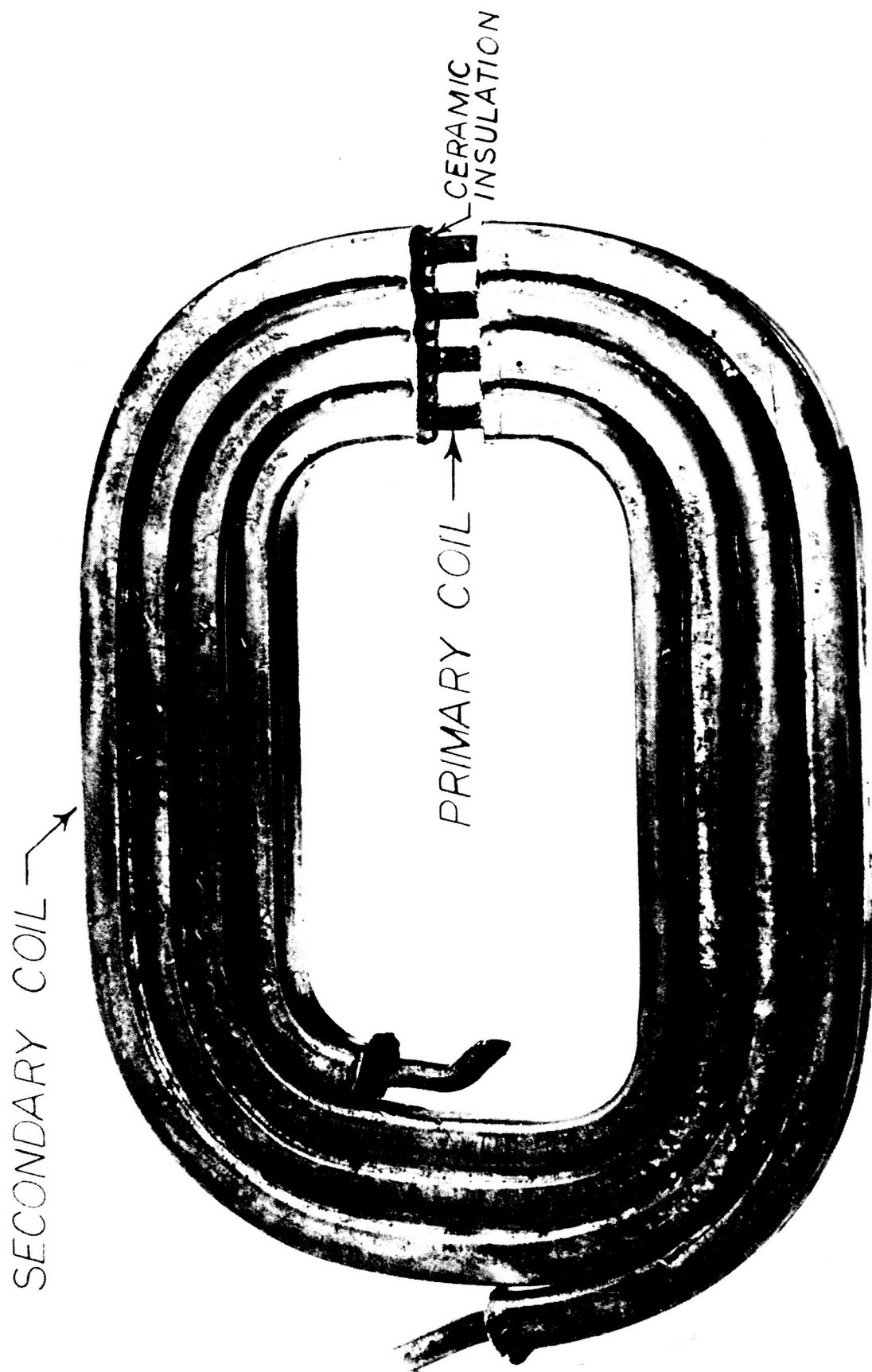
BLOCK DIAGRAM SOLID STATE VLF GENERATOR

Figure 9

SECONDARY COIL

CERAMIC INSULATION

PRIMARY COIL

FIGURE 10 OUTPUT TRANSFORMER COIL